EMISSION, DISPERSION AND LOCAL DEPOSITION OF AMMONIA VOLATILISED FROM FARM BUILDINGS AND FOLLOWING THE APPLICATION OF CATTLE SLURRY TO GRASSLAND

by
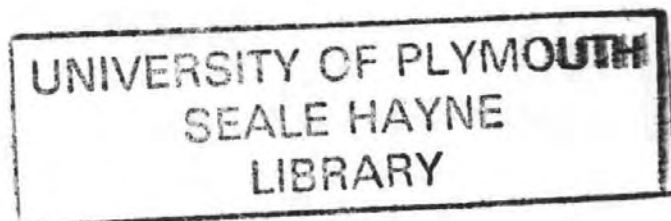
RICHARD ALEXANDER HILL

A thesis submitted to the University of Plymouth in partial fulfilment for the degree of

DOCTOR OF PHILOSOPHY

Department of Agriculture and Food Studies

In collaboration with

The Institute of Grassland and Environmental Research

JUNE 2000

ABSTRACT

EMISSION, DISPERSION AND LOCAL DEPOSITION OF AMMONIA VOLATILISED FROM FARM BUILDINGS AND FOLLOWING THE APPLICATION OF CATTLE SLURRY TO GRASSLAND

RICHARD ALEXANDER HILL

Emissions of ammonia (NH_3) into the atmosphere, principally from agricultural sources, have been implicated in the pollution of forests, moorlands and grasslands, through the subsequent deposition of reduced nitrogen (NH_x-N). Consequently, legislation has been implemented to control both the transboundary transport and local environmental impacts of NH_x. This thesis investigates the emission, dispersion and local deposition of NH_3 from two sources that are major components of national NH_3 emissions inventories, slurry applied to grassland and naturally ventilated cattle buildings.

A N balance method was identified for determining the time-average deposition of NH_3 downwind of a farm building, whilst an adapted micrometeorological flux-gradient technique was developed for estimating local deposition downwind of slurry spreading. This method used an analytical atmospheric dispersion model to provide advection corrections to the standard flux-gradient method. The UK-ADMS model, which incorporates a reasonably detailed treatment of building effects, was identified for use in determining the near-field dispersion from naturally ventilated farm buildings.

Eight field experiments were conducted to determine the emission, dispersion and local deposition of NH_3 volatilised from slurry applications. Emission fluxes during the initial runs following slurry spreading were found to depend on friction velocity, relative humidity and rainfall. Local deposition, at sufficient rates to affect local deposition budgets, was not found to occur during near-freezing conditions or following the application of fertilisers. Local deposition velocities during other periods were found to depend on the latent heat flux, temperature and the roughness length. During such periods, 14 - 18 % of the emitted NH_3 was estimated to deposit within 50 m of the source.

Experiments were also conducted at two naturally ventilated farm buildings, the Silsoe Research Institute Structures Building and a working dairy farm. Ammonia emission factors were determined for the main building and slurry lagoon at the dairy farm. A novel application of a model back-calculation method was applied to determine the emission from the lagoon. Dispersion of NH_3 from both sites was found to be adequately modelled using UK-ADMS. Approximately 2 % of the emitted NH_3 deposited within 100 – 150 m of each building. Time averaged deposition velocities calculated from the farm building studies confirmed that NH_3 was deposited to the leaf surfaces and uptaken across the leaf cuticle. Temperature dependent exchange rates were also indicated by the results of the farm building experiments, with NH_3 uptake being regulated by the assimilation potential of the plant.

The experimental results demonstrated that deposition around both sources could lead to local critical load exceedances. These were only estimated to occur within a few tens of metres downwind of slurry spreading whilst critical load exceedances were predicted at distances of up to 100 m or more downwind of the farm building. The temporal variability in local recapture found in these experiments, particularly for farm buildings, suggests that seasonal variability in the treatment of NH_3 emission and deposition should be included in atmospheric transport models. Furthermore, it is possible that transboundary transport of NH_x may increase during winter periods with peak housing emissions.

LIST OF CONTENTS

LIST OF TABLES

LIST OF FIGURES

ACKNOWLEDGEMENTS

AUTHOR'S DECLARATION

At no time during the registration for the degree of Doctor of Philosophy has the author been registered for any other University award.

The Biotechnology and Biological Sciences Research Council (BBSRC) courses on technical writing and statistics were attended. Conferences that were attended during the course of this study were:

♦ Atmospheric Ammonia: Emissions Deposition and Environmental Impacts (1995)
♦ Gaseous Nitrogen Emissions from Grasslands (1996)
♦ CAPER (1996)
♦ The 5th Annual BGS Research Conference (1997)

Publications:

Sutton M.A., Milford C., Dragosits U., Place C.J., Singles R.J., Smith R.I., Pitcairn C.E.R., Fowler D., Hill J., ApSimon H.M., Ross C., Hill R., Jarvis S.C., Pain B.F., Phillips V.R., Harrison R., Moss D., Webb J., Espenhahn S.E., Lee D.S., Hornung M., Ullyett J., Bull K.R., Emmett B.A., Lowe J. and Wyers G.P. (1998) Dispersion, deposition and impacts of atmospheric ammonia: quantifying local budgets and spatial variability. *Environmental Pollution* **102**, 349-361.

Hill R.A., Pain B.F., Parkinson R., and Phillips V.R. (1997) The role of grasslands adjacent to farm buildings and slurry spreading in capturing emitted ammonia. In: *Abstracts from the Fifth Annual BGS Research Conference.*
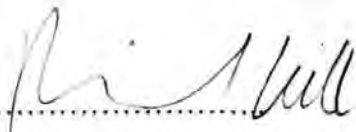
Sutton M. A., Milford C., Dragosits U., Singles R., Fowler D., Ross C. A., Hill R. A., Jarvis S. C., Pain B. F., Harrison R., Moss D., Webb J., Espenhahn S., Halliwell C., Lee D. S., Wyers G. P., Hill J. and ApSimon H. M. (1997) Gradients of atmospheric ammonia concentrations and deposition downwind of ammonia emissions, First results of the ADEPT Burrington Moor experiment. In: *Gaseous Nitrogen Emissions from Grasslands* (edited by Jarvis S. C. and Pain B. F), pp 131-141. CAB International.

Hill R. A., Pain B. F. and Parkinson R. (1996) Seasonal variability in the short-range deposition of ammonia. In: *Gaseous Nitrogen Emissions from Grasslands- Poster Proceedings and Abstracts.*

Ross C. A. and Hill R. A. (1996) Ammonia deposition to grassland from grazing animals and slurry spreading. In: *Abstracts from the Committee for Air Pollution and Environmental Research (CAPER) Conference.*

Hill R. A., Pain B. F. and Parkinson R. (1996) Short range exchanges of atmospheric ammonia, emitted from slurry, with grassland. In: *Atmospheric Ammonia: Emissions, Depositions and Environmental Impacts. Poster Proceedings* (edited by Sutton M. A., Lee D. S., Dollard G. J. and Fowler D.), pp 71-74. Institute of Terrestrial Ecology, Edinburgh.

Signed:................................. Date:.15-06-2000

1

REVIEW OF THE LITERATURE

1.1   INTRODUCTION

The deposition of anthropogenic nitrogenous compounds onto natural and semi-natural ecosystems is widely regarded to cause significant environmental damage, mostly through eutrophication and the acidification of soils. Whilst 75 % of the nitrogenous compounds emitted annually in the United Kingdom (UK) are oxidised nitrogen (NO_x-N), the smaller reduced N (NH_x-N) fraction accounts for 60 % of the total N deposition (Fowler *et al.*, 1998a). Moreover, due to the high reactivity and solubility of ammonia (NH_3) localised deposition close to sources can result in significant heterogeneity in the deposition field.

Both national and international legislation have been drafted to regulate the local scale and transboundary aspects of N deposition. Environmental impact assessments, that are fundamental in applying and policing such legislation, require the determination of the emission, dispersion and fate of atmospheric NH_3 using mathematical models. The modelling of NO_x deposition is fairly straightforward, being principally regulated by stomatal uptake to plants. However, NH_3 deposition is more difficult to model due to bi-directional surface-atmosphere exchange and the dependence of deposition rates on the poorly understood surface chemistry of the underlying vegetation. Furthermore, as most studies have concentrated on the background deposition of NH_3 over uniform areas little work has been done on the deposition close to sources. Significant deposition close to a source could result in localised pollution episodes, should the receptor location be sensitive to N deposition, or the beneficial addition of N though deposition to agricultural land. A further important aspect of local NH_3 deposition is that deposition close to a source reduces the net emission from an area and thus is important when calculating regional and national N budgets.

This chapter reviews the current literature on the sources, dispersion, deposition and effects of atmospheric NH_3 to illustrate the background and aims of the research reported later in this thesis. Details are also given of the overall project this work was part of, the Ammonia Distributions and Effects ProjecT (ADEPT), which was commissioned by the UK Ministry of Agriculture Fisheries and Food (MAFF).

1.2 SOURCES OF ATMOSPHERIC NH_3

Emissions of NH_3 into the atmosphere are dominated by terrestrial sources (ApSimon *et al.*, 1987; Pain *et al.*, 1998; Sutton *et al.*, 1995) with the seas acting principally as a sink for NH_3 (Asman *et al.*, 1995; Lee *et al.*, 1998). The majority of terrestrial NH_3 is produced from the hydrolysis of urea, the major nitrogenous constituent in urine (Bristow *et al.*, 1992), catalysed by the extracellular acting enzyme, urease, Equation 1.1. Urease is mainly produced by soil bacteria and has a ubiquitous distribution throughout many terrestrial environments. Urease activity is increased by high substrate concentrations, high water contents, and a pH greater than 6.5 (Ferguson *et al.*, 1988). The optimal temperature range for urease has been shown to be between 10 - 40 °C, though the enzyme has some activity at sub-zero temperatures (Jarvis and Pain, 1990).

$$CO(NH_2)_2 + H_2O \xrightarrow{\text{Urease}} 2\,NH_3 + CO_2$$
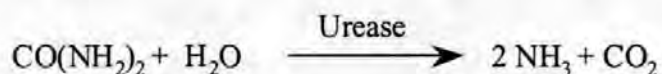
Equation 1.1: The urease catalysed hydrolysis of urea to form NH_3.

1.2.1 The volatilisation process

The volatilisation process leads to the production of gaseous NH_3 from NH_3 in solution produced by urea hydrolysis or from the application of artificial fertilisers. The three reversible reactions that control volatilisation follow a linear scheme, shown in Equation 1.2, with products of either ammonium (NH_4^+) bound as a solid form onto soil particles or gaseous NH_3.

$$NH_4^+ \rightleftharpoons NH_4^+ + H_2O \rightleftharpoons NH_3 + H_2O + H^+ \rightleftharpoons NH_3$$
$$\textit{Solid} \qquad \textit{In solution} \qquad \textit{In solution} \qquad \textit{Gaseous}$$
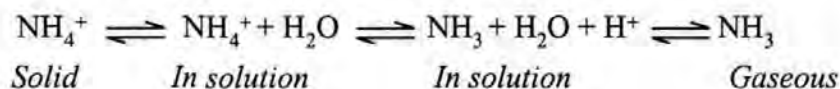
Equation 1.2: Reaction scheme for the volatilisation of NH_3.

According to Henry's law, the pressure of NH_3 gas in equilibrium with NH_3 in solution is directly proportional to the activity of NH_3 within the solution. A high rate of volatilisation therefore depends on a high concentration and activity of NH_3 in solution at the surface-atmosphere interface. Other factors enhance the formation of gaseous NH_3 such as the

removal of excess H^+ by a base, usually HCO_3^- (Jarvis and Pain, 1990), and the presence of sufficient H_2O to prevent the production of NH_4^+ on the solid phase whilst maintaining a high concentration of NH_3 in solution.

1.2.2   Non-agricultural NH₃ emissions

Non-agricultural NH_3 emissions arise from industrial processes, wild animals, domestic pets and human respiration.

1.2.2.1   Industrial NH₃ emissions

The synthesis of NH_3, conducted for the fertiliser industry, is the primary contributor to the direct emission of gaseous NH_3 from industrial processes in the UK (Sutton *et al.*, 1995) with an estimated annual emission of 5.7 kt NH_3-N (Buijsman *et al.*, 1987). Typical NH_3 emission factors for the production of mineral fertilisers are in the region of 10 kg NH_3-N for each tonne of NH_3 produced according to Wieprecht (1987), as cited in Moller and Schieferdecker (1985).

Power generation also contributes to industrial NH_3 emissions with an estimated 6 - 9 g NH_3-N being released to the atmosphere for each tonne of lignite combusted (Lee and Longhurst, 1993). In addition, road traffic has been estimated to contribute a typical emission of 25 mg NH_3-N per kilometre travelled per vehicle by Harkins and Nicksic (1967), as cited in Lee and Longhurst (1993). Due to the use of catalytic converters in modern petrol cars current emission factors are estimated to be higher, approximately 70 mg NH_3-N km^{-1}, though emissions from diesel vehicles are much smaller, <2 mg NH_3-N km^{-1} (Sutton *et al.*, 2000).

Landfill sites and the spreading of sewage sludge on land are further sources of atmospheric NH_3 (Kruse *et al.*, 1989; Sutton *et al.*, 1995). However, despite the large mass of waste disposed though both these processes, their low N contents mean that they are only minor contributors to national NH_3 emissions inventories (Sutton *et al.*, 1995). The relatively low contribution of road traffic, landfill sites and sewage treatment works to regional scale NH_3 emissions has been confirmed by Allen *et al.* (1988) who found that influences of such sites on NH_3 air concentrations were minimal.

1.2.2.2   Emissions of NH₃ from wild animals and pets

Emission factors of 0.3 kg NH_3-N $animal^{-1}$ a^{-1} and 0.1 kg NH_3-N $animal^{-1}a^{-1}$ have been determined by Sutton *et al.* (1995) for large and small seabirds respectively by rescaling

(by mass) emission factors for poultry. Though the assumption that seabirds have a comparable metabolism and dietary N intake to poultry is somewhat speculative, these types of emission factors do enable the calculation of conservative (over-predictive) estimates of the total contribution of such sources to the total UK NH_3 emission. Even so, the results indicate that seabirds are minor contributors to national NH_3 emissions, with an estimated annual emission of 0.3 kt NH_3-N from UK sources.

The contribution of domestic pets to UK NH_3 emissions have also been estimated by Sutton *et al.* (1995). Emission factors for these sources were calculated by rescaling the emission factors for sheep cited in Cass *et al.* (1982). Using this methodology emission factors of 0.13 kg N animal^{-1} a^{-1} and 0.81 kg animal^{-1} a^{-1} were determined for cats and dogs respectively. Horses are also often included in NH_3 emission inventories as pets, and again emission factors have been calculated by rescaling the emission factors for other livestock. There is a fairly wide range of uncertainty with respect to the emission factor for horses with estimates ranging from 7.7 kg NH_3-N animal^{-1} a^{-1} (Buijsman *et al.*, 1987) to 31.6 kg NH_3-N animal^{-1} a^{-1} (Kruse *et al.*, 1989). In the inventory compiled by Sutton *et al.* (1995) a value of 10 kg NH_3-N animal^{-1} a^{-1} was used with the caveat that the estimate was extremely uncertain. Wild red deer were also included by Sutton *et al.* (1995) in their inventory calculations. An emission factor was calculated of 0.9 kg NH_3-N animal^{-1} a^{-1} assuming that deer have a higher metabolic rate than sheep (by a factors of 2.5) but graze on low N status crops.

1.2.2.3   *Emissions of NH_3 from human respiration*

Elevated NH_3 concentrations within occupied residential buildings, between 13 - 85 μg NH_3 m^{-3}, have been measured by Atkins and Lee (1993). These results provide empirical evidence that urea produced by human respiration is a source of atmospheric NH_3.

An emission factor of 1.25 kg NH_3-N capita^{-1} a^{-1} was estimated by Moller and Schieferdecker (1985), based on an assumed N excretion of 5 kg N capita^{-1} a^{-1} and a further assumption that 25 % of the excreted N volatises as NH_3-N. It should be noted that this estimate includes the contribution of N lost though urine and faeces as well as through perspiration. Other emission factors have been estimated, assuming that all urea-N present on the skin surface will be volatilised as NH_3-N, of 1 kg NH_3-N capita^{-1} a^{-1} (Atkins and Lee, 1993), 250 g NH_3-N capita^{-1} a^{-1} (Cass *et al.*, 1982) and 270 kg NH_3-N capita^{-1} a^{-1}, (Healy *et al.*, 1970). Sutton *et al.* (1995) calculated a revised emission factor of 50 g NH_3-N capita^{-1} a^{-1} by reducing the estimate of Cass *et al.* (1982) by 80 % to include the

4

reduction in net emission caused by sorption onto clothing, deposition within buildings and washing.

1.2.3 Agricultural NH₃ emissions

There is consensus that NH_3 emissions from agriculture are the dominant contributor to emissions on national and international scales (ApSimon *et al.*, 1987; Moller and Schieferdecker, 1985; Pain *et al.*, 1998; Sutton *et al.*, 1995). The reason for this becomes apparent when the influence of Man on the N cycle is investigated.

Estimates suggest that 93 % of the inputs to the N cycle of most developed countries are derived from anthropogenic sources, the remainder being from biological N fixation (Kruse *et al.*, 1989). Plants are highly efficient at utilising such an increased N supply, with typical N balances for irrigated permanent grassland demonstrating that crops uptake and assimilate 90 % of applied N (Sapek, 1997). However, animals are considerably less efficient, with between 4 - 25 % of dietary N intake being assimilated (Whitehead, 1970).

The main pathway for the metabolic loss of N from livestock is through urea excretion (Bristow *et al.*, 1992). Excreted urea is typically converted to NH_3 within 24 hours through urea hydrolysis, as shown in Equation 1.1 (Ryden, 1986). The NH_3 produced can be directly lost to the atmosphere through volatilisation (Equation 1.2), can be reduced to NH_4^+ and retained on soil particles, or may be nitrified by soil bacteria. Nitrate-N can be lost from agricultural systems through leaching to aquifers or through denitrification and the subsequent gaseous emission of N_2O and N_2. Measurements suggest that losses through NH_3 volatilisation are greater by a factor of two (Pain and Thompson, 1989; Van der Molen *et al.*, 1990b) to three (Ryden, 1986) than nitrification losses.

Of the agricultural production systems, animal housing and the application of livestock wastes onto land are the major pathways for the loss of N through NH_3 volatilisation. Other agricultural practices that are smaller contributors to national NH_3 emissions include slurry storage, the grazing of livestock, emissions following fertiliser applications and the stomatal emission of NH_3 from intensively fertilised crops.

1.2.3.1 *NH₃ volatilisation following the application of slurry to land*

Volatilisation of NH_3 from cattle slurry applied to land, using conventional UK methods for surface application, can result in losses of up to 67 % of the total NH_x-N (often termed as TAN) applied depending on slurry type and method of application (Bless *et al.*, 1991;

Pain *et al.*, 1989; Pain *et al.*, 1991; Thompson *et al.*, 1990a; Van der Molen *et al.*, 1990a). Ammonia losses during slurry spreading have been estimated to be between 0.1 % and 0.3 % of the total emission (Pain *et al.*, 1991). However, a considerable increase in the rate of emission occurs once the slurry contacts the soil, with 24 - 29 % of the total loss occurring during the first hour following application and up to 85 % of total losses occurring within 12 - 24 hours (Klarenbeek *et al.*, 1993; Pain *et al.*, 1989). High initial rates of volatilisation are typically followed by a roughly exponential decrease in the emission rate, with more than 90 % of losses occurring within 96 hours following application (Pain *et al.*, 1991; Thompson *et al.*, 1990b). Volatilisation losses are regulated by meteorological factors, slurry composition, and by the method of application.

A diurnal variation in NH_3 emission from slurry has been measured in several studies with emission maxima occurring at noon and minima occurring during the early hours of morning (Bless *et al.*, 1991; Sommer *et al.*, 1991; Sommer *et al.*, 1997; Van der Molen *et al.*, 1990a). This variability correlates with changes in air temperature, wind speed and atmospheric humidity, though it should be noted that these quantities are strongly correlated in the atmosphere and disentangling their relative influences on NH_3 volatilisation is difficult.

Comparative wind tunnel experiments, conducted by Sommer *et al.* (1991), found that temperature variations were strongly correlated with NH_3 emissions. Similar experiments conducted by Menzi *et al.* (1998) demonstrated that the correlation between emission and humidity described more of the variability in their dataset than the correlation between emission and temperature. However, Menzi *et al.* (1998) noted that the correlation they found may have been highlighted because of the poor draining soils used in their experiments. Wind speed has also been found to influence the rate of NH_3 volatilisation (Menzi *et al.*, 1998; Sommer *et al.*, 1991; Thompson *et al.*, 1990b). This is thought to be due to a reduction in the gas phase resistance above the slurry (boundary layer resistance) enhancing the rate of atmospheric dispersion of emitted NH_3, and increasing the surface-atmosphere concentration gradient (Sommer *et al.*, 1991).

The loss of NH_3 through volatilisation from surface applied cattle slurry has been shown by Menzi *et al.* (1998) to be strongly correlated with the TAN content of the slurry, with a high slurry TAN content maintaining a positive surface-atmosphere concentration gradient. The dry matter content of slurry has also been found to be correlated with NH_3 emission (Sommer *et al.*, 1991; Sommer and Olesen, 1991). In the compilation of their emission

inventory, Pain *et al.* (1998) estimated that approximately 15 % of applied TAN volatilises from slurries with low dry matter contents (< 4 %) and 59 % volatilises from slurries with high dry matter contents (>8 %). The latter was including farm yard manures, produced from straw based farming systems.

The influence of dry matter content on NH_3 volatilisation is thought to be due to reduced rates of TAN infiltration into soil (and subsequent immobilisation on clay minerals) from slurries with high dry matter contents. Lower rates of NH_3 volatilisation from slurry exposed to rainfall (Pain and Misselbrook, 1997), from slurry applied at low rates (Menzi *et al.*, 1998), and from slurry applied to dry soils (Sommer *et al.*, 1991) are also thought to be due to infiltration into soil. The pH of slurry also has an influence on NH_3 emission, as the equilibrium between NH_4^+ and NH_3 in the liquid phase of slurry is pH dependent (Pain *et al.*, 1990). Acidic pH can be seen from Equation 1.2 to favour the production of NH_4^+, whilst alkaline pH favours the production of NH_3.

Different methods used to apply slurry to land have been shown to have a significant influence on the subsequent NH_3 volatilisation. Jarvis and Pain (1990) concluded that injection of slurry into soil to a depth of 150 mm reduces NH_3 volatilisation to negligible levels through the large reduction in the area of the slurry-atmosphere interface. More conventional methods of incorporation can also result in emission reductions, with up to a 90 % reduction from ploughing slurry into soil, a 78 % reduction from using a rotary harrow and a 40 % reduction from the use of tines (Pain *et al.*, 1991). The use of drag hoses to apply slurry beneath a vegetated canopy can also reduce NH_3 volatilisation by approximately 10 % when compared to conventional application techniques. This is due to plant uptake and low wind speeds beneath canopies (Bless *et al.*, 1991; Sommer *et al.*, 1993b).

This section has so far only considered NH_3 volatilisation from the application of cattle slurry to land, as this is estimated to be the largest contributor to land spreading losses. However other types of manure are also routinely spread including: poultry manure, pig manure and, to a lesser extent, sheep manure (Pain *et al.*, 1998). Approximately 3.8 Mt of poultry manure and 5.1 Mt of pig manure are produced annually in the UK (Pain *et al.*, 1998). These are mainly disposed of by spreading on agricultural land, with 35 % of the TAN applied volatilising as NH_3 from poultry manure and 15 % of the TAN applied volatilising from pig manure (Chambers *et al.*, 1997; Pain and Thompson, 1989; Pain *et*

al., 1990). The differences between these losses are, in part, due to the high dry matter content of poultry manure.

1.2.3.2   NH₃ volatilisation from farm buildings and slurry stores

In the UK, approximately 20 % of the nitrogenous compounds excreted in farm buildings and slurry stores are lost to the atmosphere through NH_3 volatilisation (Fangmeier *et al.* 1994). Emissions of NH_3 from farm buildings and slurry stores are often grouped due to their common source: housed livestock. Emissions to the atmosphere occur directly from the animal house and, following removal of wastes, from local storage facilities.

Ammonia emissions from stored slurry are principally dependent on the design of the slurry store. Slurry stored in a stirred open tank typically has a relatively homogeneous TAN content with a constant supply of NH_3 to the surface, so maintaining a positive surface-atmosphere concentration gradient (Olesen and Sommer, 1993). However, when slurry is stored in an unstirred tank, such as a lagoon, a gradient of NH_3 concentration can be formed within the store thus reducing the availability of NH_3 at the surface-atmosphere interface (Sommer *et al.*, 1993a). The emission of NH_3 from slurry lagoons can be further restricted by the formation of a crust of dried slurry (principally composed of undigested grass) on the surface of the lagoon (Voorburg and Kroodsma, 1992).

Work conducted by Pain *et al.* (1998) for the UK NH_3 emissions inventory, citing unpublished measurements from Silsoe Research Institute (SRI), determined average emission fluxes of 51 μg NH_3-N m^{-2} s^{-1} for stirred cattle slurry tanks and 24 μg NH_3-N m^{-2} s^{-1} for unstirred slurry lagoons. These values compare well with estimates from Sommer *et al.* (1993a) of 51 μg NH_3-N m^{-2} s^{-1} for stirred cattle slurry and 10 μg NH_3-N m^{-2} s^{-1} for an encrusted store. Other estimates of NH_3 emission from aerobically digested slurry produced from a biogas plant, reported in Sommer (1997), suggested that emission fluxes ranged between 3 - 104 μg NH_3-N m^{-2} s^{-1} depending on surface cover.

Data from Pain *et al.* (1998) on the distribution of NH_3 emissions between the main types of housed livestock demonstrate that cattle are the dominant source in the UK, as shown in Figure 1.1. Cattle are mostly housed in farm buildings that are ventilated through open slatted wooden boarding on the walls, "Yorkshire boarding", and through open fronting (Demmers *et al.*, 1998). Emissions from such "naturally ventilated" structures depend on the rate of ventilation and the concentration of NH_3 in the building. The concentration of

NH_3 in a building is a function of both the N excretion of the housed livestock and factors related to NH_3 volatilisation, as discussed in the previous sections (Hutchings *et al.*, 1996).
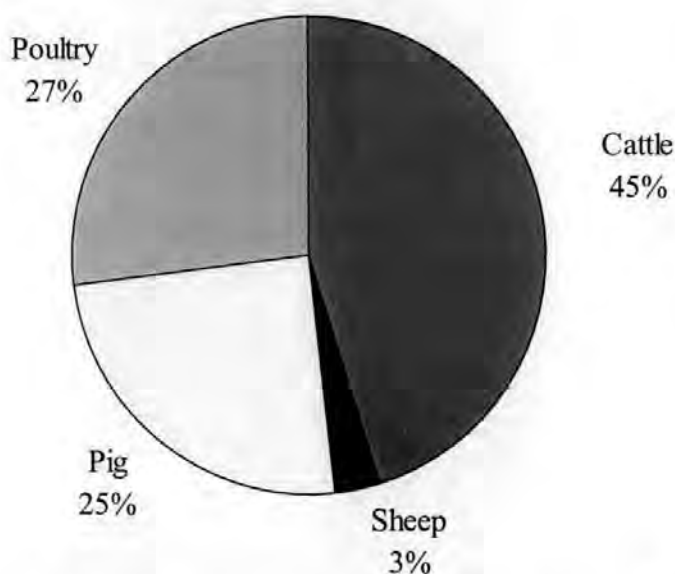
Figure 1.1:   The distribution of NH_3 emissions from different types of housed livestock in the UK. Based on data from Pain *et al.* (1998).

Field measurements conducted by Demmers *et al.* (1998) derived a typical winter emission factor of 300 µg NH_3-N s^{-1} (500 kg liveweight)$^{-1}$ for cattle housed in naturally ventilated buildings with a slurry waste management system and 186 µg NH_3-N s^{-1} (500 kg liveweight)$^{-1}$ for housed cattle with straw based systems. The reduction in housing emission from straw based systems is likely to be due to the absorption of NH_3 by the straw, reducing the area over which emissions can occur (Voorburg and Kroodsma, 1992). Hartung and Phillips (1994) suggested that the reduction in housing NH_3 emissions from straw based systems would be offset by higher land spreading losses from the high dry matter content manures and also by volatilisation from liquors produced by the manure.

Other field measurements conducted by Phillips *et al.* (1998) estimated a typical emission factor of 57 µg NH_3-N s^{-1} (500 kg liveweight)$^{-1}$ for housed cattle with a slurry collection system. The disparity between the estimates of Phillips *et al.* (1998) and Demmers *et al.* (1998) was hypothesised by Phillips *et al.* (1998) to be due to the use of different measurement techniques and differences in livestock husbandry. Theoretical calculations by Sutton *et al.* (1995) predicted emissions of NH_3 from housed livestock, based on an estimated N excretion of 33 kg N animal^{-1} a^{-1} and from an inferred volatilisation of 15 % of the excreted N. Their calculations were in good agreement with the emission estimate of

Demmers *et al.* (1998) suggesting an emission factor of 279 μg NH_3-N s^{-1} (500 kg liveweight)$^{-1}$.

Phillips *et al.* (1998) also measured NH_3 emissions during summer periods, when dairy cows are housed for 4 hours per day for milking, estimating an emission factor of 32 μg NH_3-N s^{-1} (500 kg liveweight)$^{-1}$. Phillips *et al.* (1998) noted that NH_3 emissions from housed cattle are included in the emission inventories compiled by Pain *et al.* (1998) and Sutton *et al.* (1995) without consideration of summertime emissions. The inclusion of summertime housing emissions in such inventories was shown by Phillips *et al.* (1998) to increase total agricultural NH_3-N emissions by approximately 9 %.

Research conducted in Holland by Swierstra *et al.* (1995) estimated NH_3 emissions of approximately 7 mg NH_3-N s^{-1} for 10 cattle housed on slatted floors over slurry collection tanks. Assuming a typical dairy cow weighs 550 kg (based on assumptions made by Pain *et al.*, 1998), these values can be rescaled for comparison with Demmers *et al.* (1998) and Phillips *et al.* (1998) to give a value of 624 μg NH_3-N s^{-1} (500 kg liveweight)$^{-1}$. The higher emissions measured in the aforementioned Dutch study should however be treated as the loss from the housing and manure storage combined and as such are unsurprisingly higher than the emissions measured in the UK.

Although housing and manure storage have long been recognised as sources of atmospheric NH_3, emissions from working dairy farms are unlikely to be so well delimited due to the movement of animals around the farm. Research conducted by Misselbrook *et al.* (1998) investigated the emissions of NH_3 from dairy farm collecting yards, areas where cows are held prior to milking. An annual average emission factor of 87 μg NH_3-N s^{-1} (500 kg liveweight)$^{-1}$ was calculated which would increase the overall emissions from dairy cows as calculated by Pain *et al.* (1998) by 11 %.

Field measurements of NH_3 emissions from other types of housed livestock are poorly represented in the literature. Typical emissions of 220 μg NH_3-N s^{-1} (500 kg liveweight)$^{-1}$ were measured from weaned pigs in Slovenia by Amon *et al.* (1995) whilst Pain *et al.*, (1998) cite, from unpublished research conducted by SRI, emission factors for pigs shown in Table 1.1. Clearly, the variability between these two studies is high though the results are broadly similar.

1.2.3.3   NH₃ volatilisation from grazing livestock

Field experiments conducted by Ryden and McNeill (1984) estimated that 24 % of the urea-N excreted by grazing steers volatilised as NH_3-N. Emission fluxes ranged between $0.3 - 3.9$ µg NH_3-N m^{-2} s^{-1} with the maximum fluxes occurring during warm mid-afternoon periods and the minimum fluxes occurring during overnight periods or following rainfall.

Animal Type	Flooring	
	Slatted	Straw
Dry Sows	197	108
Farrowing Sows	375	206
Boars	-	278
Fatteners: >110 kg	625	628
20-110 kg	625	628
Rearing: 0-20 kg	403	108

Table 1.1: NH_3 emission factors, in µg NH_3-N s^{-1} (500 kg liveweight)$^{-1}$, for various types of pigs from Pain *et al.* (1998).

These results compare with similar measurements made by Jarvis *et al.* (1989), showing peak emission fluxes of 2.6 µg NH_3-N m^{-2} s^{-1} and annual fluxes ranging from $1.0 - 26.7$ kg N ha^{-1}. Jarvis *et al.* (1989) demonstrated that the emission flux from grazing cattle was positively correlated with the N input to the pasture, and that higher emission fluxes were measured during rotational grazing. An emission factor for grazing cattle of 63 µg NH_3-N s^{-1} (500 kg liveweight)$^{-1}$ was calculated by Pain *et al.* (1998) assuming a typical annual N input of 174 kg N ha^{-1}.

Emissions of NH_3 from pastures grazed by sheep in Australia were estimated by Denmead *et al.* (1974). Average fluxes of 0.3 µg NH_3-N m^{-2} s^{-1} were measured with peak emissions, of 0.8 µg NH_3-N m^{-2} s^{-1}, occurring during midday periods. Emissions reduced to 0.2 µg NH_3-N m^{-2} s^{-1} during overnight periods. The N losses measured by Denmead *et al.* (1974) accounted for 27 % of the excreted urea-N. Much lower losses were reported by Jarvis *et al.* (1991) with annual average emission fluxes ranging from $1.6 - 30.6$ ng NH_3-N m^{-2} s^{-1}. Such emission fluxes were estimated to account for between 0.5 and 2.4 % of the N cycled through dung and urine. Jarvis *et al.* (1991) suggested that the lower percentage emission fluxes from sheep, when compared with the measurements by Ryden and McNeill (1984) and Jarvis *et al.* (1989), were related to species differences, the rotational grazing of cattle and differences in the exchange of gaseous NH_3 with the grazed swards.

1.2.3.4   NH₃ volatilisation from fertilised agricultural land

Emissions of NH_3 from fertilised agricultural land can occur from both the soil and vegetated canopy (Denmead *et al.*, 1976; Schjoerring *et al.*, 1993a; Sutton *et al.*, 1993c). Volatilisation of NH_3 from soil can result in a loss of 23 % of the N applied when spreading urea fertilisers onto grasslands (Pain *et al.*, 1998). Other fertiliser types result in lower percentage emissions in the order of $(NH_4)_2SO_4$, NH_4NO_3, NH_4PO_3 (Jarvis and Pain, 1990). In the inventory compiled by Pain *et al.* (1998), 1.6 % of fertiliser N applied to grassland was estimated to be emitted to the atmosphere as NH_3. Urea fertilisers have a higher capacity to emit NH_3 as urea hydrolysis does not result in the formation of H^+, as occurs from the oxidation of NH_4^+ to NH_3, Equation 1.2. The localised increase in pH following urea hydrolysis reduces the solubility of NH_3 in solution and thus promotes volatilisation. Harper *et al.* (1983) found that long-term trends in NH_3 emissions following urea fertiliser applications were not correlated with the NH_4^+ concentration in the soil, but with factors that increase the activity of urease. From this, they concluded that the rate of conversion of NH_4^+ to NH_3 was much smaller than the rate of conversion of urea to NH_3.

Net NH_3 emission from vegetation following the application of fertilisers have been measured in several studies (Harper and Sharpe, 1995; Schjoerring *et al.*, 1993a; Sutton *et al.*, 1993c; Yamulki *et al.*, 1996), with a typical diurnal pattern of emission through stomata occurring during daytime and deposition of NH_3 to leaf surfaces occurring overnight. Volatilisation of NH_3 from fertilised vegetation tends to only account for a small proportion of the fertiliser applied, 1.5 - 5.0 % (Sutton *et al.*, 1995).

In addition to stomatal emission of NH_3, senescing vegetation also can be a minor source of NH_3 (Farquhar *et al.*, 1979; Harper *et al.*, 1987; Whitehead and Lockyer, 1989). Estimates by Whitehead and Lockyer (1989) suggest that 10 % of the N in high N status decomposing grass could volatilise as NH_3, though negligible losses were measured from plants with a lower N status. A further pathway for NH_3 emission from fertilised grassland was identified by Sutton *et al.* (1997a) who measured NH_3 emission fluxes of up to 0.3 µg NH_3-N $m^{-2} s^{-1}$ over recently cut grassland.

1.2.4   Current estimates of UK NH₃ emissions

National NH_3 emission inventories have been compiled by many EU countries as part of the European Monitoring and Evaluation Project (EMEP), a multinational project responsible for monitoring and evaluating transboundary air pollutants. The "official" UK NH_3 emissions inventory submitted to EMEP was compiled by the UK Department of the

Environment (DoE), now the Department of Environment, Transport and the Regions (DETR) (DoE, 1995). This emission inventory estimated that during 1993, 260 kt of NH_3-N were emitted from agriculture in the UK. This compares with estimates for the same year of 197 kt of NH_3-N by Pain *et al.* (1998) and 370 kt NH_3-N by Sutton *et al.* (1995). An analysis of the different components that make up these inventories is given in Table 1.2.

As large uncertainties were found in the emission factors discussed in the previous sections, it is not surprising that the inventories, presented in Table 1.2, show a broad range of values. The largest difference between the emissions quoted in Pain *et al.* (1998) and Sutton *et al.* (1995) was for cattle. The reason for this difference becomes apparent when the level of detail used to compile the inventories is investigated. Sutton *et al.* (1995) applied an emission factor of 17 kg NH_3-N animal^{-1} a^{-1}, based on an "average cattle" to the 11.9 million cattle in the UK. Whilst, Pain *et al.* (1998) subdivided the UK cattle into 10 animal types (28 % of which were dairy cows) and applied emission factors to each animal type so including the effects of differing management practices.

Source	DoE (1995)	Pain *et al.* (1998)	Sutton *et al.* (1995)
Cattle	130	98.7	199
Pigs	25	23.6	34
Sheep	15	12.7	36
Poultry	25	30.2	29
Fertilisers and crops	30	32.1	28
Other farm animals	-	0.02	6
Agro-industry	-	-	1.3
Non-agricultural	35	-	36
Total	260	197.32	369.3

Table 1.2: NH_3-N (kt N) emissions from the UK for 1993.

ApSimon *et al.* (1987) calculated that large increases in UK agricultural NH_3 emissions occurred during the 1950s, with an estimated 36 % increase in emissions occurring between 1950 and 1960 and a 55 % increase in emissions occurring between 1950 and 1980. Annual NH_3 emissions during the later part of the 20th century were estimated to be reasonably constant by Dragosits *et al.* (1998) with emissions estimates of 234.5 kt NH_3-N and 232.9 kt NH_3-N calculated for 1988 and 1996 respectively.

Dragosits *et al.* (1998) estimated the annual averaged distribution of NH_3 emissions on a 5 km grid across the UK. The results showed that emissions were highest in Devon, East Anglia and the Midlands and lowest in the Highlands of Scotland. Historical trends in the geographical distribution of NH_3 emission sources were investigated by Dragosits *et al.* (1996) based on data from 1969 and 1988. Their results showed that only a slight increase had occurred in the magnitude of NH_3 emissions between these years, consistent with the findings of ApSimon *et al.* (1987). However, a very different spatial distribution of sources was observed, with NH_3 emissions in 1988 being more spatially heterogeneous than those in 1969. This reflects the reduced land area required by modern intensive agricultural management practices.

1.3 TRANSPORT OF NH_X IN THE ATMOSPHERE

The atmospheric transport of NH_3 can be partitioned into three separate phases: short-range transport and deposition, chemical reaction of NH_3 with acid gases and formation NH_4^+ particulates, and the long range transport and deposition of NH_4^+ particulates. This section reviews the literature on each of these topics.

1.3.1 Short-range transport and deposition of NH_3

Gaseous NH_3, being chemically reactive and highly soluble, has an estimated residence time in the atmosphere of 0.8 days (Moller and Schieferdecker, 1985). Losses of NH_3 from the atmosphere occur due to dry and wet deposition and chemical reactions with atmospheric acids to form particulate NH_4^+. Chemical reactions deplete NH_3 plumes by approximately 30 % per hour (Asman, 1998). Thus, significant reductions in the quantity of NH_3 in the atmosphere resulting from chemical conversions are typically only found at distances of several tens of kilometres from a source. This suggests that the removal of NH_3 from the atmosphere close to a source is dependent on deposition processes.

Asman *et al.* (1989) investigated the variation in air concentrations over a nature reserve, close to a strongly emitting agricultural area, using numerical modelling and field measurements. Air concentrations were found to reduce exponentially with distance from the source with higher air concentrations and shallower horizontal concentration gradients being observed during overnight periods. This was due to the suppression of vertical mixing in the atmosphere caused by the formation of a low-level inversion layer and due to reduced turbulence. Further modelling studies were conducted by Asman (1998) on the short-range atmospheric dispersion and dry deposition of NH_3 from agricultural sources. The model predictions of dry deposition at rates limited by turbulence and molecular

diffusion demonstrated that approximately 50 % of emitted NH_3 could be retained within 2 km from a source. Deposition was predicted to be more localised over well fertilised agricultural land, with most deposition occurring between 0 - 450 m and 0 - 1450 m of a source depending on the magnitude of the emission and the canopy compensation point.

Large scale field experiments and numerical modelling of NH_3 dispersion and deposition from slurry spreading were conducted as part of the ADEPT Project (Sutton *et al.*, 1997a; Sutton *et al.*, 1998b). These experiments measured an NH_3 compensation point of 41 µg NH_3-N m^{-3} over intensively managed cropped grassland downwind of a line source of slurry. Such a high compensation point resulted in the downwind grassland acting as a source for atmospheric NH_3, with deposition only occurring within a few tens of metres of the source, a region where surface air concentrations exceeded the compensation point.

The surface-atmosphere exchange of NH_3 over wheat stubble downwind of forced ventilated poultry buildings was investigated by Sutton *et al.* (1997b). Bi-directional NH_3 exchanges in the range –33 to +33 ng NH_3-N m^{-2} s^{-1} were observed, which were hypothesised to be driven by a soil compensation point. Emission fluxes (denoted by a positive sign) were measured during the daytime, whilst deposition fluxes (denoted by a negative sign) were typically measured overnight. Overall Sutton *et al.* (1997b) estimated that the stubble field downwind of the building was a net source of atmospheric NH_3 with a time averaged flux of +16.5 ng NH_3-N m^{-2} s^{-1}. Overnight deposition to the field was not found to significantly affect the net emissions from the area.

The long-term averaged deposition of NH_3 to woodland surrounding a poultry farm was investigated by Fowler *et al.* (1998b). They estimated deposition fluxes of 250 ng NH_3-N m^{-2} s^{-1} occurred at 15 m downwind of the building with an exponential decrease in fluxes with distance to 16 ng NH_3-N m^{-2} s^{-1} by 276 m downwind. Local deposition was estimated by Fowler *et al.* (1998b) to result in 3.2 % of the 4800 kg NH_3-N that were annually released to the atmosphere from the site being redeposited within 300 m of the source. However, Fowler *et al.* (1998b) noted that their results were sensitive to the parameterisation of dry deposition, based on bi-directional exchange measurements over a blanket bog "Auchencorth Moss". The results from Auchencorth Moss (concentration range 0.1 - 2.0 µg NH_3 m^{-3}) required a significant extrapolation to provide fluxes in the woodland (concentration range 1.6 - 42.0 µg NH_3 m^{-3}). Fowler *et al.* (1998b) noted that this uncertainty could result in up to 15 % of the source term being deposited as NH_3.

Measurements of NH_3 air concentrations and deposition fluxes around a dairy farm have been made by Sommer (1988). Ground level NH_3 air concentrations were found by Sommer (1988) to be significantly above background level within 300 m of the source. Deposition fluxes measured around the farm were significantly higher than background with an estimated annual average deposition flux, within 100 m to 200 m of the building, of 160 ng NH_3-N m^{-2} s^{-1}. Similar research conducted by Sommer and Jensen (1991) showed that fluxes remained constant at 0.75 µg NH_3-N m^{-2} s^{-1} across a distance of 40 m from a dairy building despite the reduction in NH_3 concentration over this distance from 90 µg NH_3-N m^{-3} to 45 µg NH_3-N m^{-3}. Sutton *et al.* (1993d) performed a recalculation of these data to derive a deposition velocity (V_d) that increased from 2.5 mm s^{-1} to 40 mm s^{-1} within 100 m of the farm. Sutton *et al.* (1993d) speculated that the lower deposition velocity measured close to the building was due to the saturation of the leaf surface sink for NH_3. Sommer and Jensen (1991) also noted this relationship in their data though they expressed some concern that this may have been an experimental artefact due to complex wind field that occurred near the farm building.

Ineson *et al.* (1998) estimated the deposition of NH_x to two woodlands within 1.0 km of an intensive pig farm. They estimated annual averaged NH_x-N deposition fluxes of 94 ng NH_x-N m^{-2} s^{-1} and 282 ng NH_x-N m^{-2} s^{-1} using throughfall and rainfall sampling (further details of this method can be found in Chapter 2, Section 2.3.2). Higher deposition was measured to the woodland to the east of the farm, in the prevailing wind direction. The deposition of NH_x-N in rainfall was found to be consistent between the two sites, despite the large difference in total deposition. This suggests that dry deposition of NH_3 was the dominant deposition pathway and that NH_x deposited in rainfall was likely to have been derived from more distant sources.

Measurements of air concentrations and wet deposition of NH_x close to a naturally ventilated farm building have been made by Couling (1997). Elevated NH_x concentrations were measured in rainwater up to 100 m from the building, though significant variability was found between rainfall events, with highest concentrations of NH_x in rainfall occurring during drizzle.

Deposition of NH_3 close to the source of emission may have beneficial effects, where deposition occurs onto agricultural land, due to increased agricultural production caused by the fertilisation effects of NH_3. For example, Cowling and Lockyer (1981) found a 30 % increase in shoot dry weight in plants exposed to 453 µg NH_3-N m^{-3} over 26 days.

However high rates of local deposition of NH_3 onto natural or semi-natural land close to a source may pose a significant risk of pollution. Research conducted by Pitcairn *et al.* (1998) has shown that species composition was adversely affected within 300 m of an intensive poultry farm, and that visible damage (needle loss and yellowing) occurred at sites close to the building. Ineson *et al.* (1998) have also shown that high rates of local NH_3 deposition to woodlands can result in enhanced emissions of N_2O, a gas that is thought to be responsible for 6 % of predicted climate change (IPCC, 1992). The effects of NH_3 on vegetation are considered in more detail later in this chapter.

1.3.2   Chemical conversion of gaseous NH_3 to particulate NH_4^+

Due to the very different behaviour of NH_3 gas and NH_4^+ aerosol in the atmosphere, the long-range transport of N emitted as NH_3 is a function of the rate of chemical conversion between these species. Several reaction schemes have been developed to include atmospheric chemistry in long range atmospheric dispersion models, though most are based on, or share components of, the EMEP chemistry scheme (EMEP, 1996) shown as Equation 1.3.
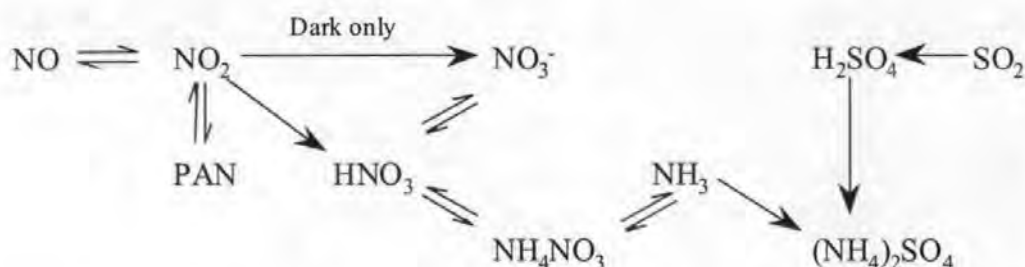
Equation 1.3: Reaction scheme for the production of NH_4^+-N aerosol from the reduction of NH_3 by HNO_3 and H_2SO_4, from EMEP (1996).

The EMEP chemistry scheme, shown in Equation 1.3, illustrates the formation of nitric and sulphuric acids in the atmosphere from emissions of NO_x and SO_2 and the subsequent reaction of these atmospheric acids with NH_3. Of these two processes, the reaction of NH_3 with sulphuric acid is irreversible, whilst the reaction of NH_3 with nitric acid is reversible with the reaction rate, and direction, being a function of the vapour pressure of nitric acid in the gas phase, determined by the ambient temperature and relative humidity (Allen *et al.*, 1989). The reaction of NH_3 with H_2SO_4 has been shown by ApSimon *et al.* (1994) to be the more significant pathway for the formation of particulate NH_4^+-N.

The reaction of NH_3 with acid gases causes the formation of opposing vertical gradients of gaseous NH_3 and particulate NH_4^+ concentrations in the atmosphere (ApSimon *et al.*,

1987), as shown in Figure 1.2. The formation of such vertical gradients can cause gas to particle conversion to be limited by the availability of atmospheric acids close to the surface, whilst close to the top of the atmospheric "mixing" layer, formation of NH_4^+ may be limited by the availability of NH_3 (ApSimon *et al.*, 1994). From these considerations it is clear that the transport of NH_x in the atmosphere is also dependent on the time lag between the merging of the rural NH_3 plume with urban or industrial H_2SO_4 plumes.
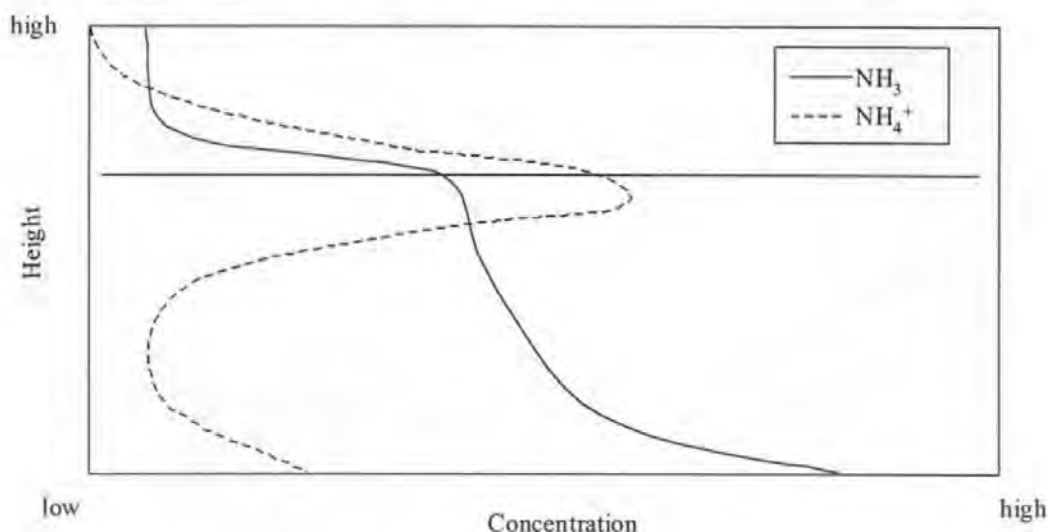
Figure 1.2:   Vertical concentration profiles of NH_3 and NH_4^+ in the atmosphere, based on ApSimon *et al.* (1987). The horizontal line shows the cloudbase.

Estimates have been made by Erisman *et al.* (1988) of the typical rates of conversion between NH_3 and NH_4^+ in the atmosphere from measurements of vertical concentration gradients, such as those shown in Figure 1.2. Erisman *et al.* (1988) simplified the complicated atmospheric chemistry by assuming that formation of NH_4^+ from NH_3 could be described by a single irreversible reaction and calculated the reaction constant to be 1.0 x 10^{-4} s^{-1} for daytime and 5.0 x 10^{-5} s^{-1} overnight. The difference between these reaction constants was thought to be due to the formation of overnight inversion layers restricting the mixing of acid gases (which were fairly evenly distributed in the atmosphere) with NH_3 (which was retained close to the surface). Other estimates of the rate of conversion of NH_3 to NH_4^+ have been made by Asman and Janssen (1987) of 8 x 10^{-5} s^{-1} based on fitting long-range atmospheric dispersion model predictions of concentrations to field measurements.

The atmospheric half-life of NH_3 can be calculated from the aforementioned estimates of the rate of conversion of NH_3 to NH_4^+ in the atmosphere, data are shown in Table 1.3. By assuming a wind speed of 1 m s^{-1} for overnight periods and 5 m s^{-1} for daytime periods and using the reaction constants calculated by Erisman *et al.* (1988), the distance at which 50

18

% of the NH_3 in the atmosphere would be converted to NH_4^+ can be calculated as 35 km for daytime and 14 km overnight. Using the above criteria chemical conversion can be calculated to have caused a 5 % reduction in NH_3 concentrations within 1 km of a source during overnight periods and a 2 % reduction during daytime.

Reference	Period	Reaction constant	Atmospheric half life	
		(s^{-1})	(s)	(hours)
Erisman *et al.* (1988)	Daytime	1.00E-04	6932	1.93
	Overnight	5.00E-05	13863	3.85
Asman and Janssen (1987)	All	8.00E-05	8664	2.41

Table 1.3: Calculation of the atmospheric chemical half-life of gaseous NH_3 from literature values of the rate constant for the formation of NH_4^+ from NH_3.

1.3.3 Long-range transport of NH_4^+

Following the previous section, it is apparent that when considering long-range atmospheric transport, over distances of several hundred kilometres, that the majority of reduced N is transported in the form of NH_4^+. As the mixing layer of the atmosphere is capped by a temperature inversion, effectively trapping material in a layer between 1 km and a few hundred metres deep, most material released into the atmosphere will either accumulate, or will be removed by deposition processes. The long-range atmospheric transport of NH_4^+ is therefore dependent on the prevailing meteorology and the time lag between emission and the NH_4^+ plume encountering rainfall and being washed out.

The influence of meteorological conditions on the long-range transport of NH_x is well illustrated by ApSimon *et al.* (1994). Their research is summarised in this review as a case study. ApSimon *et al.* (1994) used a multi-layer Lagrangian atmospheric dispersion model (Transport over Europe of Reduced Nitrogen, TERN) to investigate several days when extremely high measurements of NH_4^+ in rainwater were made at the EMEP monitoring station, Stoke Ferry. The atmospheric conditions at the time were dominated by an anti-cyclone moving south-east over the Norwegian Sea, the trajectories which advected air to Stoke Ferry are shown in Figure 1.3.

The path which the trajectories followed were the major cause of the high deposition measurements, with the first trajectories passing over the North Sea and bringing air with a relatively low NH_4^+ content. Later trajectories passed over the highest sulphur emitting region in Europe, "The Black Triangle", and then over the Netherlands where large emissions of NH_3 occurred. This combination of trajectories and low wind speeds ensured

that the air column contained high concentrations of particulate NH_4^+. The convective showers that the air column encountered on arrival at Stoke Ferry led to the high rate of wet deposition observed.
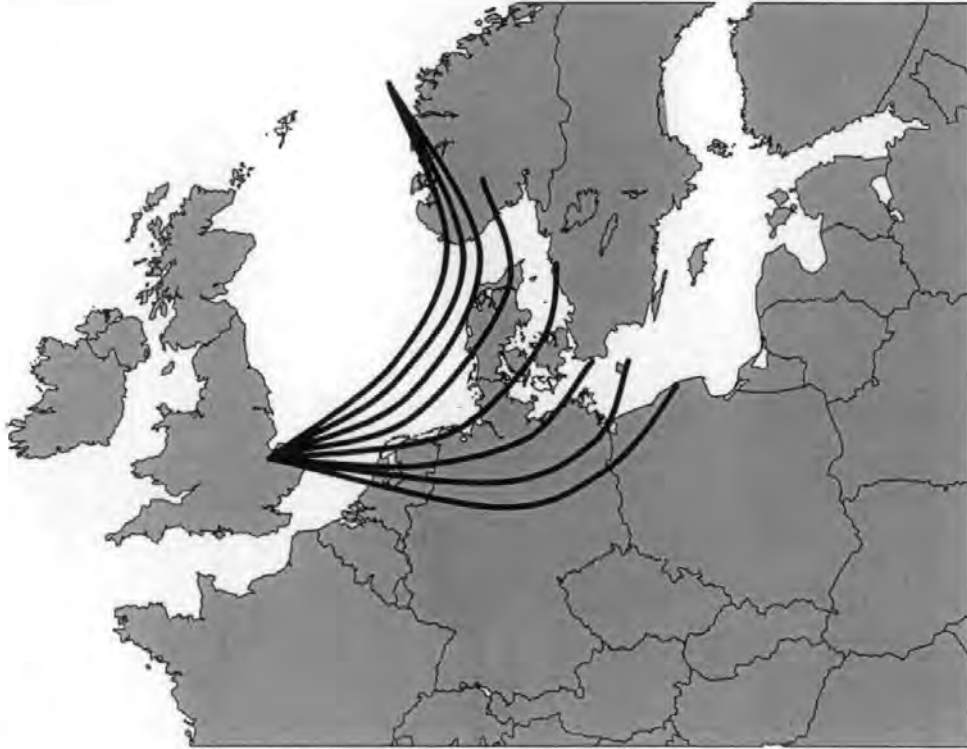
Figure 1.3:   Trajectories arriving at Stoke Ferry at 3 hourly intervals between 12:00 on 21/06/83 and 09:00 on 22/06/83. Reproduced from ApSimon *et al.* (1994).

Singles *et al.* (1988) used a modification of the TERN model, Fine Resolution Ammonia Exchange (FRAME), to calculate budgets of NH_3 emission and deposition in the UK. Similar to the conclusions of ApSimon *et al.* (1994), the wind directions which resulted in the highest net export of NH_3 from the UK were from the south-west, where NH_3-rich air formed from the high emission areas in the west and south-west of the UK, passed over the Midlands and northern England, regions that are the principal areas of NO_x and SO_x production, resulting in the formation of slow depositing particulates. Conversely, a low net export of NH_x-N was found for winds from the south to south-east, where the air column was advected over Scotland, resulting in efficient wet deposition. Overall, Singles *et al.* (1998) estimated that the UK was a net exporter of NH_3, though 66 % of NH_3 emitted in, and imported into, the UK was estimated to deposit within the national boundary.

The EMEP programme (EMEP, 1997) estimated that 80 % of the NH_3 emitted from UK sources was re-deposited within the national boundary with the remainder being deposited onto the neighbouring countries, particularly Ireland, Norway and Iceland, see Figure 1.4.

The large contribution of UK emissions to deposition over Norway and Iceland reflect the low NH_3 emission rates from these countries (Norway: 25 kt a^{-1}; Iceland: 3 kt a^{-1}). The reducing gradient in percentage contribution of UK emissions to total deposition in the Nordic countries, shown in Figure 1.4, demonstrates that the long-range transport of NH_x is restricted to around 2 - 4 Mm from the source. These values are close to the 1.5 - 3 Mm estimated by Hov and Hjollo (1994). Indeed, Galperin and Sofiev (1998) used a large area Northern Hemisphere model to predict transport of NH_x-N, finding that Russia, the USA, Canada and Europe were largely self-polluting.

Percentage of national NH_x depositions arising from UK emissions

- 0
- 1
- 2
- 3
- 5
- 7
- 80
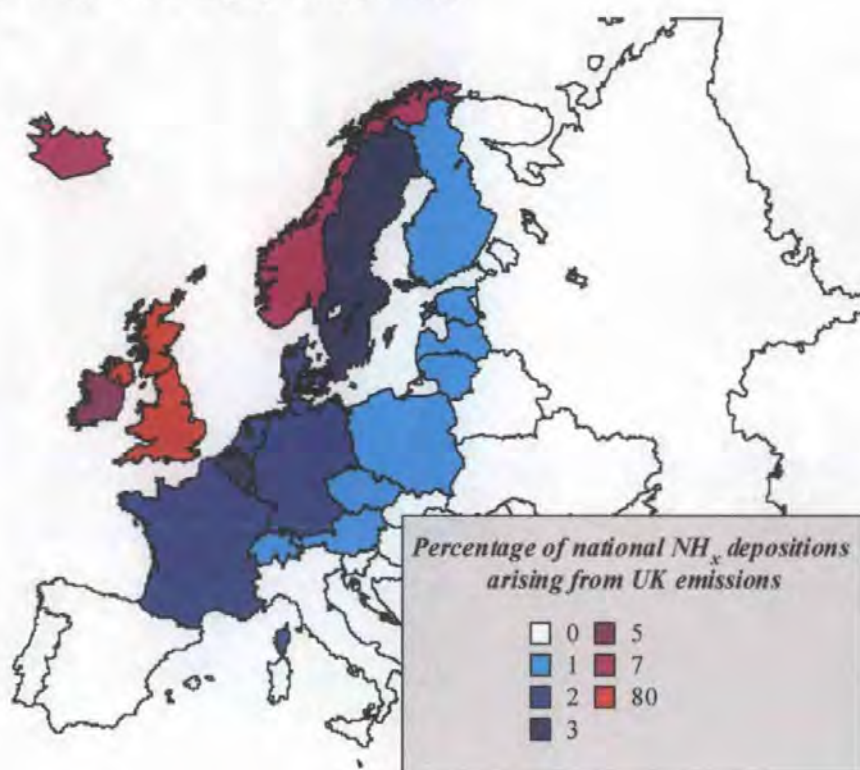
Figure 1.4: Deposition of NH_x in Europe originating from sources in the UK, shown as the percentage of deposition in each country that can be attributed to UK sources. Data were taken from EMEP (1997).

1.4   MECHANISMS OF NH_x DEPOSITION

From the previous sections of this chapter, it is clear that deposition is a critical process when investigating the fate of NH_3 released to the atmosphere. Research into the processes that remove NH_x from the atmosphere is reviewed in this section.

1.4.1   Dry deposition of gaseous NH_3

The dry deposition flux of a gas is often treated as being analogous to electric current in a circuit as described by Ohm's law. The deposition flux of NH_3 (F_{NH3-N}) can be expressed as a function of the air concentration, $\chi\{z-d\}$, at a reference height (z) above the zero plane

displacement height (d) and the cumulative resistance to transport between the reference height and the surface, R_t. A term often used when assessing gaseous deposition is the deposition velocity (V_d), defined in Equation 1.4.

$$V_d\{z-d\} = \frac{1}{R_t\{z-d\}} = \frac{F_{NH3}}{\chi\{z-d\}}$$

Equation 1.4

Several resistance models have been developed to parameterise R_t for interpreting field studies (*e.g.* Sutton *et al.*, 1993a; Sutton *et al.*, 1993b) and for including dry deposition in atmospheric dispersion models (*e.g.* Asman and Van Jaarsveld, 1992; EMEP, 1996; Russell *et al.*, 1993; Singles *et al.*, 1998). These resistance models share a common treatment of the transport of NH_3 between the atmosphere and the lower bound of the quasi-laminar sub-layer, as two resistances in series. These resistances are the atmospheric resistance (R_a), which is the turbulent resistance to vertical transport in the atmosphere, and the boundary layer resistance (R_b), which occurs due to small-scale turbulence and molecular diffusion between the roughness height and the surface. The combined resistance generated by R_a and R_b is dependent on both wind speed and surface roughness, thus deposition limited by these processes is more rapid during periods with high wind speeds and over surfaces with high roughness elements (such as forests).

Differences in the resistance modelling of NH_3 dry deposition tend to occur when parameterising the transfer between the lower bound of the surface quasi-laminar sub-layer and the site of deposition. The simplest scheme, shown in Figure 1.5, that is followed by EMEP (1996), Russell *et al.* (1993), and Asman and Van Jaarsveld (1992), is to treat the processes as following a single irreversible pathway, defined by a single fixed surface resistance (R_c). This, of course, is only applicable to surfaces where an *a priori* assumption of uni-directional fluxes can be made.

Field measurements have shown that surface resistances are strongly dependant on land use type with low values of R_c being measured over unfertilised semi-natural areas (*e.g.* Bobbink *et al.*, 1992; Duyzer, 1994; Duyzer *et al.*, 1992; Duyzer *et al.*, 1994; Sutton *et al.*, 1992; Sutton *et al.*, 1993b; Wyres *et al.*, 1992a) whilst measurements over agricultural cropland show that the surface may act as both a source and a sink for atmospheric NH_3 (*e.g.* Denmead *et al.*, 1978; Harper and Sharpe, 1995; Sutton *et al.*, 1993c). A further limitation to the usefulness of the constant R_c approach is that R_c can show a substantial diurnal variation due to its dependence on meteorological conditions, particularly temperature, relative humidity and dewfall (*e.g.* Duyzer *et al.*, 1994; Sutton *et al.*, 1993a; Sutton *et al.*, 1993b; Yamulki *et al.*, 1996).
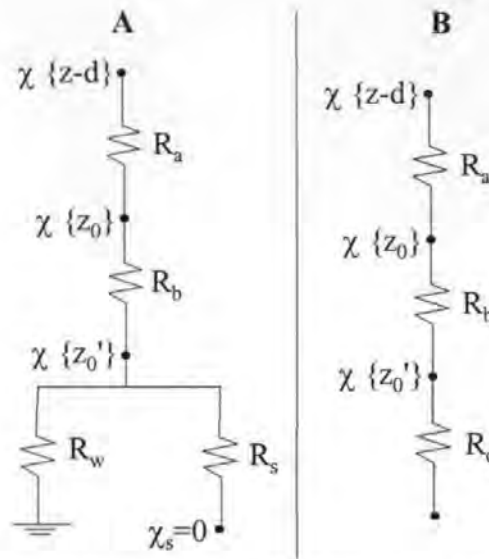
Figure 1.5:   Resistance models for NH_3 deposition. **A**: bi-directional resistance model for NH_3 deposition from Sutton *et al.* (1993a); **B**: simple uni-directional approach used in EMEP (1996). R_a: atmospheric resistance, R_b: boundary layer resistance, R_c: surface resistance, R_w: leaf surface resistance (water and waxes), R_s: stomatal resistance.

Sutton *et al.* (1993a) developed a more realistic bi-directional approach to describe the dry deposition of NH_3, shown alongside the simple approach outlined above in Figure 1.5. This approach treats deposition to the leaf surfaces and to stomata as parallel resistances, drawing NH_3 from the atmosphere *via* a canopy level air concentration, $\chi \{z_0'\}$. The mechanisms and controls of NH_3 deposition to leaf surfaces and stomata are discussed in the following sections.

1.4.1.1   Deposition of gaseous NH_3 to leaf surfaces

Field measurements of the dry deposition of NH_3 at rates higher than permissible by stomatal resistance (R_s) are summarised in Table 1.4. These measurements were made over agricultural land, upland areas and forests. Stomatal resistances for agricultural areas and forests have been estimated to be close to 60 s m^{-1} during mid-summer periods with strong insolation and surface temperatures close to 20 °C (Wesley, 1989). Stomatal resistance becomes higher during periods with extremes of temperature, low insolation or when the vegetation is dormant. The data presented in Table 1.4 demonstrate that much lower values of R_c are reported than are permissible by R_s. Sutton *et al.* (1993b) hypothesised that such high deposition rates occurred due to surface adsorption resulting from co-deposition of NH_3 with atmospheric acids or deposition to thin water films.

Reference	χ_{NH3-N} ($\mu g\ m^{-3}$)	Exchange parameters	Notes
Andersen *et al.* (1993)	0 - 4.2	V_d (mean) = 26 mm s^{-1}, V_d (max) = 20 cm s^{-1} Highest V_d during daytime, $V_d \propto$ friction velocity (u_*).	FGM, forest
Dabney and Bouldin (1990)	0 – 5.8	V_d (median) = 8.4 mm s^{-1} V_d (max)= 100 mm s^{-1}. 50 of 63 runs were emis.	FGM, Alfalfa crop
Denmead *et al.* (1976)	1.0 - 13.5	R_c = 18 – 31 s m^{-1}, R_s = 180 – 310 s m^{-1}. Emis. from ground dep. to canopy.	FGM, grazed pasture
Denmead *et al.* (1978)	1.3 – 8.2	Emis. during wet conditions, dep. during dry conditions. R_c= 0.2 – 0.5 s m^{-1}.	FGM fertilised corn
Draaijers *et al.* (1989)	4.8 & 8.7	V_d (mean)= 27 mm s^{-1}	TSM, forest
Duyzer (1994)	2.0 – 9.0	R_c (median) = 15 – 75 s m^{-1} V_d (median)= 8 – 30 mm s^{-1}	FGM, heathland
Duyzer *et al.* (1992)	0.8 - 22.3	R_c= 0 - 4 s m^{-1}, no diurnal variation in R_c observed V_d (mean) = 36 mm s^{-1}.	FGM, forest
Duyzer *et al.* (1994)	0.8- 22.3	V_d (maximum) = 100 mm s^{-1}, V_d (mean) = 20 mm s^{-1} R_c =0 (wet conditions) $R_c \propto R_s$ (dry conditions).	FGM, forest
Erisman *et al.* (1994)	0 – 20.0	R_c= 15 s m^{-1}. High R_c during dry periods or in frozen conditions. Mean V_d = 8 mm s^{-1}.	FGM heathland
Erisman and Wyers (1993)	0 – 8	R_c= 14 s m^{-1}, high R_c related to wetness and relative humidity.	FGM heathland
Houdijk and Roelofs (1991)	N/A	Flux correlated with surface area of canopy.	TSM, forests
Sutton *et al.* (1992)	0.05 – 0.65	R_c= 2 – 53 s m^{-1}, higher values for frozen surfaces.	FGM, moorland
Sutton *et al.* (1993b)	0.1- 0.8	Mean R_c = 3 – 6 s m^{-1} R_c increased to 135 s m^{-1} over calcareous grassland.	FGM, moorland, forest, grassland.
Sutton *et al.* (1997c)	0 – 3.5	R_c= 5 – 27 s m^{-1} (typically) Emis. during dry periods with low NH$_3$ concentrations	FGM, upland
Wyers *et al.* (1992b)	<0.1 - >25	V_d (median) = 30 mm s^{-1}. High dep. overnight	FGM, forest.

Table 1.4: Summary of literature measurements finding deposition rates higher than permissible by stomatal resistance. Emis: emission; Dep: deposition; TSM: fluxes estimated using throughfall sampling measurements; FGM: fluxes estimated using the flux-gradient method.

Measurements of the electrical conductance of coniferous needles were used to infer water film presence and intensity by Burkhardt and Eiden (1994). These researchers correlated the presence of water films with rainfall and relative humidity, detecting water films at

relative humidities as low as 50 %. Analysis of isolated needles showed that the correlation between humidity and electrical conductance was dependent on the deposition of airborne particles, which reduced the saturation vapour pressure of air and provided a capillary framework bridged by condensed water droplets. Overall, Burkhardt and Eiden (1994) estimated that water films, between 1 - 50 nm in thickness, were formed for over 67 % of the time in the field.

The co-deposition of NH_3 with SO_2 to leaf surfaces has been found by Erisman and Wyres (1993), McLeod *et al.* (1990), Van Breemen *et al.* (1982) and Van Hove *et al.* (1989). This process is thought to result from the acid-base reaction of NH_3 and SO_2 in the water film on leaves reducing the liquid phase concentrations of each pollutant though the formation of $(NH_4)_2SO_4$ and so preserving a favourable surface-atmosphere concentration gradient. Measurements by Erisman and Wyers (1993) suggested that an optimum molar concentration ratio for co-deposition of NH_3 with SO_2 to wet leaf surfaces was 2:1 (NH_3-N: SO_2-S). Dry deposition rates were found to reduce following extended periods with high air concentrations of NH_3 or SO_2 due to the increased alkalinity in the case of NH_3 and increased acidity in the case of SO_2 of the surface water film. During periods of low relative humidity, Erisman and Wyres (1993) found that deposition rates correlated with stomatal resistances.

A further complication to the co-deposition process was identified by Sutton *et al.* (1993a) who found enhanced emission of NH_3 from a wheat canopy (*Triticum aestivum* L.) during periods of enhanced SO_2 concentrations. This was hypothesised to be caused by the depletion of NH_3 concentrations in the atmosphere through chemical reaction and the formation of particulate $(NH_4)_2SO_4$. This would act to reduce the NH_3 concentration below the compensation point ($\chi\{z_0'\}$ in Figure 1.5) and so promote the stomatal emission of NH_3.

Reduced rates of NH_3 deposition to leaf surfaces have also been correlated with high temperatures and light wind speeds by Duyzer *et al.* (1994) and with sub-zero temperatures by Erisman and Wyers (1993) and Sutton *et al.* (1992). Both these conditions would reduce the capacitance of the surface sink for NH_3 through the direct evaporation of water layers and through the formation of ice crystals, which laboratory studies have confirmed do not interact with atmospheric NH_3 (Iribarne and Pyshnov, 1990). The surface sink for NH_3 may also become saturated when plants are exposed to high ambient NH_3 concentrations over several hours (Sommer and Jensen, 1991; Van Hove *et al.*, 1989). The

rate of saturation of the surface sink was modelled by Sutton *et al.* (1998a) though the inclusion of addition terms in the bi-directional resistance model (shown in Figure 1.5) to allow for the charging of a surface sink with deposited material and for the subsequent cuticular uptake of NH_x.

1.4.1.2   *Stomatal exchange of gaseous NH₃*

Stomatal exchange of NH_3 has been hypothesised by Sutton *et al.* (1994) to occur as a parallel process alongside the dry deposition of NH_3 to leaf surfaces. The term "exchange" is often used when discussing the role of stomata as both emission and deposition can occur depending on the concentration gradient between the atmosphere and the sub-stomatal cavity (Farquhar *et al.*, 1980). If ambient NH_3 is in excess of this compensation point deposition occurs, whilst if ambient concentrations are less than this compensation point stomatal emission of NH_3 occurs.

A review of the literature on the exchange of NH_3 between plants and the atmosphere from chamber studies is presented in Table 1.5. These studies provide good evidence of the role of stomata as relative humidities are often artificially reduced by the experimentalists to prevent bias caused by NH_3 deposition to the chamber walls. The rates of NH_3 deposition measured in all studies, with the exception of the measurements by Artyomov *et al.* (1994), were similar to rates limited by stomatal resistances ($V_d <= 10$ mm s^{-1}). Furthermore, strong correlations were found by Artyomov *et al.* (1994) and Hutchinson *et al.* (1972) between NH_3 deposition and measurements of stomatal conductance and photosythetically active radiation (PAR).

The experiments reviewed in Table 1.5 show that deposition rates, limited by stomatal resistance, increase linearly with ambient concentrations in the range of 3 μg NH₃-N m^{-3} to 164 mg NH₃-N m^{-3}. The high sorption capabilities of agricultural cultivars were shown by Whitehead and Lockyer (1987) who found no evidence of toxicity following the exposure of Italian ryegrass (*Lolium multiflorum* Lam.) to 583 μg NH₃-N m^{-3} for 33 days. Artyomov *et al.* (1994) found that dry deposition rates were independent of concentrations between 660 μg NH₃-N m^{-3} and 165 mg NH₃-N m^{-3}, though plants exposed to 535 mg NH₃-N m^{-3} showed necrotic spots, an obvious toxic response.

Deposition rates have been observed in several studies not to be linearly related to air concentrations below 3 μg NH₃-N m^{-3}. However, due to difficulties in obtaining such low concentrations in chamber experiments, most of the compensation point estimates have

been determined from micrometeorological field experiments. A summary of compensation point estimates from the literature is shown in Table 1.6.

The compensation points listed in Table 1.6 can be seen to vary with land use type, such that very low compensation points are typically measured over natural vegetation and much higher values are recorded over fertilised vegetation. This is likely to result from the increased NH_3 concentrations in the apoplast of plants with higher tissue N concentrations caused by the addition of fertilisers. Lockyer and Whitehead (1986) found that plants with a high N status may have a reduced NH_3 uptake, whilst Schjoerring *et al.* (1993a) found canopy (stomatal) emissions increased from spring barley (*Hordeum vulgare* L.) exposed to high levels of N fertiliser.

Reference	Concentration (μg NH_3-N m^{-3})	Exchange parameters	Notes
Aneja *et al.* (1986)	36 – 350	$V_d = 3 - 12$ mm s^{-1}	Used agricultural species Higher V_d during daytime
Artyomov *et al.* (1994)	658 – 164k	$V_d = 2 - 84$ mm s^{-1} V_d independent of conc.	V_d dependent on PAR
Bruckner *et al.* (1993)	6 – 23	Deposition flux linear with concentration, low level of surface deposition reported (4 - 9% of total).	Higher deposition to low N fertilised plants Higher deposition to needles than twigs
Cowling and Lockyer (1981)	9 – 453	$V_d = 3 - 14$ mm s^{-1}	Used perennial ryegrass Higher deposition velocities found for higher yielding plants.
Farquhar *et al.* (1980)	0 – 28	Linear flux with concentrations above 3 μg NH_3-N m^{-3}. $V_d = 7$ mm s^{-1}	χ {z_o'} dependent on temp
Husted and Schjoerring (1995)	0 – 23	Linear flux with conc. above 2.7 μg NH_3-N m^{-3}. $V_d = 10$ mm s^{-1}	Higher deposition during daytime
Hutchinson *et al.* (1972)	20 – 36	$V_d = 2 - 6$ mm s^{-1}	Used agricultural species. NH_3 exchange rates followed same patterns as CO_2.
Whitehead and Lockyer (1987)	11 – 584	$V_d = 3.0 - 7.4$ mm s^{-1} (low nitrate fertilisation). $V_d = 2.4 - 4.6$ mm s^{-1} (high nitrate fertilisation).	Used Italian Ryegrass. Estimated that 15-20 % of plant N maybe derived from the atmosphere

Table 1.5:   Review of the data on stomatal NH_3 deposition from chamber studies.

Another factor that regulates the NH_3 compensation point of plants, is the ambient temperature. Farquhar *et al.* (1980) found that the compensation point of French bean (*Phaseolus vulgaris* L.) increased by a factor of two for a temperature change of 26 °C to 33 °C. This was thought to occur due to higher rates of volatilisation within stomata caused by the temperature dependence of the volatilisation process.

Compensation point $\mu g\ NH_3$-N m^{-3}	Land use	Author
1.2	Intensive grassland	Dabney and Bouldin (1990)
<1	Heathland	Duyzer (1994)
0.3	Forest (Douglas fir, *Pseudotsuga menziesii*)	Duyzer *et al.* (1994)
1.4 – 3.0	Chamber (French bean, *Phaseolus vulgaris* L.)	Farquhar *et al.* (1980)
0 (winter) 0.16 (summer)	Moorland	Fowler *et al.* (1998c)
5.8 (daytime) 2.5 (dusk)	Corn crop	Harper and Sharpe (1995)
2.4 – 2.7	Chamber (barley)	Husted and Schjoerring (1995)
<0.06	Moorland	Sutton *et al.* (1992)
< 0.07	Natural vegetation	Sutton *et al.* (1993b)
1.6 – 5.8	Intensive grassland	Sutton *et al.* (1993c)
2.5 – 3.3	Arable land	Yamulki *et al.* (1996)

Table 1.6:   Field and chamber measurements of NH_3 compensation points over areas with differing land use types.

1.4.2   Dry deposition of particulate NH_4^+

Dry deposition of aerosols occurs by impaction, interception, sedimentation and diffusion. The relative importance of these processes is defined by the aerodynamic diameter of the depositing particles (Monteith and Unsworth, 1990). Deposition of particles less than 0.1 µm in diameter occurs by a similar process to deposition of gases, with turbulent diffusion in the atmosphere followed by Brownian diffusion through the laminar boundary layer. Particles with diameters greater than 10 µm are efficiently deposited through impaction, interception and sedimentation due to their high mass and inertia. A general relationship between particle diameter and deposition velocity (adapted from Monteith and Unsworth, 1990) is shown in Figure 1.6.

28
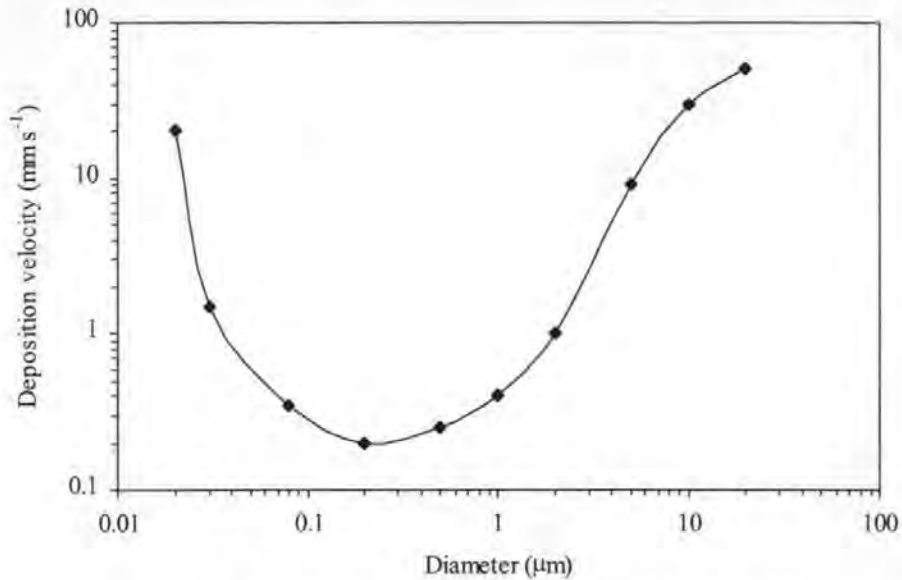
Figure 1.6: Variation of deposition velocity with particle diameter for spherical particles with a density of 1.0 g cm^{-3}. Reproduced from Monteith and Unsworth (1990).

Estimates of the size of NH_4^+ particles have been made by Sievering *et al.* (1994). These authors measured the geometric mass median aerodynamic diameter (MMAD) of NH_4^+ particulates to be 0.9 μm. The data shown in Figure 1.6 demonstrates that this corresponds to a deposition velocity of approximately 0.5 mm s^{-1}. Field measurements by Sutton (1990) and Duyzer (1994) have measured average particulate NH_4^+ deposition velocities of 1.9 and 1.8 mm s^{-1} respectively. The discrepancies between their results and theoretical predictions (discussed in Monteith and Unsworth, 1990) were likely to be due to methodological uncertainties due to difficulties in resolving shallow NH_4^+ concentration gradients.

1.4.3   Wet Deposition of NH$_x$

Wet deposition of particulate NH_4^+ in rainfall has been estimated by Asman and Van Jaarsveld (1992) to account for 72 % of the total particulate NH_4^+ deposition, the remainder being removed by the less efficient dry deposition process. Wet deposition can be thought of as occurring *via* two pathways, rainout and washout. Washout occurs when "clean" precipitation falls through a "polluted" air mass, whilst rainout is the removal of material which has been carried into the raincloud itself (Jones, 1981). Clouds can efficiently capture both gaseous NH_3 and particulate NH_4^+, due to their hydrophilic and hydroscopic chemistries. Field measurements of the "cap cloud" at Great Dun Fell in Cumbria show that 100 % capture of gaseous and particulate NH$_x$-N by cloud droplets is typical (Wells *et al.*, 1997).

Asman (1995) developed a numerical modelling methodology to investigate the below cloud scavenging of soluble gases (including NH_3) in the atmosphere, defined previously as washout. Washout efficiencies were found to reduce rapidly as the diameter of the raindrops increased above 1 mm, whilst a slight decrease in washout rate was found as droplet diameters reduced below an optimum of 0.24 mm. The typical washout coefficient for NH_3 (λ_w) was found to be a function of rainfall rate (I, in mm hour^{-1}) as shown in Equation 1.5, where $a= 9.85 \times 10^{-5}$ and $b= 0.616$. In general scavenging by washout was estimated to be an order of magnitude less efficient than scavenging by rainout.

$$\lambda_w = a\,I^{\,b}$$

Equation 1.5

Jensen and Asman (1995) modelled the washout of NH_3 and rainout of NH_4^+ 10 m from a farm building. The increase in the NH_4^+ concentration of water droplets passing through the NH_3 plume was predicted to be between 6 % and 20 % for droplets sized 0.6 mm and 0.2 mm respectively. Water droplet concentrations of NH_3 were estimated to increase by a factor of four as 0.2 mm droplets passed through the plume. However the total deposition of NH_3, including both washout and rainout was estimated to be five orders of magnitude lower than the contribution of rainout NH_4^+.

Field experiments by Couling (1997) measured a factor of six increase in the NH_4^+ concentrations of rainwater 20 m downwind of a simulated livestock building (as discussed in Section 1.3.1). The disparity between these results and the modelling estimates of Jensen and Asman (1995) may be, in part, explained by the dry deposition of NH_3 to wet deposition collectors, though this was estimated by Couling (1997) to be a small, but significant fraction (up to 26 %) of the total deposition.

A combination of the washout and rainout processes "the seeder-feeder effect" can cause localised peaks in NH_x wet deposition (CLAG,1997). This process operates when an air mass containing NH_x rises and cools as it is advected up a hillside. Water droplets condense as the air mass cools forming a cap-cloud on the top of the hill that efficiently scavenges gaseous NH_3 and particulate NH_4^+. As cloud droplets are typically between 5 μm and 10 μm in diameter (Fowler *et al.*, 1991) they efficiently deposit and are also efficiently scavenged by rainfall. Rainfall from a "seeder cloud", higher up in the atmosphere, passes through the "feeder cloud" thus washing out NH_x (RGAR, 1997).

Field measurements of the dry and wet deposition fluxes of NH_x show that wet deposition dominates the NH_x-N input to upland areas (Bower *et al.*, 1995; Sutton *et al.*, 1992).

Whilst, deposition fluxes over lowland areas are typically dominated by the dry deposition of NH_3 (Bobbink *et al.*, 1992; Draaijers *et al.*, 1989; Hesterberg *et al.*, 1996; Houdijk and Roelofs, 1991).

1.4.4   Cloud droplet interception of NH_x

Cloud droplet interception (otherwise termed as "occult deposition") occurs following the incorporation of NH_3 and NH_4^+ into cloud and fog droplets. As these droplets have a much greater size than the sub-micron NH_4^+ particulates, they efficiently impact on vegetation (as shown in Figure 1.6). Deposition fluxes of cloud droplets, containing NH_3 and NH_4^+, at the summit of Great Dun Fell have been estimated by Bower *et al.* (1995) to be higher (by a factor of 3.5) than the deposition flux of gaseous NH_3 (assuming $R_c = 0$) in the pre-cloud below the summit.

1.5   NET NH_X-N   BUDGETS   FOR   TERRESTRIAL ECOSYSTEMS

The previous sections in this chapter have shown that the surface-atmosphere exchange of NH_x is far from a simple homogeneous process. The magnitude and direction of NH_3 and NH_4^+ fluxes are determined by atmospheric chemistry and plant physiology, as well as by the prevailing meteorological conditions. This section makes a more holistic assessment of the annual budgets of NH_x for terrestrial ecosystems, reviewing field experiments on the exchanges of that occur between the atmosphere and forests, moorlands, and agricultural areas.

1.5.1   Forests

Literature estimates of the net NH_x-N fluxes to forests are shown in Table 1.7. Most of the measurements show a consistent pattern of deposition to forest though Andersen *et al.* (1993) and Wyres and Erisman (1998) both found some evidence of occasional NH_3 emission. In general deposition velocities are high and reasonably consistent between studies, ranging between 22 mm s^{-1} (Duyzer *et al.*, 1994) and 48 mm s^{-1} (Sutton *et al.*, 1993b). As discussed in Section 1.4.1 such rapid deposition is caused by both the surfaces of forests frequently being wet and the high surface roughness they present to the incoming wind field reducing the atmospheric resistance to deposition. The net deposition to forests spans a much wider range between the field studies than the range in deposition velocities, with the lowest measurements of 5 kg NH_3-N ha^{-1} a^{-1} (Sutton *et al.*, 1993b) and the highest measurements of 95 kg NH_3-N ha^{-1} a^{-1} (Draaijers *et al.*, 1989). Higher values were

generally found for forests in the Netherlands due to higher NH_3 concentrations in the atmosphere.

1.5.2   Heathland and Moorland

Literature estimates of the net NH_x-N fluxes to heathlands and moorlands are shown in Table 1.8. Fluxes ranged between 57 kg NH_x-N ha^{-1} a^{-1} (Erisman *et al.*, 1994) and 5 kg NH_x-N ha^{-1} a^{-1} (Fowler *et al.*, 1998c). Deposition fluxes measured in the UK and in Denmark were generally below 10 kg NH_x-N ha^{-1} a^{-1}, whilst estimates for the Netherlands were considerably higher. The enhanced deposition in the Netherlands was due to the higher NH_3 concentrations that moorlands and heathlands were exposed. Deposition velocities were comparatively consistent between studies with estimates ranging from 8 mm s^{-1} (Erisman *et al.*, 1994) to 33 mm s^{-1} (Sutton *et al.*, 1993b) with a median deposition velocity of 20 mm s^{-1}.

Deposition flux (kg NH_x-N ha^{-1} a^{-1})	χ_{NH3-N} (μg m^{-3})	V_d (mm s^{-1})	Location	Reference
7.6 (FGM, DD)	0 – 4 (mean 0.47)	45	Ulborg (DK)	Andersen *et al.* (1993)
95 (TSM, BD)	7 (NH_3) 4 (NH_4^+)	27 (NH_3)	Veluwe (NL)	Draaijers *et al.* (1989)
50 (FGM, DD)	5	36	Speulderbos (NL)	Duyzer *et al.* (1992)
22 – 44 (FGM, DD)	4	22	Speulderbos (NL)	Duyzer *et al.* (1994)
67 (TSM, BD)	N/A	N/A	14 Sites (NL)	Houdinjk & Roelofs (1991)
89 & 30 (TSM, BD)	N/A	N/A	2 Sites (UK)	Ineson *et al.* (1998)
5 – 29 (INF, DD)	0.5 – 2.6	25 - 67	3 Sites (UK)	Sutton *et al.* (1993b)
26 (FGM, DD)	2.6	32 (median)	Speulderbos (NL)	Wyres *et al.* (1992b)
64 (TSM, BD)	N/A	N/A	2 sites (NL)	Van Breemen *et al.* (1982)

Table 1.7:   Review of the literature on deposition of NH_x-N to forests. BD: bulk deposition, DD: dry deposition, TSM: throughfall sampling method; FGM: flux-gradient method; INF: fluxes inferred from predefined deposition velocities, NL: measurements made in the Netherlands, DK: measurements made in Denmark, UK: measurements made in the UK, N/A: data not available.

Several of the studies reviewed in Tables 1.7 and 1.8 estimated the total deposition to the field site, the bulk deposition. Dry deposition had a more significant influence on the NH_x-N inputs measured by Erisman *et al.* (1994) whilst Sutton *et al.* (1992) and Fowler *et al.* (1998c) estimated that slightly higher wet deposition occurred than dry deposition.

Deposition flux (kg NH_x-N ha^{-1} a^{-1})	χ_{NH3-N} (μg m^{-3})	V_d (mm s^{-1})	Location	Reference
30 – 45 (TSM, BD)	N/A	N/A	Heathland (NL)	Bobbink *et al.* (1992)
16 (AGM, BD)	1.9	14	Heathland (NL)	Duyzer (1994)
41 (AGM, DD) 57 (TSM, BD)	16	8	Heathland (NL)	Erisman *et al.* (1994)
2 (AGM, DD) 5 (BD)	0.05 – 0.10	25 – 5.2	Moorland (UK)	Fowler *et al.* (1998c)
8 (AGM, DD)	1.2	20	Heathland (DK)	Hansen *et al.* (1998)
2.9 (AGM, INF) 7.4 (BD)	0.45	20	Moorland (UK)	Sutton *et al.* (1992)
10 (AGM, INF) 16.5 (BD)	2.1	16	Heathland (UK)	
3.4 (AGM, DD)	0.55	19.6	Moorland (UK)	Sutton *et al.* (1993b)
2.9 (INF, DD)	0.45	20.4		
2.8 (INF, DD)	0.25	33		
19 (AGM, DD)	3	14	Heathland (NL)	Wyers *et al* (1992b)

Table 1.8:   Review of the literature on deposition of NH_x-N to heathlands and moorlands. Abbreviations are defined in Table 1.7.

1.5.3   Agricultural land

Estimates of the net exchange of NH_3 between agricultural surfaces and the atmosphere are reviewed in Table 1.9. These studies refer to the net exchange estimated over a year between the vegetation and the atmosphere. Reference should be made to Section 1.2.3 for other agricultural sources of NH_3. Most studies reviewed in Table 1.9 show that agricultural vegetation was a small net emitter of NH_3, with estimated emissions ranging between 0.4 -3.6 kg NH_3-N ha^{-1} a^{-1}.

Several of the reviewed studies estimated that agricultural areas were net sinks for atmospheric NH_3 (Goulding, 1990; Hesterberg *et al.*, 1996; Rodgers, 1978). Net deposition was estimated by Rodgers (1978) using synthetic surfaces (filter papers) as analogues to the biological leaf surfaces. Such an approach would tend to estimate that deposition fluxes were occurring even if the surrounding vegetation was emitting NH_3, particularly if the filter papers became wet. Similar methodological artefacts may explain the high rates of deposition predicted by Goulding (1990), as deposition fluxes were calculated by applying a fixed deposition velocity to air concentration measurements. From Section 1.4 of this review, it is clear that the processes controlling the magnitude and direction of surface-

atmosphere fluxes of NH_3 are much more complicated than can be explained by such a simple analysis.

Net exchange flux (kg NH_x-N ha^{-1} a^{-1})	χ NH3-N (μg m^{-3})	V_d (mm s^{-1})	Land use	Reference
-40 (INF, DD)	N/A	N/A	Arable (UK)	Goulding (1990)
+0.4 (AGM)	N/A	N/A	Permanent grassland (GR)	Grünhage *et al.* (1994)
+3.6 (AGM)	1.6 – 6.6	N/A	Arable (USA)	Harper and Sharpe (1995)
-7.4 (DD, AGM) -5.6 (WD)	7.6	1.3- 14	Extensive grassland (CH)	Hesterberg *et al.* (1996)
-4.0 (SS, DD)	2.1	6	Arable (UK)	Rodgers (1978)
+0.5 to +1.5 (AGM)	1.7 – 3.0	N/A	Arable (DK)	Schjoerring *et al.* (1993a)
-10 (INF, DD)	2.1	14.6	Unfertilised meadow	Sutton *et al.* (1993b)
+0.4 (INF)	0.93	N/A	Permanent grassland (UK)	Sutton *et al.* (1993c)
+1.8 (AGM)	2.9	0 – 16	Arable (UK)	Yamulki *et al.* (1996)

Table 1.9: Review of exchange flux measurements made over agricultural land. Positive fluxes denote emission whilst negative fluxes denote deposition. SS: fluxes calculated using a synthetic surface, WD: wet deposition, CH: measurements made in Switzerland, GR: measurements made in Germany, USA: measurements made in the United States of America. Other abbreviations are defined in Table 1.7.

1.6 DETRIMENTAL EFFECTS OF NH_X DEPOSITION

Detailed reviews of the effects of NH_x deposition have been compiled by CLAG (1994), Fangmeier *et al.* (1994), INDITE (1994) and Pearson and Stewart (1993). The effect of deposited NH_x on a receptor location is a function of the quantity deposited and the susceptibility of the vegetation or ecosystems onto which deposition occurs. The effects of NH_x deposition can be summarised as:

♦ Toxic effects on individual plants

♦ Eutrophication effects on ecosystems

♦ Acidification effects of ecosystems

1.6.1 Direct effects on plants

Direct toxic effects on plants include leaf yellowing and loss and growth defects due to plant nutrient imbalances (Pearson and Stewart, 1993; Pitcairn *et al.*, 1998; Van der Eerden

et al., 1991). The relationship between air concentration, exposure period and effect has been investigated by Van der Eerden *et al.* (1991). Their research showed that direct toxic effects are possible for heathland species, either following exposure to low concentrations (8 μg NH$_3$-N m^{-3}) over long time periods (3 months), or following exposure to high concentration (8 mg NH$_3$-N m^{-3}) over short time periods (1 hour).

The relationship between concentration and effect was found to vary between species. Survival experiments by Van der Eerden *et al.* (1991) showed that, of plants exposed to 86 μg NH$_3$-N m^{-3} for 16 months, grasses had a 100 % survival rating whilst only 30 % of bryophytes survived. Other chamber experiments, conducted by Artyomov *et al.* (1994), found that necrotic spots appeared on isolated maize (*Zea mays* L.) leaves when exposed to concentrations of 535 mg NH$_3$-N m^{-3}, over approximately 1 hour. Although the NH$_3$ concentrations in air in this experiment are unlikely to be encountered in the field, it does demonstrate the rapidity of toxic responses.

Such directly toxic responses are thought to be mediated by the rapid metabolic assimilation of NH$_3$ through the conversion of glutamate to glutamine *via* the GS/GOGAT pathway (Fangmeier *et al.*, 1994). For example, enhanced activities of glutamine sythetase (GS) have been found when plants are exposed to high concentrations of NH$_3$ (Pearson and Soares, 1998) whilst, Schjoerring *et al.* (1993b) measured increased NH$_3$ emission fluxes during periods of low GS/GOGAT activity.

Other biochemical factors regulate the ability of plants to assimilate and therefore detoxify NH$_3$. These include the production of C skeletons, energy (ATP), and reduction equivalents (NADPH and ferredoxin). As these factors are affected by environmental conditions, genetic ability and growth stage it may be expected that plants growing in cold or shaded areas, or those with slow growth rates may be particularly susceptible to the toxic effects of NH$_3$ (Fangmeier *et al.*, 1994).

The effects of increased NH$_3$ concentrations on vegetation are not necessarily detrimental. Cowling and Lockyer (1981) and Whitehead and Lockyer (1987) found that increased plant growth occurred following the exposure of plants to elevated NH$_3$ concentration with Italian ryegrass being able to obtain up to 77 % of its tissue N from the atmosphere.

Increases in plant growth rate caused by NH$_3$ deposition are not always beneficial to the plant. Assimilation and growth responses due to exposure to NH$_3$ are mainly localised to

the site of deposition, the leaves and shoots. This results in increased shoot: root ratios that may result in nutrient imbalances in the plant (Lockyer and Whitehead 1986; Ryden 1986). These imbalances occur as the increased above ground biomass places an unsustainable demand on the roots for nutrients, such as P, K, and Mg, causing reduced tissue concentrations of these elements (Ryden, 1986).

Other indirect secondary effects of nutrient and physiological imbalances can occur. These include a reduced tolerance of plants to drought stress, as increased transpirational water losses are not offset by increases in root growth (Pearson and Stewart 1993). Frost resistance also may be reduced, as plants grown in elevated concentrations of NH_3 have a prolonged growth phase in autumn which can cause the late onset of winter hardiness (Duyzer *et al.*, 1992). Pests also may benefit from the increased plant N concentrations caused by atmospheric deposition with increased insect larval growth being found to occur on ling heather (*Calluna vulgaris* L. Hull) grown in an enhanced NH_3 atmosphere (Van der Eerden *et al.* 1991).

1.6.2 Eutrophication effects

Nitrogen eutrophication occurs when the competitive balance between species in an ecosystem becomes perturbed, resulting in the dominance of "nitrophilous" species in previously diversely populated areas. Eutrophication has been identified as a contributory factor to the reduced species diversity of calcareous grassland, heathlands and forests.

Bobbink (1991) demonstrated, using N addition experiments, that tor grass (*Brachypodium pinnatum* L.) benefited from an additional N input to a greater extent than other grassland species. Furthermore, *B. pinnatum* did not suffer from phosphorus deficiency caused by the stimulation of above ground biomass at the expense of root growth. The competitive advantage gained by *B. pinnatum* enabled it to outcompete other species and thus caused a reduction in the species diversity of the ecosystem. Eutrophication has also been shown to be a problem in Dutch heathlands, with changes in species composition from mainly *C. vulgaris* and bell heather (*Erica tetralix* L.) to grasses dominated by wavy hair grass (*Deschampsia flexuosa* L.) or purple moor grass (*Molinia caerulea* L.) (Bobbink *et al.*, 1992). These changes are thought to be due to the faster growth rate of the grasses than the dwarf shrubs and their increased ability to detoxify and utilise NH_3 to gain a competitive advantage. Van der Eerden *et al.* (1991) found that enhanced NH_3 concentrations resulted in higher biomass of *C. vulgaris* when grown in monoculture. However, in a mixed culture of *C. vulgaris* and *D. flexuosa*, only *D. flexuosa* showed an increase in growth, due to the

earlier start of its growing season allowing it to intercept light above the *C. vulgaris* canopy.

Pitcairn *et al.* (1998) found a reduction in forest understory species diversity close to four farms, with nitrophilous species dominating close to the buildings. Reductions in understory species diversity, correlated with increased NH_x deposition, have also been found in the Netherlands by Van der Eerden *et al.* (1998). Original moss and lichen dominated vegetation was found to revert to grasses with reductions also being found in forest understory shrubs and an increased coverage of nitrophilous species. Reductions in the abundance of ectomycorrhizal fungi have also been found with commensurate increases in saprotrophic and parasitic fungi.

Wetlands also may be adversely affected. Baxter *et al.* (1992) removed turves of bog moss (*Sphagnum cuspidatum* Ehrh. ex. Hoffm.) from areas of high and low N deposition and subjected them to varying levels of simulated NH_x deposition in the laboratory. They found that moss transplanted from the low deposition area showed a reduced growth rate when exposed to simulated NH_x deposition, whilst the mosses from the high deposition area showed an increase in growth under the same conditions. However, Baxter *et al.* (1992) were unable to determine whether this was a physiological adaptation to high NH_x deposition.

1.6.3   Soil acidification

The deposition of NH_x has been hypothesised to significantly contribute to forest decline through soil acidification (Nihlgard, 1985). This acidification is thought to be caused by nitrification of NH_x to nitric acid by soil bacteria releasing H^+ (Draaijers *et al.*, 1989), and by plant root uptake exchanging H^+ for NH_4^+ (Fangmeier *et al.*, 1994).

The most common pathway for the nitrification of NH_4^+ in soils is *via* the action of the chemoautotrophic bacteria, *Nitrosomonas* and *Nitrobacter*. This pathway is shown in Equation 1.6. The rate of autotrophic nitrification of NH_4^+ increases with oxygen supply (therefore reduces with soil depth) and is also positively correlated with reducing soil acidity, increasing temperature and high soil NH_4^+ content (RGAR, 1997).

It is apparent from Equation 1.6 that the nitrification of NH_4^+ by soil bacteria leads to the production of two moles of hydrogen ions for each mole of NH_4^+ consumed. The co-deposition of atmospheric acids (*e.g.* H_2SO_4) with either NH_3 or NH_4^+ can further enhance

the acidification of soils (Draaijers *et al.*, 1989). Estimates by Schneider and Heij (1990), cited in Duyzer *et al.* (1994), suggest that the deposition of NH_x is responsible for 40 % of the total load of potential acid in Dutch ecosystems. Soil acidification is a particular problem in poorly buffered soils and can result in the leaching of cations (Ca^{2+}, Mg^{3+}, K^+) from forests, as well as the mobilisation in the forest soil of phytotoxic Al^{3+} (Draaijers *et al.*, 1989). These factors, along with reductions in the development of fine root hairs and mychorrhiza, can severely decrease the vitality of trees (Fangmeier *et al.*, 1994).

$$2NH_4^+ + 3O_2 \xrightarrow{\text{\textit{Nitrosomonas}}} 2NO_2^- + 2H_2O + 4H^+$$

$$2NO_2^- + O_2 \xrightarrow{\text{\textit{Nitrobacter}}} 2NO_3^-$$
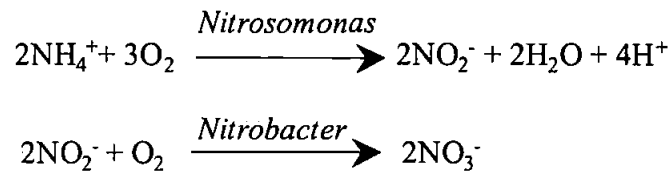
Equation 1.6: Reaction scheme for the production of nitrate ions, water and hydrogen ions from the oxidation of NH_4^+ by chemoautotrophic soil bacteria.

1.7 CRITICAL LOADS FOR REDUCED N AND ENVIRONMENTAL POLICY

1.7.1 Critical loads for reduced N

The previous sections have shown that the effects of NH_x-N deposition on the environment are diverse and depend on both the sensitivity of the receptor ecosystem and the quantity of deposition that occurs. In order to simplify the assessment of whether NH_x-N fluxes to an ecosystem have detrimental effects, the United Nations Economic Commission for Europe (UNECE) adopted the Critical Loads approach, which is defined in CLAG (1994) as:

" *a quantitative estimate of exposure to one or more pollutants below which significant harmful effects on sensitive elements of the environment do not occur according to present knowledge*"

The annual critical load of NH_x-N for an ecosystem can be viewed as a threshold below which no significant environmental harm occurs. Deposition of NH_x-N above this threshold is termed as being a critical load exceedance. Estimates of the critical loads for N for UK ecosystems have been reviewed in INDITE (1994). These values have since been further refined by Hornung *et al.* (1997), the values from which are reproduced in Table 1.10.

Critical load exceedance maps for the UK have been calculated by Sutton *et al.* (1998b). Their results showed that widespread exceedances were predicted to occur (taking into account deposition of SO_x, NO_x, and NH_x) with the critical load for acidity in forest soils

being exceeded over 76 % of rural non-agricultural land. Deposition of NH_x-N alone was estimated to be responsible for 43 % of the area over which exceedances were predicted to occur. Large-scale exceedances of critical loads are also predicted to occur across Europe, particularly in central and southern regions (Kuylenstierna *et al.*, 1998).

Receptor	Critical load (kg N ha^{-1} a^{-1})
Coniferous trees (acidic, low nitrification)	10-15
Coniferous trees (acidic, moderate to high nitrification)	20-30
Deciduous trees	15-20
Acidic coniferous forests	7-20
Acidic deciduous forests	10-20
Calcareous forests	15-20
Acidic unmanaged forests	7-15
Forests in humid climates	5-10
Lowland dry heathlands	15-20
Lowland wet heathlands	17-22
Species rich heaths and acid grasslands	10-15
Upland Calluna heaths	10-20
Arctic and alpine heaths	10-20
Calcareous grasslands	15-35
Neutral-acid grasslands	20-30
Montane-subalpine grasslands	10-15
Mesotrophic fens	20-35
Ombotrophic bogs	5-10
Shallow soft-water bodies	5-10

Table 1.10: Summary of empirical critical loads for N deposition to a variety of ecosystems. Reproduced from Hornung *et al.* (1997).

1.7.2 Environmental policy

The UNECE currently regulates the transboundary acidifying pollutants, SO_2 and NO_x, as well as transboundary volatile organic compounds (VOC), which are thought to affect human health, through the convention on Long Range Transboundary Air Pollution (LRTAP). Ammonia is not currently regulated under LRTAP though a further protocol is under development: the multi pollutant-multi effect protocol, which will include NH_3 emissions (Bull and Sutton, 1998). This protocol will regulate the emissions of the above mentioned pollutants taking into account both deposition and chemical interactions in the atmosphere.

ApSimon *et al.* (1995) reviewed the efficiencies of various methods that may be used to reduce NH_3 emissions from agriculture. They concluded that the maximum feasible emissions reduction across Europe, without radical agricultural reforms, was likely to be in the order of 30 %. The effectiveness of NH_3 reduction policies was estimated by Metcalfe *et al.* (1998a) using a long-range atmospheric dispersion model, termed the Hull Acid Rain Model (HARM), capable of simulating the atmospheric chemistry of SO_2, NO_x, NH_3 and HCl. The predictions of the HARM model demonstrated that the coupling effects of reductions in SO_x and NO_x on NH_x-N deposition were estimated to cause a 30 % reduction in total UK NH_x-N deposition, with a further reduction to 36 % being caused by a 25 % reduction in NH_3 emissions. The large reduction in NH_x-N deposition, modelled to occur from regulating emissions of SO_x and NO_x, was mainly through a reduction in the wet deposition of NH_4^+-N.

A note of caution should be applied to this analysis however, as the HARM model was found to show a poor fit to field validation data on the dry deposition of NH_x-N (Metcalfe *et al.*, 1998b) which the authors attributed to the use of instantaneous vertical mixing in the model. Large differences can be found between the percentage of total deposition which occurs by the dry deposition pathway when comparing the HARM model (13 %, Metcalfe *et al.*, 1998a) to the FRAME model, which has a more realistic "multi-layer" treatment of vertical dispersion, (49 % Singles *et al.*, 1988). As both models have comparable predictions of total annual wet deposition (112 kt: FRAME, 98 kt: HARM) it is likely that the assessment conducted using the HARM model has underestimated the dry deposition component. As the conversion of NH_3 to NH_4^+ would proceed more slowly due to the reduced concentrations of atmospheric acids, enhanced local dry deposition of NH_3 may occur following the arguments presented in Section 1.3.3, based on ApSimon *et al.* (1994).

Local deposition of NH_3 is also to be regulated with the inclusion of NH_3 emissions from agriculture under the pollutants listed in the European Community (EC) legislation on Integrated Pollution Prevention and Control (IPPC). This legislation only regulates emissions from large pig and poultry units, requiring assessments of the local environmental impacts to be performed in order for the site operators to be granted a permit to operate.

1.8   THE ADEPT PROJECT

Agriculture contributes the majority of gaseous NH_3 to the atmosphere in the UK. This NH_3 may be transported over both short and long distances and be deposited to sensitive

natural and semi-natural ecosystems. When the data in Section 1.5 on NH_x inputs is compared with the data in Section 1.7.1 on critical loads for N, it may be seen that these loads are exceeded in many sensitive ecosystems by NH_x deposition alone. Therefore, from this analysis, agricultural practices can be implicated in having significant detrimental effects on the environment. However, a major uncertainty exists in this analysis as the dry deposition of NH_3 onto land close to the site of emission has major implications on the overall transport of NH_x and its effect on local, regional and international scales.

The ADEPT project, under which this study was conducted, was funded by MAFF to investigate the spatial scale of NH_3 emissions and depositions. The project involved scientists from six UK research organisations: the Institute of Terrestrial Ecology (ITE), the Agricultural Development and Advisory Service (ADAS), AEA Technology (AEAT), Imperial College Centre for Environmental Technology (ICCET), Silsoe Research Institute (SRI) and the Institute of Grassland and Environmental Research (IGER). The role of each of the partner organisations in the ADEPT project is shown in Table 1.11.

Work package	Partner contributions
1a: Joint field experiments	ITE, IGER, ADAS, AEAT, ICCET, SRI
1b: PhDs and long term experiments	IGER, ADAS, SRI
2: Emissions mapping	ITE, ADAS
3: Atmospheric dispersion modelling	ICCET, ITE
4: Effects assessment	ITE

Table 1.11:   Work packages conducted for the MAFF ADEPT project. Reproduced from Sutton *et al.* (1998b)

A large section of the project was involved with investigating the dispersion and deposition of NH_3 close to emissions sources, which was identified as representing a large uncertainty in the calculations of critical load exceedances. Several studies were conducted to accomplish this, the most significant of which were two short-term campaign experiments designed to validate dispersion models for predicting the dispersion and deposition of NH_3 within 1 km of both a large poultry farm and a slurry strip. Additional experiments were conducted by ADAS to measure long-term averaged horizontal NH_3 fluxes around poultry farm building and by IGER to investigate other aspects of NH_3 dispersion and deposition as part of two PhD projects.

The guidelines for the two PhD projects at IGER, as detailed in the original proposal to MAFF, were as follows:

1. Determine the extent and controls over short-range deposition from field sources (i.e. grazed swards and farm waste applications).

2. Provide data and contribute to campaign measurements for validation of farm scale dispersion models.

3. Extend, in particular, the limited information that is/will be available for sources associated with grazed swards and determine the controls over apparent wide-ranging spatial and temporal variability.

4. Derive/ improve best estimate emission factors for various livestock farming sources.

These research aims were split into two projects, one investigating the emission, dispersion and deposition of NH_3 from grazing livestock, and this project investigating the emission dispersion and deposition from slurry spreading and farm buildings.

1.9   OBJECTIVES OF THIS STUDY

This study estimated the emissions, dispersion and deposition of NH_3 from two sources that are significant contributors to national NH_3 emissions: slurry spread onto grasslands and emissions from a working dairy farm.

More detailed aims and objectives were as follows:

1.   Determine the emission of NH_3 from slurry spread onto grassland and investigate the seasonal and diurnal variability.

Emission estimates, often used as input to atmospheric dispersion models, are typically expressed as annual averaged values. However, NH_3 emissions from slurry spreading have been shown in previous research to be highly intermittent with peaks in emission occurring immediately following application.

Research on this objective investigated the diurnal variability, and meteorological controls over NH_3 emission fluxes from slurry applied to grassland using the micrometeorological mass balance technique. This technique was identified from the methods review (Chapter 2). Eight field experiments were conducted at times when farmers would typically apply slurry, providing further information on the seasonal variability of NH_3 emission rates.

2.   Estimate local dispersion and deposition of NH₃ over distances less than 100 m from slurry applied to grassland and investigate the controls over deposition rates.

The local dispersion and deposition of NH₃ emitted from slurry spreading over distances of less than 1.0 km from the source is currently poorly understood and poorly represented in the scientific literature. This introduces a substantial uncertainty term in the calculation of regional, national, and international environmental impacts of NH₃. Deposition close to a source may theoretically account for a substantial reduction in the quantity of NH₃ available to be transported over longer distances, and also may result in pollution "hot spots".

The methods review highlighted the significant contribution of advection errors to micrometeorological measurements of deposition close to slurry spreading. These errors were quantified using a theoretically exact analytical atmospheric dispersion model, termed the K-theory Atmospheric Transport and Exchange Model (KATCH) which was developed in Chapter 3. An advection corrected flux-gradient method was then developed along with an experimental design for the implementation of the method in Chapter 4. Field experiments on dispersion and deposition were integrated with the emission measurements discussed in Objective 1.

3.   Derive emission factors for a naturally ventilated farm building and the associated slurry storage facility.

Emissions from housed dairy cattle are estimated to account for a substantial portion of the net UK NH₃ emissions inventory. However, the emission factors used in the inventories are based on the observations from a limited number of experimental studies. This objective aimed to derive additional emission factors for housed livestock for comparison with those currently used to construct NH₃ emissions inventories.

Emission factors were derived from field measurements made at a working dairy farm. A mass balance method was identified from the methods review for determining emissions from the naturally ventilated farm buildings, whilst a model back-calculation method was developed to derive emission factors for stored slurry.

4.   Estimate the dispersion and local deposition of NH₃ from a naturally ventilated farm building.

The local deposition of NH₃ around naturally ventilated farm buildings is currently poorly understood. Due to the emissions from buildings occurring as a relatively continuous point

source, local depositions close to such structures may cause local critical load exceedances. However, this may be partially offset by the enhanced turbulence and local dispersion that such structures generate.

Field experiments, described in Chapter 6, were conducted at the experimental SRI "Structures Building" and at the working dairy farm discussed in Objective 3. Measurements of the dispersion of NH_3 were compared with the predictions of an advanced Gaussian plume model (UK-ADMS), identified from the models review (Chapter 3) as having a reasonably detailed treatment of building effects. Whilst, local deposition was estimated using a biomonitor N balance method, identified from the methods review.

2

REVIEW OF EXPERIMENTAL METHODS TO MEASURE NH₃ FLUXES IN THE FIELD

2.1   INTRODUCTION

The aim of this thesis, discussed in Chapter 1, was to determine the emission, dispersion and local deposition of NH_3 volatilised from two sources: slurry spread onto grassland and naturally ventilated farm buildings. This chapter presents a review of the methods that are often used to estimate emission and deposition fluxes in the field. These methods can be broadly grouped into chamber methods, surface measurements and micrometeorological methods.

2.2   CHAMBER METHODS

Chamber techniques operate by restricting the volume of air with which surface-atmosphere exchanges occur, so amplifying any increases or decreases in air concentrations. The two variations of the chamber method are: closed systems, where changes in gas concentration are monitored in a finite headspace; and open systems, where a continuous flow of air passes through the chamber. Surface-atmosphere fluxes are calculated from closed and open systems according to Equations 2.1 and 2.2 respectively, where v is the volume of the headspace (in Equation 2.1) or the air throughflow (in Equation 2.2), a is the surface area covered, χ is the gas concentration (the subscript g denotes the concentration within the chamber and b denotes the background), and t is the exposure time.

$$F_\chi = \frac{v}{a} \frac{d\chi_g}{dt}$$
Equation 2.1

$$F_\chi = \frac{v(\chi_g - \chi_b)}{a\,t}$$
Equation 2.2

45

Chamber techniques have the advantage of being sensitive to relatively small fluxes and are mechanically simple to operate. Indeed, Denmead (1994) showed that chamber techniques could be more than two orders of magnitude more sensitive to surface-atmosphere CH_4 and N_2O fluxes than comparable micrometeorological methods. Chamber methods do have several important disadvantages. Often the enclosed microclimate does not represent the external meteorological conditions, such that large corrections are typically required to account for the extreme enhancement of laminar boundary layer resistance. Furthermore, surface temperatures and humidities can also be significantly enhanced within chambers and large uncertainties are often involved when extrapolating "point" chamber measurements over wider areas.

Another important limitation on the use of chamber techniques for determining the surface-atmosphere exchange of reactive gases (such as NH_3) is that adsorption may occur onto the chamber walls. This can be an important artefact under field conditions, especially when humidities and temperatures within the chamber are enhanced and condensation of water onto the chamber walls occurs (Sutton, 1990; Sutton *et al.*, 1993d).

As a result of the above concerns chamber techniques are mainly used for investigating the surface-atmosphere exchange of relatively slow depositing gases that are typically either emitted from soil, such as N_2O or CH_4, or exchanged with stomata (Denmead, 1994). The applications of chamber techniques to NH_3 measurements have largely been confined to either situations where the direction of fluxes can be presupposed (*e.g.* Ferguson *et al.*, 1988; Kissel *et al.*, 1977; Marshall and DeBell, 1980), or for controlled environment studies where the accumulation of water vapour may be reduced (*e.g.* Aneja *et al.*, 1986; Cowling and Lockyer, 1981). Because of the above artefacts, simple chamber techniques have not been widely used to determine background NH_3 exchange fluxes in the field. Dynamic chambers were used by Sutton *et al.* (1997a) to determine NH_3 exchange fluxes immediately downwind of slurry spreading, though these authors noted that their results should be treated with caution as the technique was only used as no other methods were available.

2.21   Advanced chamber methods

Developments to the simple chamber techniques have been made by Lockyer (1984), who developed a miniature wind tunnel system for estimating NH_3 volatilisation in the field, and Svensson (1994), who developed a "micrometeorological" chamber technique.

The miniature wind tunnel system, developed by Lockyer (1984), avoided the problems of unrealistically low air flows and some of the problems of condensation through the use of a high powered fan to draw air through a transparent polycarbonate tunnel. The wind tunnel system, shown diagrammatically in Figure 2.1, was designed to cover a rectangular area of 1.0 m^2 (0.5 m width by 2.0 m length). Fluxes were calculated using Equation 2.2 with the air volume through the tunnel (v) calculated from a vane anemometer at the exit of the fan housing. Air concentrations at the inlet and outlet of the tunnel (χ_b) and (χ_g) were measured using simple acid flask impingers.
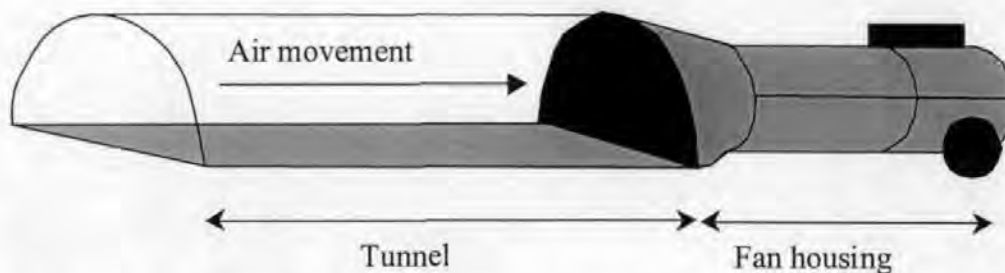
Figure 2.1:   Miniature wind tunnel, as described in Lockyer (1984), showing the fan housing and the polycarbonate tunnel.

The wind tunnel system does have some limitations that should be considered. Dew formation on the surface of the tunnel can occur, limiting the usefulness of the method when collecting overnight measurements or during daytime periods with a high humidity. Furthermore, due to the high volume flow of the system, the detection limits of the method are higher than for dynamic chamber techniques, limiting the usefulness of the method to situations where gross differences occur between χ_b and χ_g.

A further caveat of the wind tunnel method was identified by Ryden and Lockyer (1985) who compared wind tunnel and micrometeorological estimates of NH_3 emission from urea fertiliser. They found that realistic predictions of emission fluxes were only obtained when the wind speeds through the tunnels were continuously adjusted to track the ambient wind speed. Because of the aforementioned caveats, wind tunnel systems have been mainly used in comparative studies of NH_3 volatilisation. For example, Pain and Misselbrook (1997) used a wind tunnel system to determine the efficiency of different slurry application techniques, and Sommer *et al.* (1991) investigated the influence of specific meteorological conditions on NH_3 volatilisation.

Svensson (1994) developed a chamber method for estimating NH_3 fluxes in the field that claimed to apply both dynamic chamber and micrometeorological theories. A stirred dynamic chamber system was used to provide a constant ventilation rate and homogeneous above surface NH_3 concentrations. Fluxes of NH_3 were determined by applying a micrometeorological resistance analysis, as discussed in Chapter 1, Section 1.4.1. Using a resistance analysis, fluxes can be determined from the difference in concentrations between the surface, $\chi\{z_1\}$ and a reference height $\chi\{z_2\}$, and the cumulative resistances to mass transfer between the heights (R_t), shown as Equation 2.3.

$$F_\chi = \frac{\chi\{z_1\} - \chi\{z_2\}}{R_t}$$

Equation 2.3

Svensson (1994) combined Equations 2.2 and 2.3 to derive an expression for the surface concentration, $\chi\{z_1\}$, from measurements of χ_g and χ_b, and from an estimation of R_t. This is shown mathematically in Equation 2.4. It should be noted that Svensson (1994) assumed that χ_g was equivalent to $\chi\{z_2\}$ and that boundary layer resistance was the only resistance pathway to deposition. Air concentrations and boundary layer resistances were estimated from passive diffusion samplers in the chamber. It is questionable whether this method is truly micrometeorological, as, according to Svensson (1994), the surface concentration, calculated using Equation 2.4, should be substituted back into Equation 2.3. This substitution can be simplified to give Equation 2.2 (as the values of R_t cancel out) which is the formula for the standard dynamic chamber.

$$\chi\{z_1\} = \chi_g \left[1 + \left(\frac{v\,R_t}{a\,t} \right) \right] - \chi_b \left(\frac{v\,R_t}{a\,t} \right)$$

Equation 2.4

2.3 SURFACE MEASUREMENTS

Direct measurements of the quantities of deposited material are often used to estimate deposition fluxes. This type of analysis is particularly useful when the deposited substance is persistent and its atmospheric origin can be presupposed. For example, the deposition fluxes of the radioisotopes ^{131}I and ^{137}Cs following the Chernobyl accident were directly determined from surface measurements by Jackson *et al.* (1987).

The application of such a simple and robust technique to the measurement of NH_3 fluxes is complicated by NH_3 being both a substrate and product of plant metabolism (Yin *et al.*, 1998). Hence, NH_3 on leaf surfaces cannot be presupposed to have an atmospheric origin or to persist unchanged following deposition. Despite these limitations, several methods have been developed to quantify deposition fluxes using surface measurements. These

involve the use of synthetic surfaces, collection of rainfall and throughfall, the use of stable isotopes and the construction of N balances.

2.3.1   Synthetic surfaces

The simplest method to account for the interfering production or consumption of NH_3 by plant metabolism on NH_3 fluxes is to use a synthetic non-biological surface as an analogue. The realism of these synthetic surfaces is somewhat questionable, in particular following the complexity of the NH_3 deposition process, as discussed in Chapter 1, Section 1.4.1.

Speirs and Frost (1987) and Rodgers (1978) used ion-exchange resin and acidified filter papers as synthetic surfaces, pre-supposed to be analogous to soil, for investigating deposition downwind of farm buildings. These methods have the advantage of being simple to implement in the field. However, the use of acidified surfaces to trap a reactive atmospheric base will have undoubtedly caused the sampling devices to behave as perfect sinks, where deposition is only limited by the availability of NH_3 to the surface. The assumption that soils are a perfect sink for NH_3 is not supported by other measurements (*e.g.* Sutton *et al.*, 1997b) and highlights a fundamental flaw in both experiments.

Bobbink *et al.* (1992) used artificial plastic surfaces to simulate heather and determine the influences of canopy exchange processes on estimates of the "throughfall" flux of NH_3. Plastic surfaces may be a slightly better analogue to natural surfaces than the acidified media previously described, as they are not chemical sinks for NH_3. However, it is unlikely that plastics can realistically represent the waxy cuticles, thin water films and high humidities which have been shown to control deposition rates to vegetated surfaces (discussed in Chapter 1, Section 1.4.1.1). The neglection of canopy exchange processes, though deliberately excluded by Bobbink *et al.* (1992), may have led to an underestimate of the total deposition flux due the stomatal and cuticular uptake of NH_x (discussed in Chapter 1, Section 1.4.1.2).

2.3.2   Rainfall/ throughfall method

The rainfall/ throughfall method has often been used to estimate deposition of NH_x to forests, as discussed in Chapter 1, Section 1.5.1. Bulk deposition fluxes (dry and wet deposition) are typically measured by collecting samples of rainwater passing through the forest canopy, assuming that dry deposited NH_x is washed from the leaf surfaces. Dry deposition fluxes can then be estimated by subtracting the wet deposition component, determined from rainwater samples collected at an exposed location.

This method, whilst simple in theory and practice, has some important limitations. The most significant being that it assumes that deposition occurs and that canopy cycling of NH_3 is negligible. In practice, internal cycling of NH_3 within plant canopies has been found in a number of studies (*e.g.* Sutton *et al.*, 1993c; Denmead *et al.*, 1976) which could lead to the erroneous estimation of deposition fluxes during periods of net emission. This is unlikely to be an issue when studying deposition fluxes to natural forests, which are mainly sinks for NH_3 and where the research interest is often in the flux reaching the forest floor. However, the rainfall/throughfall method may be of limited use for studying other environments, both from the above considerations and due to practical problems of making representative measurements of throughfall under short vegetation.

2.3.3   Stable isotopes (^{15}N)

The most abundant isotope of nitrogen is ^{14}N, however the stable isotope ^{15}N exists at a natural abundance of 0.368 atom percent making it an ideal tracer for studying the fate of nitrogenous compounds. The flux of NH_3 between vegetation and the atmosphere can be estimated by two methods. The plant material may be enriched with ^{15}N and measurements made of the dilution resulting from atmospheric uptake of ^{14}N (*e.g.* Sommer and Jensen, 1991). Alternatively, NH_3 gas can be labelled with ^{15}N and the enrichment of unlabelled plants can be measured (*e.g.* Porter *et. al.*, 1972).

The loss or gain of ^{15}N in plants grown in the field should provide a conclusive and quantifiable method for determining surface-atmosphere fluxes. However, in practice this is often not the case. Harper and Sharpe (1998) reviewed a number of intercomparisons between fluxes estimated using micrometeorological and ^{15}N balance techniques. They found that over fertilised grassland, during periods when plants were metabolically active, ^{15}N methods predicted higher NH_3 emission fluxes (by a factor of two) than simultaneous micrometeorological measurements. Furthermore, ^{15}N methods tended to overpredict the low-level "background" NH_3 exchange by a factor of six. During periods of metabolic inactivity both methods tended to be in a good agreement.

Harper and Sharpe (1998) concluded that these differences were due to isotopic substitution of $^{15}NH_3$, emitted from the enriched plants, with $^{14}NH_3$, from the atmosphere. During periods of bi-directional exchange, where there was no net NH_3 flux, the reduction in ^{15}N would have been erroneously interpreted to imply a net NH_3 emission flux. They also suggested that emission fluxes from ^{14}N and ^{15}N sources may differ due to the preferential volatilisation of lighter $^{14}NH_3$. Evidence of this has also been reported by

Marshall and DeBell (1980) who found reduced rates of volatilisation from ^{15}N fertiliser granules.

2.3.4 N balance

A nitrogen balance may be used to estimate the surface-atmosphere exchange of NH_3 in situations where all sources and sinks of N to a plant-soil system can be quantified. Any excess or deficit of N in the system can then be attributed to surface-atmosphere exchange processes.

Nitrogen balance methods have been used by Cowling and Lockyer (1981) to determine fluxes in chamber experiments and by Sommer (1988) to determine deposition fluxes downwind of a dairy farm. Both studies controlled the N nutrition of plants grown in a glasshouse. Cowling and Lockyer (1981) used field soil as a growth media whilst Sommer (1988) used artificial "Rockwool" to enable a more accurate quantification of inputs necessary to detect ambient deposition fluxes. Surface-atmosphere fluxes were estimated from the difference between the N supplied to the plant in the glasshouse and the N recovered following field exposure.

This method has the advantage that NH_3 deposition can be investigated over an extended time period and the fate of deposited NH_3 between the various plant sinks can be determined. Furthermore, plants grown in a glasshouse are likely to represent robust analogues and net canopy exchange processes can be treated within a N balance. The N balance method does have several limitations. Not least that the determination of an accurate N budget necessitates the modification of the root environment, which obviously means that the experimental plants are no longer exact analogues to the underlying surface. Also, as atmospheric inputs to a well fertilised plant are likely (following Cowling and Lockyer, 1981) to represent a significant, though small, fraction of the total plant N, errors in the dosage of fertiliser N or in the determination of soil N can have a large influence on the estimated fluxes. For example, Sommer (1988) made a detailed consideration of the N supplied to the plant as fertiliser and as seed during the growth phase in the glasshouse, however no account was made of any atmospheric deposition that may have occurred during this period. This could have led to the overprediction of deposition fluxes in the field.

2.4 MICROMETEOROLOGICAL METHODS

Micrometeorological methods have been reviewed in detail by Baldocchi *et al.* (1988), Denmead (1983), Denmead (1994) and Monteith and Unsworth (1990). These methods estimate fluxes from measurements of near surface meteorology and the corresponding air concentrations of the property being evaluated. These methods have the advantage that they do not modify the environment over which fluxes are being evaluated and that they allow the estimation of spatially averaged fluxes. The disadvantages of micrometeorological methods include their labour intensity, their low precision (in comparison with chamber techniques) and that flux estimates are only, strictly speaking, valid for a limited number of conditions where the original assumptions underlying the methods are met.

Micrometeorological methods that are typically used to determine the surface-atmosphere exchange of trace gases can be grouped into two generic types: those that assume fluxes are constant with height in the atmosphere, and those that account for heterogeneity in the vertical flux field. Before consideration of these methods, it is important to appreciate the overall processes that occur in the region of the atmosphere being studied, hence a brief review of boundary layer meteorology follows based on the reviews of Baldocchi *et al.* (1988), Denmead (1994), Hanna *et al.* (1982), Pasquill and Smith (1983) and Monteith and Unsworth (1990).

2.4.1 Basic boundary layer meteorology

The Earth's atmosphere is comprised of four vertical layers, the troposphere, stratosphere, mesosphere and thermosphere. The troposphere is the layer of the atmosphere closest to the surface of the planet, typically extending to 10 km, and is itself subdivided into two layers, the atmospheric boundary layer (ABL) and the free atmosphere. The ABL is closely coupled to the surface by turbulent mixing and is separated from the overlying free atmosphere by an inversion layer that restricts the vertical transport of pollutants and energy.

The height of the ABL varies diurnally, due to what is termed the "stability" of the atmosphere. The ABL has a minimum height, of approximately 100 m, during cloudless overnight periods with low wind speeds when the surface acts as a sink for sensible heat (stable conditions). The maximum height of the ABL, of approximately 1300 m, occurs during cloudless daytime periods with low wind speeds when the surface acts as a source of sensible heat (unstable conditions). During overcast periods with moderate wind speeds

and minimal sensible heat fluxes (neutral conditions) the ABL has a height of approximately 800 m (Clarke, 1979).

The term "stability" relates to the ratio of mechanical to convective turbulence in the atmosphere. In the ABL turbulence forms as a chaotic pattern of swirling motions (termed eddies) and is often measured as the standard deviation of the wind speed in the horizontal, lateral and vertical planes (termed σ_u, σ_v, and σ_w respectively). Mechanical turbulence is generated by the action of both the wind and the surface, increasing with strong winds and taller roughness elements. The atmosphere is termed as being of a neutral stability when turbulence is generated purely by these mechanical processes. Convective turbulence is regulated by the surface-atmosphere heat flux. Increased turbulence occurs during periods with a strong emission of heat from the surface caused by daytime insolation whilst the absorption of heat by the surface during cloudless overnight periods acts to suppress turbulence.

The influence of stable and unstable atmospheric conditions on the vertical movement of a parcel of air is shown schematically in Figure 2.2. If a parcel of air, at a height of z_1, is moved adiabatically (without gaining or losing heat) by mechanical turbulence to a greater height (z_2) then in a stable atmosphere this parcel would then have a lower temperature than the surrounding air and sink back to z_1. Whilst, in an unstable atmosphere the parcel of air at z_2 would have a higher temperature than the surrounding air and continue to rise. Similarly an initial downwind motion (to z_3) would be suppressed in a stable atmosphere and extended in an unstable atmosphere.

The ABL is separated from the surface by the quasi-laminar sub-layer, which is also often referred to as the roughness sub-layer. This layer is formed by the frictional drag of the surface and can have a vertical extent of a few millimetres over relatively smooth surfaces such as sea, sand or short grass, and can extend to a metre or more over rough surfaces such as cities and woodland. The height to which the roughness sub-layer extends above the aerodynamic zero plane displacement height (termed d) is denoted by the roughness length (z_0).

The surface layer exists immediately above the roughness sub-layer. Fluxes are approximately constant with height within the surface layer and air concentrations show marked vertical gradients. The surface layer accounts for approximately 10 % of the depth of the ABL. The remainder of the ABL is accounted for by the mixed layer. Fluxes in this

layer are no longer constant with height due to mixing, in the case of gases, and expansion of the ABL in the case of heat fluxes.
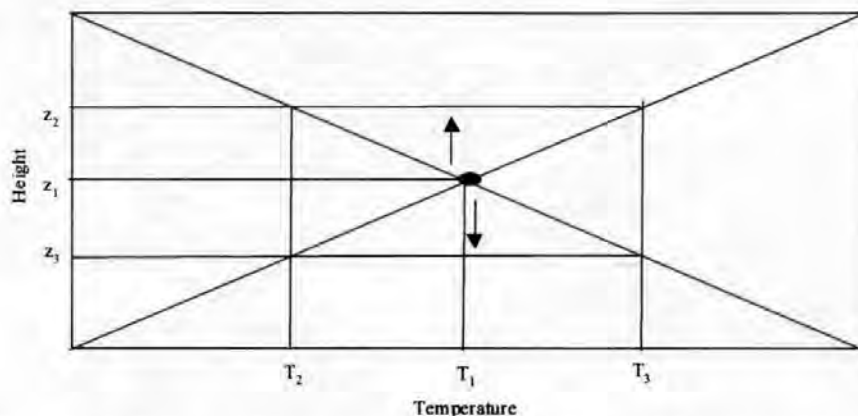
Figure 2.2:   The influence of temperature gradients in a stable atmosphere (shown as a blue line) and an unstable atmosphere (shown as a red line) on the vertical dispersion of a parcel of air.

2.4.2   Methods assuming a constant flux layer

The development of a constant flux layer in the atmosphere requires an extensive homogeneous upwind area, termed the fetch. The typical "rule of thumb" used to estimate the fetch requirements for micrometeorological measurements suggests that fetch to height ratios are in the order of 100:1. Hence, a constant flux layer 1 m in height will develop across 100 m of upwind fetch. The fetch requirements for micrometeorological methods have been investigated in more detail by Horst and Weil (1994) using an analytical atmospheric dispersion model. They found that fetch to height ratios were weak functions of the roughness length, with smoother surfaces having slightly higher fetch to height ratios. The more significant factor determining the fetch to height ratio was found to be the stability of the atmosphere with strongly stable atmospheric conditions requiring fetch to height ratios of 1000:1 or more. Unstable atmospheric conditions were found to require fetch to height ratios between 50:1 to 100:1 whilst neutral conditions required fetch to height ratios between 100:1 and 200:1.

Constant flux layer micrometeorological methods can be grouped into two categories, those which estimate surface-atmosphere fluxes directly and those which estimate fluxes from concentration gradients, assuming that molecular and turbulent diffusion are analogous.

2.4.2.1   *Eddy-correlation method*

The eddy-correlation method estimates surface fluxes directly from turbulent fluctuations in vertical wind speed (w') and the corresponding fluctuations in air concentration (χ'). The method assumes that above an emitting surface higher air concentrations occur associated with eddies moving upwards in the atmosphere and conversely lower concentrations are associated with downward eddies. The net flux can be determined from the time-average of these correlated fluctuations, shown in Equation 2.5.

$$F_\chi = \overline{w'\chi'}$$
Equation 2.5

The eddy-correlation method requires the rapid simultaneous measurements, both spatially and temporally of air concentrations and vertical wind speeds. As eddy size increases with height above the surface, due to the shearing stress generated by the surface roughness elements, the determination of fluxes over relatively smooth agricultural surfaces, where fetch may be limited, requires fast response instrumentation (<1 hz) to resolve the small eddy sizes close to the surface. This has, to date, prevented the determination of NH₃ fluxes using the eddy correlation method as rapid response instruments sensitive enough to measure ambient NH₃ concentrations are not currently available.

2.4.2.2   *Flux-gradient methods*

Flux-gradient methods assume that turbulent diffusion and molecular diffusion are analogous, hence the turbulent flux can be defined as the product of the vertical concentration gradient and the eddy diffusivity (K_χ), Equation 2.6.

$$F_\chi = -K_\chi \frac{\partial \chi}{\partial z}$$
Equation 2.6

The eddy diffusivity for matter may be calculated directly, assuming "similarity theory". That is, that equality exists between eddy diffusivities for heat, water vapour and matter. Sensible heat flux (C) can be calculated using Equation 2.7 where K_H is the eddy diffusivity for heat, T is the potential (adiabatic) temperature, ρ is the density of air and C_p is the specific heat capacity of air.

$$C = -\rho\, C_p\, K_H \frac{\partial T}{\partial z}$$
Equation 2.7

Latent heat flux (λE) can be calculated, in a similar form, from the vertical gradient of absolute humidity (E) and the latent heat of vaporisation of air (λ), Equation 2.8.

$$\lambda E = -K_E\, \lambda \frac{\partial E}{\partial z}$$
Equation 2.8

A simple surface energy balance assumes that the net radiation to the surface (R_n) is equivalent to the fluxes of sensible heat (H), latent heat (λE) and soil heat (G), shown in Equation 2.9.

$$R_n = H + \lambda E + G \qquad \text{Equation 2.9}$$

The eddy diffusivity for heat (or latent heat or matter) can be calculated by combining Equations 2.7 to 2.9 and rearranging to form Equation 2.10.

$$K_\chi = K_H = K_E = \frac{(R_n - G)}{(\rho_a C_p \, \delta T/\delta z) + (\lambda \, \delta E/\delta z)} \qquad \text{Equation 2.10}$$

This method has been used by Denmead *et al.* (1974) to study NH₃ fluxes from grazed pasture and has been shown to produce results with a precision of +/- 40 %. Errors in the determination of NH₃ concentration profiles were found to dominate the error term. The energy balance method is limited to situations where R_n-G is well defined. Thus, K_χ calculated using this method becomes uncertain during overcast daytime periods or overnight.

Eddy diffusivity can also be calculated from the vertical gradients of wind speed and temperature using the aerodynamic gradient method. This method initially defines the momentum flux (τ) in the constant flux layer using the flux-gradient relationship shown in Equation 2.11.

$$\tau = -\rho \, K_M \frac{\partial u}{\partial z} \qquad \text{Equation 2.11}$$

The momentum flux can be also derived directly from the tangential eddy velocity $(u*)$ using Equation 2.12.

$$\tau = -\rho \, u_*^2 \qquad \text{Equation 2.12}$$

The eddy velocity (or friction velocity) is defined in Equation 2.13, where k is the von Karman constant, defined as the ratio of eddy size to height above the ground (approximately 0.4), Φ_M is a non-dimensional stability correction factor for momentum and d is the zero plane displacement height, the increase in aerodynamic height caused by the influence of the surface roughness elements.

$$u_* = \frac{k(z - d)\partial u / \partial z}{\Phi_M} \qquad \text{Equation 2.13}$$

The zero plane displacement height is difficult to evaluate, often being derived using trial and error methods from the curvature of the log-linear wind speed profile in neutral stability conditions. An example of such an analysis is shown in Figure 2.3

Equations 2.11 to 2.13 can be rearranged to give an expression for the eddy diffusivity for momentum, shown as Equation 2.14.

$$K_M = \frac{k\, u_*(z-d)}{\Phi_M}$$

Equation 2.14
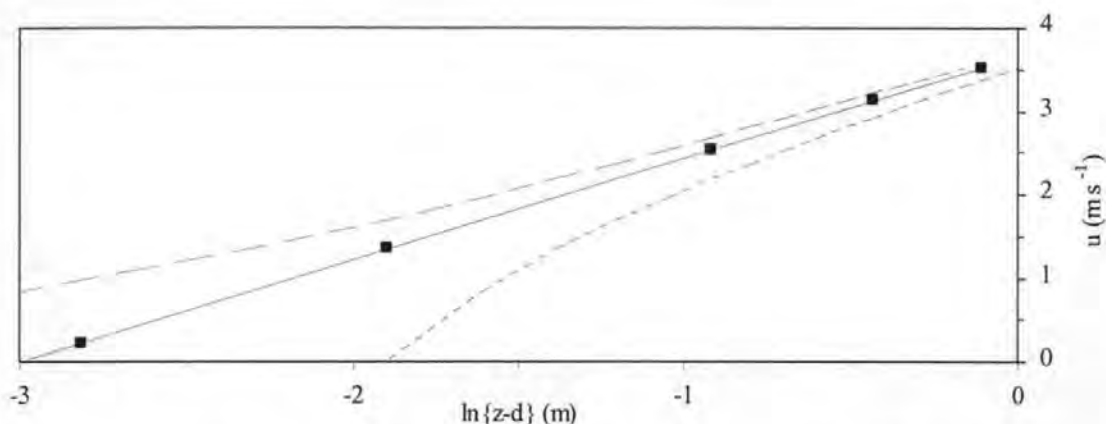
Figure 2.3: Determination of the zero plane displacement height from measurements of wind speed close to the surface (■), correct d: ——, d underestimated: ---, d overestimated: -----.

Analogous expressions may be defined for eddy diffusivities for heat and matter, Equations 2.15 and 2.16 respectively.

$$K_H = \frac{k\, u_*(z-d)}{\Phi_H}$$

Equation 2.15

$$K_\chi = \frac{k\, u_*(z-d)}{\Phi_\chi}$$

Equation 2.16

For neutral conditions Φ_M, Φ_H, and Φ_χ all equal unity. Relationships for stable conditions were defined by Webb (1970), Equation 2.17, and for unstable conditions were defined by Dyer and Hicks (1970), Equation 2.18. The term L is the Monin-Obukhov stability length.

$$\Phi_M = \Phi_H = \Phi_\chi = 1 + \left(\frac{5.2\,(z-d)}{L}\right)$$

Equation 2.17

$$\Phi_M^2 = \Phi_H = \Phi_\chi = \left[1 - \left(\frac{16\,(z-d)}{L}\right)\right]^{-0.5}$$

Equation 2.18

The Monin-Obukhov stability length, defined in Equation 2.19, is a function of the fluxes of sensible heat and momentum and is approximately constant with height in the surface layer. L has a rather loose definition of being the modal height at which equal magnitudes of Turbulent Kinetic Energy (TKE) are generated (or consumed) by convective and

mechanical forces. In Equation 2.19, T is the temperature in Kelvin and g is acceleration due to gravity.

$$L = -\frac{u_*^3 \, \rho \, C_p T}{k \, g \, C}$$

Equation 2.19

It is clear that some circularity exists when using the Equation 2.19 to calculate L, as L is a function of the sensible heat flux (C). Hence L is often inferred from the semi-empirical relationship between L and the gradient Richardson's number (Ri), which is defined as the height dependent ratio of the production (or consumption) of TKE by convective forces to the production of TKE by wind shear. Several mathematical parameterisations of the Richardson's number are available, however a commonly used form was derived by Sutton (1990), shown as Equation 2.20.

$$Ri = \frac{(z-d)g \, \delta T/\delta \ln(z-d)}{T\left[\delta u/\delta \ln(z-d)\right]^2}$$

Equation 2.20

The Monin-Obukhov stability length can be defined from the Richardson's number in stable conditions using Equation 2.21 (Webb, 1970) and in unstable conditions using Equation 2.22 (Dyer and Hicks, 1970).

$$L = \frac{z-d}{Ri}$$

Equation 2.21

$$L = \frac{\left[1-(5.2Ri)\right](z-d)}{Ri}$$

Equation 2.22

The calculation of the surface-atmosphere fluxes could be made by substituting the value for K_χ from Equation 2.16 back into Equation 2.6. Alternatively an eddy concentration (χ_*) can be calculated using Equation 2.23 and fluxes can then be calculated as the product of the eddy velocity and eddy concentration, Equation 2.24.

$$\chi_* = \frac{k(z-d)\partial\chi/\partial z}{\Phi_\chi}$$

Equation 2.23

$$F_\chi = -u_* \chi_*$$

Equation 2.24

The determination of u_* and χ_* from Equations 2.13 and 2.23 requires curve fitting to the curvilinear vertical gradients, hence it is often preferable to linearize the logarithmic profiles by integration with respect to height (Sutton, 1990). For stable and neutral conditions Equations 2.23 and 2.13 can rearranged and integrated with respect to height to yield Equations 2.25 and 2.26, where Ψ_M, Ψ_H and Ψ_χ denote integrated stability correction factors. Formulae for unstable conditions are identical to Equations 2.25 and 2.26 except Ψ_M and Ψ_χ should be subtracted from $\ln(z\text{-}d)$.

$$u\{z-d\} = \frac{u_*}{k}\left[\ln(z-d)+\Psi_M\right] - \frac{u_*}{k}\ln(z_0)$$

Equations 2.25

$$\chi\{z-d\} = \frac{\chi_*}{k}\left[\ln(z-d)+\Psi_\chi\right] - \frac{\chi_*}{k}\ln(z\{\chi=0\})$$

Equations 2.26

Integrated stability correction factors for stable atmospheric conditions have been derived by Thom (1975), shown in Equation 2.27, and for unstable conditions by Paulson (1970) shown in Equations 2.28 to 2.30.

$$\Psi_M = \Psi_H = \Psi_\chi = \frac{5.2\,(z-d)}{L}$$

Equations 2.27

$$\Psi_M = -2\ln\left(\frac{1+x}{2}\right) + \ln\left(\frac{1+x^2}{2}\right) - 2\,TAN^{-1}(x) + \frac{\pi}{2}$$

Equation 2.28

$$\Psi_H = \Psi_\chi = -2\ln\left(\frac{1+x^2}{2}\right)$$

Equations 2.29

Where TAN^{-1} is in radians and

$$x = \left[1 - \frac{16\,(z-d)}{L}\right]^{0.25}$$

Equations 2.30

Equation 2.25 can be solved using linear regression analysis treating the term $u\{z-d\}$ as the y-variable and $\left[\ln(z-d)+\Psi_M\right]$ or $\left[\ln(z-d)-\Psi_M\right]$ as the x-variable. The eddy velocity can then be calculated from the gradient of the regression (u_*/k) and z_0 can be determined from the y-intercept ($[u_*/k]\ln[z_0]$). The eddy concentration and the height at which concentrations equal zero, $z\{\chi=0\}$, can be evaluated from a similar analysis of Equation 2.26. Fluxes can then be directly calculated from the eddy concentration and eddy velocity using Equation 2.24. A similar analysis can be performed to calculate sensible and latent heat fluxes using Equations 2.7 and 2.8.

Whilst the aerodynamic gradient method is theoretically robust, except immediately above or within a vegetated canopy (Raupach and Legg, 1984), the application of the method in the field unavoidably introduces some error terms. These errors relate to uncertainties in the determination of the stability correction terms, measurement uncertainties and uncertainties due to the violation of the constant flux layer assumptions.

The correction factors for non-neutral atmospheric stability are semi-empirical and fairly approximate. Hence, during extremely stable or unstable conditions the correction terms become large and fluxes become increasingly more uncertain. This is particularly a problem during periods when large-scale shifts in stability occur (dusk and dawn). As a

result for these uncertainties Yamulki *et al.* (1996) avoided determining fluxes in non-neutral conditions altogether, whilst other researchers (*e.g.* Sutton, 1990) often flag data collected during extremely non-neutral conditions as being highly uncertain.

Measurement uncertainties can also influence the determination of fluxes using the gradient method. Errors in u_* are typically small, with 95 % confidence intervals being typically less than 10 % of the mean (Duyzer *et al.*, 1992). As NH_3 is a notoriously difficult gas to measure in the field, it is often the determination of NH_3 concentration gradients that dominate error terms. For example, errors in NH_3 concentration measurements reported by Sutton (1990) and Duyzer *et al.* (1992) resulted in random errors in the determination of fluxes that typically exceeded the magnitude of the flux. Heat fluxes are considerably less problematic and generally measurement errors range between 10 - 30 % (Baldocchi *et al.*, 1988) and are attributed to the semi-empirical stability correction factors. Further corrections are often required for slow depositing gases to account for the vertical variation in the density of air, however as NH_3 fluxes often result in pronounced vertical gradients these correction factors are widely ignored.

A further limitation of the aerodynamic gradient method can occur due to the violation of the constant flux layer assumption. Horst and Wiel (1994) found that fetch to height ratios can exceed 1000:1 during stable conditions and can be up to 200:1 for neutral conditions. As a result, measurements made using the "rule of thumb" fetch to height ratio of 1:100 were shown by Horst and Wiel (1994) to be in error by 20 % for neutral conditions and more than 50 % for stable conditions. Furthermore, advection errors, due to heterogeneity in the upwind source or sink field, and storage errors, due to temporal variations in the concentration measurements, can significantly affect flux determinations. Sutton *et al.* (1993a) derived simplified formulae for the calculation of storage fluxes (F_{st}), shown as Equation 2.31, and advection fluxes (F_{ad}), shown as Equation 2.32. They found that errors due to these processes were important when considering measurements of slow depositing gases measured at large heights above the surface, though for NH_3 fluxes, errors were thought to be small (in the region of 10 – 20 %). Advection errors are increasingly significant close to strongly emitting sources and, due to their height dependence, are difficult to account for using Equation 2.32. Consequently, advection errors present a major limitation to the determination of fluxes using flux-gradient methods in such regions.

$$F_{st}\{z-d\} = -\frac{d\chi}{dt}(z-d)$$
<div align="right">Equation 2.31</div>

$$F_{ad}\{z-d\} = -u\frac{d\chi}{dx}(z-d)$$

Equation 2.32

2.4.3   Methods that do not assume a constant flux layer

It is clear from the above considerations that whilst constant flux layer methods can estimate fluxes over large uniform areas they can be in substantial error over short fetches or when determining fluxes in regions where advection errors may occur. Consequently, micrometeorological mass balance methods were developed to estimate fluxes from relatively small plots (<50 m fetch) such as fields treated with slurry or grazed pasture.

The mass balance method, developed by Denmead *et al.* (1977), has a simpler theoretical basis than the constant flux layer methods previously discussed. Surface vertical fluxes are estimated from the difference between the integrated horizontal advective flux entering and exiting a plot. The mass balance method assumes that lateral dispersion is negligible and that the horizontal advective flux is much greater than the horizontal diffusive flux.

Wilson and Shum (1992) investigated the assumption that lateral dispersion could be ignored using a "Random Walk" atmospheric dispersion model. This model is discussed in detail in Chapter 3, Section 3.2.3. Their numerical experiments focussed on the dispersion of material from a circular source to instrumentation at the centre of the source, a method often used in the field to estimate NH_3 emission fluxes. They found that lateral dispersion became a significant transport pathway when the source size was small (radius < 10 m) or had a high aerodynamic roughness length (z_0= 0.1 m). Errors in the method due to lateral dispersion could be as high as 52 % in extreme situations (radius = 2.5 m, z_0= 0.1 m). However, for more usual situations the error terms were less than 10 % (radius = 20 m, z_0 = 0.01 m).

The assumption that the horizontal advective flux is much larger than the horizontal turbulent diffusive flux (the dispersion of material against the mean wind) was investigated in wind tunnel studies by Raupach and Legg (1984) and numerically by Phillip (1997). Raupach and Legg (1984) found that the horizontal turbulent diffusive flux could account for approximately 10 % of the net flux, though the relative importance was found to reduce with distance from the source. Phillip (1997) confirmed the results of Raupach and Legg (1984) finding that the influence of the horizontal turbulent diffusive flux on the net vertical flux, and on downwind air concentrations, was negligible.

Denmead *et al.* (1977) demonstrated that a two dimensional mass balance may be constructed, as shown in Equation 2.33, where X' is the fetch, χ_g is the downwind concentration and χ_b is the upwind concentration.

$$F_\chi = \frac{1}{X'} \int_{z_0}^{z_p} \overline{\chi_g u} - \overline{\chi_b u}\ dz \qquad\qquad \text{Equation 2.33}$$

Measurements of the vertical profile of horizontal flux ($\overline{\chi u}$) are integrated between the surface (z_0) and the top of the plume (z_p), as shown in Equation 2.33. This integration is often conducted numerically, using either trapezium or Simpson's rules. The measurement of vertical profiles of horizontal flux can be labour intensive and logistically difficult due to the upper height of the plume varying with fetch and atmospheric stability. Typical ratios of fetch to plume height are in the order of 1:10, hence measurements would be required at a height of 5 m at the centre of a 50 m radius plot.

A simplified mass balance method was suggested by Wilson *et al.* (1982) and verified by Wilson *et al.* (1983). This method was developed using a "Random Walk" atmospheric dispersion model to investigate the vertical distribution of the ratios of horizontal to vertical flux in the atmosphere. A height (termed z_{inst}) was identified which, for a given roughness length and fetch, the ratio of horizontal to vertical flux was approximately independent of the stability of the atmosphere. An example of such a calculation is shown in Figure 2.4. Wilson *et al.* (1982) tabulated values of the z_{inst} height for various scenarios, allowing the experimental calculation of surface-atmosphere fluxes from measurements at a single height.
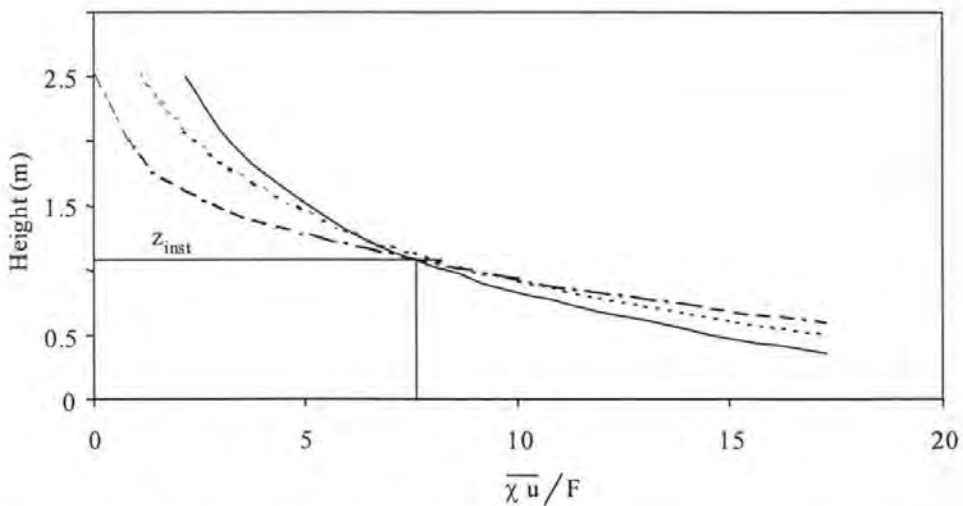
Figure 2.4: Model simulation of the height dependence of the ratio of horizontal to vertical flux estimated for three stability conditions (········: neutral, ———: highly unstable and –·–·–: highly stable). Reproduced from Wilson *et al.* (1983).

McInnes *et al.* (1985) evaluated the z_{inst} method against measurement data and the predictions of an analytical atmospheric dispersion model. They found that errors in individual measurements of air concentration, or horizontal flux, could lead to significant errors when determining fluxes using the z_{inst} method. McInnes *et al.* (1985) advocated the use of dispersion model predictions and measurements at several heights thus reducing the error terms. However, this conclusion is open to some criticism, as it does not address whether the error terms associated with the z_{inst} method could have been reduced by collecting multiple samples at the z_{inst} height.

The work of McInnes *et al.* (1985) does highlight the most significant limitation of the mass balance method, that is, that the method becomes unreliable when $\overline{\chi_g u} \longrightarrow \overline{\chi_b u}$. This has resulted in the use of the mass balance method being restricted to situations where the experimental area is a significant source, such as the emission of NH₃ from a slurry treated field.

A mass balance analysis can also be useful for determining the emission flux from naturally ventilated farm buildings. However, the application of the previously described micrometeorological techniques would be inappropriate given the complex flows and inhomogeneous source distributions that characterise such structures.

Assuming that there is no significant import of atmospheric NH₃ into the building, fluxes (in mass s^{-1}) can be calculated from the buildings ventilation rate (v) and the average air concentration of NH₃ in the building ($\overline{\chi_g}$), Equation 2.34.

$$F_\chi = v \, \overline{\chi_g}$$ Equation 2.34

Equation 2.34 is simple to solve for forced ventilated buildings (*e.g.* Amon *et al.*, 1995), however when investigating the emission from a naturally ventilated building both v and $\overline{\chi_g}$ terms can show a considerable spatial variability.

Demmers *et al.* (1998) used a passive tracer, carbon monoxide (CO), to determine the mean ventilation rate of a building. A CO mass balance was constructed from measurements of the difference in CO concentration at the inlets (χ_i) and outlets (χ_o) of the building divided by the emission flux (F_{CO}), shown in Equation 2.35. Inlets and outlets were specified from temperature differences (such that ambient air entering the building

would be cooler than air exiting the building) or were specified from differences in CO air concentrations.

$$v = \frac{\chi_i - \chi_o}{F_{CO}}$$

Equation 2.35

Air concentrations of NH$_3$ within the building were measured with a modified chemiluminescence NO$_x$ analyser following the oxidation of NH$_3$ to nitric acid. Ventilation rates were determined at the same points as NH$_3$ concentrations, allowing the calculation of point mass fluxes (μg s^{-1}) which could be integrated to estimate the overall flux from the building. This method allowed the calculation of high time resolution fluxes of NH$_3$ from the building. However, Demmers *et al.* (1998) were critical of the flux estimations during periods of high external wind speed, when the method to determine the ventilation rate performed poorly and the more dilute air concentrations (< 220 μg NH$_3$-N m^{-3}) were difficult to detect.

A theoretically simpler method was developed by Phillips *et al.* (1998) using passive flux samplers, "Ferm tubes" as described in Ferm (1986). Ferm tube samplers, described in full in Chapter 6, Section 6.2.2, allow the direct calculation of fluxes across a plane. The net flux across a plane (either horizontal or vertical) was calculated by applying the Ferm tube samplers in pairs facing in opposite directions. The net emission flux for each ventilation point was then calculated as the product of the average net flux and the open face area of the ventilation point (*A*) being evaluated. The net emission flux from the building was calculated as the algebraic sum of the emission fluxes occurring at each of the openings, shown as Equation 2.35.

$$F_\chi = \sum \frac{\overline{u\chi}}{A}$$

Equation 2.35

Phillips *et al.* (1998) validated their method using 32 pairs of Ferm tubes mounted in the Yorkshire boarding and roof of the naturally ventilated Silsoe Research Institute (SRI) Structures Building. The flux from the building, estimated using the Ferm tube samplers, was compared with the predefined release rate of NH$_3$ in the building. Phillips *et al.* (1998) found that 62 % of the released NH$_3$ was accounted for using their method. They attributed the underestimate to the offset between the inlet of the Ferm tube samplers and the Yorkshire boarding of the building. The empirical correction factor determined from the capture-recapture experiment was applied by Phillips *et al.* (1998) to subsequent field experiments.

2.5   SELECTION OF METHODS

This section presents the selection of suitable methods to determine the emission and local deposition of NH_3 volatilised from slurry applied to grassland and from naturally ventilated farm buildings.

The mass balance method was selected to determine NH_3 emissions from slurry spreading as it is both simple and robust. This method was preferable to flux-gradient techniques as it does not require a large uniform upwind fetch. The application of slurry to a large area (such as 200 m x 200 m) would be highly labour intensive and very unlikely to produce a region of constant flux due to the time lapse between the first and last applications.

The Ferm tube method, developed by Phillips *et al.* (1998), was selected to measure emission fluxes from naturally ventilated farm buildings, based on its lower cost and lower labour intensity when compared with the CO balance method (Demmers *et al.*, 1998). Errors due to the offset of the Ferm tubes samplers were identified as being a weakness of the method. The empirical correction factor, discussed in Phillips *et al.* (1998), was applied to account for these errors.

As slurry is often spread on relatively uniform agricultural land, many of the criteria are met for the application of micrometeorological techniques to estimate local surface-atmosphere exchange fluxes. However, a significant advection correction was required in order to apply conventional flux-gradient methods within an advected plume. These advection corrections were investigated using an analytical atmospheric dispersion model, the identification and development of this model is detailed in Chapter 3. The verification of the corrected flux-gradient method is discussed in Chapter 4.

The N balance method, as used by Cowling and Lockyer (1981) and Sommer (1988), was selected for determining the local surface-atmosphere exchange of NH_3 downwind of the farm building. This method is well suited for determining time-average (net) fluxes and has the ability to provide some insight into the physiological processes that regulate NH_3 deposition to plants. Weaknesses of this method were identified relating to the accurate determination of the inputs to the N balance. Therefore, the methods used by Cowling and Lockyer (1981) and Sommer (1988) were revised in Chapter 6 to consider replicate sampling, experimental controls and background samples. Furthermore, a spike-recapture experiment was conducted in Chapter 7 to experimentally validate the revised method.

3

REVIEW, SELECTION AND DEVELOPMENT OF SHORT-RANGE ATMOSPHERIC DISPERSION MODELS

3.1   INTRODUCTION

Previous chapters in this thesis have reviewed the literature and identified methods used by other researchers to measure the surface-atmosphere exchange of NH_3. However, methods were also required to evaluate the atmospheric dispersion of NH_3 and to determine the advection terms to enable the use of flux-gradient micrometeorological methods close to a source. Atmospheric dispersion is typically evaluated using numerical models. A selection of these models is reviewed in this chapter and appropriate models to simulate short-range dispersion and deposition from slurry applications and farm buildings were identified.

3.2   REVIEW OF MODELLING METHODS

Atmospheric dispersion models that are typically used to estimate the short-range dispersion of gases can be grouped into three categories. In the order of increasing complexity, these are: Gaussian plume, K-theory, and Random Walk. The general equation for most mathematical treatments of atmospheric diffusion is shown in Equation 3.1, where u, v and w are the alongwind, crosswind, and vertical components of the wind field respectively and x, y and z are the related co-ordinates from the plume centreline (Pasquill and Smith, 1983).

$$\frac{\partial \chi}{\partial t} = -\left[\frac{\partial(u\chi)}{\partial x} + \frac{\partial(v\chi)}{\partial y} + \frac{\partial(w\chi)}{\partial z} \right]$$ Equation 3.1

Pasquill and Smith (1983) showed that in a turbulent system properties have both mean and turbulent components, illustrated in Equation 3.2.

$$u = \bar{u} + u', \quad v = \bar{v} + v', \quad w = \bar{w} + w', \quad \chi = \bar{\chi} + \chi' \qquad \text{Equation 3.2}$$

Using the decomposition illustrated in Equation 3.2, Equation 3.1 can be rearranged to give Equation 3.3, from which the majority of atmospheric dispersion models are derived.

$$\frac{\partial \chi}{\partial t} = -\bar{u}\frac{\partial \chi}{\partial x} - \bar{v}\frac{\partial \chi}{\partial y} - \bar{w}\frac{\partial \chi}{\partial z} - \left[\frac{\partial(\overline{u'\chi'})}{\partial x} + \frac{\partial(\overline{v'\chi'})}{\partial y} + \frac{\partial(\overline{w'\chi'})}{\partial z} \right] \qquad \text{Equation 3.3}$$

3.2.1 Gaussian plume models

Gaussian plume models, discussed in detail in Clarke (1979) and Pasquill and Smith (1983), are widely used to predict short-range atmospheric dispersion, over distances of up to a few tens of kilometres from a source. The equation for turbulent diffusion (Equation 3.3) can be solved analytically assuming steady state conditions, homogeneous turbulence, and a constant wind speed with height (for example see Yeh and Huang, 1975). The resulting equation, predicting ground level air concentrations downwind of a surface point source in an unbounded atmosphere (that is, without the physical blocking of dispersion by an upper inversion layer), is a Fickian expression of turbulent diffusion, Equation 3.4.

$$\chi\{x, y, z = 0\} = \frac{F_\chi}{2\pi \bar{u} \, \sigma_z \, \sigma_y} \exp\left(\frac{-y^2}{2\sigma_y^2} \right) \qquad \text{Equation 3.4}$$

Where F_χ is the emission flux, σ_y and σ_z are the lateral and vertical standard deviations of the plume and x, y and z are the alongwind, crosswind and vertical positions of the receptor point along the centreline of the plume.

Simple "turbulence typing" schemes are often used to determine appropriate values for σ_y and σ_z following the determination of the "stability class" of the atmosphere. The separation of atmospheric stability, which has a continuous variation, into discrete stability classes was originally proposed by Pasquill (1961). In general, the stability of the atmosphere is separated into six classes ranging from A-F. These classes correspond to a range of conditions from highly unstable (A) to neutral (D) through to highly stable (F). Golder (1972) derived a relationship between the Pasquill (1961) stability classes and the Monin-Obukhov stability length (L) for a range of roughness lengths.

Several researchers have proposed schemes for calculating σ_y and σ_z, for details refer to the reviews of Gifford (1976) and Pasquill and Smith (1983). As an example, the parameterisations of Briggs (1974) for the determination of σ_z and the turbulent component of σ_y, termed σ_{yt}, are shown in Table 3.1. The calculation of σ_y accounting for both σ_{yt} and

the meandering of the plume caused by wind direction fluctuations is shown in Equation 3.5, σ_θ is the standard deviation of the wind direction in radians.

Pasquill Class	σ_{yt} (m)	σ_z (m)
A	$0.22\,x\,(1+0.0001\,x)^{-0.5}$	$0.20\,x$
B	$0.16\,x\,(1+0.0001\,x)^{-0.5}$	$0.12\,x$
C	$0.11\,x\,(1+0.0001\,x)^{-0.5}$	$0.08\,x\,(1+0.0002\,x)^{-0.5}$
D	$0.08\,x\,(1+0.0001\,x)^{-0.5}$	$0.06\,x\,(1+0.0015\,x)^{-0.5}$
E	$0.06\,x\,(1+0.0001\,x)^{-0.5}$	$0.03\,x\,(1+0.0003\,x)^{-1}$
F	$0.04\,x\,(1+0.0001\,x)^{-0.5}$	$0.016\,x\,(1+0.0003\,x)^{-1}$

Table 3.1:   Formulae recommended by Briggs (1974) for estimating dispersion in open country conditions, valid for downwind distances (x) between 100 m and 10 km.

$$\sigma_y = \sqrt{\sigma_{yt}^{\,2} + (\sigma_\theta x)^2}$$

Equation 3.5

The Gaussian plume formula has several advantages over other modelling methods. These include the conceptual simplicity of the method, and, due to the symmetry of the plume calculations, the ease of which if can be modified.

Dispersion from an elevated point source, including the reflection of material at the surface and at the upper inversion layer height (a) can be calculated by introducing virtual source reflection terms. These reflection terms are denoted as $f\{h,z,a\}$ and are shown in Equation 3.6. Air concentrations from elevated sources can be calculated from the product of Equations 3.4 and 3.6.

$$f\{h,z,a\} = \exp\left[\frac{-(z-h)^2}{2\sigma_z^{\,2}}\right] + \exp\left[\frac{-(z+h)^2}{2\sigma_z^{\,2}}\right] + \exp\left[\frac{-(2a+z+h)^2}{2\sigma_z^{\,2}}\right] +$$
$$\exp\left[\frac{-(2a+z-h)^2}{2\sigma_z^{\,2}}\right] + \exp\left[\frac{-(2a-z+h)^2}{2\sigma_z^{\,2}}\right] + \exp\left[\frac{-(2a-z-h)^2}{2\sigma_z^{\,2}}\right]$$

Equation 3.6

3.2.1.1   *Modifications to account for line and area sources*

Dispersion from other types of sources, such as line sources and area sources, can be simply calculated by modifying the lateral dispersion term in Equation 3.4. Pasquill and Smith (1983) demonstrate that dispersion from an infinitely long line source of unit width could be calculated from the crosswind integration of the product of Equations 3.4 and 3.6, shown as Equation 3.7. Smith (1995) derived an analytical expression to describe dispersion from a finite line source, shown in Equation 3.8. The term Y in Equation 3.8 is the length of the source.

$$\chi\{x,z\} = \frac{F_\chi}{\sqrt{2\pi} \, u \, \sigma_z} \, f\{h,z,a\}$$

Equation 3.7

$$\chi\{x,y,Y,z\} = \chi\{x,z\} \, 0.5 \left[erf\left(\frac{y+0.5Y}{\sqrt{2} \, \sigma_y}\right) - erf\left(\frac{y-0.5Y}{\sqrt{2} \, \sigma_y}\right) \right]$$

Equation 3.8

Smith (1995) also demonstrated a method to solve Equation 3.8 for a finite area source orthogonal to the wind (*i.e.* for wind blowing straight across a strip in the *x*-direction). Due to the complexities of reflections in the vertical, Equation 3.8 could not be integrated in the *x*-direction analytically and had to be solved by numerical integration. This integration was made between the limits of the downwind distance from the windward edge of the source (*x*) and the sum of *x* and the fetch (*X'*), Equation 3.9, where *x'* related to the positions of the individual sub-strips.

$$\chi\{x,X,y,Y,z\} = \int_x^{x+X'} \chi\{x',y,Y,z\} \, dx'$$

Equation 3.9

Of course, Equation 3.9 only relates to the situation where the wind direction is orthogonal to the source, a condition that rarely occurs in the field. Hence, it was desirable to derive an expression to account for the effects of any wind direction on the source. Smith (1995) presented the concept of sub-dividing an area source into a large number of finite width strips, which unlike the strips in Equation 3.8, are aligned orthogonal to the mean wind direction rather than to the overall dimensions of the source. Hence, both the width of individual strips (*Y'*) and their centreline offsets (*y'*) vary between strips in the more complex model, as shown in Figure 3.2. Unfortunately, Smith (1995) did not provide further expressions to determine the positions and dimensions of each of the contributory sub-strips.

3.2.1.2   Modifications to account for deposition

Wet and dry deposition also can be simply included in Gaussian plume models. Deposition processes are often treated by reducing the source term in the models (Jones, 1981). Effective source terms, F_χ' and F_χ'', can be derived to model the depletion of air concentrations due to dry and wet deposition respectively. The depleted source term due to dry deposition can be calculated from Equations 3.10 and 3.11 whilst the depleted source term due to wet deposition can be calculated from the time-of–flight (*t*) and the washout co-efficient (λ_w), as shown in Equation 3.12.

$$F_\chi' = F_\chi \, \exp(F_d\{x\})^{v_d/u}$$

Equation 3.10

$$F_d\{x\} = -\sqrt{\frac{2}{\pi}} \int_0^x \frac{1}{\sigma_z} \left[\begin{array}{c} \exp\left(-\dfrac{h^2}{2\sigma_z^{\,2}}\right) + \exp\left(-\dfrac{(h+2a)^2}{2\sigma_z^{\,2}}\right) \\[2mm] + \exp\left(-\dfrac{(h-2a)^2}{2\sigma_z^{\,2}}\right) \end{array} \right] \partial x'$$

Equation 3.11

$$F_\chi'' = F_\chi \exp(-\lambda_w t)$$

Equation 3.12

The overall depleted source term due to both wet and dry deposition processes (F_χ''') can be calculated using Equation 3.13.

$$F_\chi''' = \frac{F_\chi' F_\chi''}{F_\chi}$$

Equation 3.13
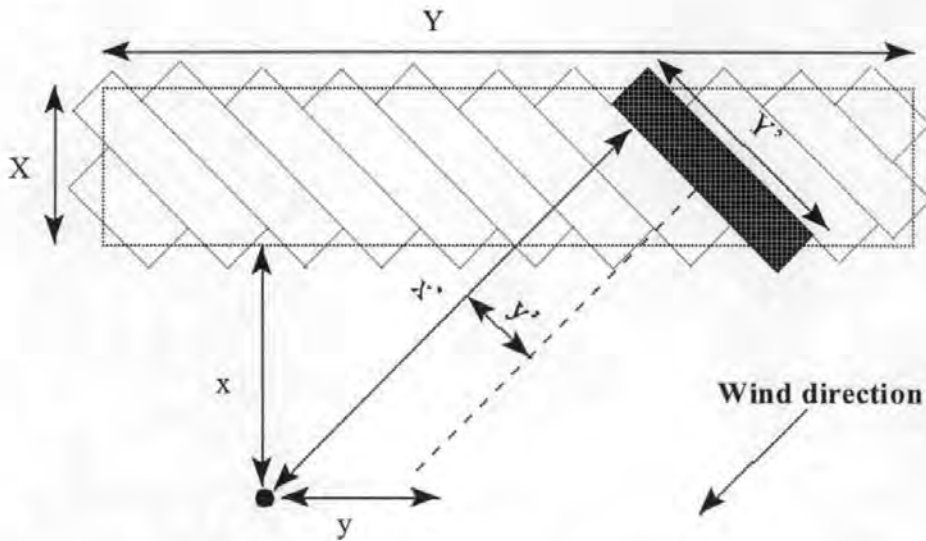
Figure 3.1:   A conceptual method to determine dispersion from an area source with any incident wind angle, from Smith (1995).

Horst (1977) criticised the source depletion method, as, due to the finite rate of vertical dispersion, dry deposition causes a reducing depletion of air concentrations with height above the ground. Horst (1977) derived the more complex surface-depletion model to include the vertical variation in plume depletion, shown in Equation 3.14.

$$\chi_{dep}\{x,z\} = \chi_{no\,dep}\{x,z\} - \int_0^x V_d \chi_{dep}\{x',z_0\} D_f\{x-x',z\} \partial x'$$

Equation 3.14

Where D_f is a dispersion factor defined as

$$D_f\{x,z\} = \frac{\chi\{x,z\}}{F_\chi}$$

Equation 3.15

Equation 3.14 is more difficult to solve than Equation 3.10 as depleted surface concentrations are required to calculate depleted elevated concentrations. Hence, Equation 3.14 must be initially solved iteratively to calculate an array of depleted surface concentrations, using each successive calculation of $\chi_{dep}\{x',z_0\}$ to calculate the subsequent

70

values. An initial assumption is also required to begin the calculations: that is that $\chi_{dep}\{x'\rightarrow 0, z_0\} = \chi_{no\ dep}\{x', z_0\}$. Once calculated, the array of depleted surface concentrations can be fed back into Equation 3.14 to allow the calculation of elevated depleted concentrations. Note that for both surface depletion and source depletion methods, V_d should be referenced to a height close to the surface (often z_0 is used).

A comparison between downwind vertical concentration profiles, calculated using the source depletion and surface depletion models is shown in Figure 3.2. As discussed by Horst (1977), the source depletion model overestimates ground level air concentrations and therefore the deposition flux. However, results from both models are usually close, leading to the conclusion of Corbett (1981) that the source depletion method was an adequate approximation for use within 100 km of a source.
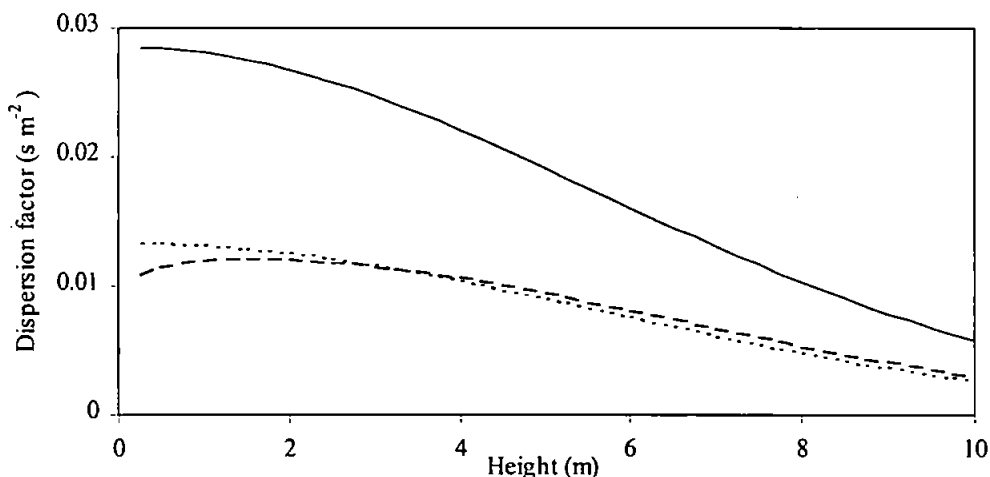
Figure 3.2: Comparison between crosswind integrated vertical concentration profiles determined using source depletion and surface depletion models. ———— : no deposition ········· : deposition calculated using a source depletion model, − · − · − : deposition calculated using a surface depletion model. Model calculations were made for $u = 5$ m s^{-1}, stability class D (Briggs parameterisation), $x = 100$ m, source height = 0 m, $V_d = 0.04$ m s^{-1}.

Horst (1984) developed a method to correct the simple source depletion model for the enhanced depletion of concentrations close to the surface. This model used a shape function, termed $P\{x,z\}$, to modify the Gaussian dispersion factor in Equation 3.11. This shape function was initially applied to calculate the overall depletion factor (F_χ') and subsequently applied to calculate concentrations above the ground level. The computational requirements for the method are quoted as being similar to those of the source depletion method, whilst the results are similar to those obtained with the surface depletion method.

3.2.1.3   Modifications to account for vertically inhomogeneous wind speeds

The previous sections have dealt with Gaussian plume formulae which assume that wind speed is constant with height. This is a reasonable assumption for advection in the mixed layer of the atmosphere, where wind speeds vary slowly with height, or for dispersion from tall industrial stacks (*e.g.* Clarke, 1979), with models for stack releases often extrapolating wind speeds from measurements at 10 m to the height of the chimney. However, an alternative approach is required for dealing with near surface level sources.

Carruthers *et al.* (1993) suggested using the wind speed extrapolated to the plume midpoint, $\bar{z}\{x\}$, where the midpoint is calculated using Equation 3.16. Alternatively, Smith (1995) suggested using the wind speed at the receptor height (z). However such a method is only applicable for near-field dispersion and is inappropriate for evaluating ground level air concentrations as, according to Equation 3.14, when $u = 0$ so $\chi = \infty$.

$$\bar{z}\{x\} = \frac{\int_o^\infty z\chi\{x,z\}\,\partial z}{\int_o^\infty \chi\{x,z\}\,\partial z}$$

Equation 3.16

3.2.1.4   Modifications to account for vertically inhomogeneous turbulence

The modification of Equation 3.14 to account for the vertical distribution of atmospheric turbulence is one of the major innovations of the "next generation" Gaussian plume model, the UK Atmospheric Dispersion Modelling System (UK-ADMS), as discussed in Carruthers *et al.* (1994).

The product of Equations 3.4 and 3.6 is used in the UK-ADMS model to calculate concentrations in neutral and stable atmospheric conditions. However σ_z and σ_y are determined, using Equations 3.17 and 3.18, from the vertical and lateral standard deviations of the turbulence velocities (σ_w and σ_v respectively) at the mean plume height as defined by Equation 3.16. Where, N is the buoyancy frequency, t is the travel time, and b is an empirical factor to ensure a smooth transition between the solution for elevated and surface releases.

$$\sigma_z = \sigma_w t \left(\frac{1}{b^2} + \frac{N^2 t^2}{1+2Nt} \right)^{-0.5}$$

Equations 3.17

$$\sigma_{yt} = \sigma_v t \left(1 + 15.6^{1/3}\, \frac{u_* t}{a} \right)^{-0.5}$$

Equations 3.18

The turbulence velocities, friction velocity and buoyancy frequency are calculated in the UK-ADMS boundary layer structure module, detailed in Carruthers and Weng (1992). These calculations use input data of wind speed and atmospheric stability, so obviating the need for the use of a turbulence-typing scheme.

For convective conditions a skewed Gaussian distribution is calculated using the convective velocity scale (w_*), Equation 3.19. The formulae for the calculation of dispersion in convective conditions use two Gaussian distributions and as such are more complex than those described above. Reference should be made to Carruthers *et al.* (1994) for further details.

$$w_*^3 = -\frac{u_*^3 h}{k\,L}$$ Equations 3.19

3.2.1.5   *Modifications to account for the effect of buildings on dispersion*

The modification of Gaussian plume models to calculate dispersion from a variety of sources over flat terrain has been discussed in previous sections. However, the aims of this thesis, detailed in Chapter 1, include the estimation of dispersion close to farm buildings, where the dispersion of material is likely to be influenced by the physical presence of the buildings.

The effects of buildings on local flows and dispersion have been reviewed in Hosker (1984). Hosker (1984) concluded that the regions influenced by the flow around the building could be subdivided as follows: the upwind face, the local re-circulation zone and an extensive far-field turbulent wake.

A complex re-circulating flow field can develop at the upwind face of a building as the stagnation pressure of the incident airflow increases with height, due to the wind speed shear. A stagnation point occurs at roughly two thirds of the height of the building (Hanna *et al.*, 1982). This pressure gradient forces the airflow downward thus creating a re-circulating zone, shown in Figure 3.3.
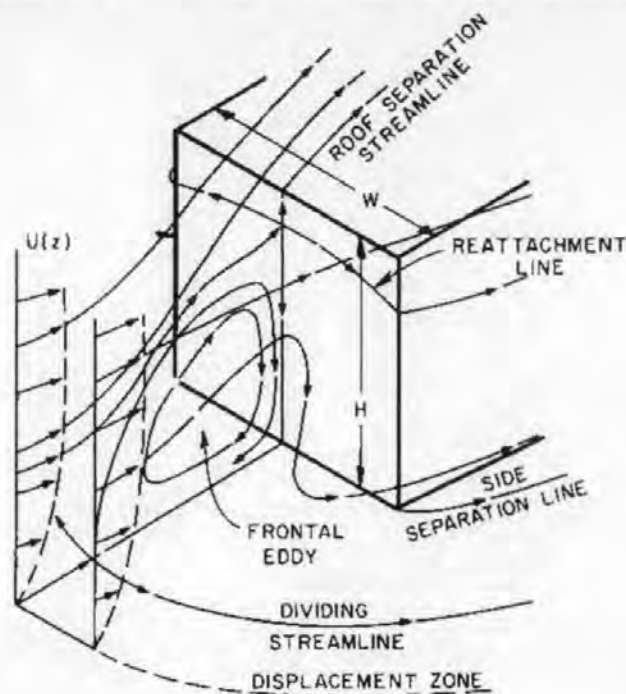
Figure 3.3:   Dispersion upwind of a building. Reproduced from Hosker (1984).

A larger cavity wake is created at the downwind side of a building. This region acts to entrain released material due to rapid mixing and re-circulation of turbulent eddies and the separation of wake flow from the mean flow that occurs over the roof and sides of the building. An impression of the turbulence and flow in and around the downwind cavity wake of a building is shown in Figure 3.4. In general, the cavity wake is thought to extend to approximately 1.5 times the building height in the vertical direction and 2.5 to 3.0 times the building width in the lateral direction (Dawson *et al.*, 1991). The mixing of material between the entrainment wake and the surrounding flow occurs through both advection and the momentary collapse of the entrainment wake (Robins *et al.*, 1997).

The simple model of the entrainment wake downwind of a building is only valid for wind directions orthogonal to the face of the building. Wind tunnel modelling, conducted by Huber (1989), showed that maximum ground level concentrations increased by a factor of between two and three for dispersion from a building at an oblique angle to the wind as opposed to that at an orthogonal angle to the wind. This results from the formation of strong roof corner vortices which efficiently transfer material into the main wake (Hosker, 1984).

A far-field turbulent wake occurs in the region following the reattachment of the mean flow streamlines to the surface. The far field wake is a region of enhanced turbulence,

reduced wind speed and can be affected by persistent trailing vortices particularly from a building at an oblique angle to the mean wind direction (Robins *et al.*, 1997).
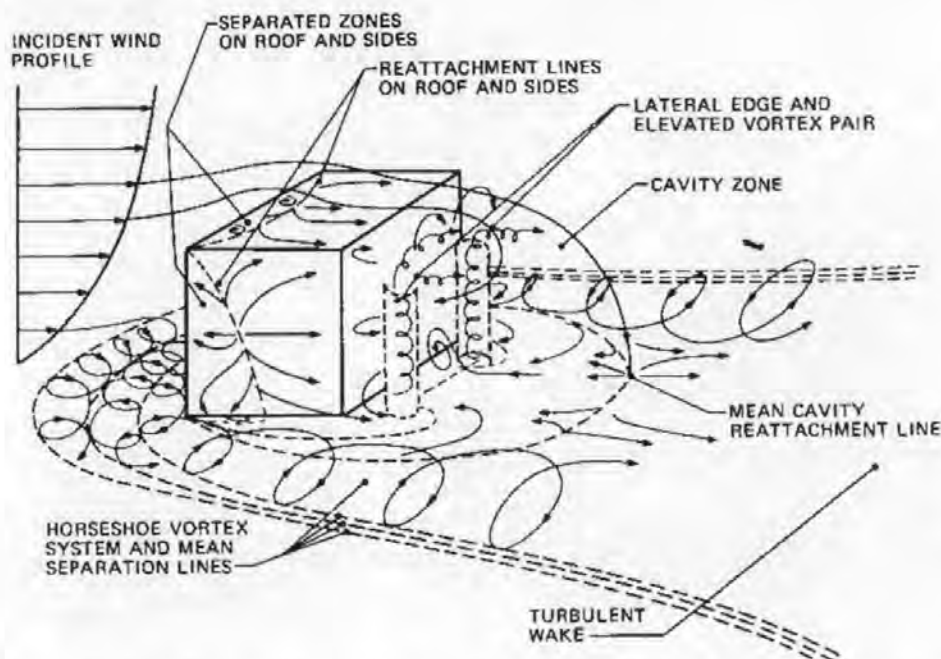
Figure 3.4: Cavity wake and flow downwind of a building. Reproduced from Hosker (1984)

Clearly, both flow and dispersion around a building are complex and difficult to treat realistically in a simple Gaussian plume model. Indeed, Computational Fluid Dynamics models are often used (*e.g.* Hill, 1997) which explicitly solve the equations governing pressure, flow and dispersion. However such modelling techniques are computationally expensive, two hours of meteorological data took five days to process in Hill (1997), and have been found to be sensitive to the initial specification of boundary conditions (Cowan *et al.*, 1997). Hence, interest remains in modifying simple models to perform complex problems.

A simple model for a fully entrained release, as is likely to occur from a farm building, was presented in Jones (1983). The height of the release was modified to a third of the building height, whilst a "virtual source" model was used to simulate the enhanced dispersion caused by the cavity wake. This virtual source model used the standard Gaussian plume model given by Equations 3.4 and 3.6 with the sigma terms modified according to Equation 3.20. Where H_b and W_b are the height and width of the building respectively.

$$\sigma_z{'}(x) = \sigma_z(x) + \frac{H_b}{3}, \ \sigma_y{'}(x) = \sigma_y(x) + \frac{W_b}{3} \hspace{3cm} \text{Equation 3.20}$$

A more complex model was developed by Robins *et al.* (1997) for integration with UK-ADMS. This model subdivided the flow around a building into five regions, shown in Figure 3.5, corresponding to the regions discussed in Hosker (1984).
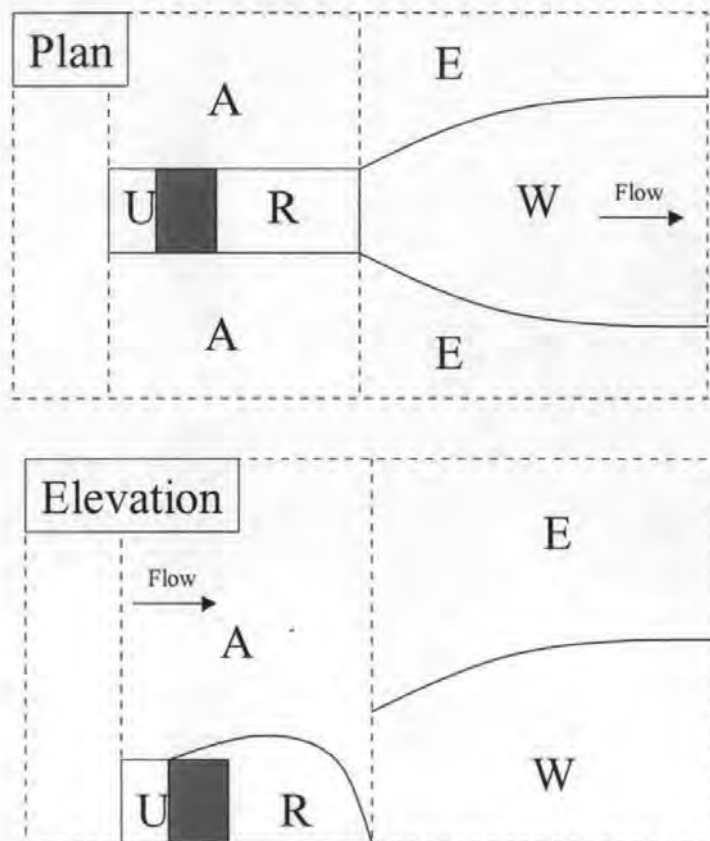
Figure 3.5:   Regions of the flow modelled using the UK-ADMS building wake model. A: remainder of the perturbed flow around the building, E: region external to the wake, R: re-circulating flow, W: turbulent wake, U: upwind region. Adapted from Robins *et al.* (1997).

A dual plume model was applied by Robins *et al.* (1997) for releases that were not fully entrained in the cavity wake. This model assumed that material entering the cavity wake would be uniformly dispersed and act as a second three dimensional volume source on re-emission. The near wake region (N) was assumed to be a re-circulating zone of constant air concentrations across the entire width of the building when $W_b < 3H_b$ or, when this condition is not met, a region of constant concentration in the central part of the near field wake of width $3H_b$. The dimensions of this region were assumed to be parallel sided in the x-y directions and elliptical in the x-z plane.

Concentrations in the surrounding region (S), generated by upwind sources, were calculated using the standard UK-ADMS Gaussian plume model formulae with the plume

centreline displaced by the mean streamline deflection. A constant eddy viscosity model was used to calculate the dimensions of the main turbulent wake region (W). Atmospheric dispersion in this region was calculated using the standard UK-ADMS Gaussian plume model with a reduced advection speed and modified dispersion coefficients (σ_y and σ_z) to account for the increased turbulence and reduced wind speed close to the building. Dispersion in the external region (E) was modelled accounting for the modification of plume trajectories caused by secondary flow generated by the decay of the main wake.

3.2.2 K-theory models

The application of K-theory to atmospheric dispersion has been discussed in Chapter 2 and forms the basis of many of the micrometeorological techniques used to estimate the surface-atmosphere exchange of trace gases. K-theory is also a popular method for modelling atmospheric dispersion (*e.g.* Asman, 1998; ApSimon *et al.*, 1994; Singles *et al.*, 1998).

Equation 3.3 can be shown to simplify to yield Equation 3.21 by assuming that $\bar{v} = \bar{w} = 0$ (*i.e.* that flow is over uniform flat terrain), steady state conditions occur, and by replacing the eddy flux terms in Equation 3.3 with their flux-gradient analogues (as discussed in Chapter 2, Sections 2.4.2.1 and 2.4.2.2). K_y and K_z in Equation 3.21 are the lateral and vertical eddy diffusivities and S is a source function.

$$u\frac{\partial \chi}{\partial x} = \frac{\partial}{\partial y}\left(K_y\ \frac{\partial \chi}{\partial y}\right) + \frac{\partial}{\partial z}\left(K_z\ \frac{\partial \chi}{\partial z}\right) + S\{x, y, z\}$$
$\qquad\qquad$ Equation 3.21

Assuming that there are no sources or sinks of material and that dispersion occurs from a infinite length line source (concentrations are termed as crosswind integrated), Equation 3.21 reduces to give Equation 3.22. This equation can be solved either analytically or numerically, using a finite difference scheme. It should be noted that following similarity assumptions K_z is replaced by K_χ in Equation 3.22.

$$u\frac{\partial \chi}{\partial x} = \frac{\partial}{\partial z}\left(K_\chi\ \frac{\partial \chi}{\partial z}\right)$$
$\qquad\qquad$ Equation 3.22

An "exact" analytical solution to Equation 3.22 was derived by Yeh and Huang (1975), assuming that profiles of wind speed (u) and eddy diffusivity could be approximated by simple power functions in the form of Equations 3.23 and 3.24. $K_\chi\{z_{ref}\}$ and $u\{z_{ref}\}$ are eddy diffusivity and wind speed at a reference height (z_{ref}) and β and α are the indexes of their vertical distributions.

$$K_\chi\{z\} = K_\chi\{z_{ref}\}\left(\frac{z}{z_{ref}}\right)^\beta$$

Equations 3.23

$$u\{z\} = u\{z_{ref}\}\left(\frac{z}{z_{ref}}\right)^\alpha$$

Equations 3.24

Huang (1979) reanalysed the Yeh and Huang (1975) function to derive expressions for both point and line sources, assuming that lateral diffusivity could be approximated by the Gaussian σ_y term. The formula for calculating dispersion from a surface or elevated infinite length line source without consideration of reflection terms at the upper inversion height is shown in Equation 3.25.

$$\chi\{x,z\} = \frac{F(z\,h)^p\,z_{ref}^{\ \beta}}{\lambda\,K_H\{z_{ref}\}\,x}\exp\left(-\frac{u\{z_{ref}\}\,z_{ref}^{\ r}(z^\lambda + H^\lambda)}{\lambda^2\,K_H\{z_{ref}\}\,x}\right)$$
$$\cdot I_{-v}\left(\frac{2u\{z_{ref}\}\,z_{ref}^{\ r}(zH)^q}{\lambda^2\,K_H\{z_{ref}\}\,x}\right)$$

Equations 3.25

Where I_{-v} is the modified Bessel function of the first kind and order $-v$ and v, λ r, p, and q are determined from the exponents of the wind speed and eddy diffusivity vertical profiles using Equations 3.26 to 3.30.

$$v = \frac{1-\beta}{\lambda}$$

Equations 3.26

$$\lambda = \alpha - \beta + 2$$

Equations 3.27

$$r = \beta - \alpha$$

Equations 3.28

$$p = \frac{1-\beta}{2}$$

Equations 3.29

$$q = \frac{\lambda}{2}$$

Equations 3.30

Equations 3.21 and 3.22 can also be solved numerically for situations where horizontal homogeneity cannot be assumed ($\overline{v} \neq \overline{w} \neq 0$) and variable meteorological conditions occur during the travel time of the plume using finite difference numerical techniques. Such schemes initially define a numerical grid structure with meteorological conditions applied to each cell. A vertical column of grid cells is often used when considering two-dimensional dispersion (in the x and z directions) (*e.g.* Singles *et al.*, 1998 and Asman, 1998). A further advantage of the numerical solution method is that surface fluxes can be easily incorporated as boundary conditions for the grid cells closest to the surface. This has a particular advantage for NH_3 research as complex deposition models can be applied and

changes in deposition velocity and roughness length due to variable land use types can be modelled.

The disadvantages of using a finite difference numerical method to solve Equation 3.21 or 3.22 are that they are computationally expensive and that numerical artefacts may occur when modelling dispersion close to a surface source (Pasquill and Smith, 1983). These artefacts are generated by the finite difference methods as material is assumed to be homogeneously distributed within each grid cell. Thus, exaggerated rates of vertical or horizontal dispersion will be predicted should the vertical distribution of grid cells not be sufficiently well resolved to approximate the steep vertical concentration gradients found close to a sources or the numerical timestep be sufficiently short to resolve the horizontal concentration gradient.

Further limitations on the general application of K-theory are discussed in Raupach and Legg (1984) and Pasquill and Smith (1983). These refer to the difficulties in applying K-theory to regions close to tall vegetated canopies or above the constant flux layer of the atmosphere. Another limitation, discussed in Hanna *et al.* (1982), is that K-theory models are only valid for the situation where the scale of atmospheric eddies are less than the scale of the plume. Hence, whilst K-theory is valid for ground level releases it fails when predicting dispersion from elevated sources.

3.2.3 Random Walk models

Previously discussed models describe the average behaviour of large numbers of dispersing molecules or particulates over time periods that are long in comparison to the time between the point of emission and the measurement location. An alternative method is to estimate the trajectory followed by an individual "particle" and to calculate the time averaged concentration as the sum of a large number of such "particles" that pass a receptor point during the duration of the measurement. The trajectories followed by an individual particle are randomised by the turbulent fluctuations that are encountered in the atmosphere. Such motions are often described as following a "drunkards walk" (Pasquill and Smith, 1983). A brief overview follows of the Random Walk modelling techniques described in Wilson *et al.* (1981a) and Wilson *et al.* (1981b).

The two dimensional (*x, z*) "Random Walk" model was developed by Wilson *et al.* (1981a) to track the positions of a large number of passive "particles" as they moved though a modelled atmosphere. This type of system is described as *Lagrangian* as the motions that

affect the position of a particle vary with time. This system contrasts with *Eulerian* motions that are not time dependent (*e.g.* $\bar{u}\{z\}$).

Wilson *et al.* (1981a) assumed that the fluctuating component of the horizontal wind, $u'\{t\}$, had a negligible influence on the dispersion of a particle when the travel time between the source and receptor was long in comparison with the timescale of the horizontal velocity fluctuations. Hence, the horizontal motion of a particle was expressed using the height dependent Eulerian horizontal velocity, from the familiar logarithmic wind profile equations (Chapter 2, Section 2.4).

Lagrangian vertical velocity fluctuations ($w'\{t\}$) are not constant over time as particles further from the surface experience motions with increasing time scales. Assuming that the vertical velocity scale (σ_w) is height independent then σ_w can be calculated for stable and neutral conditions using Equation 3.31. While, the height dependence of σ_w can be modelled in unstable conditions using Equation 3.32.

$$\sigma_w = 1.25\, u_*$$

Equation 3.31

$$\sigma_w = 1.25\, u_* \cdot \left(1 + 4.1\frac{z}{-L}\right)^{1/3}$$

Equation 3.32

The height dependent Lagrangian timescale, $\tau_L\{z\}$, of these motions can be calculated for neutral conditions using Equation 3.33, for stable conditions using Equation 3.34, and for unstable conditions using Equation 3.35.

$$\tau_L\{z\} = \frac{0.5\, z}{\sigma_w}$$

Equation 3.33

$$\tau_L\{z\} = \frac{0.5\, z \left(1 + 5\frac{z}{L}\right)^{-1}}{\sigma_w}$$

Equation 3.34

$$\tau_L\{z\} = \frac{0.5\, z \left(1 - 6\frac{z}{L}\right)^{0.25}}{\sigma_w}$$

Equation 3.35

The change in horizontal and vertical positions of each particle following a time step (Δt) can be calculated from the Lagrangian timescales and the instantaneous horizontal and vertical velocities using Equations 3.36 and 3.37 respectively.

$$\Delta x = u\{z\}\, \frac{\tau_L\{z\}}{\tau_L\{H\}}\, \Delta t_H$$

Equations 3.36

$$\Delta z = w_L\{t_H\} \frac{\tau_L\{z\}}{\tau_L\{H\}} \Delta t_H$$

Equations 3.37

Where H is a reference height and $w_L\{t_H\}$ is a random function of t_H calculated from a Gaussian distribution with a standard deviation of σ_w, and a mean of zero.

A bias velocity was added by Wilson *et al.* (1981b) to the instantaneous vertical velocity to account for convective (unstable) conditions. This bias velocity is defined in Equation 3.38.

$$\overline{w_L} = \sigma_w\{z\}\,\tau_L\{z\} \frac{\partial \sigma_w}{\partial z}$$

Equation 3.38

The predictions of the Random Walk model were compared with those of an analytical K-theory model (as discussed in Section 3.2.2) by Wilson *et al.* (1981a) and Wilson *et al.* (1981b). They concluded that both models produced almost identical results for dispersion downwind of an area source in the constant flux layer. This conclusion has since been confirmed by McInnes *et al.* (1985) and Sommer *et al.* (1995). The predictions of the Random Walk model (the z_{inst} method) have been shown to agree well with measured NH_3 concentration profiles by Pain *et al.* (1989), Sommer *et al.* (1995) and Wilson *et al.* (1983).

The main advantage of using the Random Walk modelling approach is that it can reliably simulate atmospheric dispersion within a canopy, where K-theory is not thought to be valid (Raupach and Legg, 1984). The main disadvantage of this modelling method is the computational expense of the calculations, requiring the tracking of approximately 5000 particles in order to obtain a single smooth vertical profile (Wilson *et al.*, 1983).

3.2.4   Selection of modelling methods

Three generic modelling methodologies have been reviewed in the previous sections of this chapter: Gaussian plume, K-theory and Random Walk. This section identifies the best methodology from these in order to address the original thesis aims (detailed in Chapter 1, Section 1.9) of modelling dispersion from ground level area sources (slurry applied to grassland) and farm buildings.

The Gaussian plume model is the least suitable of the reviewed modelling methods for estimating dispersion from ground level sources. This is due to the assumptions that wind speed and turbulence are vertically homogeneous in the simple versions of this model (*e.g.* Clarke, 1979) and homogeneous about the plume mid-point in the more complex versions of the model (Carruthers *et al.*, 1994). The K-theory finite difference models also are

difficult to apply in situations where there are strong vertical and horizontal gradients, which can result in exaggerated "numerical" diffusion. Modelling dispersion using analytical K-theory solutions compares well with Random Walk solutions for dispersion from area sources. Both these methods have been shown to agree with experimental data and both have a robust physical basis. However, the analytical K-theory solution is simpler to compute and is similar to the micrometeorological methods often used to calculate vertical NH_3 fluxes. Hence analytical K-theory modelling was identified as the most suitable approach for investigating dispersion close to a surface NH_3 source. The development and numerical testing of a K-theory model is detailed in later sections of this chapter and a comparison with field measurements is shown in Chapter 5.

The most scientifically robust methods to simulate building influenced dispersion are Computational Fluid Dynamics (CFD), as applied by Hill (1997). However these methods incur a high cost, both computationally and financially, and are sensitive to the specification of the boundary conditions of the modelling domain. CFD techniques are therefore best applied when investigating dispersion over short time periods when high resolution input data can be used. This thesis aims to estimate the time-average dispersion of NH_3 released from a farm building and therefore a more general approach is required. Gaussian plume models are simple to modify to include some of the generic aspects of dispersion in the wake of a building. The most scientifically robust method for including building influenced dispersion in such a simple model was identified as the building effects module contained in UK-ADMS (Robins *et al.*, 1997). The realism of the UK-ADMS model, using the buildings effects module was investigated in Chapter 7 by comparing the model predictions with field measurements.

3.3 DEVELOPMENT AND TESTING OF A K-THEORY MODEL

The analytical K-theory model developed by Huang (1979), describes the atmospheric dispersion of a non-depositing "passive" tracer over uniform flat terrain within the constant flux layer. This model assumes that wind speed and eddy diffusivity profiles can be approximated by simple power law functions. An operational model to predict the dispersion of NH_3 from a field spread with slurry, required the modification of the original Huang (1979) model to consider the geometry of a surface level area source and to include a realistic treatment of the dry deposition process. Chemical conversion of NH_3 in the atmosphere need not be included in a short-range model (<1 km from the source) as the

rates of chemical conversion (discussed in Chapter 1) are not thought to be sufficiently rapid to cause a substantial depletion of air concentrations.

This section reviews the assumption that power laws can simulate micrometeorological wind speed and eddy diffusivity profiles and presents an optimised method for this necessary simplification. The extension of the Huang (1979) modelling approach to consider area source geometries and dry deposition is also considered.

3.3.1   Testing and optimising the power law profiles

A fundamental assumption of the theory published by Huang (1979) is that complex micrometeorological profiles of wind speed and eddy diffusivity can be realistically approximated by simple power laws. These power laws enable the two dimensional advection-diffusion equation to be solved analytically. Methods to fit power law profiles to micrometeorological profiles are discussed in Tirabassi *et al.* (1986).

Micrometeorological equations to describe the wind speed profile, corrected for all atmospheric stabilities, are discussed in Chapter 2, Section 2.4.2.2. Simple power law profiles are often used to approximate the rather complex micrometeorological profiles. These power law profiles can be defined in terms of the wind speed and eddy diffusivity at a reference height and the indexes of their vertical distributions (α for wind speed and β for eddy diffusivity). The power law indexes can be calculated using Equations 3.39 and 3.40.

$$\alpha = \frac{u\{z_{ref}\} - \bar{u}}{\bar{u}}$$ Equation 3.39

$$\beta = \frac{K_\chi\{z_{ref}\} - \overline{K_\chi}}{\overline{K_\chi}}$$ Equation 3.40

Where the terms $\bar{u}$ and $\overline{K_\chi}$ are calculated by Equations 3.41 and 3.42.

$$\bar{u} = \frac{1}{z_{ref}} \int_{z_0}^{z_{ref}} u\{z\}\, dz$$ Equations 3.41

$$\overline{K_\chi} = \frac{1}{z_{ref}} \int_{z_0}^{z_{ref}} K_\chi\{z\}\, dz$$ Equations 3.42

Theoretically the power law profiles should realistically simulate their micrometeorological counterparts as the advective and eddy fluxes between the ground and the reference height are preserved by Equations 3.41 and 3.42 and the wind speed and eddy

diffusivity at z_{ref} are preserved by Equations 3.39 and 3.40. However, the indexes of the power law profiles are not independent of height and so the choice of reference height may influence the shape of the profile and so the performance of the model.

3.3.1.1   Testing power law wind speed profiles

The index of the wind speed profile (α) is a function of the Monin-Obukhov stability length (L) and roughness length (z_0). Figure 3.6 shows the relationship between z_{ref} and α for different values of L and z_0. Greatest deviation from the assumption of height independence can be seen when the profiles have a high degree of curvature caused by high roughness lengths and non-neutral atmospheric stabilities.
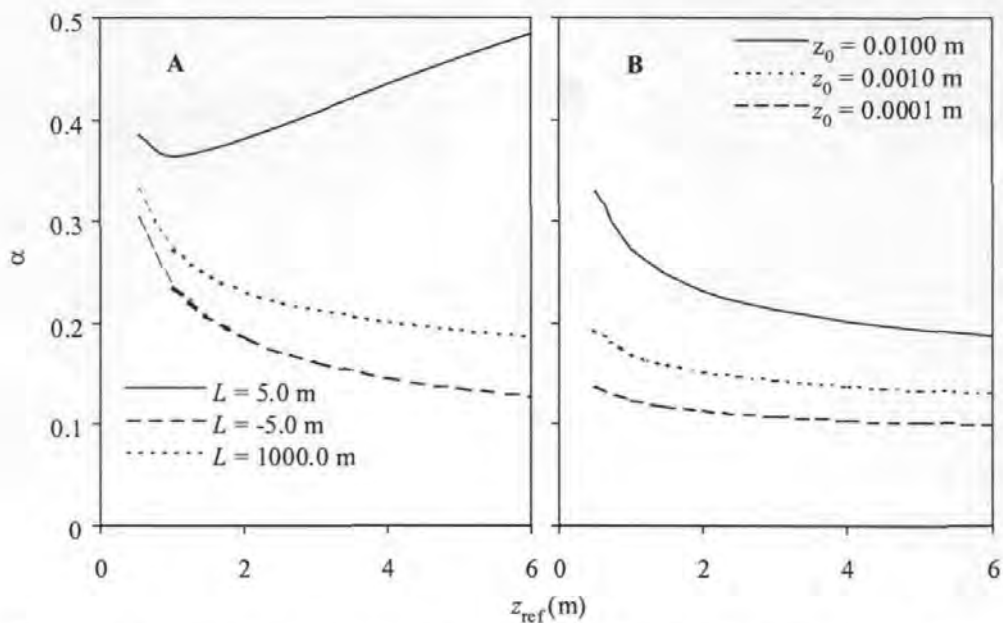
Figure 3.6:   Dependence of the index of the power law wind profile (α) on the reference height z_{ref} for **A**: variable Monin-Obukhov stability length (L), $z_0 = 0.01$ m: and **B**: variable roughness lengths (z_0), $L = 1000$ m.

3.3.1.2   Testing power law eddy diffusivity profiles

Theoretically the index of the power law eddy diffusivity profile (β) should be independent of reference height. However, due to the approximate nature of the power law parameterisation height dependence may be found, particularly when micrometeorological profiles show a high degree of curvature. The variation in β with z_{ref} is purely a function of the Monin-Obukhov stability length. Results are shown in Figure 3.7.

3.3.1.3   Optimising the power law profile fitting method

As single values of α and β were required by the model for mass to be conserved it was important that the errors associated with the dependence of these parameters on z_{ref} were minimised. Figures 3.6 and 3.7 show that a pronounced height dependence of α and β occurred during non-neutral stability conditions, with a high roughness length. It was clear that one must treat model predictions made during such conditions with caution. However, as the experiments conducted for this thesis were designed to realistically represent agricultural practices, the exclusion of such conditions would be inappropriate. An alternative solution was to identify an optimal reference height that minimised the error in model predictions across the height range of the field measurements.
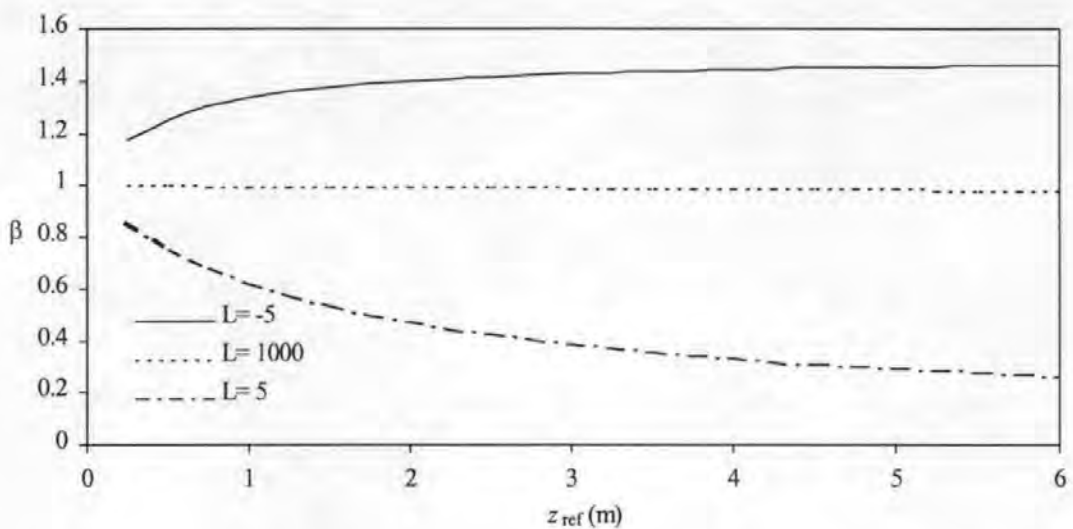
Figure 3.7:   Dependence of the index of the power law eddy diffusivity profile (β) on the reference height z_{ref} for neutral (L= 1000 m), stable (L= 5 m) and unstable (L= -5 m) atmospheric conditions.

Figures 3.8 and 3.9 compare micrometeorological (MM) and power law (POW) profiles of wind speed and eddy diffusivity respectively, calculated for contrasting atmospheric stabilities using power law reference heights of 1.0 m and 6.0 m. Due to the dependence of the power law indexes α and β on z_{ref} the micrometeorological and power law profiles diverge as the measurement height differs from z_{ref}. As the model was required to predict concentrations close to the surface then the best profile fit was concluded to be that calculated for a z_{ref} height of 1.0 m.
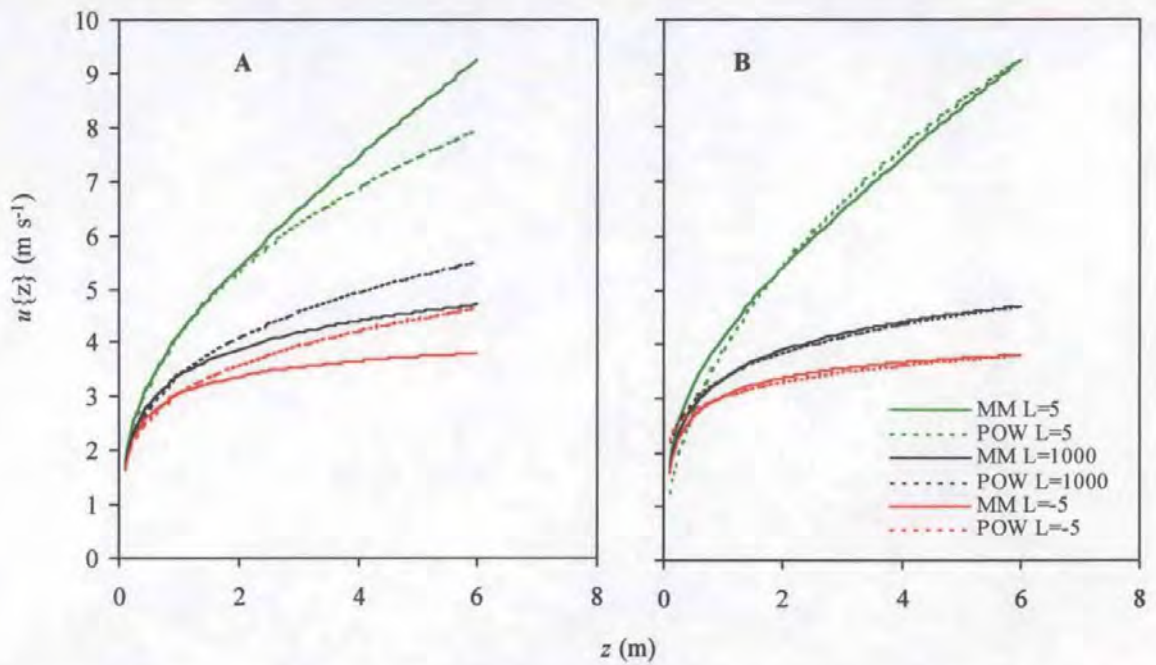
Figure 3.8:   Comparison of micrometeorological (MM) and power law (POW) wind speed profiles for three Monin-Obukhov stability lengths at two power law reference heights. **A**: z_{ref}= 1 m, **B**: z_{ref}= 6 m.
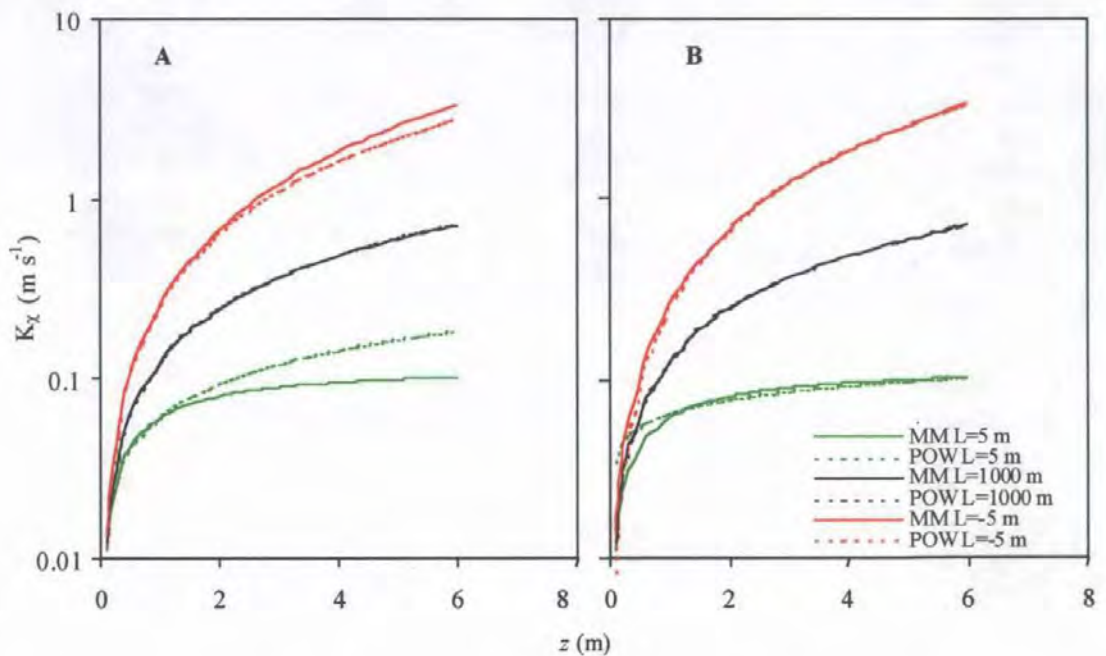
Figure 3.9:   Comparison of micrometeorological (MM) and power law (POW) eddy diffusivity profiles for three Monin-Obukhov stability lengths at two power law reference heights. **A**: z_{ref}= 1 m, **B**: z_{ref}= 6 m.

A two dimensional model was written, using the Huang (1979) solution, to investigate the variability in air concentrations caused by the choice of z_{ref}. The model was run using input

data of highly stable atmospheric conditions ($L= 5$ m) over a surface with a roughness length of 0.01 m. Vertical concentration profiles were modelled at three distances (10 m, 50 m and 100 m) from a uniformly emitting infinitely long line source (width= 15 m) and four values of z_{ref} were tested (0.5 m, 1 m, 3 m and 6 m). Results of this modelling study are presented in Figure 3.10.
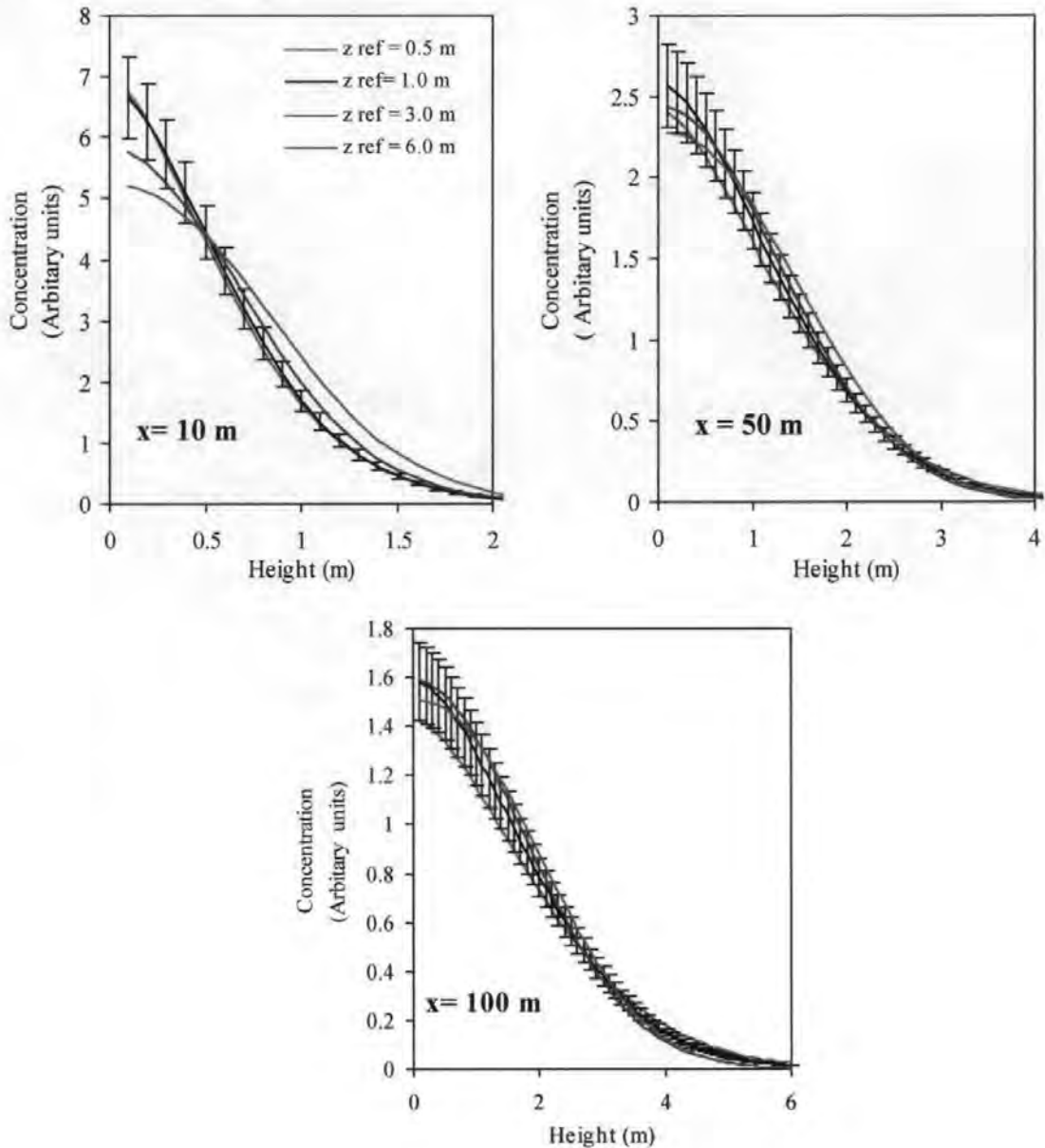
Figure 3.10: Comparison of modelled concentration profiles in stable conditions ($L= 5$ m) for a surface roughness length of 0.01 m using z_{ref} values of 0.5 m, 1.0 m, 3.0 m, and 6.0 m. Error bars are shown for +/- 10 % of the value of the profile for $z_{ref} = 1.0$ m. Three distances downwind of a strip source of width 15 m are shown.

The results shown in Figure 3.10 demonstrated that near surface air concentrations, at a downwind distance of 10 m, were underestimated when reference heights above 3 m were used. Better estimates of air concentrations at 10 m downwind of the source were made

using power law profile reference heights of 1.0 m or 0.5 m. Concentrations calculated at 50 m downwind were relatively insensitive to the choice of z_{ref}. Concentration profiles were also found to be relatively insensitive to the choice of z_{ref}, between 1.0 m and 6.0 m, at a downwind distance of 100 m, though the model predictions for $z_{ref} = 0.5$ m underestimated concentrations by approximately 10 %. As Figures 3.10 and 3.11 show a good agreement between micrometeorological and power law wind speed and eddy diffusivity profiles for $z_{ref} = 1.0$ m, the underprediction of concentrations when $z_{ref} = 0.5$ m can be explained as an artefact of the power law parameterisation. Similar results were obtained from tests conducted in neutral and unstable atmospheric conditions.

In conclusion, the errors associated with using power law profiles of wind speed and eddy diffusivity were minimised by using a power law reference height of 1.0 m. Errors in the predictions of the analytical K-theory models could be high if the z_{ref} value was not chosen with care, particularly when values of z_{ref} were considerably greater than the upper height of the plume or considerably lower than the plume mid height. Despite the poor agreement between power law and micrometeorological wind speed and eddy diffusivity profiles at heights greater than 3.0 m for a z_{ref} value of 1.0 m these inaccuracies were not evident in the concentration predictions. In conclusion, the Huang model was found to have a sound theoretical basis and to be theoretically capable of predicting the dispersion of NH_3 with a precision greater than 90 %.

3.3.2 Inclusion of source geometry effects in the model

Smith (1995) published several methods to include sources of different geometries in Gaussian plume models, as discussed in Section 3.2.1.1. Due to the similar analytical basis of the Gaussian plume and analytical K-theory approaches, such methods can be interchanged between the modelling methodologies. The source geometry effects that were considered when modelling dispersion from a field spread with slurry were those of an infinitely long area source, a finite length area source orthogonal to the wind, and a finite length area source at an oblique angle to the wind.

3.3.2.1 Simulation of dispersion from an infinitely long area source

Due to the linearity of the advection diffusion equation, (Equation 3.3) concentrations from several interacting plumes can be superimposed. Smith (1995) showed that concentrations downwind of an infinitely long, and finitely wide area source could be simulated by simply summing the contribution from a series of line sources spaced at intervals across the strip, Equation 3.9. The intervals between these line source elements determine the accuracy of

the numerical integration method, however the computation time increases as finer intervals are used. The optimal strip source integration interval was determined by investigating the variation in downwind concentrations for a range of integration intervals, results are shown in Figure 3.11. The reduction in integration interval, shown in Figure 3.11, caused an obvious increase in the precision of the predicted downwind concentrations. This increase was more apparent closer to the source. An optimal integration interval was determined of 0.1 m as the error in concentrations, even at 1.0 m downwind of the source, was less than 2 %.
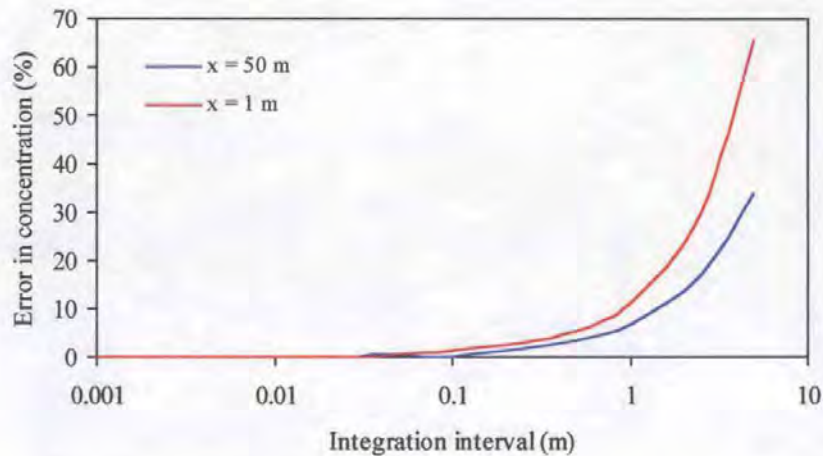
Figure 3.11:   Relationship between integration interval and the error in the resulting ground level concentration at 1 m and 50 m downwind of a 15 m wide infinite length area source. Other model parameters were $L= 1000$ m, $u_*= 0.3$ m s^{-1}, $z_0= 0.01$ m, $d= 0$ m and $z_{ref} = 1.0$ m.

3.3.2.2   Simulation of dispersion from a finite length area source orthogonal to the wind

Smith (1995) derived an analytical expression for integrating the Gaussian plume equation across the length of a finite line source, shown in Equation 3.8. Following the recommendation of Huang (1979), that lateral dispersion is closely approximated by the Gaussian σ_y term, the Gaussian method for determining dispersion from a finite length line source can be simply applied to an analytical K-theory model by substituting the $\chi\{x,z\}$ term from the K-theory model given by Equation 3.25 into Equation 3.8. The Briggs (1974) parameterisation of σ_{yt}, presented in Table 3.1, was used with stability classes derived from the Monin-Obukhov stability length following the recommendations of Golder (1972). It should be noted that, strictly speaking, the Briggs (1974) parameterisation is only applicable at distances greater than 100 m from a source. However, the back-extrapolation of the Briggs formulae can be justified as close to the

89

centreline of a long area source dispersion is largely unaffected by σ_y. Additional tests using a variety of schemes for calculating σ_y confirmed the insensitivity of the area source model to the specification of σ_{yt}.

3.3.2.3   *Simulation of dispersion from a finite length area source at an oblique angle to the wind*

Smith (1995) extended the method for estimating dispersion from a line source orthogonal to the mean wind direction to consider oblique wind angles, as discussed in Section 3.2.1.1. To the authors knowledge the methods of calculating values of y' and Y' have not been previously published. General forms of the trigonometric equations were derived to calculate values of x', y' and Y' (see Figure 3.1 for definitions) from input data on source dimensions, receptor position and wind direction. The resulting computational module, termed "SOURCEGEO", is detailed in Appendix 1.

The SOURCEGEO module was verified by comparing the numerical calculations of strip offsets and dimensions with hand calculations for the simple case of a source subdivided into five strips. The results of the K-theory dispersion model using the SOURCEGEO module were also compared with similar predictions from the infinite source model described in the previous section. The results of this comparison, shown in Figure 3.12, demonstrate that both models produced similar predictions when edge effects could be assumed to be insignificant. And, as to be expected, when the wind angle increased so the predictions diverged

3.3.2.4   *Simulation of dry deposition*

The surface depletion method, developed by Horst (1977), discussed in Section 3.2.1.2, was applied to include dry deposition in the K-theory model. This method was initially derived by Horst (1977) for use with the Gaussian plume dispersion model, though the K-theory dispersion calculations were simply included by substituting $\chi \{x,z\}$ from the K-theory model (given by Equation 3.25) into Equations 3.14 and 3.15.

A further modification was made to the Horst (1977) approach to model deposition downwind of an infinitely long area source. The dispersion factor, $D_f \{x\text{-}x', z\}$ in Equation 3.14 refers to the dispersion from the downwind sinks, hence the K-theory $D_f \{x\text{-}x', z\}$ was calculated by substituting Equation 3.25 into Equation 3.15. However $\chi_{no\ dep} \{x,z\}$ and $\chi_{dep} \{x',z= z_0\}$ both refer to dispersion from the source and therefore were calculated by

numerical integration of Equation 3.25 across the width of the strip, as discussed in Section 3.3.2.1. A further point to note is that Equation 3.14 only applies for crosswind integrated concentrations (*i.e.* downwind of an infinitely long source). When significant lateral dispersion terms apply, depleted concentrations were calculated by rescaling the results from Equation 3.25 by the ratio of $\chi_{no\,dep}\{x,y,z\}$ to $\chi_{no\,dep}\{x,z\}$.
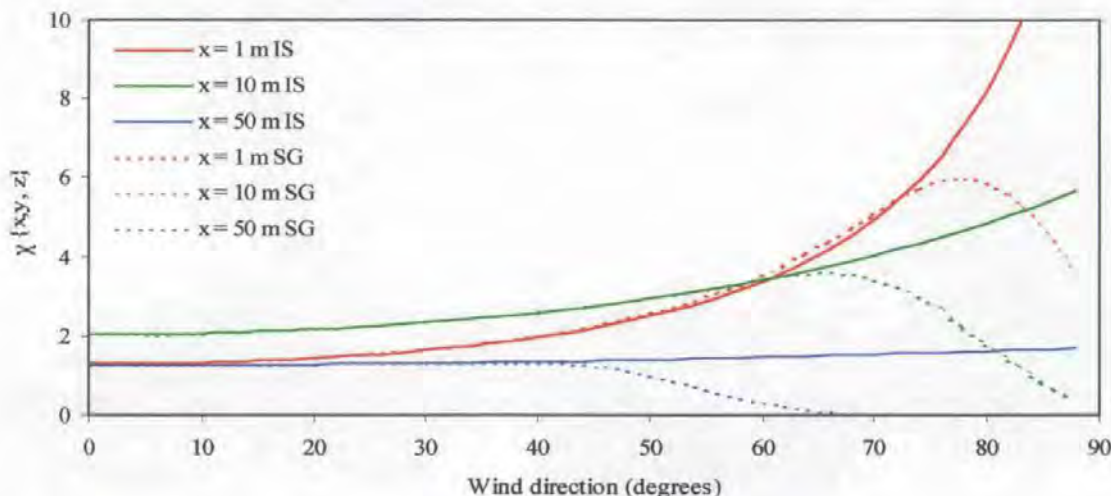
Figure 3.12: Comparison of the variation of air concentrations with centreline wind direction offset predicted using an analytical K-theory model with the source geometry of an infinite length area source (IS) and a finite length area source (SG). Three downwind receptor distances were used (0.1 m, 10 m and 50 m) and all simulations were made using input data of source width = 15 m, source length = 160 m, L = 1000 m, u_* = 0.3 m s^{-1}, z_0 = 0.01 and d = 0 m.

As Equation 3.14 was integrated numerically, a similar analysis to that shown in Figure 3.11 was required to determine the appropriate integration interval. Mean ground level concentrations, averaged between the downwind edge of the source and the receptor position, were determined for a range of atmospheric stability conditions and deposition integration intervals. The results of these tests are shown in Figure 3.13. An optimal integration interval of 0.1 m was identified from Figure 3.13 as only slight errors (4 – 6 %) were found during stable and neutral conditions. In unstable conditions the error terms increased to 12 %, though as the application of the stability correction factors becomes uncertain during such conditions a small error due to deposition integration interval was deemed tolerable.

3.3.2.5 Model implementation

An operational atmospheric dispersion model, specifically designed to provide realistic predictions of dispersion and local deposition downwind of a surface area source (NH_3

volatilisation from slurry treated grassland), was developed following the considerations detailed in the previous sections of this chapter. The model, referred to in later chapters, as the K-theory Atmospheric Transport and exCHange (KATCH) model, was coded in Visual Basic Applications Edition within the spreadsheet program Microsoft (MS) Excel. The KATCH model was implemented within MS Excel to reduce the demand for "front-end" coding and to allow the model to interchange data directly with other spreadsheets used to process meteorological and emissions data. The source code for the KATCH model and a description of the architecture of the program can be found in Appendix 1.
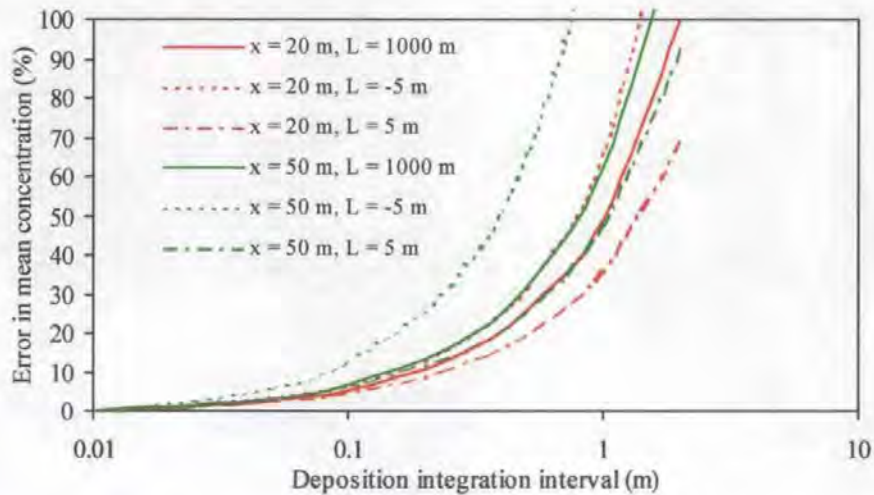
Figure 3.13: Variation in mean ground level concentration, over distances of 20 m and 50 m, with different values of deposition integration interval. Three atmospheric stabilities were used as model input ($L = 5$ m, $L = -5$ m and $L = 1000$ m), other model input were: strip width = 15 m, $u_* = 0.3$ m, $z_0 = 0.01$ m, $V_d = 0.04$ m s^{-1}, emission integration interval = 0.1 m.

3.3.3   Comparison between K-theory and Random Walk models

The Random Walk model developed by Wilson *et al.* (1981a), detailed in Section 3.2.3, was a very different dispersion modelling approach to that implemented in the KATCH model. However, the Random Walk model has been shown to produce realistic dispersion predictions for surface area sources (Wilson *et al.*, 1983). Furthermore, the Random Walk model has also been shown to agree well with the predictions of other K-theory models (Wilson *et al.*, 1981a; Wilson *et al.*, 1981b and McInnes *et al.*, 1985). Hence, the predictions of the Random Walk model provided a good dataset to verify that the KATCH model produced reasonable results. Prediction of vertical dispersion (as the non-dimensional ratio of horizontal to vertical flux) were transcribed from the graphs in Wilson *et al.* (1982) and Wilson *et al.* (1983). Comparable flux ratios were calculated using the KATCH model, results of this intercomparison are shown in Figure 3.14.
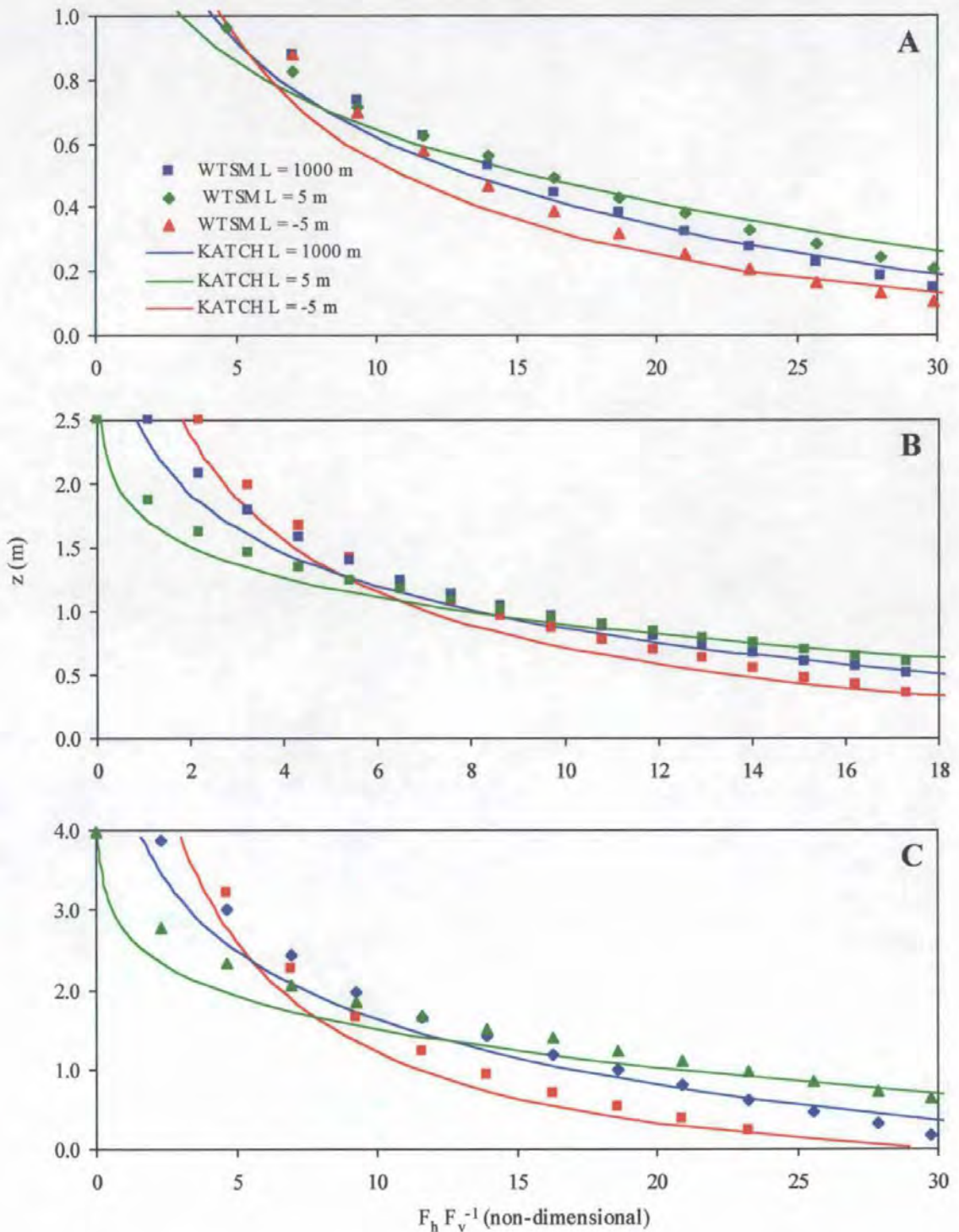
Figure 3.14: Comparison between vertical profiles of the non-dimensional ratio of horizontal to vertical flux predicted by two models: KATCH and the Random Walk model discussed in Wilson *et al.* (1981a) and Wilson *et al.* (1981b), termed WTSM. **A**: $z_0 = 0.002$ m, $X' = 20$ m, $d = 0$ m; **B**: $z_0 = 0.01$ m, $X' = 50$ m, $d = 0$ m; **C**: $z_0 = 0.005$ m, $X' = 25$ m, $d = 0.15$ m. Data in Figures **A** and **B** were transcribed from Wilson *et al.* (1982) whilst data in Figure **C** were transcribed from Wilson *et al.* (1983).

A good agreement was found between the predictions of both the KATCH and Random Walk models, shown in Figure 3.14, with the majority of predictions from both models

being within 20 % of each other. This provided some confidence that the KATCH model produced realistic dispersion predictions. A full validation of the KATCH model using field measurements was conducted in Chapter 5, Section 5.3.

3.4   CONCLUSIONS

Atmospheric dispersion models that could be used to determine the dispersion of NH_3 released from slurry spreading and from farm buildings have been reviewed in this chapter and appropriate models to fulfil the objectives of this thesis, as presented in Chapter 1 were identified. The UK-ADMS Gaussian Plume model, which has a detailed building effects module was selected for the farm buildings study, whilst a physically realistic analytical K-theory atmospheric dispersion model (KATCH) was developed for the slurry spreading experiments. The underlying assumptions of the KATCH model, relating to the realism of power law profiles of wind speed and eddy diffusivity, were tested and, where appropriate optimised. Further modifications were included in the KATCH model to account for area sources, the influence of oblique and orthogonal wind directions and to include a realistic treatment of dry deposition. Tests were also conducted to optimise the numerical integration techniques used to calculate dispersion and deposition from an area source. The KATCH model was shown to produce similar dispersion predictions to the Random Walk model developed by Wilson *et al.* (1981a) and Wilson *et al.* (1981b).

4

EMISSION, DISPERSION AND LOCAL DEPOSITION OF NH₃ VOLATILISED FROM CATTLE SLURRY: METHODS

4.1 INTRODUCTION

Methods used in this thesis to determine the emission, dispersion and local deposition of NH_3 released from slurry spreading are presented in this chapter. Method used by other researchers to estimate the surface-atmosphere fluxes of NH_3 were reviewed in Chapter 2. The micrometeorological mass balance method was identified, from the methods reviewed, as being suitable for estimating NH_3 emission fluxes in the field, although no methods could be identified to robustly estimate deposition fluxes immediately downwind of slurry applications.

Atmospheric dispersion models were reviewed in Chapter 3 and a physically realistic K-theory model was developed to predict downwind air concentrations, including both dispersion and deposition processes. This atmospheric dispersion model (termed KATCH) provided information on two important areas of uncertainty when considering surface-atmosphere exchange downwind of slurry spreading. These were: the advection terms for inclusion in micrometeorological methods and the influence of deposition on downwind concentrations.

This chapter presents the development and verification of a novel micrometeorological method for estimating the surface-atmosphere exchange of NH_3 over agricultural land immediately downwind of slurry spreading. This method was developed using micrometeorology and atmospheric dispersion modelling to solve the flux-gradient equation accounting for local advection. An experimental design for applying this method

is also presented in this chapter along with the instrumentation that was used to implement the experimental design.

4.2   DEVELOPMENT OF A MICROMETEOROLOGICAL METHOD

The short-range deposition of NH_3 was numerically investigated using the atmospheric dispersion model (KATCH) discussed in Chapter 3. This model used an analytical solution of the advection/ diffusion equation, and an "exact" method to include deposition. The predictions of this model were shown, in Chapter 3, to compare well with the predictions of another "physically realistic" model, the "Random Walk" model developed by Wilson *et al.* (1981a) and Wilson *et al.* (1981b).

The influence of dry deposition, at rates likely to be encountered in the field, on downwind vertical NH_3 concentration profiles was investigated using the KATCH model. Model simulations were conducted representing dispersion and deposition, from a field treated with slurry, as an infinite length area source. The model predictions, shown in Figure 4.1, demonstrate that dry deposition can substantially reduce near-surface air concentrations downwind of a source, with the depletion of air concentrations reducing with height due to the finite rate of vertical dispersion. A further point to note from Figure 4.1 is that the influence of deposition on downwind concentrations approached a maximum at $V_d > 0.09$ m s^{-1}. This was due to aerodynamic resistance limiting diffusion of material across the concentration gradient.
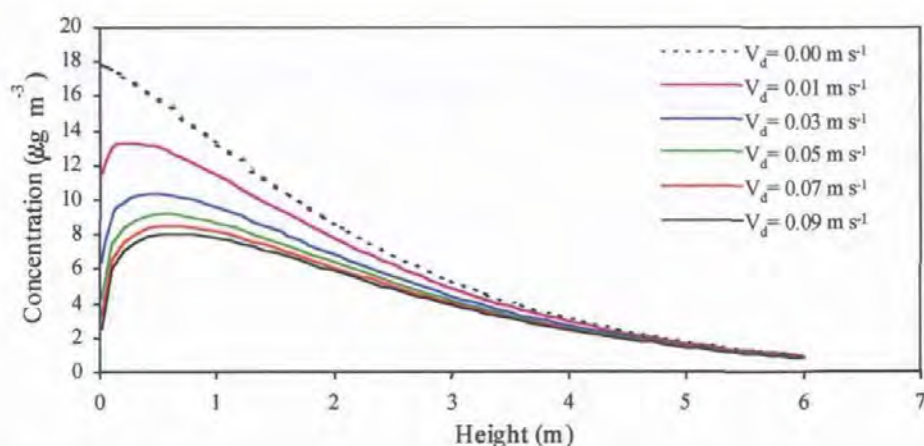
Figure 4.1:   Modelled concentrations at 50 m from an infinitely long surface strip source (15 m width) emitting NH_3 at 10 µg m^{-2} s^{-1}. Meteorological data were $u_* = 0.3$ m, $z_0 = 0.01$ m, $d = 0.01$ m, $L = 1000$ m.

Deposition velocities and fluxes could be estimated from a direct comparison of measured and modelled vertical concentration profiles. This method is subsequently referred to as the "direct profile comparison method". However, as the depletion of concentrations due to dry deposition varies with height, fluxes and the uncertainties of the fluxes should be biased towards concentrations closer to the surface.

The aerodynamic gradient method, discussed in Chapter 2, calculates fluxes from the gradient in air concentrations. However, the constant flux layer assumptions, that are implicit in the method, are invalid close to a strongly emitting source. Simple corrections for advection, which assume that the contribution of the advective flux to air concentrations is constant with height, have been presented by Sutton *et al.* (1993a). However these advection corrections are not valid when there are strong vertical and horizontal concentration gradients, such as found close to a source. Furthermore, the aerodynamic gradient method assumes that the surface flux is constant across the measurement area, which is also unlikely to be valid immediately downwind of a source. An improved method for correcting the aerodynamic gradient method for advection errors, and to include the effects of variable surface fluxes was developed using the KATCH model.

4.2.1   Correcting the aerodynamic gradient method for local advection

The influence of deposition on an advected plume was discussed in Chapter 3, Section 3.2.1.2. An exact method for modelling deposition was developed by Horst (1977), the surface depletion method, shown in Equation 3.14. This method modifies an undepleted plume from a source, with a crosswind integrated air concentration at a downwind point, $\chi_{no\,dep}\{x, z\}$, by subtracting of the "negative" air concentration at the point $\{x, z\}$ generated by the downwind deposition flux, termed $\chi_{neg}\{x, z\}$, Equation 4.1

$$\chi_{dep}\{x,z\} = \chi_{no\,dep}\{x,z\} - \chi_{neg}\{x,z\} \qquad \text{Equation 4.1}$$

Equation 4.1 can be simply rearranged to remove the source advection term from the depleted downwind air concentration, Equation 4.2.

$$-\chi_{neg}\{x,z\} = \chi_{dep}\{x,z\} - \chi_{no\,dep}\{x,z\} \qquad \text{Equation 4.2}$$

Making the assumption that surface fluxes are horizontally homogeneous, Equation 4.2 can be used to calculate the downwind deposition flux from the flux-gradient relationships discussed in Chapter 2, Section 2.4.2.2.

The validity of the assumption of horizontal homogeneity was tested by running the KATCH model with three input deposition velocities (0.01 m s^{-1}, 0.05 m s^{-1} and 0.10 m s^{-1}). Meteorological input data were used that approximate the most common UK meteorological conditions ($u\{10$ m$\}= 5$ m s^{-1}, stability class D), as discussed in Clarke (1979) and an appropriate surface roughness for short grassland ($z_0= 0.01$ m) was applied.

Results, shown in Figure 4.2, demonstrate that the assumption of horizontally homogeneous surface fluxes is invalid close to a source, with an exponential decline in surface flux with downwind distance. The horizontal gradient of flux over distance was greatest immediately downwind of the source, with steeper initial gradients being associated with the higher deposition velocities. Horizontal gradients in deposition flux tended to become less dependent on the deposition velocity further from the source.
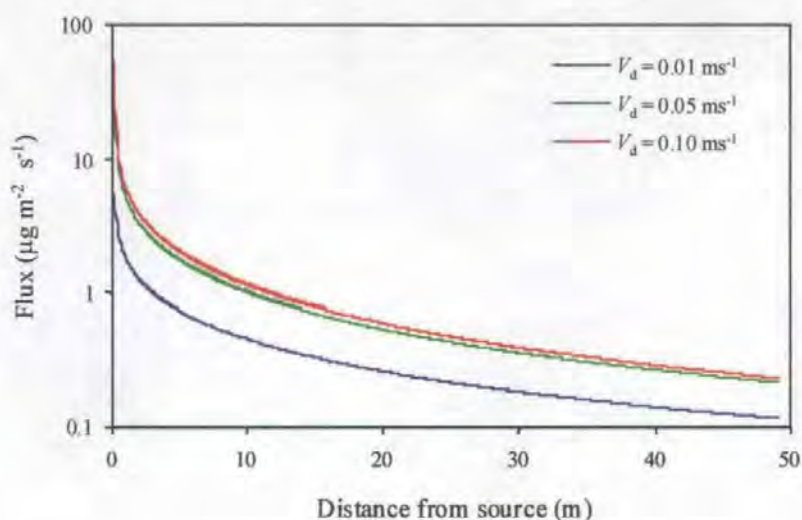
Figure 4.2:   Modelled vertical fluxes downwind of a uniformly emitting surface area source 15 wide and of an infinite lateral extent. Meteorological input data for the KATCH model were: $u_*= 0.3$ m s^{-1}, $L= 1000$ m, $d= 0$ m, $z_0= 0.01$ m, emission flux $= 10$ µg m^{-2} s^{-1}.

4.2.2   Correcting the aerodynamic gradient method for variable surface fluxes

Correction for the violation of the horizontal homogeneity assumption presented a more complex problem than the correction for source advection. This was due to the horizontal gradient in surface flux being a function of the deposition velocity. This introduced something of a paradox in the development of a method to estimate deposition velocities in the field.

The variability in surface fluxes with height above d was investigated. The KATCH model was run for two scenarios: a horizontally variable upwind surface flux (as shown in Figure 4.2) and a constant upwind surface flux. The same input meteorological data as discussed in the previous section were used. The aerodynamic gradient method was used to calculate fluxes from χ_* and u_*, with χ_* being derived across each 0.1m height interval from the vertical gradient of $\chi_{neg}\{x, z\}$. The results are shown in Figure 4.3.
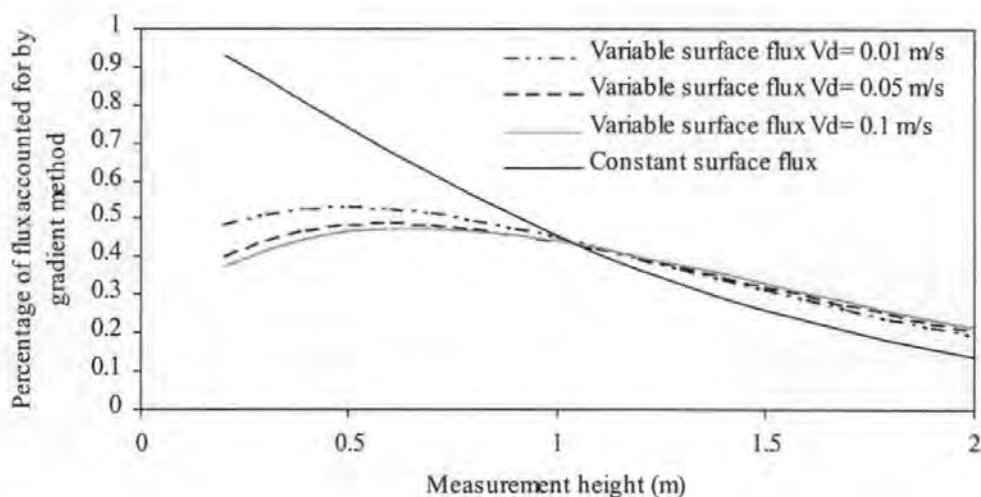
Figure 4.3:   Variation in advection corrected surface flux with height above the ground at 20 m downwind of a 15 m wide infinite length surface level area source. Plots are shown for horizontally homogeneous upwind surface fluxes and for horizontally variable upwind surface fluxes (as shown in Figure 4.2). KATCH model input were $u_*= 0.3$ m, $L= 1000$ m, $z_0= 0.01$ m, $d= 0$ m. The correction for source advection was made using an emission flux of 1.0 $\mu g\ m^{-2}\ s^{-1}$.

The horizontally homogeneous upwind surface flux plot, in Figure 4.3, showed a fetch to height ratio of approximately 100:1, with over 90% of the flux being accounted for by measurements within 0.2 m of the surface. The model runs for horizontally variable surface fluxes showed that the vertical gradient of $\chi_{neg}\{x, z\}$ accounted for 40 - 50 % of the vertical flux. This region was found to extend to 1.0 m from the surface and encompassed a variation of only 20 %. Slight differences were found between each of the three deposition velocities used as model input, however similar proportions of the input flux were calculated when profiles were used across the range 0.1 to 1.0 m. This analysis demonstrated that the magnitude of the variable surface flux could be estimated by multiplying the flux calculated using the advection corrected gradient method by a correction factor of approximately 2.0.

A better estimate of the magnitude and error of the correction factor was made by comparing the advection corrected gradient method flux predictions with fluxes calculated directly by the model. The advection corrected gradient method was used to calculate the deposition flux downwind of the source at each distance using gradients of $\chi_{dep}\{x,z\}$ and $\chi_{no\ dep}\{x,z\}$ generated by the model. These fluxes were compared with the fluxes directly output from the model determined from the product of $\chi_{dep}\{x,z_0\}$ and V_d.

Fluxes were compared at six downwind distances (between 10 m and 60 m from the source), for three input deposition velocities (0.01 m s⁻¹, 0.05 m s⁻¹ and 0.10 m s⁻¹), for three stability conditions (L= 5 m, L= 1000 m and L= -5 m) and for two source fetches (15 m and 30 m). This analysis gave 108 data points for comparison and was assumed to include such a large variation in the input data that any calculated correction factor would be applicable across a wide range of field measurements. The results of this comparison are shown in Figure 4.4. It should be noted that the stability corrections, detailed in Chapter 2, Section 2.4.2.2, were applied when calculating fluxes in non-neutral conditions.
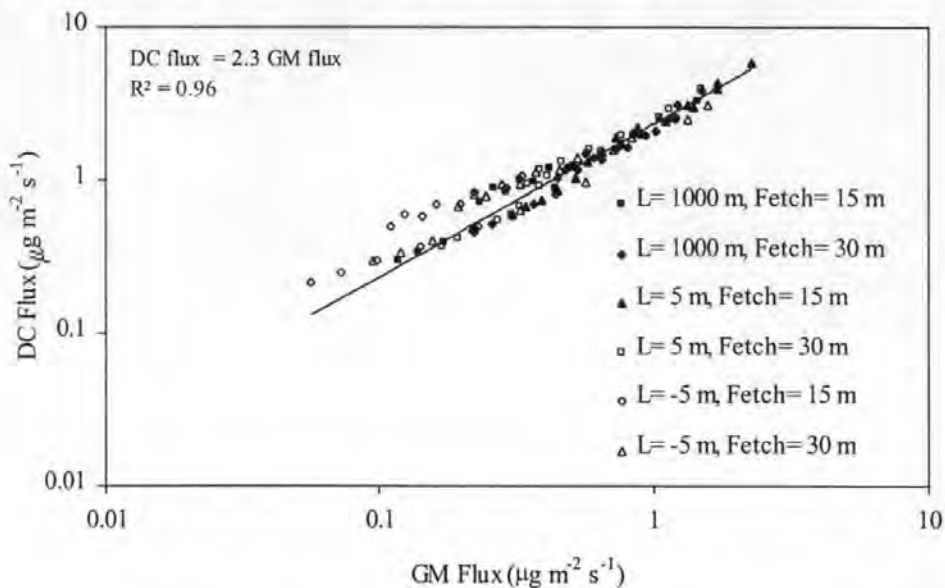
Figure 4.4: Comparison between fluxes calculated with the advection corrected gradient method (GM Flux) and those output directly from the KATCH model (DC Flux). Each data series comprised of 18 data points generated by running the KATCH model for three input deposition velocities (0.01 m s⁻¹, 0.05 m s⁻¹ and 0.10 m s⁻¹) and for six downwind distances (between 10 m and 60 m). Other input data that were constant in the model were: u_*= 0.3 m s⁻¹, z_0= 0.01 m, source emission flux = 10 µg m⁻² s⁻¹.

Figure 4.4 shows that fluxes estimated using the advection corrected gradient method (GM Flux) are approximately linearly proportional to those calculated using an exact reference

method (DC Flux). Using a simple regression analysis the y-intercept was not found to be significantly different from zero and the R^2 value showed that 96 % of the variation in the reference fluxes was accounted for by the advection corrected gradient method. The gradient term was found to be significantly different from both zero and unity showing that the observed relationship was real and that the advection corrected gradient method (without a correction for variable surface fluxes) underpredicted the deposition flux.

The variable surface flux correction factor was approximated from the non-dimensional gradient term in the regression equation (= 2.3) shown in Figure 4.4. This term was only approximately constant, being a function of the gradient in surface fluxes and their respective footprints. The largest departure from this approximation occurred during highly unstable atmospheric conditions when a lower fraction of the flux–profile close to the source was accounted for by the advection corrected gradient method. During such conditions, the direct profile comparison method, discussed at the beginning of this section, would produce more realistic flux estimates.

The dataset used to generate Figure 4.4 was further analysed to determine the ratio of the GM Flux, corrected for the non-uniform surface flux, to the DC Flux at each of the six downwind distances. The results of this comparison, shown in Figure 4.5, demonstrated that the vertical fluxes calculated using the corrected gradient method were within 20 % of the target value up to 40 m from the source in neutral and stable atmospheric conditions. Larger uncertainties were found when applying the corrected gradient method in highly unstable conditions with errors in the flux determination that could exceed 60 %. A further point to note was that the corrected gradient method may only be applied close to the source as the results were highly uncertain for all stability conditions, fetches and deposition velocities beyond 60 m.

4.2.3 Sensitivity of the advection corrected gradient method to input data

The previous section used the KATCH model to investigate advection corrections and to simulate field data. The input data used to model these two scenarios were identical, enabling the theoretical basis of the method to be investigated. Of course, data obtained in the field is seldom, if ever, exact. Thus, it was important to determine the sensitivity of the corrected gradient method to the inevitable variability in the data used to parameterise the KATCH model when making the advection correction.

The KATCH model was used to simulate vertical profiles of $\chi_{dep}\{x, z\}$ measured in the field and to determine the advection correction by predicting $\chi_{no\ dep}\{x, z\}$. In the sensitivity study the KATCH model input data used to predict $\chi_{no\ dep}\{x, z\}$ were varied to simulate the random errors that could occur in field measurements. The model was used to generate depleted concentration profiles, for three input deposition velocities (0.01 m s⁻¹, 0.05 m s⁻¹ and 0.10 m s⁻¹). The reference case for the sensitivity analysis was chosen to represent the most commonly occurring meteorological conditions, neutral atmospheric stability ($L=$ 1000 m), and a moderate wind speed gradient ($u_* = 0.3$ m s⁻¹, $z_0 = 0.001$ m, $d = 0$ m). The source emission flux was arbitrarily set to 10 µg m⁻² s⁻¹, however, as relative changes were being investigated the actual value of emission flux had no significance on the results.
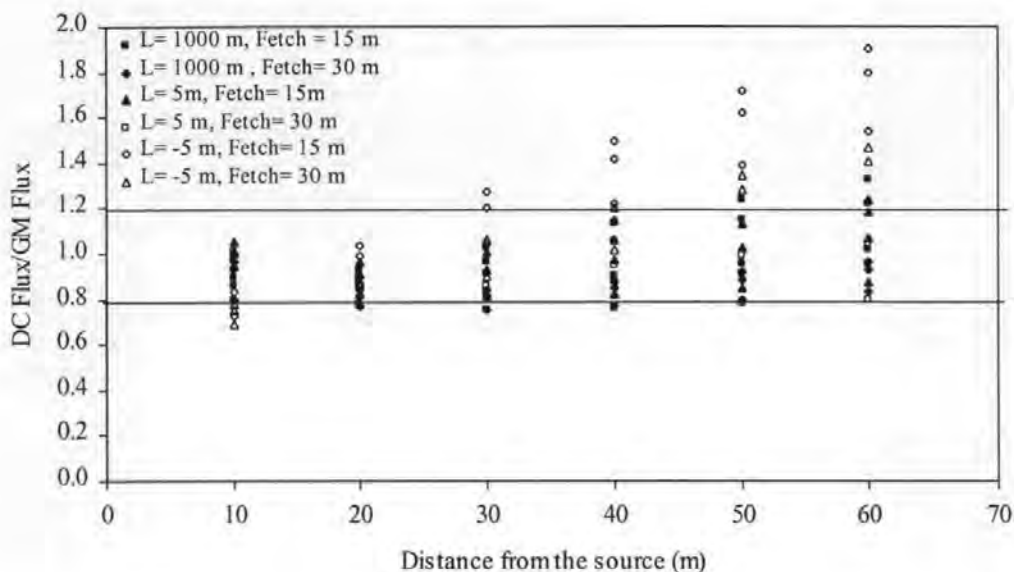
Figure 4.5: Variability in the gradient method calculation of vertical fluxes (GM Flux) referenced to a direct calculation of vertical flux from the KATCH model (DC Flux). Data were generated using the method described in Figure 4.4 and the variable surface flux correction factor (= 2.3) was applied to the GM Fluxes. Horizontal lines indicate deviations in the GM Flux of +/- 20 % from the DC Flux.

A strip width of 15 m was used, as Figure 4.5 demonstrated that this was likely to present a conservative (over predictive) estimate of variability, whilst still representing the field experiments discussed later in this chapter. The wind angle was varied rather than varying the fetch and downwind distance independently as both these distances were accurately measured in the field and variations are more likely to occur due to inaccuracies in wind direction measurements. Results of this analysis are shown in Table 4.1.

Parameter	Change	Change in flux (%)		
		$V_d = 0.01$ m	$V_d = 0.05$ m	$V_d = 0.10$ m
Emission, F	Increase 30 %	100.1	46.5	40.1
(μg m^{-2} s^{-1})	Increase 20 %	66.7	31.0	26.8
	Increase 10 %	33.4	15.5	13.4
	Reduce 10 %	-33.4	-15.5	-13.4
	Reduce 20 %	-66.7	-31.0	-26.8
	Reduce 30 %	-100.1	-46.5	-40.1
Stability length, L	250 m	1.7	0.2	1.1
(m)	50 m	12.8	2.9	7.3
	5 m	125.1	37.0	94.8
	-250 m	-5.1	-1.4	-2.6
	-50 m	-22.4	-5.8	-10.9
	-5 m	-235.9	-73.9	-72.4
Wind angle, θ	to 10°	-2.2	-1.0	-0.9
(degrees)	to 20°	-14.1	-6.4	-5.4
	to 30°	-32.9	-14.9	-12.7
	to 40°	-63.1	-28.5	-24.4
	to 50°	-103.3	-46.7	-39.9
z_0	Increase 50 %	-18.6	-8.6	-7.5
(m)	Increase 100 %	-32.6	-15.1	-13.1
	Increase 200 %	-53.5	-24.8	-21.5
	Increase 300 %	-69.1	-32.1	-27.7
u_*	Increase 5 %	-16.2	-4.6	-3.2
(m s^{-1})	Increase 10 %	-50.2	-14.2	-9.9
	Increase 50 %	-237.3	-67.1	-46.7
d	0.05 m	-11.2	-11.2	-11.2
(m)	0.10 m	-23.0	-23.1	-23.1
	0.20 m	-51.5	-51.6	-51.7

Table 4.1:   Sensitivity analysis on the advection corrected gradient method. Reference case which the deposition fluxes were calculated for was: $u_* = 0.3$ m s^{-1}, $z_0 = 0.001$ m, $d= 0$ m, $L= 1000$ m, fetch $= 15$ m, strip length $= 160$ m, $x =30$ m, $y = 0$ m.

4.2.3.1   Results of the sensitivity analysis

Clearly, from Table 4.1, calculations of vertical fluxes using the ACG method were prone to large systematic errors if the dispersion model, used for making the advection correction, was supplied with incorrect input data. This was particularly true when the downwind fluxes were small proportions of the advected flux (when $V_d < 0.01$ m s^{-1}). The flux estimates were found to be insensitive to the value of stability length (L) across the range of moderate stability ($L= 50$ m), neutral stability ($L= 1000$ m) and moderate

instability (L= -50 m), with a maximum error of 22 %. Unsurprisingly, large errors were found when extremely erroneous parameterisations of atmospheric stability were used (L = -5 m and L = 5 m). This may limit the usefulness of the method during periods of rapidly fluctuating extreme stabilities (dusk and dawn).

Errors in the parameterisation of wind profiles ($u*$, z_0 and d) also could significantly affect the reliability of the ACG method. Fluxes were found to be relatively insensitive to the value of d with an extreme overestimation only causing an error in the flux determination of 55 %. Larger variations were found when $u*$ and z_0 were varied with maximum errors in the determination of fluxes, for V_d= 0.01 m s⁻¹, of 237 % and 69 % respectively. Again, the uncertainty in the method reduced as the deposition velocity increased. Such extreme errors in the determination of wind speed profiles were unlikely to occur in the field, as wind speeds were measured to a precision of +/- 3 %.

Inaccuracies in the determination of wind directions were found to have little influence on the error term for the surface flux measurements between the range 10 - 30°. Wind angles in error by greater than 40° could contribute a significant error term to surface flux estimates. However, as modern wind vanes have a typical precision of +/- 6° such errors were unlikely to have been encountered in the field.

Errors in the determination of the emission flux from the source were found to be a significant source of error in the estimation of surface fluxes, with a 20 % error in the emission estimate resulting in an 67 % error in the surface flux when V_d = 0.01 m s⁻¹. As field measurements of NH_3 emission from slurry applications can have error terms in excess of 10 % (Ryden and McNeill, 1984; Wilson and Shum, 1992) it was important to minimise the effect of these errors on the deposition flux predictions. This was accomplished by comparing the field measurements of air concentrations above the region depleted by surface deposition with the KATCH model predictions. A further check was made by comparing the gradient method predictions with those made using the direct profile comparison method, discussed at the beginning of this section.

4.2.4 Estimating the confidence limits of the ACG method

The previous sections have shown that uncertainties in the ACG method arise from the advection correction term, the variable surface flux correction term, the stability correction term as well as uncertainties in the values of $u*$ and $\chi*$. Assuming that wind speeds have been measured to a precision of +/- 3 %, that the atmosphere is not highly stable or highly

unstable and that emission data have been measured to a precision of 10 %, then the error in the determination of fluxes due to the advection correction (including the $u*$ term in Equation 2.24) can be determined from the smallest values of component error terms in Table 4.1.

Further errors, arising from the variable surface flux correction term, should not affect the measured fluxes by more than +/- 20 %, assuming that measurements have been made within 40 m of the source and that atmospheric conditions are not highly unstable. The overall error in the flux was estimated from these component error terms using a "root mean sum of squares" method. Random errors were estimated to be within approximately 44 % of the mean for a V_d of 0.01 m s^{-1} and 22 % for a V_d of 0.10 m s^{-1}.

Analyses of errors have been included in several papers on the use of the gradient method to determine NH₃ fluxes (*e.g.* Duyzer *et al.*, 1994; Sutton, 1990; Wyers *et al.*, 1992a) with consensus that errors in the determination of fluxes are dominated by the uncertainty in the measurement of NH₃ gradients. These errors typically result in 95 % confidence limits of the flux determinations ranging from 50 % to greater than 100 % of the mean values. An error in the $\chi*$ term of 50 % was included in the "root mean sum of squares" analysis discussed in the previous paragraph. This increased the overall confidence limits of ACG method to between 66 % for a V_d of 0.01 m s^{-1} and 54 % for a V_d of 0.1 m s^{-1}. This demonstrated that an approximate estimate of the overall error in fluxes determined using the ACG method could be derived solely from the error in $\chi*$. The 95 % confidence limits of $\chi*$ were determined from the error in the gradient $\chi\{z-d\}$/stability corrected $\ln(z-d)$.

4.2.5   Calculation of the theoretical maximum deposition velocity ($V_{d\,max}$)

Deposition velocities are often calculated by simply dividing the measured flux by an air concentration referenced to some predefined height above the ground (typically 1.0 m) as shown in Equation 1.4. However, when considering the deposition velocity downwind of a slurry application it was inappropriate to reference deposition velocities to heights above the surface laminar boundary layer as fluxes could not be assumed to be constant with height above this layer (see Chapter 2, Section 2.4.1). Hence, deposition velocities determined in this thesis follow the convention used when modelling atmospheric deposition and are referenced to the roughness height (z_0). The theoretical maximum deposition velocity, between z_0 and the surface, (termed $V_{d\,max}$) could therefore be calculated as the reciprocal of the boundary layer resistance (R_b), where R_b was calculated

from the friction velocity and the sub-layer Stanton number (B), as shown in Equation 4.3 (Owen and Thomson, 1963).

$$R_b = \frac{1}{B\, u_*}$$ Equation 4.3

The sub-layer Stanton number was calculated from the turbulent Reynolds number (Re_*) and the Schmidt number (Sc) according to the semi-empirical expression, shown in Equation 4.4 (Garland, 1977). Re_* and Sc were defined in Equations 4.5 and 4.6. In Equations 4.5 and 4.6, v is the kinematic viscosity of air, quoted as 1.46×10^{-5} m^2 s^{-1} at an ambient temperature of 15 °C by Monteith and Unsworth (1990) and D_{NH3} is the diffusion coefficient for NH_3 in air, quoted as 2.20×10^{-5} m^2 s^{-1} at 15 °C by Massman (1998). Both v and D_{NH3} vary with ambient temperature, increasing by approximately 3 % for each 5 °C increase in temperature, however as R_b was found to show very little temperature dependence across the range 0 – 25 °C (less than 1 % maximum change in value) no temperature corrections were made. Moreover, Sutton (1990) found that estimates of R_b could differ by up to 50 % depending on which semi-empirical parameterisation was used.

$$B = \frac{1}{1.45\, Re_*^{0.24}\, Sc^{0.8}}$$ Equation 4.4

$$Re_* = \frac{z_0\, u_*}{v}$$ Equation 4.5

$$Sc = \frac{v}{D_{NH_3}}$$ Equation 4.6

4.2.6 Estimation of deposition velocities using the corrected gradient method

Deposition velocities were calculated using the ACG method by comparing the field measurements of the vertical flux with the predictions of the KATCH model. The model was used to predict the flux for a range of input deposition velocities, using the same meteorological and emission data as measured in the field. The confidence limits of the deposition velocities were calculated by comparing the upper and lower confidence limits of the deposition flux, calculated from the error in χ_*, with the range of fluxes predicted by the model. An example of the use of this method to determine the mean deposition velocity and the associated confidence limits is shown in Figure 4.6.

Due to the variability in field measurements, the upper confidence limit of the deposition flux could be greater than the maximum flux permitted by boundary layer resistance and the lower confidence limit could be less than zero. In these cases the confidence limits of the deposition velocity were expressed as <0 and >$V_{d\,max}$ respectively.
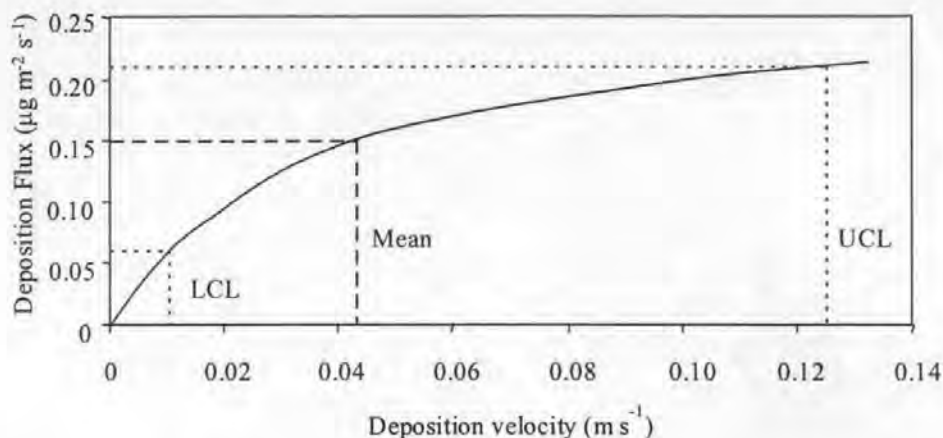
Figure 4.6: Estimation of deposition velocities from a comparison of measured flux data with the modelled relationship between deposition flux and deposition velocity. Example data shows a mean deposition flux of 0.15 μg m^{-2} s^{-1} (V_d= 0.04 m s^{-1}) with upper and lower confidence limits (UCL and LCL) of 0.21 μg m^{-2} s^{-1} (V_d= 0.12 m s^{-1}) and 0.06 μg m^{-2} s^{-1} (V_d= 0.01 m s^{-1}).

4.3 EXPERIMENTATION

The experimental methods used to measure the emission, dispersion and local deposition of NH_3 volatilised from slurry spreading are presented in this section, the results of these field experiments are detailed in Chapter 5. An experimental design, allowing the methods to be simultaneously applied as required by the ACG method is also presented.

4.3.1 Methods to estimate NH₃ emissions from slurry spreading

The micrometeorological mass balance method, discussed in Chapter 2, Section 2.4.3, was applied to estimate the emission flux of NH_3 from slurry. The mass balance method was applied to a long rectangular area source of slurry to prevent errors arising from lateral dispersion (as discussed in Wilson and Shum, 1992). This also provided a downwind field of crosswind integrated concentrations, necessary for the application of the ACG method. Profiles of the horizontal NH_3 flux were measured at the downwind edge of the slurry strip and at 10 m upwind of the source. Upwind horizontal flux profiles were measured at a distance from the leeward edge of the slurry strip to prevent the possible contamination of the samplers by the horizontal turbulent diffusive flux ("back diffusion").

Three samplers, at an equal spacing, were used to determine the upwind horizontal flux profile, whilst six samplers, with an exponential vertical arrangement, were used to determine the downwind horizontal flux profile. Horizontal fluxes of NH_3 were measured

directly using passive flux samplers attached to 3.5 m high aluminium masts. Vertical fluxes of NH_3 were estimated using Equation 2.33, with the vertical integration of the upwind and downwind horizontal flux profiles calculated using the trapezium rule (Berkley, 1988). The fetch (X') across the slurry strip was calculated from the width of the strip (X) and the wind angle normal to the strip (θ) using Equation 4.7. The fetch for each run was determined from the average of the fetches calculated for each value of θ returned by the wind vane.

$$X' = \frac{X}{\cos(\theta)}$$

Equation 4.7

4.3.1.1 *Theoretical basis of the passive flux sampler method*

Passive flux samplers (often termed "shuttles"), developed by Leuning *et al.* (1985), were used to measure the horizontal fluxes of NH_3. The design and mounting of these samplers is shown in Figure 4.7.
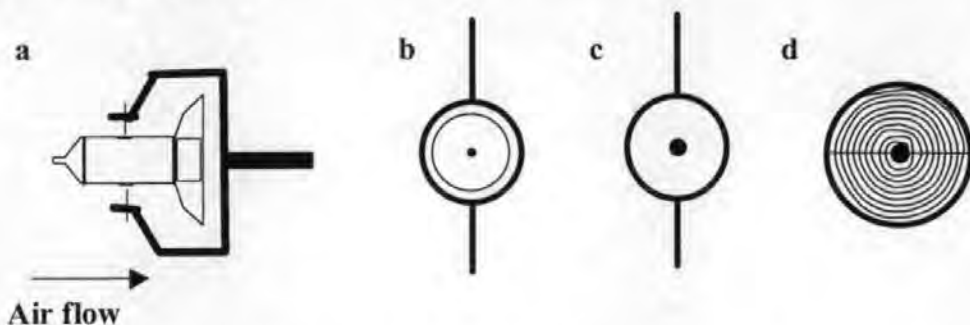
Figure 4.7: Diagram of the Leuning *et al.* (1985) passive flux samplers showing: **a/** the sampler, in longitudinal view, mounted on a bracket for field use, **b/** the sampler in transverse view showing the tail section and outlet orifice, **c/** the sampler in transverse view showing the nose section and inlet orifice, **d/** the sampler in transverse view with tail section removed showing the coiled stainless steel interior.

Leuning *et al.* (1985) demonstrated that the airflow through the sampler was linearly proportional to the ambient wind speed. The ambient horizontal NH_3 flux ($\overline{\chi u}$) was calculated from the mass of NH_3 collected by the sampler (M_{NH3-N}), the effective cross sectional area (A') and the duration which the sampler was exposed in the field (t), using Equation 4.8.

$$\overline{\chi u} = \frac{M_{NH_3-N}}{A' t}$$

Equation 4.8

The effective cross sectional area of the sampler (A') was calculated from the surface area of the outlet orifice (A), the sampler discharge coefficient (C) and the sampler drag

coefficient (C_d) using Equation 4.9. Values of these properties, as detailed in Leuning *et al.* (1985), are shown in Table 4.2.

$$A' = CA \, C_d^{0.5}$$

Equation 4.9

Cross sectional area (A) (m^2)	Discharge coefficient (C) (non dimensional)	Drag coefficient (C_d) (non dimensional)
3.85 10⁻³	0.62	1.0

Table 4.2: Values of the properties used to calculate the effective cross sectional area (A') of the passive flux samplers, as described in Leuning *et al.* (1985).

Gaseous NH_3 was stripped from the airflow passing through the samplers by diffusion onto oxalic acid crystals deposited on a thin coiled stainless steel plate, shown in Figure 4.7. Leuning *et al.* (1985) maximised the internal surface area of the sampler and minimised the distance between the stainless steel coils in order to ensure that the interior of the sampler behaved as a perfect sink for NH_3, even at high air concentrations and wind speeds up to 12 m s⁻¹. Leuning *et al.* (1985) found that the maximum amount of NH_3 that could be trapped in the sampler was 7 mg NH_3-N and that the sampler was still 98 % efficient when 3 mg NH_3-N were deposited onto the internal surfaces. Less than 0.4 mg NH_3-N were extracted from the samplers in the experiments described in Chapter 5, demonstrating that saturation effects would have been negligible.

Samplers, equipped with tail fins, were mounted between two vertically opposing needles on a steel bracket to permit continuous rotation into the mean direction of the wind. Needles were carefully sharpened to a fine point before each experiment to ensure that the sampler tracked wind direction changes even at very low wind speeds. Leuning *et al.* (1985) found that, whilst samplers could stall at wind speeds less than 1.0 m s⁻¹, only slight differences in horizontal fluxes (<5 %) were measured between samplers facing up to 35° from the mean wind angle. Samplers, used in this study, were observed to track wind direction changes at wind speeds less than 0.5 m s⁻¹ which was attributed to the use of finer needles.

4.3.1.2 Preparation of passive flux samplers

Due to the ubiquitous distribution of NH_3 in the environment considerable attention was paid to ensure that the samplers were not contaminated before, or during, an experiment. A de-contaminant (Decon 90) was used to remove any NH_3 from the surfaces of the glassware used for the analytical work. Latex gloves were used when preparing and

extracting the passive flux samplers to prevent any contamination arising from NH_3 present on skin.

The passive flux samplers were easily disassembled for preparation or sample extraction in the laboratory. Figure 4.8 shows a disassembled passive flux sampler. Two different tail sections were used: a section equipped with fins and an outlet orifice for field use (Section C-1) and a solid tail section for use in the laboratory (Section C-2).
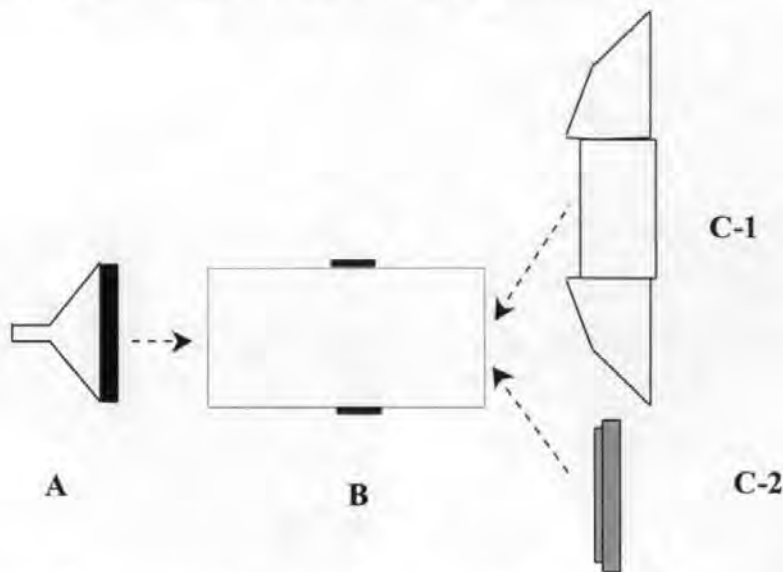
Figure 4.8:   A disassembled passive flux sampler showing A: nose section, B, mid section, C-1 tail section for field application showing tail fins, C-2 tail section used during laboratory work.

The internal and external surfaces of the samplers were thoroughly washed, prior to field application, to remove any background NH_3 contamination from the laboratory air, or from previous use. Samplers, used in Experiments 1 - 4, were cleaned with two 40 ml washes of de-ionised water, introduced into each sampler through Section A prior to a 30 s agitation period. Samplers used in Experiments 5 - 8 were flushed for 15 s with a stream of de-ionised water to reduce the laboratory preparation time. Tests showed that changing the cleaning protocol did no affect the performance of the sampler, though provided a significant saving in laboratory time. This allowed the more frequent exchange of samplers between the laboratory and field, and thus shortened run times.

Excess water was shaken from each sampler, prior to drying with a volatile organic solvent. Section B was sealed using Section C-2 prior to the introduction of 30 ml of analytical grade acetone or methanol into the sampler through Section A. The assembly was shaken for 15 s to ensure that the excess water and the solvent were well mixed, after

sealing Section A with a rubber bung. Following agitation, Section C-2 was removed and the sampler was inverted in a fume cupboard to allow the solvent to evaporate.

Once dried, the stainless steel interior of the sampler was coated with oxalic acid crystals. The mid section was again sealed with Section C-2 prior to the introduction of 30 ml of 30 g l^{-1} oxalic acid dissolved in either acetone or methanol through Section A. The nose section was sealed with a rubber stopper and the sampler was shaken for 30 s to ensure an even coating of the acid on all the internal surfaces. Excess oxalic acid was poured from the samplers and the samplers were allowed to dry in a fume cupboard for approximately 600 s. Concentrations of NH_3 in the laboratory air were occasionally measured. A typical value being 5 μg NH_3-N m^{-3}. No detectable increase in blank values were found between shuttles dried in laboratory air and those dried in an "NH_3 free" air stream provided by passing air through a chamber of oxalic acid crystals bound to glass wool.

4.3.1.3   *Field application of the passive flux samplers*

Two identical sets of samplers were used to enable the laboratory work and field sampling to be conducted concurrently. Passive flux samplers, coated with oxalic acid crystals, were prepared for field use by placing a rubber stopper in the nose section (A) and attaching Section C-1 onto Section B. A small piece of tape was placed over the orifice of Section C-1 to seal the sampler.

Samplers were transported to the field site and carefully placed between the needles of the sampler brackets attached to the sampling masts. The duration of the sampling period was calculated from the time that the stopper sealing the inlet orifice and the tape sealing the outlet orifice were removed. When runs occurred consecutively, samplers were simply exchanged. Each sampler was given a unique identifying number to allow the tracking of positions in the sampling arrangement.

4.3.1.4   *Extraction of passive flux samplers*

Samplers were returned to the laboratory following exposure in the field. The tail section (C-1) was replaced with Section C-2 and a 40 ml aliquot of de-ionised water was introduced through the inlet orifice. The automatic dispenser, used to supply the 40 ml aliquot of de-ionised water, was calibrated to +/- 0.1 % prior to, and during, each experiment. Each sampler was then agitated for 30 s to allow the formation of an equilibrium solution of ammonium oxalate. Approximately 25 ml of the extractant from each sampler was stored at –15 °C for chemical analysis. The mass of NH_3 collected by

each sampler was calculated as the product of the volume of water introduced into the sampler (in litres, l) and the concentration of NH_3 in the solution (in mg l^{-1}).

4.3.1.5 Chemical analysis of samples

The NH_4^+-N concentration in the extractant from the each sampler was determined using the reaction between monochloramine and phenolic compounds under oxidising conditions to form a blue indophenol dye (wavelength = 660 nm). Reactions of this type were first described by Berthelot (1859). The reaction scheme used in this study was based on the modified Berthelot reaction described by Krom (1980), shown in Figure 4.9.
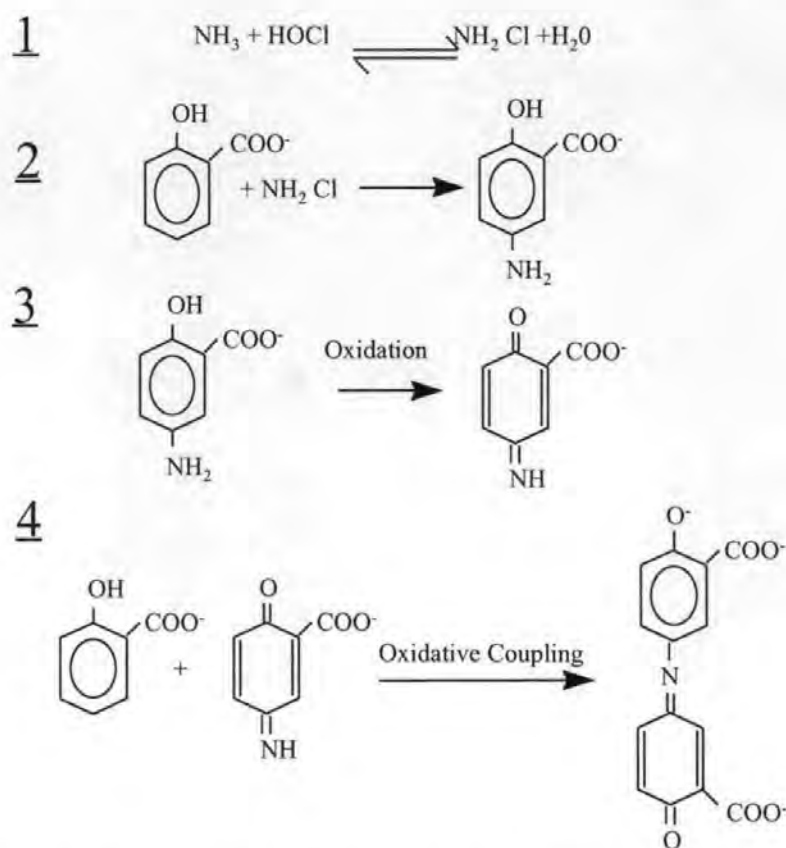
Figure 4.9: Reaction scheme for the production of indophenol from the oxidation of NH_3. Figure reproduced from Krom (1980).

The initial formation of monochloramine was achieved through the oxidation of NH_3 by hypochlorate, produced from the hydrolysis of sodium di-chloroisocyanurate. Monochloramine then reacted with sodium salicylate to form 5-aminosalicylate, which was oxidised, using nitroprusside as a catalyst, to benzoquinone mono-imine. This was then passed through a further oxidative coupling stage with sodium salicylate, promoted by nitroprusside, to form a blue indophenol dye.

Sodium hydroxide was used to buffer the pH to 12 during the formation of monochloramine. Tri-sodium citrate and potassium sodium tartrate were used as chelating agents, reducing the interference caused by dissolved metals such as calcium and magnesium (Searle, 1984). Interferences were further reduced by the dialysis of samples at the higher standard range. Samples were not dialysed at the lower standard range to increase the overall sensitivity of the reaction.

The modified Bethelot reaction was implemented on a dedicated continuous flow analysis (CFA) system (Skalar, UK), shown in Figure 4.10. The advantage of this system over manual methods was that a higher degree of uniformity could be produced in the analysis and that large batches of samples could be analysed (approximately 200 per day).
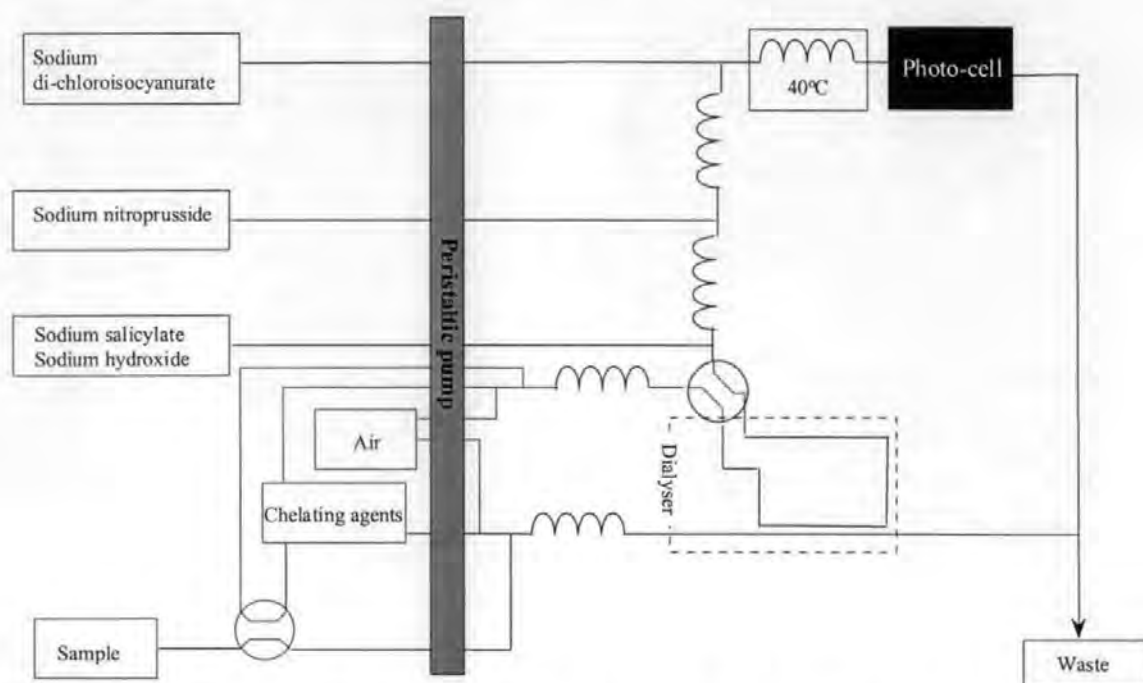
Figure 4.10: Schematic diagram of the CFA system used for the determination of NH₃ concentrations in samples. Valves shown in configuration for the dialysis of high range samples. $\bigwedge\!\bigwedge\!\bigwedge$: mixing coil, $\ominus$: valve, $\boxed{\text{₄₀°C}}$: heater bath.

The CFA system drew 0.5 ml of sample from each 2 ml sample vial on an automated carousel. All the flow rates through the system were controlled using calibrated tubing with suction being provided by a peristaltic pump. The initial eight samples in a run were standards, made up in the sample matrix (oxalic acid), ranging to 10 mg l^{-1} NH₄$^+$-N or 500 μg l^{-1} NH₄$^+$-N. Samples were separated with air bubbles and run through the photocell ever 30 s, preceded by a wash. Differences between the sample and wash peaks were proportional to the NH₃ concentration of the sample. The signal produced by the samples

running through the photocell was processing by a proprietary analogue to digital converter (Skalar, UK) and stored on a microcomputer. The highest sample of either standard range (10 mg l^{-1} NH_4^+-N / 500 µg l^{-1} NH_4^+-N) and a wash (the sample matrix, oxalic acid) were run through the photo cell to correct for any slight baseline drifts following every 10 samples.

Analytical quality control (AQC) samples were tested at random intervals during a sample run. These samples were prepared and checked by the laboratory supervisor to provide an independent verification of the analytical results. Runs were rejected when any of the AQC standards were more than 10 % higher or lower than the target value. Typically, differences between the analytical measurements and the target values of the AQC samples were less that 5 %. A further verification test was organised as part of the ADEPT project to determine the variability in NH_3 analysis between the five participating laboratories. This intercomparison confirmed that analyses were performed to within 5 % of the target value, with results of a similar precision being found from the other participating laboratories.

The relatively poor performance of NH_4^+-N analysis in comparison with other routine spectro-photometric analyses such as NO_3^- -N, which is typically within 1 % of the target value, highlights the need for a robust system of quality control. The cause of the poor performance was likely to be due to the contamination of samples and reagents by background NH_3.

4.3.1.6   *Precision of the determination of NH₃ horizontal fluxes*

The passive flux samplers were estimated by Leuning *et al.* (1985) to have a typical precision of +/- 5 %. This was tested in the field by triplicate sampling, applying three samplers at a single height. A range of sampler error, expressed as a coefficient of variation (100 $\sigma_\chi/\overline{\chi}$), was found between extremes of 1 % and 30 %. A typical sampler error of 10 % was calculated from the average of the measured coefficients of variation (n= 25). Similar sampler errors have been found for other methods routinely used to measure atmospheric NH_3 (Sommer *et al.*, 1995; Sutton, 1990; Sutton *et al.*, 1997a).

4.3.1.7   *Reducing the contamination of unexposed samplers*

Methanol was used as the solvent for drying and coating the passive flux samplers in Experiments 5 – 8, due to the presence of high concentrations of NH_3 in the analytical

grade acetone (approximately 2 mg NH_3-N l^{-1}). This resulted in high but consistent blank samples being measured during Experiments 1 - 4, typically 16 µg NH_3-N sampler^{-1}, with a slight variation between solvent batches.

Blanks were reduced to 1.6 µg NH_3-N sampler^{-1} in the subsequent experiments through the replacement of acetone with methanol. Methanol was found to contain considerably less NH_3 than found in acetone (<0.5 mg NH_3-N l^{-1}) and NH_3 concentrations were further reduced by scrubbing each 2.5 l bottle of solvent with 10 g Dowex 50/10W Ion-exchange resin.

Assuming a limit of detection twice the standard deviation of the blank value and that field measurements were made over a 4 hour period with a wind speed of 3 m s^{-1} the detection limit of the samplers, expressed as an ambient air concentration, would be 3 µg NH_3-N m^{-3} and 0.3 µg NH_3-N m^{-3} for samplers charged with oxalic acid in acetone and methanol respectively. As the concentrations downwind of slurry were considerably greater than these estimated limits of detection, negligible effects of the high blank values were found at all sites, with the exception of Site 1 (background).

Experiments were restricted to the period within 48 hours following the spreading of slurry. This was due to the relatively high limit of detection of the shuttle samplers and the questionable assumptions of using a mass balance method when only slight differences occur between upwind and downwind horizontal fluxes. Whilst this period was likely to be sufficiently long to enable the majority of the NH_3 emissions to be accounted for, the total emissions measured in the field experiments are likely to slightly underestimate the overall volatilisation of NH_3.

4.3.2 Methods to estimate NH_3 deposition downwind of slurry spreading

The ACG method was used to estimate NH_3 deposition downwind of the slurry strip. This method required the measurement of vertical profiles of NH_3 air concentrations downwind of the slurry strip. Passive flux samplers were also used to calculate the downwind air concentrations of NH_3 by dividing the measured horizontal NH_3 flux by the wind speed at the sampler height. The use of passive flux samplers to measure downwind air concentrations meant that no further error terms were introduced into the experiments caused by the well documented systematic differences between methods used to measure NH_3 concentrations (Sommer *et al.*, 1995; Sutton *et al.*, 1997a).

Vertical NH_3 concentration profiles over the downwind grassland were measured at a single site during Experiments 1 and 2, whilst two downwind sites were used in later experiments. The use of two downwind sites enabled the investigation of the variation in deposition velocities with downwind distance and provided some replication of the flux determinations. A further check on the reproducibility of the measurements was made by using paired experiments during broadly similar conditions.

Vertical concentration profiles were measured to 4.5 m and 6.0 m above the ground at the two downwind sites. Six passive flux samplers were typically used at the closest site and eight samplers were typically used at the furthest site. The majority of samplers were placed below a height of 2.0 m in order to maximise the number of measurements in the region of the plume likely to be depleted by surface deposition. The measurements made above the depleted concentration zone provided confirmation that the KATCH model correctly predicted non-depositing dispersion and so provided a further check on the reliability of the results.

4.3.3 Meteorological methods

The methods used to determine the emission flux, the local deposition flux and the dispersion of NH_3 required the precise measurement of the on-site meteorology. In addition, the meteorological measurements provided useful data to help interpret the field measurements. The meteorological data required by each of the methods and required for the interpretation of results are detailed in Table 4.3.

4.3.3.1 Wind speed measurements

Wind speed profiles were measured using sensitive cup anemometers (model A100, Vector Instruments, Clwyd, UK) that were mounted at approximately exponentially increasing heights on the side arms of a 3 m high aluminium meteorological mast. The anemometers were powered by a 12 V battery and produced a voltage output that was linearly proportional to the wind speed (gradient = 0.78 m s^{-1} V^{-1}, y-intercept = 0 V). The voltage output of each anemometer was recorded on a multi-channel datalogger (Squirrel 1000, Grant Instruments, Cambridge, UK) at intervals of 10 s. The voltages recorded at each 10 s interval were averaged over 120 s by the datalogger and stored in the datalogger's random access memory (RAM). Data were downloaded from the datalogger at the end of each experiment. The anemometers were pre-calibrated by the manufacturer to a precision of +/- 3 %. This was routinely checked throughout the experiments by measuring the wind speed from several anemometers at the same height.

Method	Data required	Meteorological measurement required
Mass balance	Wind angle normal to the slurry strip	Wind direction
Advection corrected gradient method	Wind speed at sampler height Stability correction factor KATCH model predictions Zero-plane displacement height	Wind speed profile Temperature profile Wind direction
KATCH model	Friction velocity Monin-Obukhov stability length Roughness length Zero-plane displacement height Wind direction	Wind speed profile Temperature profile Wind direction
Interpretation of results	Surface temperature Surface humidity Sensible heat flux Latent heat flux	Wind speed profile Temperature profile Humidity profile

Table 4.3:   Meteorological data requirements of the experiments to measure the emission, dispersion and local deposition of NH_3 and used for interpreting the results.

4.3.3.2   Wind direction measurements

A wind vane (W200, Vector Instruments, Clwyd, UK), aligned to magnetic north, was used to measure wind direction. The wind vane was powered by the same 12 V battery as the anemometers and produced an output, between –6.7 V and 6.7 V, that was linearly related to the wind angle in degrees from south (gradient = $45°\ V^{-1}$, y-intercept = $0°$). Wind angles in degrees from north were calculated by rotating the wind directions through $180°$. Any negative wind angles were rotated through a further $360°$ to ensure that all wind directions were output as positive degrees from north. The wind vane was mounted (at 1.5 m) on an opposing arm of the meteorological mast to the anemometer. This height was chosen to allow the accurate sighting of the wind vane to the north. The typical errors in the measurement of wind directions using this device were determined by the manufacturer to be +/- $6.0°$

4.3.3.3   Air temperature measurements

Air temperatures were measured using four high precision thermistors (CT-UU, Grant Instruments). These were proprietary sensors, developed by the manufacturer to be used with the Squirrel 1000 datalogger, and so did not require any post-processing or calibration

factors. The manufacturer's claims of errors less than +/- 0.1 °C were tested and confirmed by an intercomparision of all the thermistors in a constant temperature environment. An aluminium coated plastic shield was placed over the main body of the temperature probe, leaving the tip of the probe containing the thermistor, exposed to the passing airflow to prevent the temperature readings from being influenced by direct solar radiation. The radiation shields and thermistors were mounted, using fine wire mesh brackets, on the opposite sides of the meteorology mast to the lowest four anemometers.

4.3.3.4   Humidity measurements

Relative humidities were measured using two systems: miniature relative humidity sensors ("Tinytalk", Gemini Dataloggers, Chichester, UK) and a conventional aspirated psychrometer system (Delta-T Devices, Cambridge, UK). The aspirated psychrometer system, used in Experiments 1 and 2, was unavailable for later experiments. The *Tinytalk* sensors comprised of a "cracked chromium oxide" relative humidity sensor with an integrated miniature datalogger powered by an internal battery. The precision of the *Tinytalk* system was verified to be +/- 5 % of the mean RH value by an intercomparison of three loggers. A good agreement was found between the aspirated psychrometers and the *Tinytalk* loggers (gradient = 1.0, y-intercept = 0, R^2 = 0.92) across a range of relative humidities (30 – 100 %).

Saturation vapour pressure (e_s) was calculated from measurements of air temperature using a modified Hooper's polynomial equation (Sargent, 1980). Vapour pressure (e) for the aspirated psychrometer system was calculated from wet bulb (T_w) and dry bulb (T) temperatures using Equation 4.10, where P_c is the psychrometer constant and ρ is the density of air.

$$e = e_s - P_c \rho (T - T_w)$$ Equation 4.10

Relative humidity (RH) was calculated from the vapour pressure and saturation vapour pressure using Equation 4.11. As the *Tinytalk* sensors measured RH directly Equation 4.11 was rearranged to allow the calculation of e, shown as Equation 4.12.

$$RH = 100 \left(\frac{e}{e_s} \right)$$ Equation 4.11

$$e = e_s \left(\frac{RH}{100} \right)$$ Equation 4.12

Three *Tinytalk* humidity sensors were used to estimate the vertical profile of vapour pressure. These instruments were mounted on the meteorological mast underneath the

thermistors to enable the precise determination of saturation vapour pressure from the ambient temperature measurements.

4.3.4   Methods used to apply cattle slurry to grassland

Dairy cattle slurry was spread onto the surface using a modified slurry injector with the injector tines raised. This method of slurry application was chosen, over the conventional splash plate technique, as it was possible to produce a clearly delimited and uniformly slurried plot. This was an essential criterion, as a clear distinction was required between the strongly emitting slurry source and any sources or sinks of NH_3 in the adjacent grass canopy. The slurry injector was calibrated by the manufacturer to discharge slurry at several pre-defined rates. An application rate of 39 tonnes ha^{-1} was used in this study as this was both a realistically high rate (MAFF, 1998a) and allowed the treated area to the spread quickly, ensuring that emissions were uniform.

4.3.4.1   Analysis of the slurries used

A litre of slurry was collected from the tanker following spreading. This sample was immediately returned to a laboratory, distant from any sensitive analytical areas, and analysed for pH using a pH meter (Model 3305, Sentek, UK). Following this, the slurry sample was acidified to a pH <5 and refrigerated prior to analysis for NH_4^+-N and dry matter.

Ammonium concentrations in the slurry samples were determined using an ion-selective electrode (Sentek, UK). A calibration curve was determined prior to the slurry analysis using standard solutions ranging to 3000 mg NH_4^+-N l^{-1}. Following which, the ion-selective electrode and a reference electrode were placed a 100 ml subsample of the cattle slurry. The potential difference between the two electrodes was displayed on a digital meter. After several minutes, the reading stabilised enabling the determination of the slurry NH_4^+-N concentration from a comparison between the measured potential difference and the calibration curve.

The dry matter content of the slurry was determined following the measurement of the NH_4^+-N concentration. A sample of the slurry was poured into a weighed aluminium tray. The liquid slurry and the tray were then re-weighed to determine the total mass of the slurry. The dry matter content, expressed as a percentage dry weight to total weight, was calculated from the re-weighing of the sample and tray after the sample had been dried in an oven at 70 °C for 48 hours.

4.3.5   Experimental design and field sites

The generic experimental design for the field experiments, incorporating the methods discussed in the previous sections, is shown in Figure 4.11. Equipment were arranged in an array, at $90°$ to the slurry strip. The background mast and meteorological mast were positioned upwind of the source, with the remainder of the sampling masts positioned downwind of the slurry.

Two field sites were used for conducting the micrometeorological experiments, Middle Wyke Moor and Halse. Both sites were owned and operated by the Institute of Grassland and Environmental Research (IGER) and were located within 2 km of the laboratories. Most experiments were conducted on Middle Wyke Moor as it had been dedicated to this project. Halse, which was used by several research groups at IGER, was only used for Experiments 1 and 2, as Middle Wyke Moor was waterlogged. Further information on the field sites is given in Table 4.4.

Site	National grid reference	Soil type	Area (ha)	Soil pH (in water)
Middle Wyke Moor	SX 663977	Clay Loam (Hallsworth series)	7.9	5.6
Halse	SS 669008	Sandy Loam (Credition series)	7.7	5.8

Table 4.4:   Characteristics of the field sites used in the micrometeorological experiments. Soil classification taken from Findlay *et al.* (1984).

The sites were selected based on micrometeorological criteria of horizontal homogeneity. Both sites were reasonable flat and covered by established and uniform swards of perennial ryegrass (*Lolium perenne* L.). Undisturbed upwind fetches of between 200 m and 300 m were available depending on the wind direction. The micrometeorological suitability of the sites was confirmed by the existence of good logarithmic wind profiles, measured to 3 m above the surface.

Another important criterion for the field experiments was that no strong NH_3 sources should be upwind of the field sites. The closest strong NH_3 sources to Middle Wyke Moor and to Halse were dairy farms at 0.8 km to the north and 1.5 km to the west respectively. Tests using the UK-ADMS atmospheric dispersion model (detailed in Chapter 3), assuming that 250 dairy cows were housed in the farms and that a 500 m^2 surface area open slurry store was present, showed that these sources should typically contribute less than 0.5 µg NH_3-N m^{-3} to downwind air concentrations at the distances being measured.
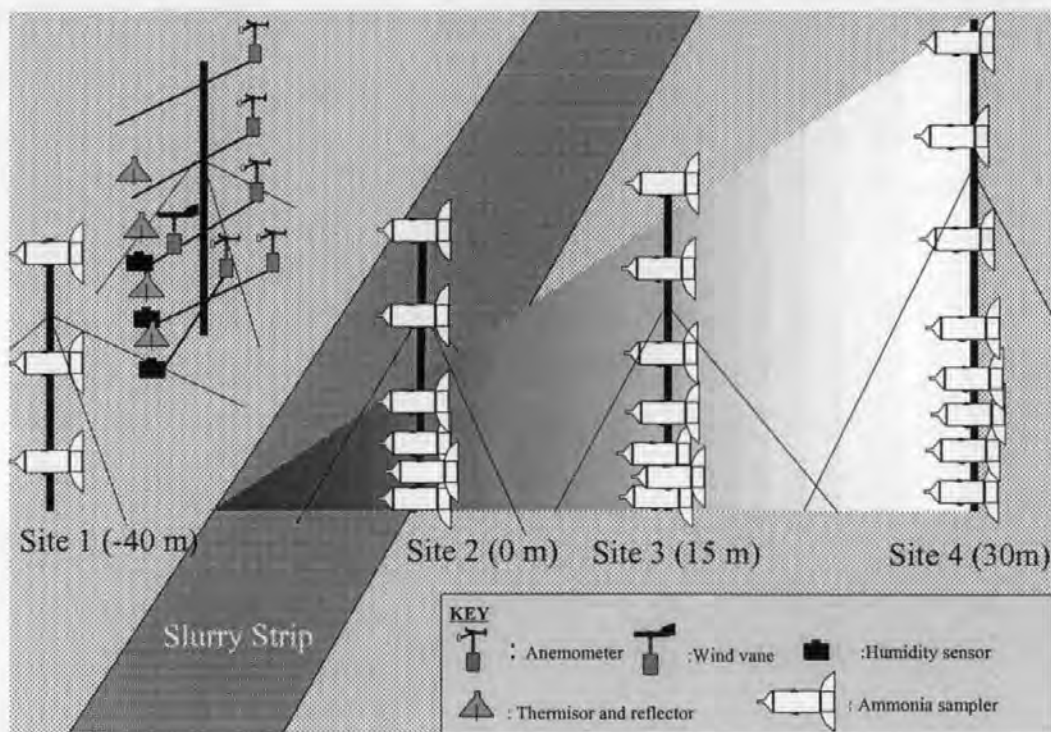
Figure 4.11:   Schematic diagram (not to scale) of the equipment and set up of the micrometeorological experiments.

4.3.6   Timing of the field experiments

The eight field experiments were designed to investigate the emission, dispersion and local deposition of NH_3 at different points during the year when a farmer may decide to spread slurry. Experiments were timed to coincide with the following agricultural practices.

- Slurry application during winter periods.
- Slurry application following the harvesting of pasture grass for silage (conducted three times throughout the growing season).
- Autumn applications onto fields previously harvested for silage to empty slurry stores prior to the indoor overwintering of livestock.

The application of slurry to grassland during winter periods is rare, as the ground conditions are often unsuitable, and is discouraged as leaching of N into watercourses may occur (MAFF, 1998b). However, experiments conducted during winter periods provided contrasting meteorological conditions to other periods thoughout the year. The specific timings of the field experiments are shown in Table 4.5

4.4   CONCLUSIONS

Methods to determine the emissions and dispersion of NH_3 volatilised from slurry spreading have been discussed in Chapters 2 and 3 respectively. A novel micrometeorological method for measuring the surface-atmosphere exchange in a variable

flux layer downwind of a strongly emitting source was developed in this chapter and shown to be reasonably robust and theoretically valid. Equipment used to implement these methods were discussed and a general experimental design was developed. Furthermore, field sites that were suitable for micrometeorological measurements were identified and described. The experimental testing of the micrometeorological method and experimental results are presented in Chapter 5.

Experiment	Number of runs	Slurry application type	Experiment times		
			Start (GMT)	End (GMT)	Duration (hours)
1	6	Winter	06/12/95 13:30	08/12/95 16:30	51.0
2	5	Winter	14/12/95 12:23	16/12/95 08:20	43.9
3	6	After 1st cut silage [a]	28/06/96 10:56	30/06/96 09:16	46.3
4	4	After 2nd cut silage [a]	24/07/96 14:13	26/07/96 15:13	49.0
5	7	After 3rd cut silage (Autumn)	15/10/96 11:39	17/10/96 17:06	53.5
6	6	After 3rd cut silage (Autumn)	30/10/96 10:46	01/11/96 09:49	47.1
7	7	Before 1st cut silage	15/05/97 09:26	16/05/97 15:47	30.4
8	6	After 1st cut silage	18/06/97 10:45	19/06/97 20:38	33.9

Table 4.5: Timing and duration of the experiments to estimate the emission, dispersion and local deposition of NH₃ volatilised from slurry spreading. All experiments were conducted on grassland that had not received a recent fertiliser application (within 8 weeks) with the exception of the experiments marked [a] where measurements were made immediately following fertiliser applications.

5

EMISSION, DISPERSION AND LOCAL DEPOSITION OF NH₃ VOLATILISED FROM CATTLE SLURRY: RESULTS

5.1 INTRODUCTION

This chapter presents the results of eight experiments to investigate the emission, dispersion and local deposition of NH_3 volatilised from dairy cattle slurry applied to agricultural grassland. These experiments were conducted between December 1995 and June 1997 at two field sites in south-west England: Halse and Middle Wyke Moor.

The experimental methods are detailed in full in Chapter 4. In brief, the micrometeorological mass balance method (as first used by Denmead *et al.*, 1977) was applied to estimate the emission flux of NH_3 from an area treated with cattle slurry. This emission flux was used, alongside measurements of the prevailing meteorological conditions, as input data to a physically realistic analytical K-theory model of atmospheric dispersion (KATCH), discussed in Chapter 3. The vertical concentration profiles, downwind of the slurry strip, predicted by the model were compared with the field measurements. Where the model predictions for non-depositing dispersion were in good agreement with the field measurements no downwind deposition was interpreted to have occurred. The Advection Corrected Gradient (ACG) method, discussed in Chapter 4, Section 4.2, was applied to calculate the magnitude and uncertainty bounds of the deposition flux when air concentrations measured close to the ground did not fit the model predictions for non-depositing dispersion. Errors due to uncertainties in emission data were reduced by comparing measured and modelled air concentrations above the surface depletion zone.

Local NH_3-N budgets were constructed for each experiment, evaluating the total mass of NH_3-N emitted from the slurry treated plot and the mass locally deposited. These budgets were calculated using the KATCH model with input deposition velocities, emission fluxes and meteorological data derived from the field experiments. An idealised source, defined as a 160 m x 30 m strip subject to a wind direction parallel to the experimental array (termed as an on-axis wind direction), was used in the budget calculations. This removed the variability between experiments in downwind distances and strip dimensions caused by wind direction changes and differing experimental designs. An assessment was also conducted to determine the downwind deposition fluxes that would occur if the surface behaved as a perfect sink for NH_3 and deposition between the roughness height (z_0) and the surface was limited only by boundary layer resistance (R_b). These theoretical maximum deposition velocities were denoted as $V_{d\ max}$. Deposition velocities throughout this chapter are referenced to z_0 as discussed in Chapter 3, Section 3.2.1.2 and Chapter 4, Section 4.2.5.

5.2 ENVIRONMENTAL CONDITIONS

The experiments were timed to coincide with the typical seasonal pattern of agricultural slurry applications, providing information on the likely variability and controls over the emission, dispersion and deposition processes. The precise timing and locations of the experiments are discussed in Chapter 4, Section 4.3.6. Further information on the agricultural management of the field sites is presented in Table 5.1. Field experiments were conducted over a wide range of meteorological conditions, a summary of the meteorological data for each experiment, collected at the local Environmental Change Network (ECN) monitoring site, is shown in Table 5.2. The dimensions of the slurry treated plots and the chemical composition of the slurries used are shown in Table 5.3. The slurries used in the field experiments were of a consistent composition, having approximately 1.0 g l⁻¹ NH_x-N (TAN), a slightly acidic to neutral pH and a dry matter content of 5 %. Further details of the methods used to apply slurry during these experiments and of the analytical techniques used to analyse the slurries are discussed in Chapter 4, Section 4.3.4.1.

5.3 INTERPRETATION OF EXPERIMENTAL RESULTS

The experimentally measured NH_3 concentration profiles were interpreted using the KATCH model detailed in Chapter 3. The numerical algorithms, upon which this model was based, were tested and parameterised to produce physically realistic predictions of air concentrations and dry deposition within the constant flux layer of the atmosphere.

Experiment	Site	Sward height (m)	Management	Fertilised within 8 weeks
1	HA	0.5	Fallow	✗
2	HA	0.5	Fallow	✗
3	MWM	0.1	Silage cropping	✓
4	MWM	0.2	Silage cropping	✓
5	MWM	0.1	Post silage grazing	✗
6	MWM	0.1	Post silage grazing	✗
7	MWM	0.3	Silage cropping	✗
8	MWM	0.2	Fallow	✗

Table 5.1: Details of the agricultural management of the field sites for each of the slurry spreading experiments. Site codes are: HA: Halse, MWM: Middle Wyke Moor.

Experiment	Air temperature {1.0 m} (°C)			Relative humidity {1.0 m} (%)			Wind speed {2.0 m} (m s⁻¹)			Wind direction {1.0 m} (°)		Precipitation (mm)
	Mean	Max	Min	Mean	Max	Min	Mean	Max	Min	Mean	σ	Total
1	0.9	5.4	-2.7	92	100	72	2.6	6.1	0.4	122	27	Snow
2	1.4	3.8	0.0	80	98	56	5.3	7.1	3.6	84	9	Snow
3	13.7	18.5	11.0	81	96	56	3.9	5.7	2.5	304	19	1.2
4	15.8	23.5	8.3	74	98	46	2.1	4.5	0.3	271	57	0.0
5	8.6	13.1	3.6	79	97	60	2.8	5.6	0.3	229	48	6.2
6	11.6	13.8	9.4	84	97	65	4.2	7.4	1.1	263	34	3.0
7	12.2	16.8	5.7	79	97	50	3.4	7.2	0.7	149	40	0.0
8	14.1	18.7	8.9	79	96	59	2.0	4.0	0.6	238	43	2.2

Table 5.2: Summary of the meteorological conditions occurring during the field experiments. Mean, minima and maxima are shown along with the standard deviation of the mean wind direction.

5.3.1   Validation of the KATCH model

An empirical validation of the KATCH model was conducted, as it was important to check that the model predictions were unbiased before they were used to interpret field data. This section presents the results of the model validation and illustrates the interpretation of some of the field data.

A comparison was made between the predictions of the KATCH model and the field measurements at the immediately downwind site (Site 2 in Figure 4.11). The mass of NH_3 in the plume passing the NH_3 samplers at this site was assumed to be conserved, enabling

the dispersion of NH_3 to be modelled as analogous to the dispersion of a passive (non-depositing and chemically inert) tracer.

Experiment	Slurry characteristics			Application details				
	TAN (g l⁻¹)	Dry matter (%)	pH	Strip width (m)	Strip length (m)	Distance to Site 3 (m)	Distance to Site 4 (m)	TAN Applied (kg NH$_x$-N)
1	1.10	5.0	7.2	30	160	32	-	20.6
2	1.20	5.0	7.2	30	160	32	-	22.5
3	1.22	4.7	7.3	30	160	15	30	22.8
4	0.95	4.5	6.4	30	160	10	30	17.8
5	0.77	5.2	6.6	15	160	10	25	7.3
6	1.27	5.1	6.7	15	160	10	25	11.9
7	0.99	4.6	6.6	15	160	15	30	9.3
8	0.95	4.8	6.8	15	160	15	30	8.9

Table 5.3:   Slurry analysis and plot dimensions for the experiments to measure the emission, dispersion and local deposition of NH_3. Details of analytical techniques used to analyse the slurries are given in Chapter 4, Section 4.3.4.1. Distances to Sites 3 and 4 were measured from the downwind edge of the slurry strip, these sites are defined in Figure 4.11.

Dry deposition was neglected from the modelling assessment at Site 2 as counter-gradient exchange (if present) should not affect measurements made at heights significantly above the canopy (Raupach and Legg, 1984). Gas to particle conversion could also be expected to have an insignificant effect on NH_3 concentrations at any of the sites used in the field experiments as typical gas to particle conversion rates (discussed in Chapter 1, Section 1.3.2) result in NH_3 having an atmospheric chemical half life of 2 - 4 hours (Asman and Janssen, 1987; Erisman *et al.*, 1988). Given the travel time of NH_3 between the source and the samplers at Site 2 is typically around 10 s then gas to particle conversion was likely to cause a maximum reduction in concentrations of approximately 0.1 %. Moreover, in such rural areas, concentrations of atmospheric acid species (SO_x and NO_x) capable of scavenging NH_3 from the plume are typically too low to permit rapid gas to particle conversion (Sutton *et al.*, 1997a).

When validating atmospheric dispersion models it is important to ensure that like quantities are compared and that the modelled and measured variables are truly independent. The use of passive flux samplers, discussed in Chapter 4, Section 4.3.1.1, enabled the direct calculation of both horizontal flux and emission (vertical) flux. A non-

dimensional ratio of horizontal to vertical flux was used as a measure of the rate of vertical dispersion. This ensured that the field measurements and model predictions were independent (*i.e.* the measured emission flux was not required as input to the model).

Similar flux ratios were calculated using the KATCH model. The model was run using the site topography, sampler heights and measured meteorological data ($u*$, z_0, L, d and θ). A unit emission flux ($1.0 \, \mu g \, m^{-2} \, s^{-1}$) was used as input to the model, producing output of concentrations per unit emission. Modelled horizontal fluxes at the sampler heights were calculated by multiplying the modelled concentrations per unit emission by the wind speed, calculated using the same meteorological data as used as input to the model. This produced a modelled horizontal flux per unit emission flux, which was exactly analogous to the measured flux ratio. The results of the comparison are presented in Figure 5.1.
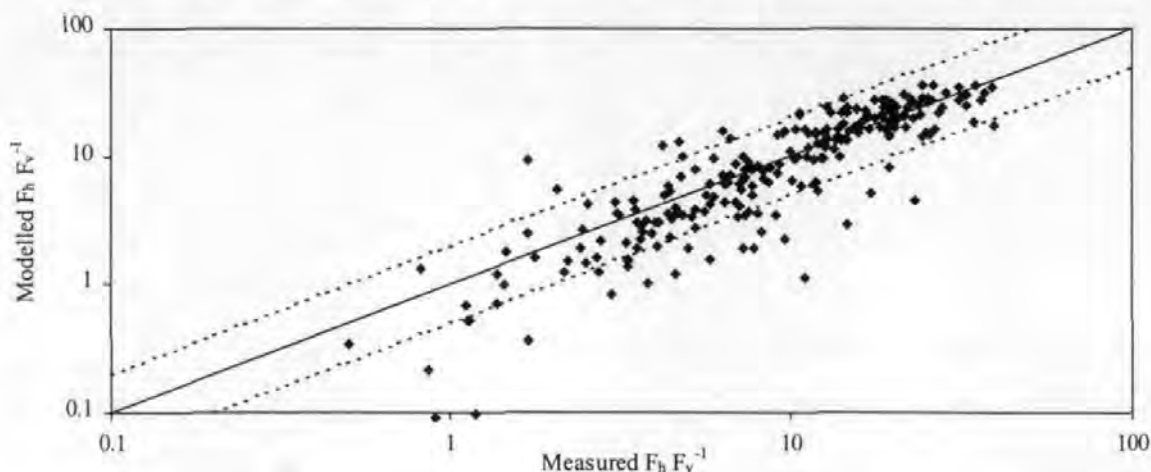
Figure 5.1:   Comparison between measured and modelled ratios of horizontal flux (F_h) to vertical flux (F_v). All the data from the field experiments are included. Lines are shown to indicate an exact fit of modelled results to measured results (—) and the fit expected if the comparison is within a factor of two (·········).

The comparison between the KATCH model predictions and the field measurements, shown in Figure 5.1, illustrates that the general trends in the field data were well described by the model. A regression analysis was performed on the data showing that the y-intercept was not significantly different from zero and that the gradient was not significantly different from unity. The R^2 value of the regression fit showed that 73 % of the variation in the measurements was accounted for by the model. Further tests were made on the data shown in Figure 5.1 to evaluate the accuracy of the predictions. These tests showed that 83 % of the model predictions were within a factor of 2.0 of the field measurements and that 38 % of the model predictions were within +/- 20 % of the field measurements.

127

The variability observed in Figure 5.1 is typical of atmospheric measurements and reflects the uncertainties in determining input meteorological data, emissions fluxes and horizontal fluxes. The influence of the uncertainty in the measurement of emission fluxes and horizontal fluxes was investigated by refining the data presented in Figure 5.1 to only consider periods when emissions were high and vertical NH_3 profiles were well defined. This was achieved by restricting the comparison to the first two runs of each experiment. The results of this comparison are presented in Figure 5.2.
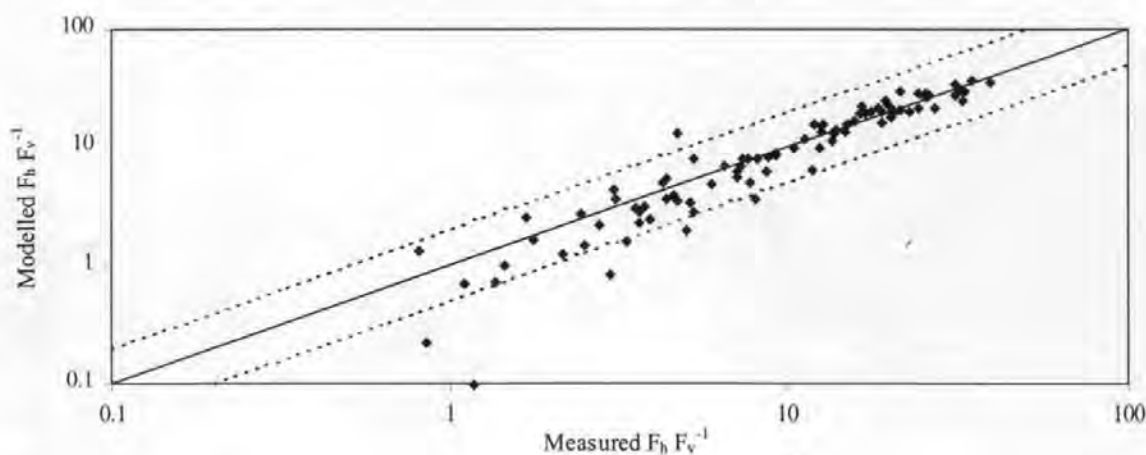
Figure 5.2: Comparison between measured and modelled ratios of horizontal flux (F_h) to vertical flux (F_v) for the initial two runs of each experiment. Lines are shown to indicate an exact fit of modelled results to measured results (——) and the fit expected if the comparison is within a factor of two (---------).

The agreement between the KATCH model predictions and the field measurements, shown in Figure 5.2, was much better that that shown in Figure 5.1. The R^2 value for the sub-set of data shown in Figure 5.2 demonstrated that 93 % of the variation in the measurements was accounted for by the model and 92 % of the model predictions were within a factor of 2.0 of the field measurements. Additionally, 56 % of model predictions were within +/- 20 % of the field measurements. This analysis demonstrates that much of the scatter in Figure 5.1 was due to the well recognised difficulties in measuring vertical and horizontal NH_3 fluxes during periods of low emission.

The processes of atmospheric dispersion and gradient transfer apply equally to sources and sinks of material in the atmosphere. As the surface depletion model has a theoretically exact basis (Horst, 1977), the deposition model was also assumed to be valid based on the conclusions of the previous section. A true experimental validation of the deposition model is beyond the scope of this thesis. Such a study, similar to the work conducted by

Doran and Horst (1985) on particulate deposition, would involve further detailed field experiments using a gas other than NH_3 for which the deposition behaviour is sufficiently well known that an exact "reference" value could be compared with the model predictions.

5.3.2 Model interpretations of field data

This section compares some of the field data with the predictions of the KATCH model, demonstrating the methods used to estimate deposition fluxes. The data presented in this section demonstrate two scenarios: where little or no deposition of NH_3 occurs; and where the field measurements are interpreted to suggest a non-zero deposition flux. Further quantitative analyses of the vertical profiles, made using the ACG method, are discussed in later sections of this chapter.

5.3.2.1 *Measured NH₃ profiles interpreted to show a zero deposition flux*

The simplest profile interpretations were made when the measured vertical NH_3 concentration profiles conformed to the predictions of the atmospheric dispersion model without the inclusion of deposition. In this situation it was concluded that either no NH_3 deposition occurred, or that the NH_3 deposition flux was not large enough to significantly affect the local emission budgets (< 5 % of the emitted NH_3 locally deposited) across the scale measured (30 - 50 m downwind). Examples of these types of profiles measured during Experiments 2, 3, and 4 are shown in Figure 5.3.

5.3.2.2 *Measured NH₃ profiles where a non-zero deposition flux is estimated*

A more complex approach, described in Chapter 4, was used to interpret NH_3 concentration profiles to determine dry deposition fluxes. These direct profile comparisons were made using the KATCH model parameterised with deposition velocities of 0.02, 0.04, 0.06, 0.08, and 0.10 m s^{-1}. Profiles that conformed to the KATCH model predictions, with the inclusion of dry deposition, were further investigated using the ACG method to estimate the magnitude and uncertainty bounds of the deposition flux.

Examples of profiles that were interpreted to determine a deposition flux are shown in Figure 5.4. The KATCH model predictions of air concentrations depleted by surface deposition are well represented by the field measurements, giving some additional confidence in the deposition model. The predicted shapes of the vertical concentration profiles, in particular the inversion in concentration gradient close to the surface, provides further empirical evidence that deposition processes occurred.
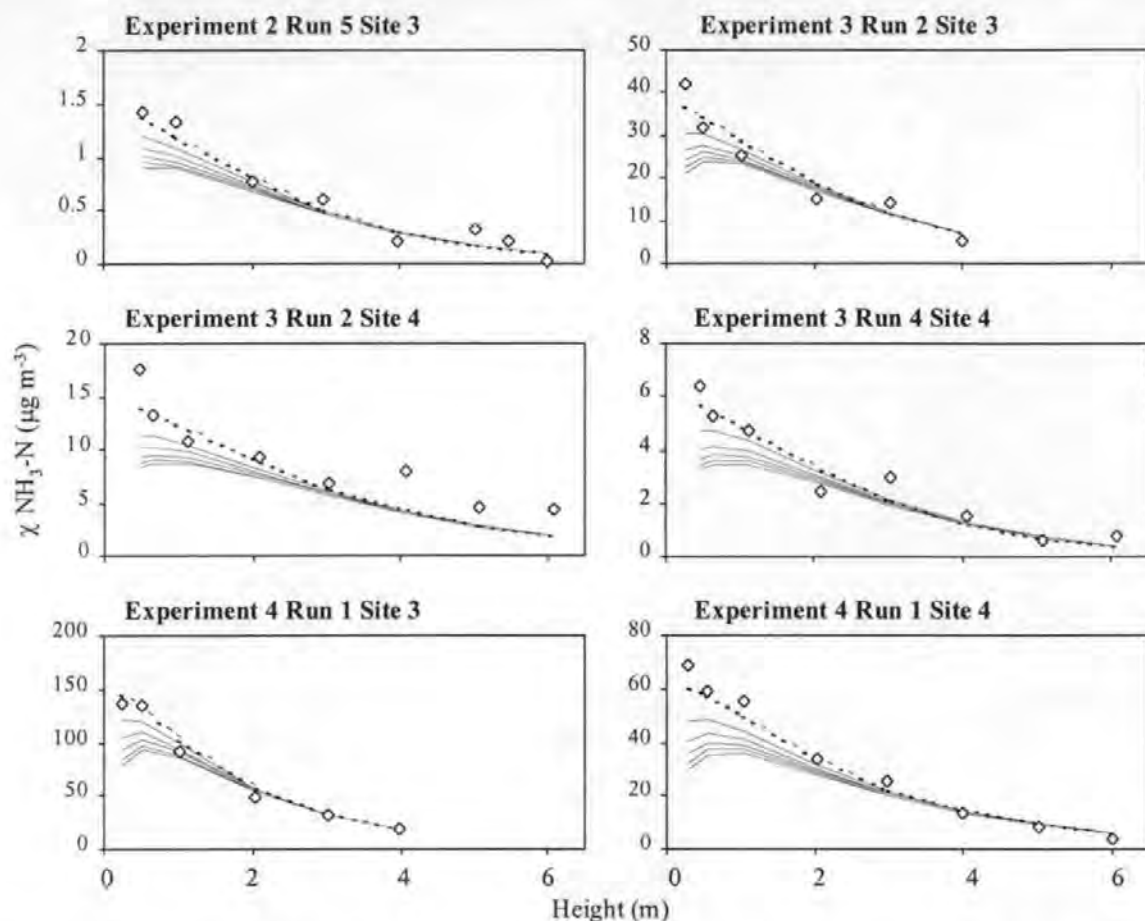
Figure 5.3: Examples of measured concentration profiles interpreted using the KATCH model to suggest that no deposition flux occurred over the downwind grassland. Measured concentration:◇, model fit without deposition:------ , model fit with deposition: —— (V_d varied between 0.02 and 0.10 m s^{-1}). It should be noted that the y-axis varies between plots.

5.4 ANALYSIS OF EXPERIMENTAL RESULTS

5.4.1 Experiment 1: 06/12/95 - 09/12/95

Experiment 1 was conducted at Halse during the winter of 1995, and was designed to simulate a period when farmers often spread slurry to reduce the volume of waste contained in their slurry stores. This experiment also provided an opportunity to investigate an extreme in meteorological conditions and to examine local exchange budgets during conditions when stomatal uptake of NH₃ would be negligible.

5.4.1.1 Meteorological conditions

Meteorological conditions measured during Experiment 1 are presented in Figure 5.5. The surface was covered with a thin layer of snow during the first run of the experiment with frozen surface conditions persisting for the initial three runs. Low surface relative humidities were measured during periods when the surface was frozen with increases in surface relative humidity measured following the snowfall during the penultimate run.
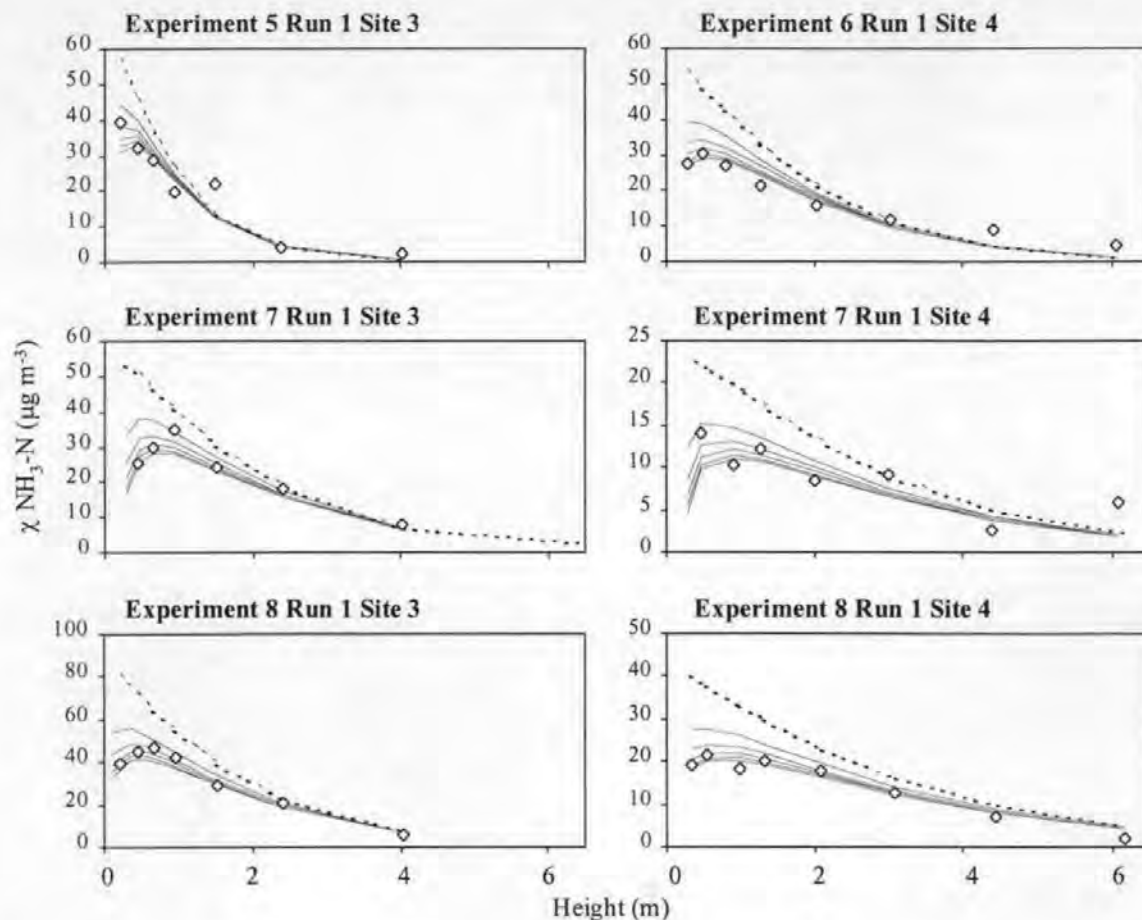
Figure 5.4:   Examples of measured concentration profiles interpreted using the atmospheric dispersion model where deposition fluxes have been estimated. Measured concentration: $\diamond$, model fit without deposition: $\cdots\cdots$, model fit with deposition: —— (V_d varied between 0.02 and 0.10 m s^{-1}). It should be noted that the y-axis varies between plots.

5.4.1.2   *NH₃-N emission*

The emission of NH_3-N from the slurry strip during Experiment 1 is shown in Figure 5.6. Fluxes of NH_3 measured during the first run of the experiment accounted for 55 % of the total NH_3 emission. The mean emission flux reduced by almost an order of magnitude during Run 2, following the characteristic exponential decline in emission rate caused by the depletion of liquid phase NH_3 concentrations on the surface of the slurry (*e.g.* Genermont *et al.*, 1998). Despite the continuing depletion of the surface NH_3 concentrations, emission of NH_3 increased slightly between Runs 2 and 3, correlating with increases in friction velocity and temperature. Emission fluxes continued to increase during Run 4, though mean friction velocity decreased slightly, suggesting either the dependence of emission fluxes on surface temperature or that a peak in NH_3 emission correlated with the measured peaks in friction velocity and latent heat flux. Runs 5 and 6 showed a much reduced NH_3-N emission rate, possibly due to the capping, and on melting, dilution effects of the observed snowfall.
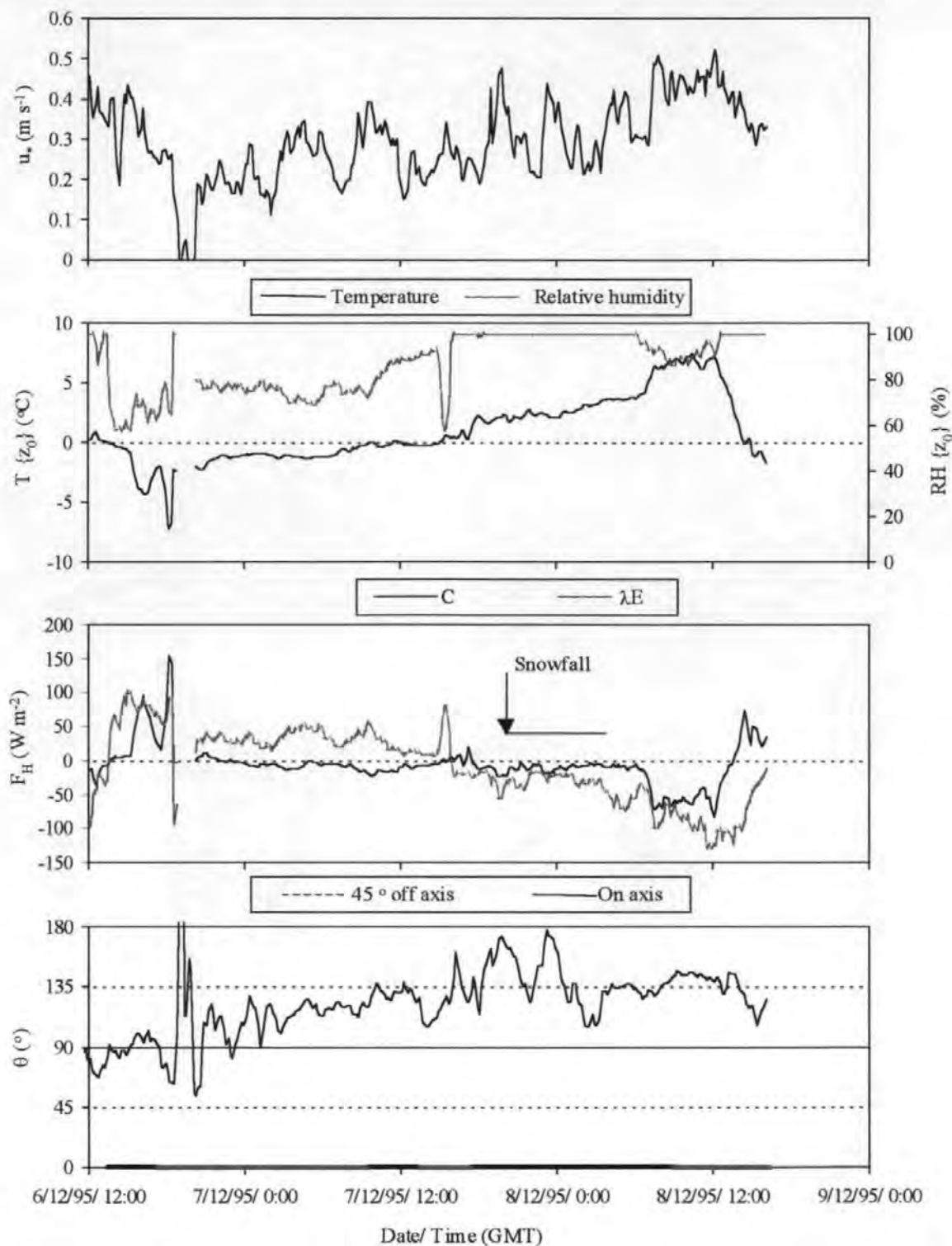
Figure 5.5: Meteorological data recorded during Experiment 1. Run times are shown as bars on the x-axis. Friction velocity: u_*, surface temperature: $T\{z_0\}$, surface relative humidity: $RH\{z_0\}$, heat flux: F_H, sensible heat: C, latent heat: λE, wind direction: θ. Horizontal lines on the wind direction plot show the "on axis wind direction" (the wind direction parallel to the experimental array) and +/- 45° from the on-axis wind direction, termed "45° off-axis".

5.4.1.3   Estimation of local NH₃ deposition

The concentration profile measured downwind of the slurry strip, at Site 3, during Run 1 corresponded with the midpoint of the KATCH model predictions for non-depositing dispersion and for a deposition velocity of 0.02 m s^{-1}. The profile interpretation for this run was determined using the ACG method, results are shown in Table 5.4. A deposition flux of 1.2 +/- 7.0 µg NH₃-N m^{-2} s^{-1} was estimated, corresponding to a deposition velocity of 0.01 m s^{-1}. Deposition velocities estimated by both direct profile interpretation and using the ACG method were much lower than the estimated deposition velocity limited by boundary layer resistance ($V_{d\,max}$) of 0.06 m s^{-1}. This suggested that the frozen conditions and low surface humidities measured during this run had resulted in a surface resistance to NH₃ deposition of approximately 80 s m^{-1}.

Figure 5.6:   Time series of NH₃-N emission fluxes from the experimental area treated with slurry during Experiment 1.

The profile interpretations for Runs 2 and 4 were reasonably well described by the KATCH model predictions for non-depositing dispersion, demonstrating that the surface strongly resisted NH₃ deposition (*i.e.* $R_c = \infty$). Concentration profiles for Runs 3, 5 and 6 were not sufficiently well defined to be interpreted using the KATCH model.

Run	Flux NH₃-N (µg m^{-2} s^{-1})		Deposition velocity (m s^{-1})
	ESTIMATED	$R_c = 0$	ESTIMATED
1	-1.2 +/- 7.0	-3.8	0.01 (<0, >$V_{d\,max}$)

Table 5.4:   Profile interpretations for Experiment 1 (Site 3) calculated using the ACG method.

A NH_x-N budget was calculated for Experiment 1, using the method discussed in Section 5.1. Results, shown in Table 5.5, demonstrate that, as a high proportion of the total NH_3 emission occurred during Run 1, the uncertainty in the deposition estimate during this run dominated the uncertainty of the combined results. Deposition over the grassland to 50 m downwind, at a rate limited by boundary layer resistance (*i.e.* deposition at $V_{d\ max}$) was estimated to result in a reduction in the net emission from the site of 22 %. However, due to the high surface resistance encountered during the field experiment, the estimated reduction in the net emission was 4 %.

Run	V_d (m s⁻¹)		Flux NH_3-N (µg m⁻² s⁻¹)			Mass flux (kg NH_3-N)			Deposited (%)	
	R_c= est	R_c= 0	Slurry	R_c= est	R_c= 0	Slurry	R_c= est	R_c = 0	R_c = est	R_c = 0
1	0.01	0.06	21	0 to -0.90	-3	1.4	-0.09	-0.3	7	21
2	0	0.04	1.9	0	-0.3	0.54	0	-0.1	0	22
3	N/A	0.06	2.3	N/A	-0.3	0.15	N/A	-0.04	N/A	23
4	0	0.05	3.1	0	-0.4	0.22	0	-0.05	0	23
5	N/A	0.06	0.47	N/A	-0.06	0.13	N/A	-0.03	N/A	23
6	N/A	0.08	0.63	N/A	-0.08	0.08	N/A	-0.02	N/A	23
			TOTAL			2.51	-0.09	-0.54	4	22

Table 5.5:　NH₃-N budget calculated for Experiment 1 using the KATCH model. Calculations were made of the deposition to 50 m downwind of the source assuming a 30 m wide slurry strip with a length of 160 m subject to an on-axis wind direction. R_c= est: surface resistance to deposition estimated from the profile measurements, R_c= 0: no surface resistance assumed.

5.4.2　Experiment 2: 14/12/95 - 16/12/95

Experiment 2 provided additional data on the emission and fate of NH_3 during winter conditions. Due to the general similarity in meteorological conditions measured between Experiments 1 and 2, this experiment also enabled the reproducibility of the previous experimental results to be confirmed.

5.4.2.1　Meteorological conditions

Meteorological conditions measured during Experiment 2 are shown in Figure 5.7. The experiment was conducted during slightly warmer and less humid conditions than Experiment 1, with a stronger mean wind speed. The only period of snowfall occurred during Run 4, whilst the surface was clear of snow for the remainder of the experiment.
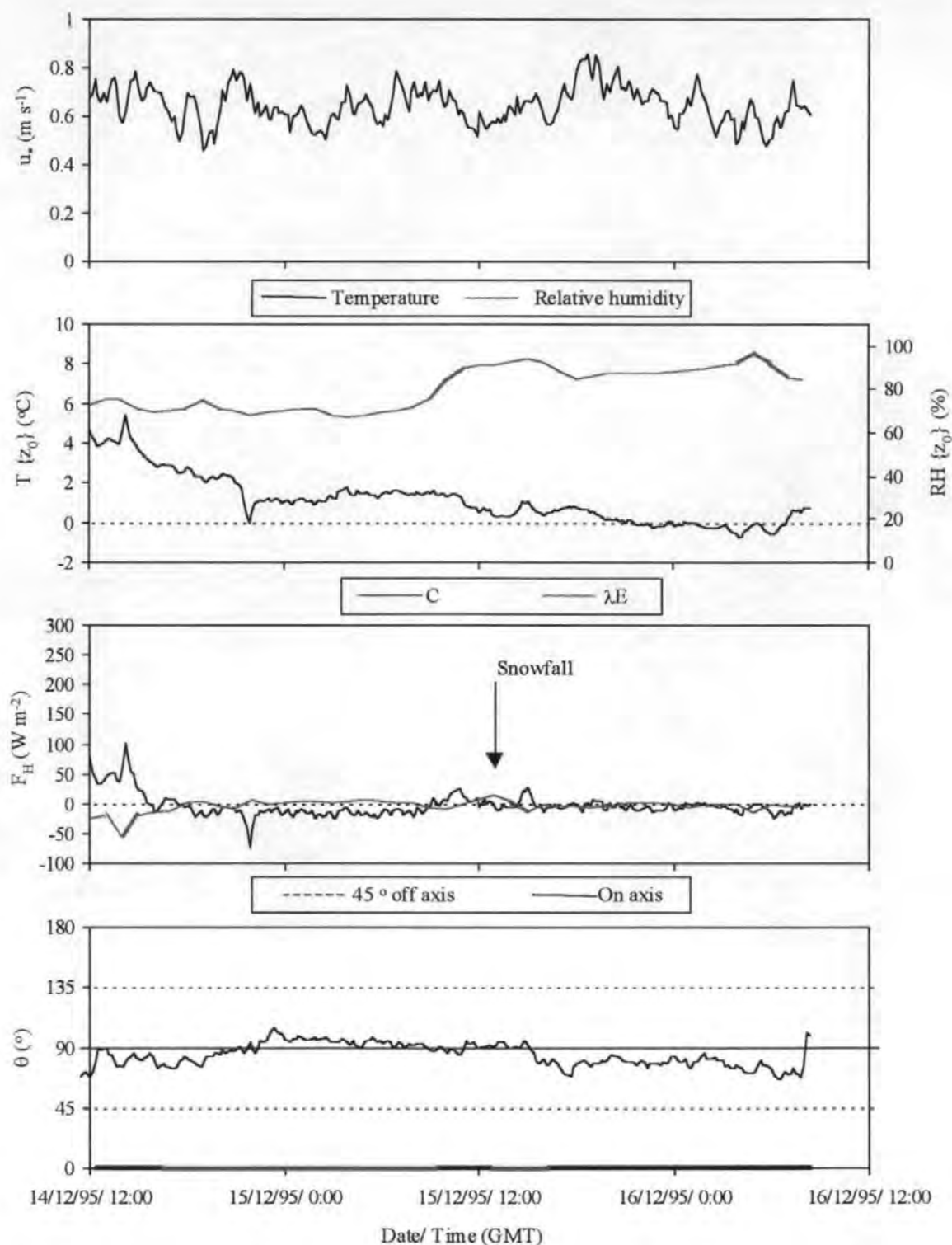
Figure 5.7:   Meteorological data recorded during Experiment 2. Run times are shown as bars on the x-axis. Abbreviations are defined in Figure 5.5.

5.4.2.2 NH_3-N emission

The emission of NH_3-N from the slurry strip is shown in Figure 5.8. A very strong initial flux of NH_3 from the slurry strip was measured, accounting for 61 % of the total emission measured during the experiment. A rapid reduction in NH_3 emission occurred between

Runs 1 and 2, which was likely to be related to the depletion of the liquid phase NH_3-N concentrations (as discussed in Section 5.4.1.2).

Emission fluxes continued to reduce during Run 3, whilst an increase in emission flux was measured during Run 4. As friction velocities, temperatures and relative humidities were relatively constant between Runs 3 and 4 these results suggest that the enhanced NH_3 emission correlated with the emission of latent heat from the surface. Emission fluxes reduced considerably during Run 5, suggesting that either the frozen surface conditions acted to prevent NH_3 emission or that liquid phase NH_3-N concentrations were too low to sustain a strongly positive surface-atmosphere concentration gradient.
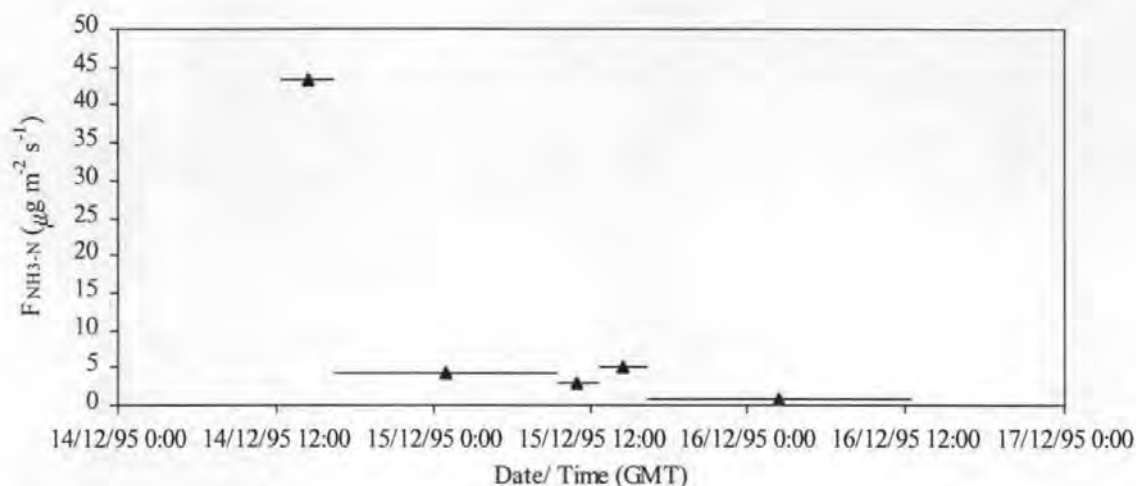
Figure 5.8:   Time series of NH_3-N emission fluxes from the experimental area treated with slurry during Experiment 2.

5.4.2.3   Estimation of local NH₃ deposition

The NH_3 concentration profile measured at Site 3 during Run 1 was in good agreement with the midpoint of the KATCH model predictions for non-depositing dispersion and for a deposition velocity of 0.02 m s⁻¹. The concentration profile measured during this run was analysed using the ACG method. The results, shown in Table 5.6, demonstrated that a surface resistance to NH_3 deposition of 90 s m⁻¹ was present. The concentration profiles measured during Runs 2 and 5 agreed with the predictions of the KATCH model for non-depositing dispersion providing further evidence that a strong surface resistance to NH_3 deposition was present. Concentration profiles measured during Runs 3 and 4 were not sufficiently well resolved to be interpreted to determine local NH_3 deposition, though the approximate magnitudes of concentrations measured in the field were predicted by the model.

The estimated emission and local deposition budget for Experiment 2 is shown in Table 5.7. Though deposition velocities, assuming R_c= 0, were higher during Experiment 2 than during Experiment 1 the total maximum deposition flux reduced between the experiments. This was due to the increased wind driven vertical dispersion that occurred during Experiment 2, which reduced the concentration of NH$_3$ at the surface and thus limited the quantity of NH$_3$ available to deposit. The deposition velocity estimated during Experiment 2 was much lower than $V_{d\ max}$ demonstrating that a high surface resistance to deposition occurred. The estimated deposition, to 50 m downwind of the source, during this experiment was found to reduce the overall net emission of NH$_3$ by 2 % and the net emission during Run 1 by 4 %.

Run	Flux NH$_3$-N (μg m^{-2} s^{-1})		Deposition velocity (m s^{-1})
	ESTIMATED	R_c= 0	ESTIMATED
1	-1.4 +/- 2.0	-6.7	0.01 (<0, 0.03)

Table 5.6:   Profile interpretation results for Experiment 2 (Site 3) using the ACG method.

Run	V_d (m s^{-1})		Flux NH$_3$-N (μg m^{-2} s^{-1})			Mass flux (kg NH$_3$-N)			Deposited (%)	
	R_c= est	R_c= 0	Slurry	R_c= est	R_c= 0	Slurry	R_c= est	R_c= 0	R_c= est	R_c= 0
1	0.01	0.11	43	-1.0	-5.4	3.1	-0.12	-0.64	4	21
2	0.00	0.11	4.4	0.0	-0.55	1.3	0.0	-0.27	0	21
3	N/A	0.10	3.0	N/A	-0.37	0.17	N/A	-0.04	N/A	21
4	N/A	0.10	5.0	N/A	-0.63	0.31	N/A	-0.07	N/A	21
5	0.00	0.11	0.79	0.0	-0.10	0.22	0.00	-0.05	0	21
			TOTAL			5.05	-0.12	-1.06	2	21

Table 5.7:   NH$_3$-N budget calculated for Experiment 2 using the KATCH model. Calculations were made of the deposition to 50 m downwind of the source assuming a 30 m wide slurry strip with a length of 160 m subject to an on-axis wind direction. R_c= est: surface resistance to deposition estimated from the profile measurements, R_c= 0: no surface resistance assumed.

5.4.3   Experiment 3: 28/06/96 - 30/06/96

Experiment 3 was conducted in warm summer conditions following the typical agricultural practice of harvesting pasture grass to provide silage for winter fodder. The sward height, post cutting, was approximately 0.1 m and NH$_4$NO$_3$ fertiliser was applied to the site seven days before the start of the experiment.

Unfortunately, results from the passive flux samplers during the initial two runs of the experiment failed the quality control checks due to contamination in the laboratory. Consequently, no emission data or profile interpretations were available for these runs.

5.4.3.1   *Meteorological conditions*

The meteorological conditions encountered during Experiment 3 contrasted with those recorded in the previous experiments as clear diurnal cycles of wind speed, surface temperature, surface relative humidity and heat fluxes were found. A brief heavy shower occurred shortly after the start of the experiment, followed by two periods of light rain during Run 2.

5.4.3.2   *NH₃-N emission*

Emission fluxes from the slurry strip, measured during Experiment 3, are shown in Figure 5.10. Data for Runs 1 and 2 are not presented due to the aforementioned problems with the NH_3 horizontal flux measurements during these runs. The NH_3 emission flux measured during Run 3 of Experiment 3 was similar in magnitude to the flux measured during Run 3 of the previous experiments. This suggests that comparable patterns of emission had occurred during Runs 1 and 2 of Experiment 3 as were found in the previous experiments. A large increase in the emission of NH_3 from the slurry strip was measured during Run 4, coincident with increases in friction velocity, surface temperature, the emission of latent heat and a reduction in surface humidity. These conditions would act to reduce the water content of the slurry and thus concentrate NH_3 at the surface and promote volatilisation. Emission fluxes measured during Runs 5 and 6 were similar in magnitude to measurements made during Run 3.

5.4.3.3   *Estimation of local NH₃ deposition*

Two sites, positioned at 15 m and 30 m from the windward edge of the slurry strip, were used in Experiment 3 to investigate any possible variation in deposition velocities with downwind distance. With the exception of measurements at Site 3 during Run 4 (which showed too much scatter to be interpreted), all the measured profiles were well described by the KATCH model predictions for non-depositing dispersion, indicating that a strong surface resistance to NH_3 deposition was present.

An NH_3 budget calculated using the KATCH model with the meteorology and deposition velocity estimates from Experiment 3 is shown in Table 5.8. Despite the $V_{d\ max}$ values,

estimated during Experiment 3, being high (0.07 - 0.10 m s^{-1}) the high surface resistance measured during the experiment prevented any significant deposition of the emitted NH_3.

Figure 5.9:   Meteorological data recorded during Experiment 3. Run times are shown as bars on the x-axis. Abbreviations are defined in Figure 5.5.

F NH3-N (μg m^{-2} s^{-1})

12
10
8
6
4
2
0

28/06/96 00:00   28/06/96 12:00   29/06/96 00:00   29/06/96 12:00   30/06/96 00:00   30/06/96 12:00

Date/time (GMT)

Figure 5.10: Time series of NH₃-N emission fluxes from the experimental area treated with slurry during Experiment 3.

Run	V_d (m s^{-1})		Flux NH₃-N (μg m^{-2} s^{-1})			Mass flux (kg NH₃-N)			Deposited (%)	
	R_c= est	R_c= 0	Slurry	R_c= est	R_c= 0	Slurry	R_c= est	R_c= 0	R_c= est	R_c= 0
1	N/A	N/A	N/A	N/A	N/A	N/A	N/A	N/A	N/A	N/A
2	N/A	N/A	N/A	N/A	N/A	N/A	N/A	N/A	N/A	N/A
3	0.0	0.07	2.9	0.0	-0.41	0.57	0.0	-0.14	0	24
4	0.0	0.10	9.9	0.0	-1.26	0.88	0.0	-0.19	0	21
5	0.0	0.08	2.7	0.0	-0.36	0.29	0.0	-0.06	0	22
6	0.0	0.07	2.0	0.0	-0.26	0.42	0.0	-0.09	0	22
			TOTAL	2.16	0.0.	-0.48			0	22

Table 5.8: NH₃-N budget calculated for Experiment 3 using the KATCH model. Calculations were made of the deposition to 50 m downwind of the source assuming a 30 m wide slurry strip with a length of 160 m subject to an on-axis wind direction. R_c= est: surface resistance to deposition estimated from the profile measurements, R_c= 0: no surface resistance assumed.

5.4.4   Experiment 4: 24/07/96 – 26/07/96

Experiment 4 was conducted in the middle of the summer, and included periods with semi-calm conditions and strong insolation. These conditions were not ideal for conducting micrometeorological experiments as wind directions were very variable and the strongly convective conditions increased the uncertainties associated with the semi-empirical stability correction factors.

5.4.4.1   Meteorological conditions

Meteorological conditions measured during Experiment 4 are shown in Figure 5.11. This experiment was conducted during a dry period with stronger insolation than encountered

during the previous experiments. The strong insolation was responsible for the pronounced diurnal variability in the measured meteorological conditions and resulted in very low surface humidities during daytime periods.

Figure 5.11:   Meteorological data recorded during Experiment 4. Run times are shown as bars on the x-axis. Abbreviations are defined in Figure 5.5.

5.4.4.2   NH₃-N emission

The pattern of NH_3 -N emission measured during Experiment 4 is shown in Figure 5.12. As found in previous experiments, strong NH_3-N emission fluxes were measured during Run 1 with a substantial reduction in emission during the subsequent runs. A reduced rate of NH_3 emission was measured during Run 2, which correlated with low friction velocities, low surface temperatures and high surface relative humidities. An NH_3-N emission flux of 2.4 $\mu g\ m^{-2}\ s^{-1}$ was measured on the second day of the experiment suggesting that NH_3 emission fluxes would continue after the experiment had finished.

5.4.4.3   Estimation of local NH₃ deposition

The KATCH model was used to interpret the downwind vertical NH_3-N concentration profiles using a time series of 10 minute averaged meteorological data. The effects of "off-axis" wind directions on dispersion were modelled using the SOURCEGEO module, discussed in Chapter 3, Section 3.3.2.3. These modifications to the modelling approach were used to account for the trends and fluctuations in wind directions and other meteorological conditions encountered throughout this experiment.
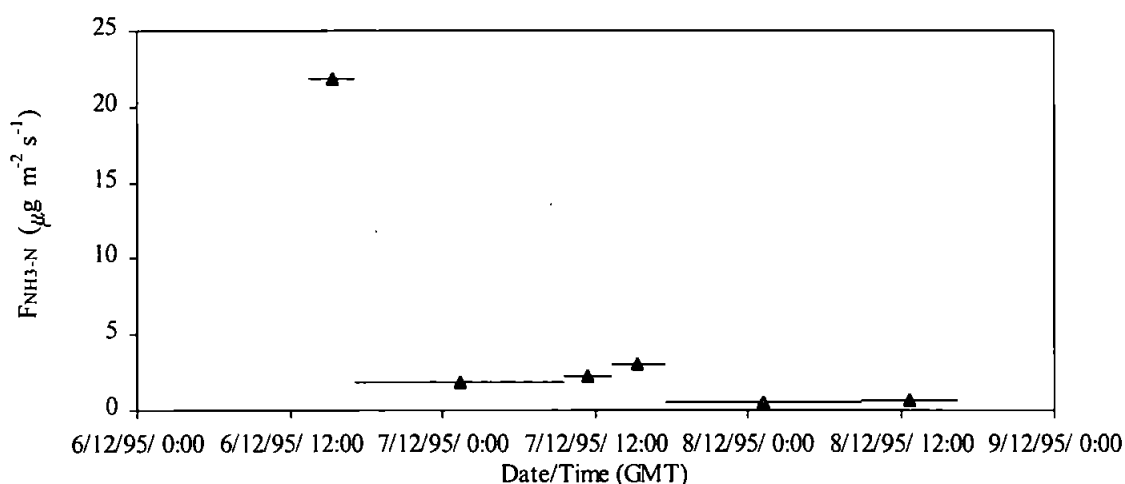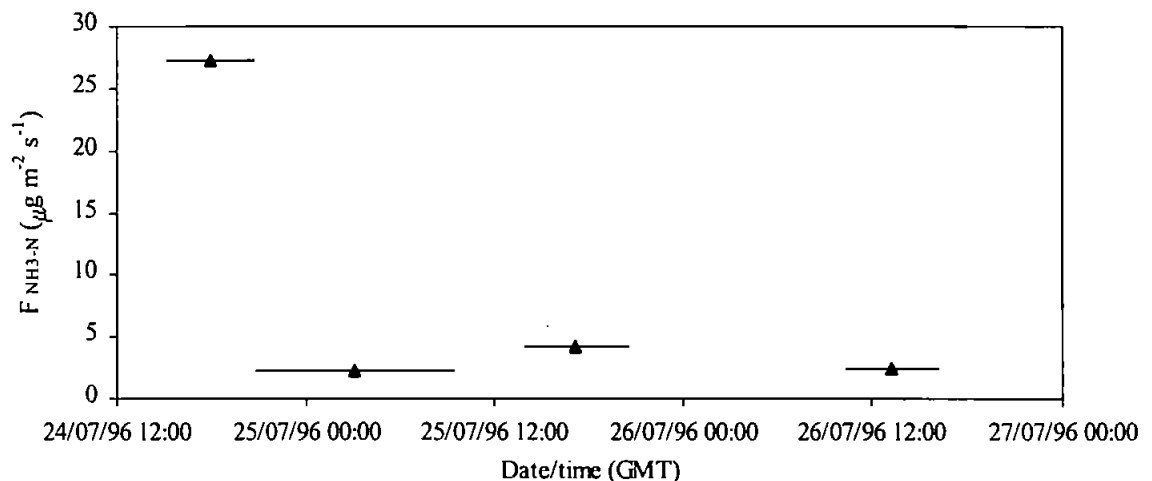

Figure 5.12:   Time series of NH_3-N emission fluxes from the experimental area treated with slurry during Experiment 4.

The NH_3-N concentration profiles measured at Sites 3 and 4 during Run 1 were in close agreement with the KATCH model predictions for non-depositing dispersion, demonstrating that little deposition of NH_3 occurred. Profiles measured at these sites during Run 2 were found to conform to the KATCH model predictions for depositing dispersion and were further investigated using the ACG method, results are shown in Table 5.9. Estimated deposition fluxes were slightly higher than $V_{d\ max}$, though the confidence limits of the flux estimates showed that the best estimate of the deposition velocity for this

run was that at $V_{d\,max}$. No interpretation of the concentration profiles could be made for Run 3 due to the highly variable wind directions. Air concentrations measured at Site 3 during Run 4 showed a good agreement to the KATCH model predictions for non-depositing dispersion, although the results at Site 4 were too variable to be interpreted.

Run	Flux NH₃-N ($\mu g\ m^{-2}\ s^{-1}$) ESTIMATED		Flux NH₃-N ($\mu g\ m^{-2}\ s^{-1}$) $R_c = 0$		Deposition velocity ($m\ s^{-1}$) ESTIMATED	
	Site 3	Site 4	Site 3	Site 4	Site 3	Site 4
2	-1.9 +/- 2.2	-1.6 +/- 1.9	-1.5	-1.1	$>V_{d\,max}$ (<0, $>V_{d\,max}$)	$>V_{d\,max}$ (<0, $>V_{d\,max}$)

Table 5.9:   Profile interpretations for Experiment 4 calculated using the ACG method.

An NH₃-N budget for Experiment 4 is presented in Table 5.10. A high proportion of the net emission during Run 2 was estimated to deposit, despite the suppression of turbulence limiting the maximum deposition velocity to 0.03 m s⁻¹. Conversely during periods when the atmosphere was highly unstable, and NH₃ was rapidly vertically transported, deposition at $V_{d\,max}$ only reduced budgets by 17 %. The field estimates of NH₃ deposition suggested that rapid deposition fluxes did not occur during the daytime and that deposition fluxes during the overnight periods coincided with reduced rates of NH₃-N emission from the slurry. In total, approximately 4 % of the emitted NH₃ was estimated to deposit within 50 m of the slurry strip during this experiment.

Run	V_d ($m\ s^{-1}$)		Flux NH₃-N ($\mu g\ m^{-2}\ s^{-1}$)			Mass flux (kg NH₃-N)			Deposited (%)	
	R_c = est	R_c = 0	Slurry	R_c = est	R_c = 0	Slurry	R_c = est	R_c = 0	R_c = est	R_c = 0
1	0.00	0.08	28	0.0	-3.5	2.70	0.00	-0.56	0	21
2	0.03	0.03	2.3	-0.49	-0.49	0.50	0.18	-0.18	36	36
3	N/A	0.06	5.3	N/A	-0.55	0.62	N/A	-0.11	N/A	17
4	0.00	0.05	2.4	0.0	-0.23	0.24	0.00	-0.04	0	17
			TOTAL			4.10	-0.18	-0.89	4	22

Table 5.10:   NH₃-N budget calculated for Experiment 4 using the KATCH model. Calculations were made of the deposition to 50 m downwind of the source assuming a 30 m wide slurry strip with a length of 160 m subject to an on-axis wind direction. R_c= est: surface resistance to deposition estimated from the profile measurements, R_c= 0: no surface resistance assumed.

5.4.5   Experiment 5: 15/10/96 – 17/10/96

Experiment 5 was conducted during autumn 1996 to investigate a period when farmers typically empty slurry stores in preparation for the indoor overwintering of cattle. The

sward height was relatively short (0.1 m) as the field site had been recently grazed, though cattle were removed from the site seven days before the start of the experiment.

5.4.5.1   *Meteorological conditions*

Meteorological data measured during Experiment 5 are shown in Figure 5.13. The experiment was conducted during humid overcast conditions with numerous precipitation events. Moderate wind speeds were recorded during the first 24 hours of the experiment with near-calm conditions being recorded around midnight 17/10/96. The meteorology encountered on the final day of the experiment was influenced by the development of convective atmospheric conditions, with a strong correlation between measurements of friction velocity and surface heat flux.

5.4.5.2   *NH_3-N emission*

The emissions of NH_3-N from the slurry applied at the start of this experiment are shown in Figure 5.14. The initial NH_3 emission flux measured during Run 1 of this experiment was weaker than that measured during the previous experiments, accounting for 42 % of the total NH_3 emission. This was likely to be due to the lower TAN content of the slurry and the leaching of NH_x from the slurry into the ground, with a possible further dilution caused by the rainfall. The emissions during the initial four runs of this experiment followed the familiar exponential reduction due to depletion of the surface NH_3 concentrations. Further evidence for the environmental controls of NH_3 emission are suggested by the considerable reduction in emission measured during Run 5, a period when a frost developed and wind speeds slowed to around 0.5 m s⁻¹. Following a familiar pattern, as wind speeds and temperatures increased during the daytime (Runs 6 and 7), so NH_3 emissions increased. In total 16 % of the TAN applied as slurry volatilised as NH_3 during this experiment.

5.4.5.3   *Estimation of local NH_3 deposition*

Initial profile interpretations, made using the KATCH model, suggested that NH_3 deposition occurred during Runs 1 and 2. Statistically significant deposition fluxes were estimated using the ACG method from measurements at Site 3 during Run 1 and at Site 4 during Run 2, results are shown in Table 5.11. The results at the other sites also suggested that atmospheric deposition was occurring, though a lower confidence was attached to the magnitude estimates. Deposition velocities of 0.02 m s⁻¹ and 0.04 m s⁻¹, corresponding to surface resistances of 41 s m⁻¹ and 16 s m⁻¹, were estimated from the deposition fluxes measured during these runs.
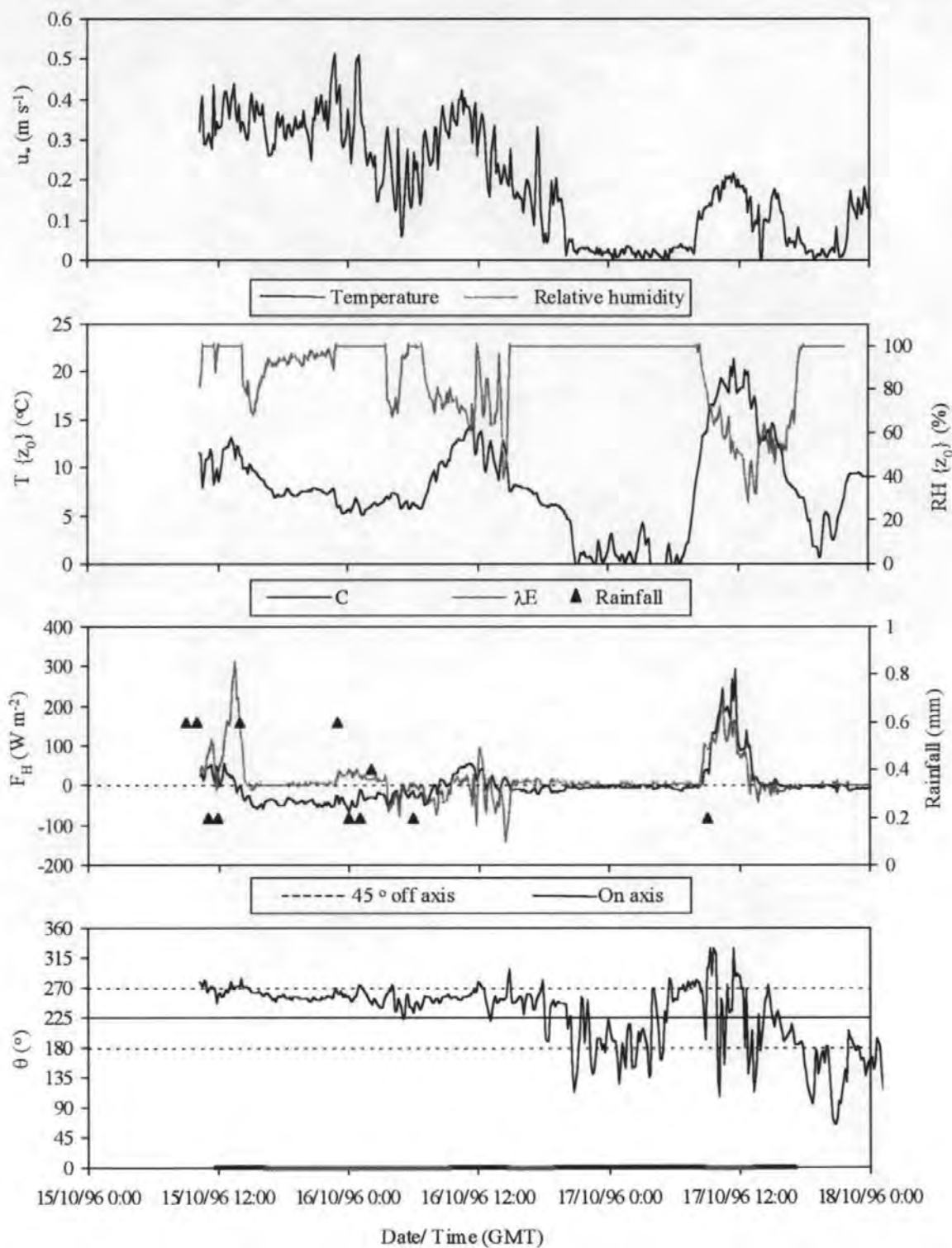
Figure 5.13:   Meteorological data recorded during Experiment 5. Run times are shown as bars on the x-axis. Abbreviations are defined in Figure 5.5.
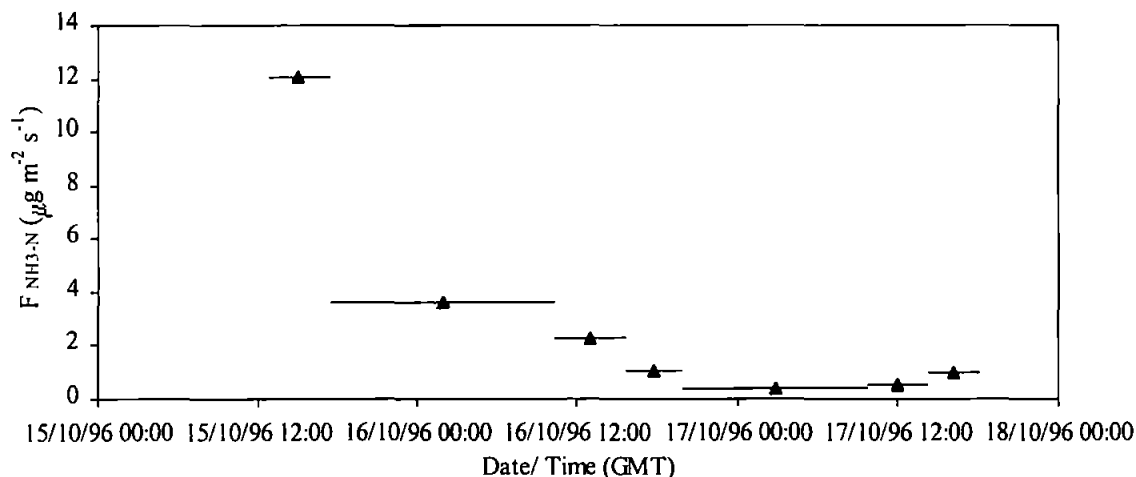
Figure 5.14:   Time series of NH₃-N emission fluxes from the experimental area treated with slurry during Experiment 5.

Direct model interpretations of the concentration profiles measured during Runs 3, 4 and 5 suggested that deposition downwind of the source did not occur. However, as there was considerable scatter between the model predictions and the measurements, particularly at Site 3, large uncertainties are attached to these interpretations. Surface humidities were high during these periods and there were short periods of heavy rain, conditions where deposition fluxes were expected. The lack of evidence of deposition suggests that the sink for atmospheric NH₃, the leaf surfaces of the grass, had reached a saturation point during the first two runs of the experiment and thereafter strongly resisted NH₃ deposition.

Due to the light winds, weak NH₃ emission fluxes from the slurry strip, and strong surface heat fluxes ($L= -2$ m) the vertical concentration profiles measured during Run 6 could not be interpreted. The concentration profiles measured during Run 7 were also difficult to interpret though there was some evidence that little, if any, deposition occurred.

The NH₃-N budget for Experiment 5 is shown in Table 5.12. The maximum deposition fraction ($V_{d\ max}$) during this experiment was more variable than had been previously found. Estimated deposition fractions at $V_{d\ max}$ ranged between 10 - 40 %. The maximum deposition corresponded to the calm stable conditions of Run 5, whilst the minimum corresponded to the unstable conditions measured during Run 6. The deposition fluxes which occurred during the initial two runs of Experiment 5 accounted for a reduction of 12 % and 20 % of the NH₃-N emitted respectively. In total 14 % of the emitted NH₃ was estimated to deposit within 50 m.

Run	Flux NH₃-N (µg m⁻² s⁻¹) ESTIMATED		Flux NH₃-N (µg m⁻² s⁻¹) $R_c=0$		Deposition velocity (m s⁻¹) ESTIMATED	
	Site 3	Site 4	Site 3	Site 4	Site 3	Site 4
1	-1.6 +/- 0.8	-2.8 +/- 5.4	-3.3	-1.8	0.02 (0.01, 0.04)	$>V_{d\,max}$ (<0, $>V_{d\,max}$)
2	-0.5 +/- 1.1	-0.45 +/- 0.35	-1.1	-0.6	0.02 (<0, $>V_{d\,max}$)	0.04 (0.01, $>V_{d\,max}$)

Table 5.11:   Profile interpretations for Experiment 5 calculated using the ACG method.

Run	V_d (m s⁻¹)		Flux NH₃-N (µg m⁻² s⁻¹)			Mass flux (NH₃-N)			Deposited (%)	
	R_c= est	R_c =0	Slurry	R_c= est	R_c= 0	Slurry	R_c= est	R_c= 0	R_c= est	R_c= 0
1	0.02	0.11	12	-0.87	-1.8	0.97	-0.12	-0.24	12	24
2	0.04	0.09	3.6	-0.43	-0.56	1.1	-0.21	-0.27	20	26
3	0.0	0.09	2.2	0.0	-0.31	0.21	0.00	-0.05	0	23
4	0.0	0.05	1.1	0.0	-0.18	0.08	0.00	-0.02	0	28
5	0.0	0.01	0.35	0.0	-0.08	0.08	0.00	-0.03	0	40
6	N/A	0.04	0.50	N/A	-0.03	0.04	N/A	-3.73	N/A	10
7	N/A	0.03	0.97	N/A	-0.16	0.06	N/A	-0.02	N/A	27
					TOTAL	2.32	-0.33	-0.58	14	25

Table 5.12:   NH₃-N budget calculated for Experiment 5 using the KATCH model. Calculations were made of the deposition to 50 m downwind of the source assuming a 30 m wide slurry strip with a length of 160 m subject to an on-axis wind direction. R_c= est: surface resistance to deposition estimated from the profile measurements, R_c= 0: no surface resistance assumed.

5.4.6   Experiment 6: 30/10/96 – 01/11/96

This experiment was conducted to supplement and, to some extent, replicate the results of Experiment 5 providing additional data on the emission and fate of NH₃ volatilised from autumn applications of cattle slurry. As 65 mm of rainfall were recorded between Experiments 5 and 6 it was assumed that any NH₃ deposited onto the vegetation during the previous experiment would have been removed.

5.4.6.1   Meteorological conditions

The meteorological conditions measured during Experiment 5 are presented in Figure 5.15. In general, the experiment was conducted during a period of high surface humidity with frequent light drizzle occurring during Runs 3, 4, 5 and 6. A strong correlation between the diurnal variations in friction velocity, surface temperature and surface sensible heat flux was observed. The latent heat fluxes measured during this experiment demonstrated that evapotranspiration occurred during midday periods though the net surface-atmosphere latent heat flux was directed towards deposition at other times.
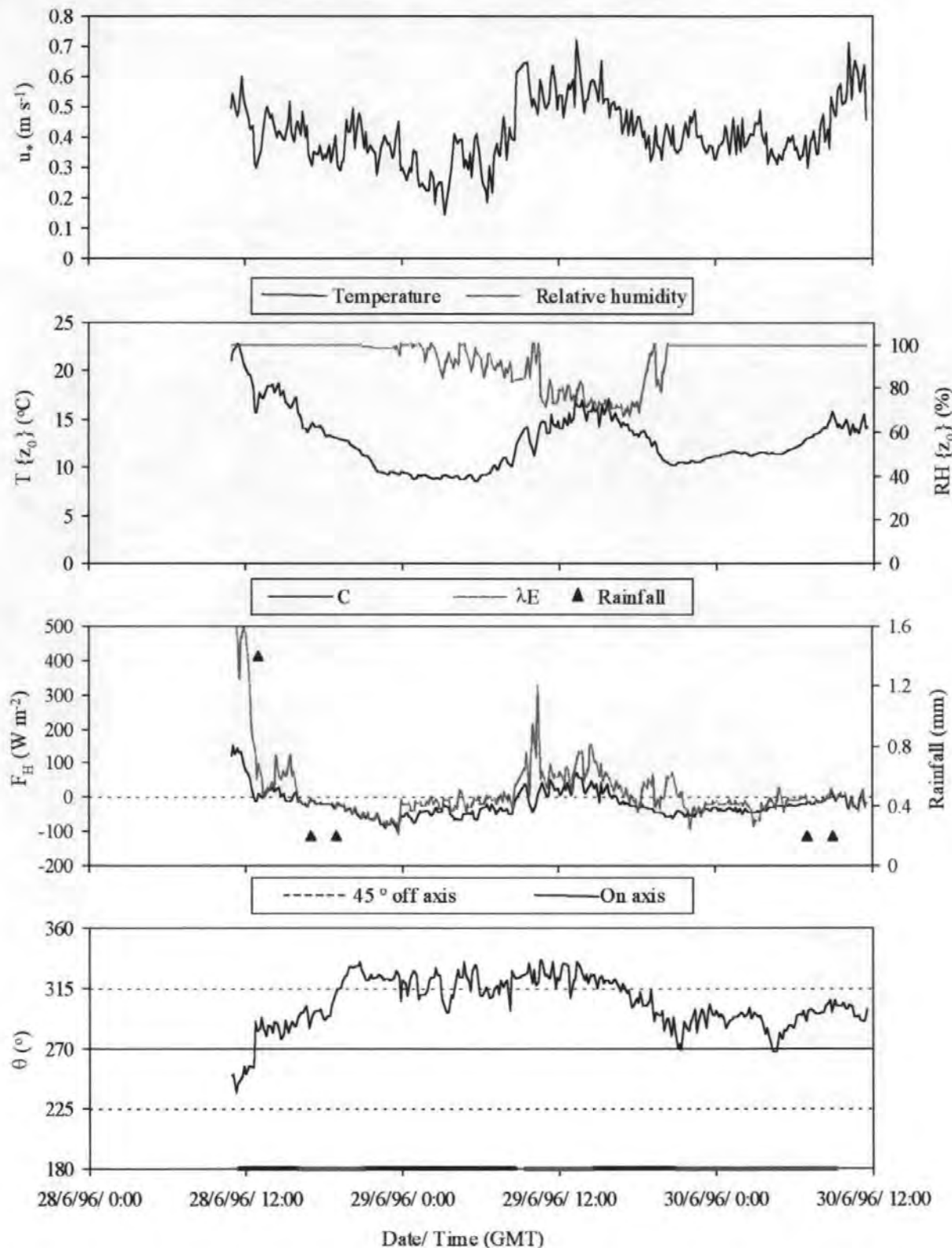
Figure 5.15:   Meteorological data recorded during Experiment 6. Run times are shown as bars on the x-axis. Abbreviations are defined in Figure 5.5.
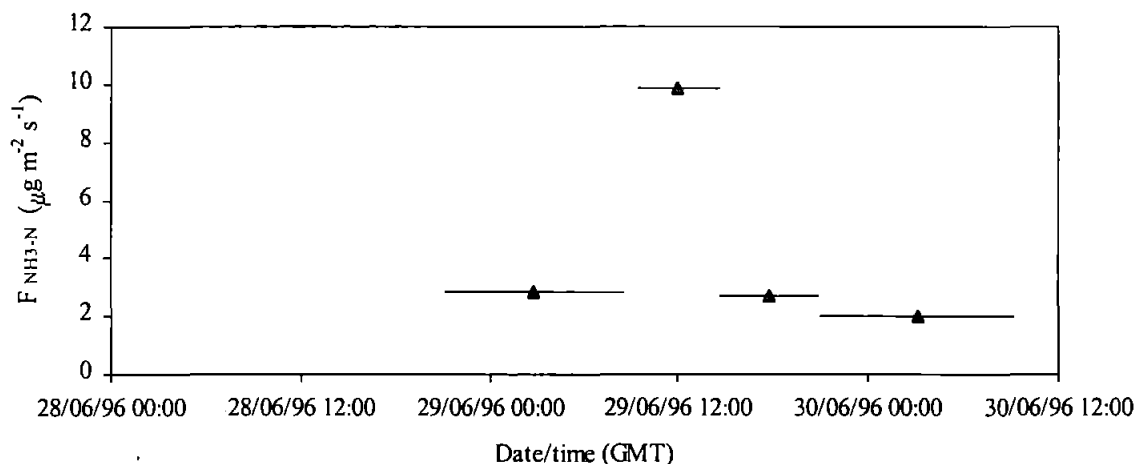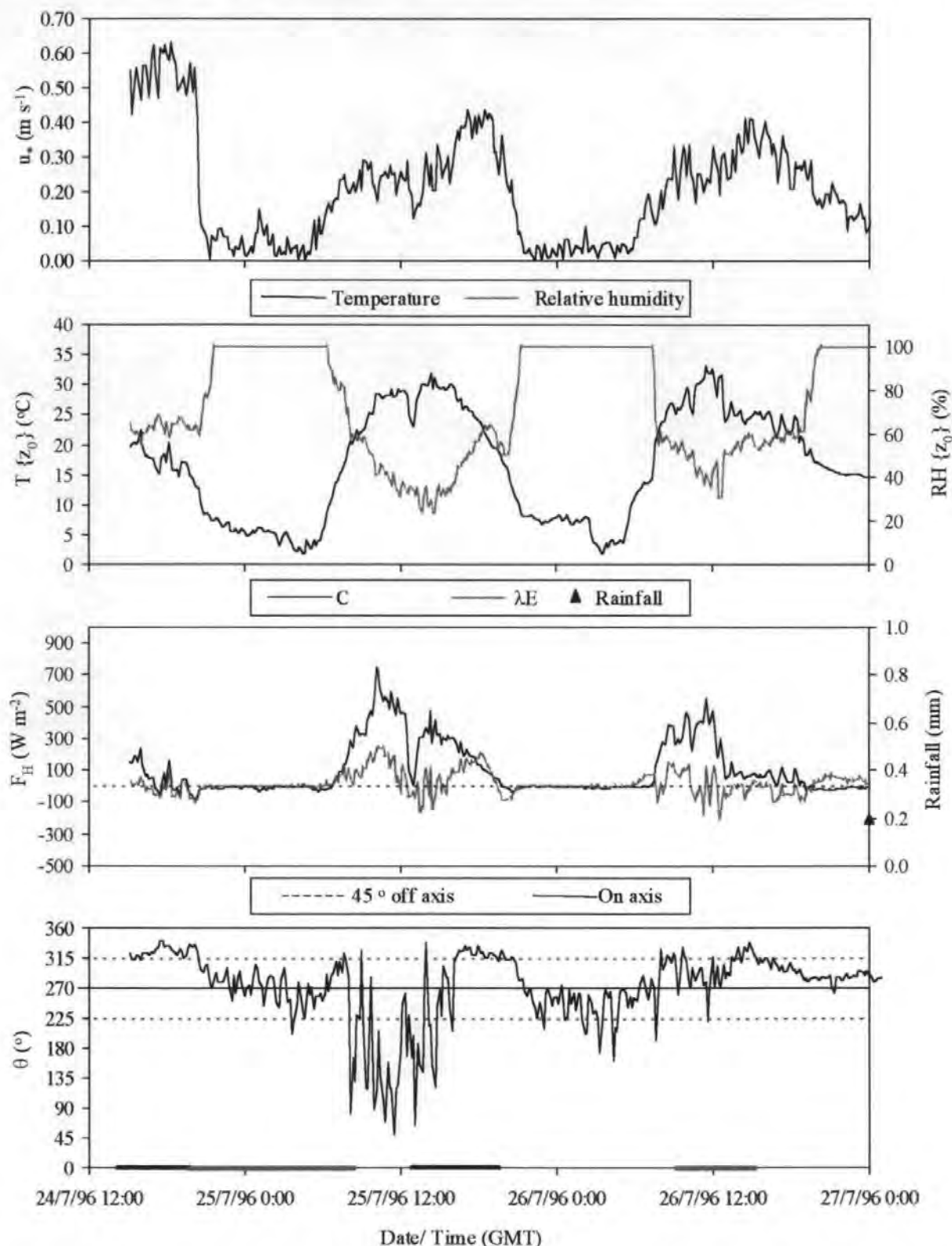
5.4.6.2   NH₃-N emissions

A familiar pattern of NH₃ emissions occurred, as shown in Figure 5.16, with strong emission fluxes occurring immediately following spreading and an exponential reduction

148

in emission flux over the subsequent runs. This experiment showed that NH_3 emission fluxes measured during overnight periods were lower than those measured during the adjacent daytime periods, demonstrating the dependence of emission fluxes on wind speed and surface temperature. Furthermore, the difference in NH_3 emissions measured during Runs 4 and 5 suggest some dependence of emission rates on rainfall and possibly surface heat flux.

In total 20 % of the applied NH_x was volatilised during this experiment with 29 % of the total NH_3-N volatilisation occurring during the initial experimental run. The relatively high proportion of NH_3 emitted demonstrates that the observed precipitation was not sufficient to leach NH_3 into the soil. In addition, the high surface humidity was likely to have both prevented the slurry from drying out and restricted the emission during the initial run.
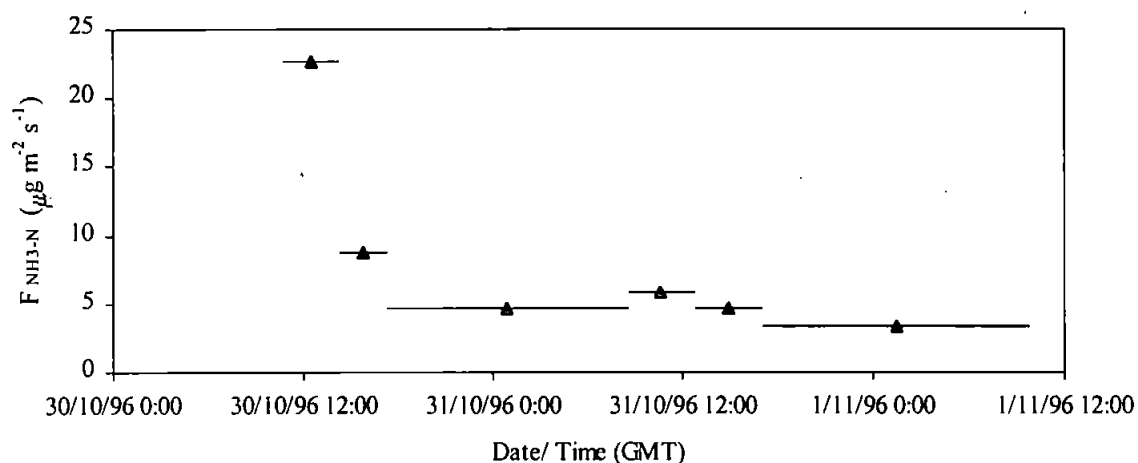
Figure 5.16: Time series of NH_3-N emission fluxes from the experimental area treated with slurry during Experiment 6.

5.4.6.3   Estimation of local NH₃ deposition

Initial interpretations of the measured NH_3 concentration profiles, using the KATCH model, provided some evidence that deposition fluxes occurred during much of the experiment. The KATCH model was re-run using the transient simulation method, described in Section 5.4.4.3, to account for the off-axis wind directions recorded during Runs 5 and 6. Measurements at Site 4 during these runs were in reasonable general agreement with the model predictions. However, due to the measured concentrations being close to background levels these results were not subjected to further analysis. ACG method interpretations of the remaining results are shown in Table 5.13.

The ACG method interpretation of the NH_3 concentration profiles recorded during Run 1 showed that both measurement sites were in good agreement over the magnitude of the

149

deposition velocity, 0.02 m s⁻¹. This velocity was much lower than $V_{d\ max}$ (0.09 m s⁻¹) suggesting a surface resistance of 39 s m⁻¹. Run 2 did not show such a clear agreement between the downwind measurement sites, with the more distant site recording a flux and uncertainly bound of equal magnitude. A deposition velocity of 0.01 m s⁻¹ was determined from the more precise results at Site 3, showing that surface resistance to NH_3 deposition had increased to 83 s m⁻¹. Profiles measured during Run 3 also showed a discrepancy between the two downwind sites, though in this case the more precise determination was made at Site 4, showing that deposition occurred at $V_{d\ max}$ (*i.e.* $R_c = 0$). This reduction in surface resistance was coincident with the surface humidity reaching saturation point, demonstrating the high affinity of wet surfaces to gaseous NH_3. Surface resistances increased during Runs 4, 5 and 6 to 16 s m⁻¹, 42 s m⁻¹ and 190 s m⁻¹ respectively. The increase in surface resistance over time indicated that sink saturation was occurring.

The budget for an idealised source, constructed using the deposition velocities and meteorology measured during Experiment 6, is presented in Table 5.14. Due to the constant meteorological conditions, a reasonably constant maximum deposition fraction of between 22 % and 27 % was estimated throughout this experiment. The peak $V_{d\ max}$ occurred during the stable overnight conditions measured during Run 3. The surface resistances encountered in the field restricted the estimated deposition fractions for all the runs except Run 3. In total, 4.8 kg of NH_3-N were emitted, with 15 % of the emission estimated to locally redeposit. This compares with an estimated 25 % local recapture that would have occurred if the surface had behaved as a perfect sink for NH_3 deposition.

Run	Flux NH₃-N (µg m⁻² s⁻¹) ESTIMATED		Flux NH₃-N (µg m⁻² s⁻¹) $R_c= 0$		Deposition velocity (m s⁻¹) ESTIMATED	
	Site 3	Site 4	Site 3	Site 4	Site 3	Site 4
1	-2.5 +/- 3.4	-1.8 +/- 0.67	-6.1	-3.3	0.02 (0, 0.08)	0.02 (0.01, 0.04)
2	-1.0 +/- 0.77	-1.3 +/- 1.3	-2.7	-1.4	0.01 (0.005, 0.03)	0.06 (0, >$V_{d\ max}$)
3	-0.89 +/- 3.3	-0.81 +/- 0.32	-1.6	-0.83	0.02 (<0,>0.1)	0.06 (0.02, >0.10)
4	-0.90 +/- 1.6	N/A	-1.6	-0.85	0.04 (0, >$V_{d\ max}$)	N/A
5	-0.54 +/- 1.5	N/A	-1.1	-0.61	0.02 (0, >$V_{d\ max}$)	N/A
6	-0.12 +/- 0.18	N/A	-0.9	-0.49	0.005 (<0, 0.01)	N/A

Table 5.13:   Profile interpretations for Experiment 6 calculated using the ACG method.

Run	V_d (m s⁻¹)		Flux NH₃-N (µg m⁻² s⁻¹)			Mass flux (NH₃-N)			Deposited (%)	
	R_c= est	R_c= 0	Slurry	R_c= est	R_c= 0	Slurry	R_c= est	R_c= 0	R_c= est	R_c= 0
1	0.02	0.09	22	-1.6	-3.0	1.4	-0.17	-0.31	12	22
2	0.01	0.06	8.8	-0.58	-1.3	0.45	-0.05	-0.11	11	25
3	0.06	0.06	4.7	-0.79	-0.78	1.3	-0.35	-0.34	28	27
4	0.04	0.11	5.8	-0.57	-0.81	0.42	-0.07	-0.10	16	23
5	0.02	0.13	4.7	-0.27	-0.65	0.35	-0.03	-0.08	10	23
6	0.005	0.09	3.4	-0.10	-0.50	0.98	-0.05	-0.24	5	24
					Total	4.84	-0.71	-1.18	15	24

Table 5.14: NH₃-N budget calculated for Experiment 6 using the KATCH model. Calculations were made of the deposition to 50 m downwind of the source assuming a 30 m wide slurry strip with a length of 160 m subject to an on-axis wind direction. R_c= est: surface resistance to deposition estimated from the profile measurements, R_c= 0: no surface resistance assumed.

5.4.7 Experiment 7: 15/05/97 – 16/05/97

This experiment was conducted during springtime, a period when dairy farmers are typically preparing to make the first harvest of grass for silage production and often dispose of slurry accumulated over the winter. This experiment was designed to simulate the application of slurry onto cut grassland with the NH₃ plume dispersing over an uncut adjacent field. The experimental site had not been recently fertilised and the sward height over the uncut area was 0.4 m.

5.4.7.1 Meteorological conditions

The meteorological conditions measured during Experiment 7 are shown in Figure 5.17. The meteorological data showed a strong correlation between the diurnal variation in friction velocities, sensible heat fluxes and surface temperatures, typical of periods with strong insolation and convective daytime meteorological conditions. The surface relative humidity was high (>90 %) for much of the experiment and strong daytime evapotranspiration fluxes were observed, suggesting a high soil water content and high rates of daytime photosynthesis.

5.4.7.2 NH₃-N emissions

The pattern of NH₃ emissions measured during Experiment 7 is shown in Figure 5.18. The initial flux of NH₃ from the slurry treated plot accounted for 48 % of the total measured emission. Emission fluxes reduced rapidly during Runs 2 and 3 with a further reduction

occurring during the overnight Run 4, correlating with low surface temperatures and light wind speeds.
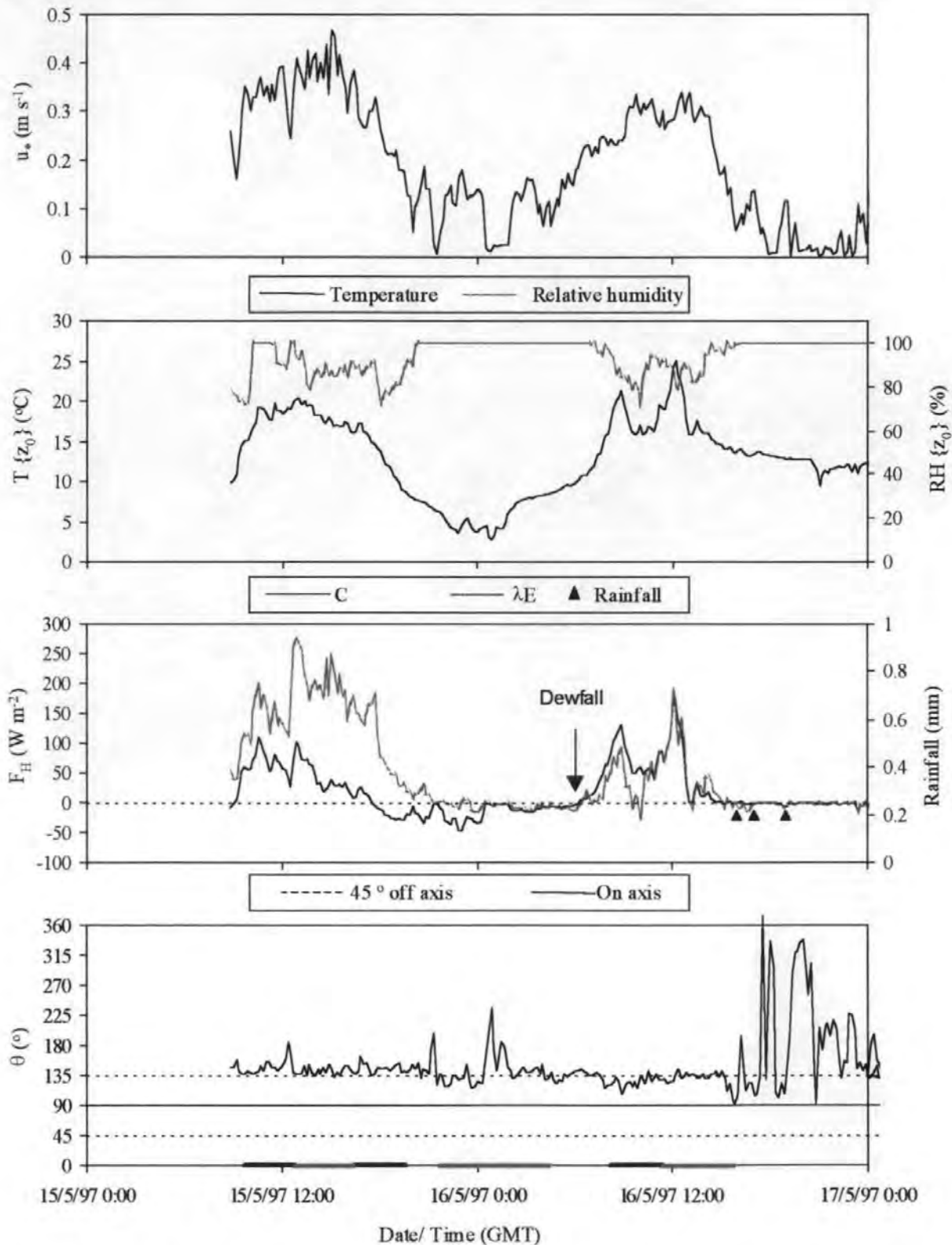
Figure 5.17: Meteorological data recorded during Experiment 7. Run times are shown as bars on the x-axis. Abbreviations are defined in Figure 5.5.

A pronounced increase in NH$_3$ emission occurred during Run 5, correlating with increases in wind speed, surface temperature and surface heat flux. However, a decline in NH$_3$ emission occurred during Run 6, the following afternoon, which may have been caused by the changing meteorological conditions or by the continued reduction in the liquid phase TAN concentrations on the surface of the slurry. In total 11 % of the TAN applied as slurry volatilised during this experiment.

5.4.7.3   *Estimation of local NH₃ deposition*

The direct comparison of measured and modelled concentration profiles indicated that deposition over the downwind area occurred during much of the experiment. However, data collected during Run 3 were in a good agreement with the KATCH model predictions for non-depositing dispersion, indicating that NH$_3$ deposition during this run was negligible. Concentration profiles measured at Site 4 during Runs 3 and 4 were too close to background levels to be robustly interpreted and so were excluded from the analysis.
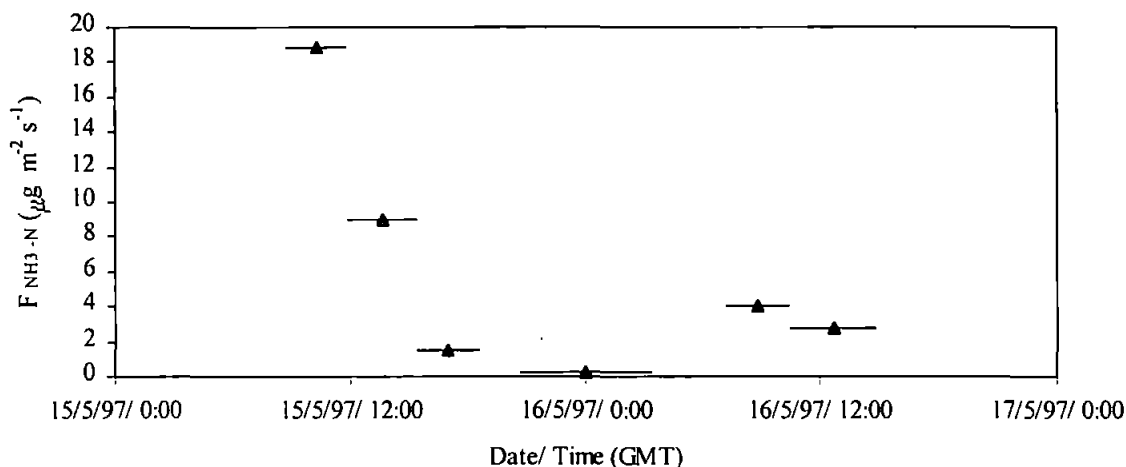
Figure 5.18:   Time series of NH$_3$-N emission fluxes from the experimental area treated with slurry during Experiment 7.

ACG method determinations of the deposition fluxes measured during Experiment 7 are shown in Table 5.15. The interpretation of the profiles measured during Run 1 showed that NH$_3$ deposited to the surface at a rate slightly lower than permissible by R_b indicating an approximate surface resistance of 11 s m^{-1}. Deposition velocities increased to $V_{d\ max}$ during Run 2, coincident with less convective atmospheric conditions, a reduction in surface temperature, and an increase in friction velocity and latent heat flux. Deposition velocities measured during Runs 3 and 4 were found to be much lower that $V_{d\ max}$, demonstrating an increase in surface resistance. Surface resistances reduced during Run 5 with deposition again occurring at $V_{d\ max}$, possibly due to the wetting of the surfaces caused by the

overnight dew formation. Deposition did not occur during Run 6, by which time the overnight dew had evaporated.

Run	Flux NH_3-N (μg m^{-2} s^{-1}) ESTIMATED		Flux NH_3-N (μg m^{-2} s^{-1}) $R_c = 0$		Deposition velocity (m s^{-1}) ESTIMATED	
	Site 3	Site 4	Site 3	Site 4	Site 3	Site 4
1	-2.4 +/- 2.4	-0.62 +/- 1.3	-2.9	-1.3	0.04 (<0, $>V_{d\,max}$)	0.02 (<0, $>V_{d\,max}$)
2	-1.8 +/- 1.5	-2.0 +/- 1.7	-1.7	-0.80	0.08 (0.005, $>V_{d\,max}$)	$>V_{d\,max}$ (0.02, $>V_{d\,max}$)
3	0.0	N/A	-0.29	-0.18	0	N/A
4	-0.02 +/- 0.04	0	-0.07	-0.05	0.0025 (0,0.02)	0
5	-1.0 +/-0.19	-0.37 +/- 0.64	-0.75	-0.45	$>V_{d\,max}$ (0.06, $>V_{d\,max}$)	0.04 (0, $>V_{d\,max}$)
6	0.0	N/A	-0.49	-0.30	0	N/A

Table 5.15: Profile interpretations for Experiment 7 calculated using the ACG method.

An NH_3-N budget was constructed using the deposition velocities and meteorology measured during Experiment 7. The results are presented in Table 5.16. Deposition close to $V_{d\,max}$ would have resulted in between 20 - 34 % of the NH_3 emitted during each of the experimental runs being locally recaptured, with the highest recapture occurring during the stable atmospheric conditions measured during Run 4. In total, 16 % of the emitted NH_3 was estimated to locally deposit compared with a theoretical maximum of 22 %.

Run	V_d (m s^{-1})		Flux NH_3-N (μg m^{-2} s^{-1})			Mass flux (NH_3-N)			Deposited (%)	
	R_c= est	R_c= 0	Slurry	R_c= est	R_c= 0	Slurry	R_c= est	R_c= 0	R_c= est	R_c= 0
1	0.04	0.07	19	-1.9	-2.4	1.0	-0.17	-0.22	17	22
2	0.08	0.08	9.0	-1.2	-1.2	0.57	-0.12	-0.13	22	22
3	0.00	0.06	1.5	-0.13	-0.21	0.08	0.00	-0.02	0	24
4	0.003	0.02	0.28	-0.02	-0.05	0.03	0.00	-0.01	0	32
5	0.06	0.06	4.1	-0.49	-0.49	0.22	-0.05	-0.05	20	20
6	0.00	0.05	2.7	0.0	-0.35	0.21	0.00	-0.04	0	21
			TOTAL			2.12	-0.34	-0.46	16	22

Table 5.16: NH_3-N budget calculated for Experiment 7 using the KATCH model. Calculations were made of the deposition to 50 m downwind of the source assuming a 30 m wide slurry strip with a length of 160 m subject to an on-axis wind direction. R_c= est: surface resistance to deposition estimated from the profile measurements, R_c= 0: no surface resistance assumed.

5.4.8   Experiment 8: 18/06/97 – 19/06/97

This experiment was conducted on Middle Wyke Moor early in the summer of 1997. The field site was set aside for the remainder of 1997, following the silage cut in May, and thus provided an opportunity to investigate the deposition of NH_3 to an area of unfertilised short grass. This contrasted with Experiment 3 where fertiliser had been applied to the cut sward. Some re-growth of the sward had occurred after the field was cropped, with the sward height measuring 0.2 m.

5.4.8.1   Meteorological conditions

The meteorological conditions measured during this experiment are shown in Figure 5.19. Weather conditions were typical of early summer, with periods of moderate wind speeds and strong surface heat fluxes. Several periods of isolated rainfall occurred during the experiment, though the corresponding peaks in surface relative humidity were short lived. In general, surface humidities were consistently high due to the evapotranspiration flux from the soil and vegetation.

5.4.8.2   NH₃-N emissions

The NH_3 emission fluxes measured from the slurry strip during Experiment 8 are presented in Figure 5.20. A clear exponential decline in NH_3 emission was found with little diurnal variability. This was possibly due to the relatively consistent meteorological conditions encountered throughout this experiment. As with the other experiments, a high proportion of the total NH_3 emission occurred during the initial period following slurry spreading (50 %). In total 14 % of the TAN applied as slurry volatilised as NH_3-N during this experiment.

5.4.8.3   Estimation of local NH₃ deposition

Direct KATCH model interpretations of the measured NH_3 profiles provided evidence that deposition of NH_3 occurred during the first four experimental runs. Ammonia concentration profiles measured during Run 5 were in good agreement with the model predictions for non-depositing dispersion, whilst results for Run 6 were harder to interpret, due to the very low concentrations measured. However, these measurements were generally better described by the model fit for non-depositing dispersion. Concentration profiles measured during Runs 1 - 4 were further investigated using the ACG method to estimate the local deposition fluxes, the results of this analysis are shown in Table 5.17.
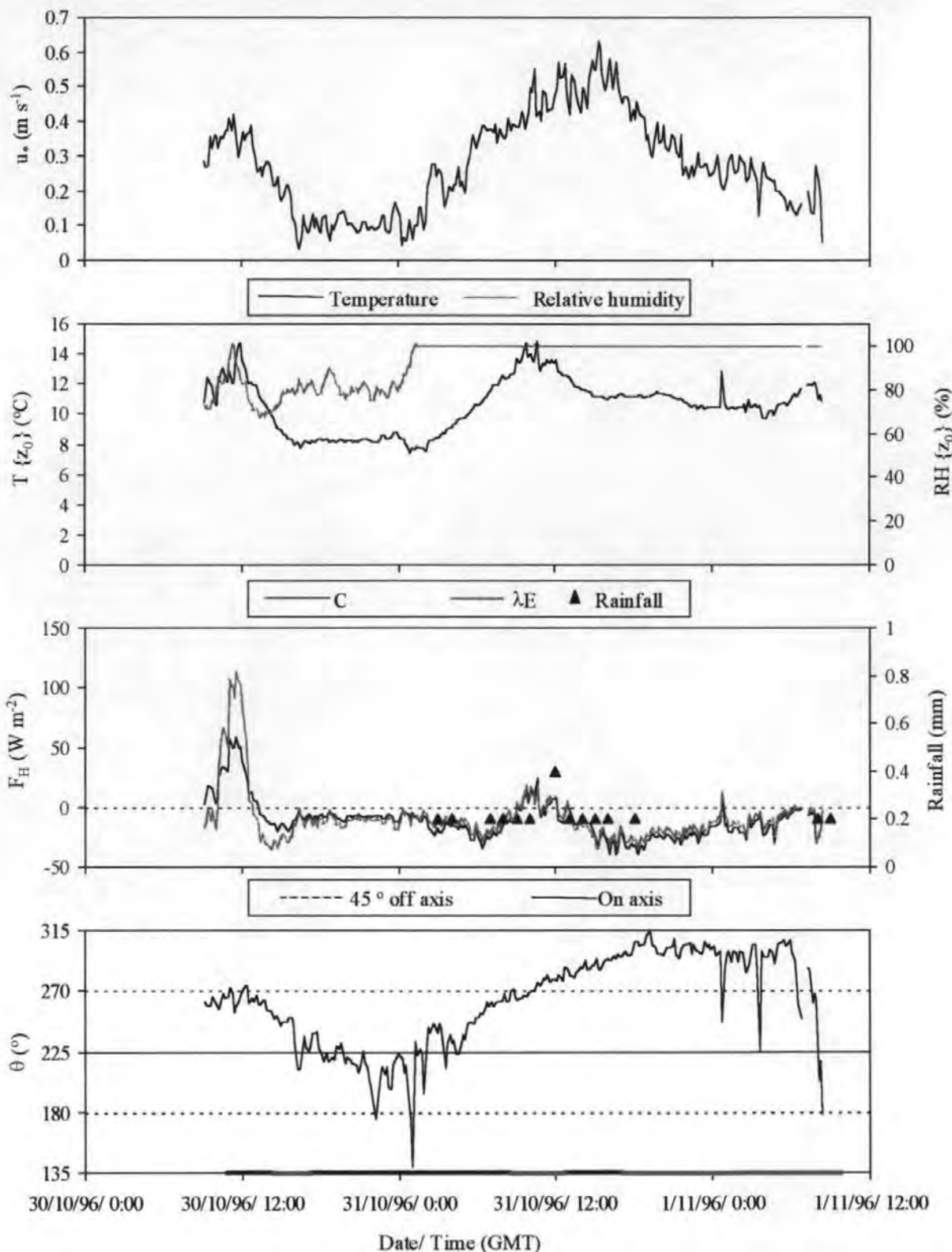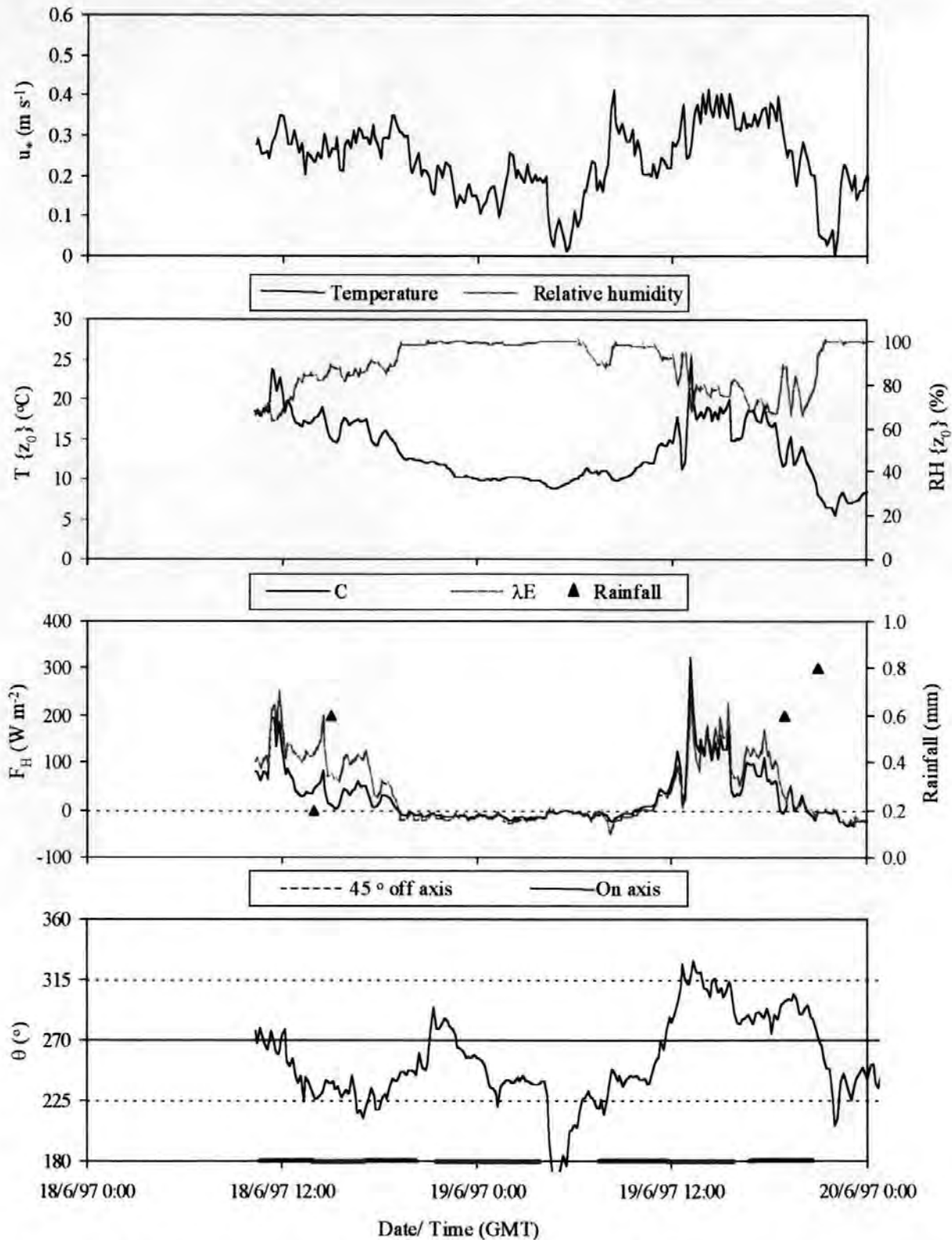
Figure 5.19: Meteorological data recorded during Experiment 8. Run times are shown as bars on the x-axis. Abbreviations are defined in Figure 5.5.

Deposition velocities of 0.06 m s^{-1} and 0.03 m s^{-1} were estimated from the profile interpretations of the data at Sites 3 and 4 during Run 1. Though these deposition velocities differ in magnitude, the assessment of the error attached to each value suggested that they were not statistically different. Hence, the more precise value, from Site 3, which

156

demonstrated that deposition was limited only by boundary layer resistance, was taken as a more representative estimate. Similarly, data collected during Run 2 were interpreted to suggest that deposition occurred at $V_{d\,max}$.

Deposition velocities were estimated to reduce slightly below $V_{d\,max}$ during Runs 3 and 4, corresponding to surface resistances of 19 s m^{-1} and 5 s m^{-1}. Whilst, no detectable deposition occurred during the final two runs of the experiment. The absence of deposition during these runs was not correlated with any change in meteorological conditions and thus was assumed to be due to saturation of the surface NH₃ sinks.
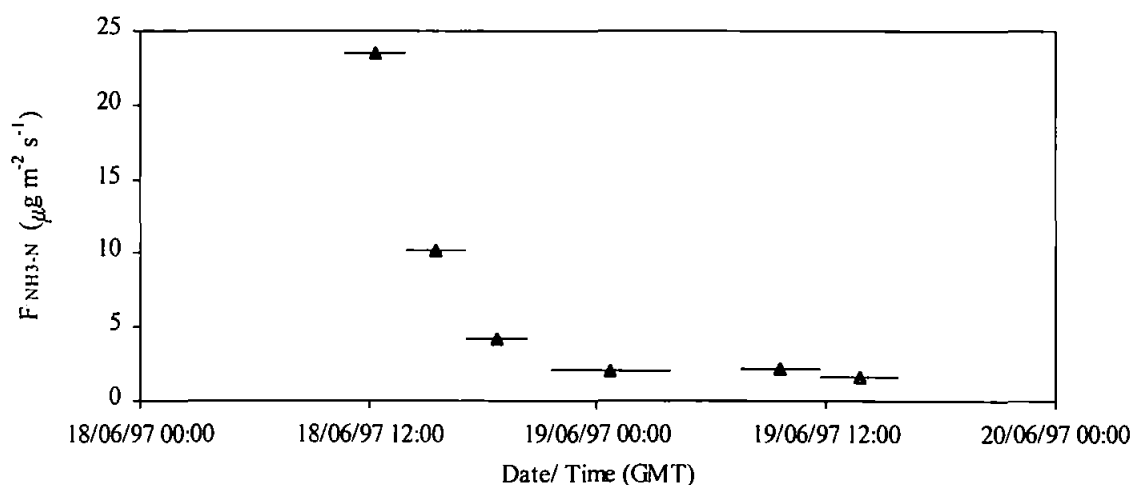
Figure 5.20:   Time series of NH₃-N emission fluxes from the experimental area treated with slurry during Experiment 8.

Run	Flux NH₃-N (µg m^{-2} s^{-1}) ESTIMATED		Flux NH₃-N (µg m^{-2} s^{-1}) $R_c = 0$		Deposition velocity (m s^{-1}) ESTIMATED	
	Site 3	Site 4	Site 3	Site 4	Site 3	Site 4
1	-4.1 +/- 0.7	-1.7 +/- 1.1	-4.2	-2.4	0.06 (0.04, >$V_{d\,max}$)	0.03 (0.01, >$V_{d\,max}$)
2	-2.2 +/- 1.5	-1.2 +/- 0.4	-1.9	-1.1	0.06 (0.01, >$V_{d\,max}$)	0.06 (0.04, >$V_{d\,max}$)
3	-0.51 +/- 0.3	-0.26 +/- 0.9	-0.83	-0.49	0.03 (0.01, 0.06)	0.02 (<0, >$V_{d\,max}$)
4	-0.15 +/- 1.6	-0.26 +/- 0.2	-0.45	-0.27	0.01 (<0, >$V_{d\,max}$)	0.04 (0, >$V_{d\,max}$)
5	0.00	0.00	-0.43	-0.25	0.00	0.00
6	N/A	0.00	-0.28	-0.16	N/A	0.00

Table 5.17:   Profile interpretations for Experiment 8 calculated using the ACG method.

An NH₃-N budget was calculated using the meteorological conditions and deposition velocities measured during Experiment 8. Results are presented in Table 5.18. Deposition at $V_{d\,max}$ was estimated to reduce the net emission from the site by 19 - 27 %, with the highest value occurring during the stable overnight conditions that occurred during Run 4.

In total 18 % of the emitted NH_3 was estimated to be locally re-deposited from a theoretical maximum recapture of 21 %.

Run	V_d (m s^{-1})		Flux NH₃-N (µg m^{-2} s^{-1})			Mass flux (NH₃-N)			Deposited (%)	
	R_c= est	R_c= 0	Slurry	R_c= est	R_c= 0	Slurry	R_c= est	R_c= 0	R_c= est	R_c= 0
1	0.06	0.06	23	-2.7	-2.7	1.3	-0.25	-0.25	19	19
2	0.06	0.06	10	-1.3	-1.3	0.56	-0.12	-0.12	21	21
3	0.03	0.07	4.2	-0.42	-0.57	0.23	-0.04	-0.05	17	23
4	0.04	0.05	2.0	-0.3	-0.32	0.22	-0.05	-0.06	25	27
5	0.00	0.06	2.1	0.0	-0.30	0.16	0.00	-0.04	0	23
6	0.00	0.07	1.6	0.0	-0.19	0.11	-0.00	-0.02	0	19
					TOTAL	2.58	-0.46	-0.54	18	21

Table 5.18:   NH₃-N budget calculated for Experiment 8 using the KATCH model. Calculations were made of the deposition to 50 m downwind of the source assuming a 30 m wide slurry strip with a length of 160 m subject to an on-axis wind direction. R_c= est: surface resistance to deposition estimated from the profile measurements, R_c= 0: no surface resistance assumed.

5.5   DISCUSSION

5.5.1   NH₃ emissions

Similar patterns of NH₃ emission were found in each experiment. A strong initial pulse of NH₃ emission was typically observed, followed by an extended period of weaker fluxes. Most experiments showed some diurnal variation in NH₃ emissions, which was associated with the diurnal variability in friction velocity, surface heat fluxes and surface temperature. Such variability in NH₃ emissions has also been described by Bless *et al.* (1991), Sommer *et al.* (1991), Sommer *et al.* (1997) and Van der Molen *et al.* (1990a),.

The total emission flux[1] (calculated for a 30 m x 160 m source) varied between experiments, with the highest net emission being measured during Experiment 3 (5.3 kg NH₃-N) and the lowest net emission being measured during Experiment 7 (2.1 kg NH₃-N). The seasonal trends in the total emission fluxes were examined by investigating the percentage of NH₃-N emitted as a function of the TAN applied, results are shown in Figure 5.21. The average emission measured during the experiments, expressed as a percentage

---

[1] The total emission fluxes for Experiments 4, 7 and 8 were calculated including an interpolation between periods where measurements were not available, see Figures 5.12, 5.18 and 5.20.

of TAN applied was 18 %. This is broadly consistent with the emission factor from Pain *et al.* (1998) of 15 % of TAN volatilising from slurries with a low dry matter content (<4 %).
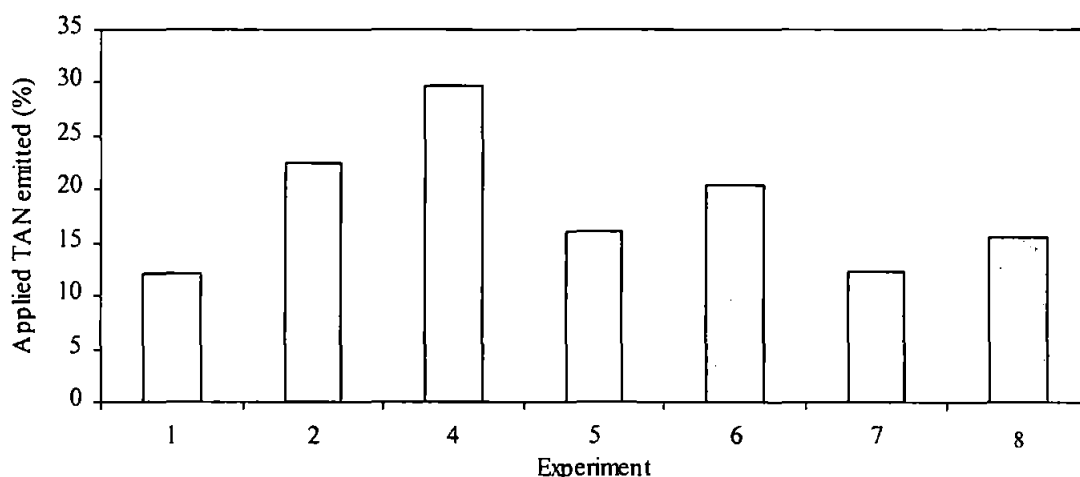
Figure 5.21:   Pattern of NH$_3$-N emission expressed as a percentage of the TAN (NH$_x$-N) applied as slurry. Experiment 3 was excluded, as the initial pulse of NH$_3$ emission was not recorded.

Correlations between the net emission fluxes (in kg NH$_3$-N), measured during each experiment, and the average meteorological variables (detailed in Table 5.2) and slurry characteristics (detailed in Table 5.3) were investigated using linear regression analysis. The results, shown in Table 5.19, demonstrated that none of the meteorological variables or slurry characteristics correlated with the net NH$_3$-N emission flux at the 95 % confidence level. Slurry TAN content correlated with the NH$_3$-N emission flux at the 80 % confidence level and explained 30 % of the variation in emission. The correlation between net NH$_3$ emission and applied TAN demonstrated the dependence of emission rates on a strong surface-atmosphere NH$_3$ concentration gradient.

Menzi *et al.* (1998) also found that much of the variation in NH$_3$ emissions could be explained by the TAN applied, though the R^2 value reported by Menzi *et al.* (1998) was higher (81 %). Slurry dry matter content has been strongly correlated with NH$_3$ emission by Sommer *et al.* (1991) and Sommer and Olesen (1991). This correlation was not apparent in this study, although this was likely to be due to the uniformity in slurry dry matter contents between the experiments.

Menzi *et al.* (1998) also correlated the NH$_3$ emissions (in kg ha^{-1}) with the TAN concentrations in the slurry, the application rate (termed *AR*, in t ha^{-1}) and the humidity and

temperature of the atmosphere (expressed as the saturation deficit, *SD*). These correlations were used by Menzi *et al.* (1998) to develop a simple empirical model to predict NH_3 emission, shown in Equation 5.1. The predictions of this model were compared with the experimental measurements of net NH_3 emission; results are shown in Figure 5.22. In general, the regression model presented in Menzi *et al.*, (1998) overpredicted the net emission, though described 54 % of the variation in the emission measurements.

$$F_{NH3-N} = (19.41\,TAN + 1.10\,SD - 9.51)\,(0.02\,AR + 0.36)$$ Equation 5.1

	Air temperature (°C)			Relative humidity (%)			Wind speed (m s⁻¹)			Rain (mm)	Slurry composition		
	Mean	Max	Min	Mean	Max	Min	Mean	Max	Min	Total	*DM* (%)	pH	*TAN* (kg)
M	0.02	0.01	0.07	-0.08	0.30	-0.05	0.50	0.12	0.60	-0.26	-0.74	-0.25	4.52
C	3.38	3.40	3.23	9.73	-25.43	6.43	1.98	2.89	2.99	4.10	7.21	5.27	-1.09
R^2	0.01	0.00	0.06	0.09	0.07	0.09	0.18	0.01	0.25	0.18	0.02	0.00	0.30
P {M}	0.84	0.89	0.59	0.51	0.58	0.51	0.34	0.81	0.25	0.35	0.77	0.91	0.20
P {C}	0.03	0.05	0.01	0.31	0.63	0.17	0.27	0.35	0.01	0.00	0.56	0.72	0.75

Table 5.19:   Regression analysis of the trends in total NH_3-N emission (kg per 160 m x 30 m strip) with meteorological conditions and slurry composition. *DM*: Slurry dry matter content, *TAN*: NH_x-N applied as slurry; *M*: gradient, *C*: y-intercept, R^2: correlation statistic squared, *P*: probability.
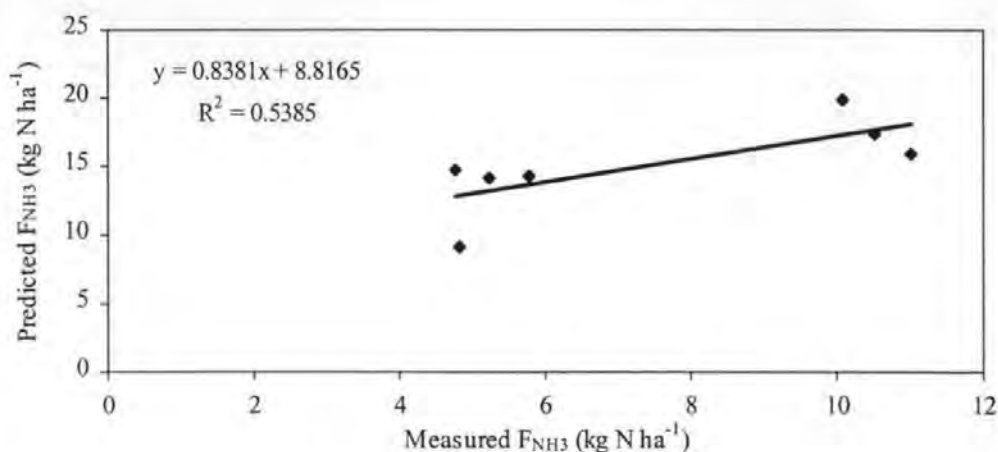
Figure 5.22:   Comparison between the measured net emissions from the slurry spreading experiments with emission predictions derived from the empirical model discussed in Menzi *et al.* (1998), shown as Equation 5.1.

Ambient temperature, wind speed and relative humidity have been found to correlate with NH_3 emission by Sommer *et al.* (1991) and Menzi *et al.* (1998) though these trends were not observed in this analysis. The likely reason for this disparity was that the correlations

determined by Sommer *et al.* (1991) and Menzi *et al.* (1998) were from field scale wind tunnel experiments, where wind speed could be set and temperatures and humidities can be somewhat buffered by the tunnel. As the field measurements reported herein were made across a wide range of varying environmental conditions, disentangling the true controls over NH_3 emission was more difficult.

A second regression analysis was performed to investigate the controls over NH_3 emissions during the first run of each experiment. Environmental conditions were more constant during these runs as emission fluxes were not affected by previous depletion of slurry TAN concentrations and, due to the short duration of the first run of each experiment, meteorological conditions were also reasonably constant. Results are shown in Table 5.20.

	u_*	z_0	C	λE	R_b	T	RH	Rainfall	DM	pH	TAN
	(m s⁻¹)	(m)	(W m⁻²)	(W m⁻²)	(s m⁻¹)	(°C)	(%)	(mm)	(%)		(kg NH_x-N)
M	58.78	145.43	0.07	-0.10	-0.64	-0.35	-0.58	-18.08	-5.84	15.16	1.78
C	1.39	20.83	22.39	29.58	33.23	28.12	68.59	26.46	52.92	-78.48	-10.11
R^2	0.75	0.08	0.05	0.43	0.07	0.07	0.31	0.31	0.02	0.23	0.34
$P\{M\}$	0.01	0.54	0.62	0.11	0.58	0.57	0.19	0.19	0.74	0.28	0.17
$P\{C\}$	0.83	0.03	0.01	<0.01	0.08	0.01	0.07	<0.01	0.54	0.40	0.66

Table 5.20: Regression analysis of the trends in initial NH_3-N emission (in $\mu g\ m^{-2}\ s^{-1}$) with meteorological conditions and slurry composition. *DM*: Slurry dry matter content, *TAN*: NH_x-N applied as slurry; *M*: gradient, *C*: y-intercept, R^2: correlation statistic squared, *P*: probability.

A significant correlation (at the 99 % confidence level) was found between the friction velocity and the initial NH_3 emission flux, shown in Table 5.20. This correlation was due to the flux-gradient relationship between the emission and u_*, as shown in Equation 2.24. Furthermore, atmospheric and boundary layer resistances to vertical transport reduce as u_* increases.

Previous research on the correlation between NH_3 emission fluxes and wind speed (Menzi *et al.*, 1998; Sommer *et al.*, 1991 and Thompson *et al.*, 1990b) supports the correlation between u_* and NH_3 emission discussed above (as $u_* \propto u$). However, these researchers found that wind speed was not a major factor determining the net emission. Indeed, experiments reported herein have shown that the suppression of NH_3 emission during periods of near-calm conditions was often followed by a pulse of emission when friction velocities increased. This suggests that friction velocity limits the transport of NH_3 from

the surface of the slurry, explaining the apparent accumulation of surface NH_3 during periods when friction velocities are reduced.

The TAN applied was only correlated with the initial NH_3-N emissions at the 80 % confidence level, suggesting that the surface concentration of NH_3-N during the initial experimental run was not a major limiting factor. A positive correlation, at the 90 % confidence level, was found between the NH_3-N emission flux and latent heat flux (λE). However, a subsequent analysis found that the correlation between λE and emission was an artefact of the strong correlation between λE and $u*$. Other trends (significant at the 80 % confidence level) showed that NH_3 emissions were reduced by high surface humidities and by rainfall. Similar results have been found by Menzi *et al.* (1998) and Pain and Misselbrook (1997) respectively, leading to the conclusion that high humidities and rainfall suppress NH_3-N emission by diluting slurry TAN concentrations and washing NH_x-N into the soil. A multiple regression analysis was performed to assess the amount of variation in the initial emission fluxes that could be explained by the combination of $u*$, *RH*, and rainfall. The regression equation, shown as Equation 5.2, was found to describe 97 % of the variation in initial emission fluxes.

$$F_{NH3-N} = 53.38\ u* - 12.83\ Rainfall - 0.11\ RH + 13.56 \qquad \text{Equation 5.2}$$

5.5.2 NH₃ dispersion

The analytical atmospheric dispersion model (KATCH) was found to realistically predict the dispersion of NH_3 downwind of the slurry treated plots. Moreover, Figures 5.1 and 5.2 demonstrate that much of the variability between the model predictions and the measurements could be attributed to measurement uncertainties. A good agreement was found between the KATCH model predictions and the NH_3 concentration profiles measured over the downwind grassland, at heights above the surface depletion zone, as shown in Figures 5.3 and 5.4. The model also produced realistic predictions of downwind concentrations during periods of extremely non-neutral atmospheric stability, demonstrating the robustness of the stability correction factors used in the model.

Several other studies have demonstrated a good agreement between the predictions of analytical K-theory models of atmospheric dispersion and field measurements. These include similar work investigating NH_3 emissions from surface applied slurry by McInnes *et al.* (1985) and Sommer *et al.* (1995). Also, Brown *et al.* (1997) and Tirabassi *et al.* (1986) compared the predictions of similar models based on the Huang (1979) theorem

with both wind tunnel and field measurement data. They concluded that the models produced realistic predictions of vertical dispersion from both elevated and surface sources.

5.5.3 Local NH₃ deposition

Deposition at a rate limited by R_b was modelled to cause the net deposition, within 50 m of a 30 m wide area source, of between 21 - 25 % of the emitted NH₃ over the duration of each experiment. The maximum deposition during each of the experimental runs was not as consistent as the cumulative values, with up to 40 % of the emitted NH₃ depositing during highly stable overnight periods and only 10 % depositing during highly unstable daytime conditions. The differences between these values result from the dilution of surface concentrations due to rapid vertical mixing during unstable periods and the entrainment of NH₃ close to the surface during stable periods. Similar predictions of 31 % of emitted NH₃ depositing within 100 m of a 1.0 m high point source and 30 % of the emitted NH₃ depositing within 50 m of a 15 m wide area source have been reported by Asman (1998) and Sutton *et al.* (1997b).

Seventy seven vertical NH₃ concentration profiles were measured downwind of the slurry treated plots. Fifty eight of the measured profiles were of a sufficiently high definition to be interpreted to estimate the local surface-atmosphere exchange of NH₃, 26 of these profiles were interpreted, by direct comparison with the KATCH model predictions, to show that no detectable NH₃ deposition occurred ($V_d < 0.005$ m s^{-1}). Deposition fluxes were estimated using the ACG method, developed in Chapter 4, from the remaining 32 profiles. However, only 13 of these were found to be significantly different from zero, with errors due to the estimation of NH₃ gradients predominating.

Despite the uncertainties in individual measurements, comparable estimates of surface atmosphere exchange were often recorded when two downwind monitoring sites were used. Furthermore, similar patterns of surface exchange were observed from experiments conducted during similar environmental conditions, providing a further check on the reproducibility of the results reported herein. Similar uncertainties in the determination of fluxes using micrometeorological flux-gradient methods have been reported in Duyzer *et al.* (1994) and Sutton (1990).

Field estimates of the deposition of NH₃ were made using the methods discussed above. Strong surface resistances (R_c) to NH₃ deposition were estimated during many of the

experimental runs. Indeed, deposition at a rate sufficient to affect the local emission-deposition budget (above approximately 5 % of the emitted NH_3-N re-depositing) was only estimated to occur during Experiments 5 - 8.

The strong surface resistances to NH_3 deposition estimated during Experiments 1 and 2 were attributed to low surface temperatures and relative humidities that would restrict deposition to the leaf surfaces, as shown by Erisman *et al.* (1994), Erisman and Wyers (1993) and Sutton *et al.* (1993a). The metabolic inactivity of the vegetation during Experiments 1 and 2 may also have restricted the deposition of NH_3, both through reduced stomatal uptake (Wesley, 1989) and through the reduced cuticular uptake of NH_3 deposited to the surfaces (Sutton *et al.*, 1998a).

High surface resistances to NH_3 deposition were also estimated during Experiments 3 and 4, which were conducted over recently fertilised grassland. High surface resistances during such conditions are likely to have resulted from the reduced capacitance of the surface sink for NH_3 and through an increased internal plant compensation point. Similar results were found in the ADEPT "Burrington Moor" campaign experiment presented in Sutton *et al.* (1997a) and Sutton *et al.* (1997b). The results reported herein provide some confidence that the estimated local recapture from the campaign experiments, made using simple dynamic chambers, can be reproduced by field scale micrometeorological experiments.

Not all the runs measured during Experiment 4 showed evidence of a strong surface resistance to NH_3 deposition. Surface resistance was estimated to approach zero during the overnight run of Experiment 4, which was possibly due to deposition to dew formed on the leaf surfaces. The subsequent fate of the NH_3 deposited to the dew film was difficult to discern as the profiles measured the following morning were poorly defined and could not be robustly interpreted with the KATCH model. However, surface level air concentrations were considerably higher at both downwind measurement sites than were predicted by the KATCH model, providing some evidence of re-emission.

Lower surface resistances were measured during Experiments 5 - 8, with 14 – 18 % of the emitted NH_3 being estimated to deposit within 50 m of the source. A general pattern of increasing surface resistance was measured over the course of each experiment. The increase in surface resistance over time suggests that either sink saturation may have been occurring, or that surface level NH_3-N concentrations were reaching an equilibrium with the reducing ambient NH_3-N concentrations caused by the decline in emission from the

slurry strip. Saturation of the surface sink for NH_3 is likely to be hastened by low rates of metabolic uptake of surface NH_x-N as suggested by Sutton *et al.* (1998a).

The regulation of deposition by such processes may explain the shorter duration of deposition fluxes found in Experiment 5 when compared with Experiment 6 and Experiment 7 when compared with Experiment 8. In general, Experiments 5 and 7 showed very rapid reductions in NH_3 emission fluxes from the slurry, which, assuming NH_x-N accumulates on the surface, was likely to significantly perturb the surface-atmosphere concentration gradient and result in higher surface resistances developing. It was also likely that the extended period over which deposition fluxes were measured during Experiment 6 was related to the persistent light rainfall that occurred, increasing the capacitance of the surface sink.

A statistical analysis was performed to investigate the correlation between the estimated deposition velocities (including zero values) and the specific micrometeorological and emission conditions that occurred during each run that profile interpretations were available. Results are shown in Table 5.21. A strong positive correlation was found between deposition velocity and the measured latent heat flux. This correlation can be explained by the rapid cuticular uptake and metabolism of deposited NH_3 by metabolically active plants (Sutton *et al.*, 1998a). Furthermore, the formation of thin water films close to open stomata has been shown by Burkhardt and Eiden (1994) to result in enhanced deposition fluxes. The abundance of surface water, either as soil water for evaporation or as a high plant water potential for transpiration, would be required to sustain a strongly positive latent heat flux. Either of these conditions would be likely to enhance the deposition of a soluble gas such as NH_3.

	u_* (m s⁻¹)	z_0 (m)	C (W m⁻²)	λE (W m⁻²)	R_b (s m⁻¹)	R_{seb} (s m⁻¹)	$T\{z_0\}$ (°C)	RH (%)	Rainfall (mm)	Emission (μg m⁻² s⁻¹)
M	-18.88	-281.13	0.10	0.18	-0.31	0.00	1.31	0.32	4.70	0.37
C	24.78	25.35	17.00	13.23	24.44	19.55	4.56	-8.61	17.37	15.86
R^2	0.01	0.08	0.04	0.20	0.03	0.01	0.13	0.03	0.02	0.02
$P\{M\}$	0.48	0.08	0.27	0.006	0.30	0.52	0.03	0.35	0.44	0.38
$P\{C\}$	0.01	<0.01	<0.01	<0.01	<0.01	<0.01	0.54	0.77	<0.01	<0.01

Table 5.21: Regression analysis of the trends in NH_3-N deposition velocity (mm s⁻¹) with meteorological conditions and emissions M: gradient, C: y-intercept, R^2: correlation statistic squared, P: probability.

A positive correlation was found between deposition velocity and temperature that was significant at the 95 % confidence level. As the metabolic activity of plants is temperature dependent then this correlation may be explained in similar physiological terms to the correlation between latent heat flux and NH_3 deposition. Indeed, measured latent heat fluxes and temperatures were found to be correlated ($R^2 = 0.13$, $P = 0.03$). An additional cause of the correlation between deposition velocity and temperature was likely to be the low affinity of NH_3 for frozen surfaces, as shown by the laboratory experiments of Iribarne and Pyshnov (1990).

The roughness length (z_0) was found to negatively correlate with deposition velocity at the 90 % confidence level. As deposition velocities in this study were referenced to the z_0 height, this correlation was likely to result from the shorter diffusion path between z_0 and the surface for small values of z_0. It should be noted that R_b and z_0 were also correlated, though R_b was found have a poorer correlation with deposition velocity.

A multiple regression analysis was performed, investigating the dependence of the deposition velocity on λE, T {z_0} and z_0. The results show that 30 % of the variation in the deposition velocity could be explained by these variables. The remaining 70 % of the variation could not be investigated statistically, though was likely to result from the saturation of surface sinks following fertiliser applications and following sustained periods of deposition. Indeed, if values of deposition velocity equal to zero were removed from the multiple regression analysis then variations in λE, T {z_0} and z_0 were found to describe 57 % of the variation in the estimated deposition velocity.

5.5.4   Local environmental impacts of slurry applications

The previous section has dealt with the controls over local deposition and the potential for recapture of NH_3 downwind of the field experiments. However another important aspect that should be considered is the potential for local pollution, often quantified through the critical load framework, discussed in Chapter 1. A typical value for the critical load for N deposition to moorlands, the most likely local receptor ecosystems for emissions from sources in the south-west of England, is around 10 kg N ha⁻¹ (Hornung *et al.*, 1997).

Deposition downwind of the field experiments was found to reduce the net emission from the source by up to approximately 20 %. Deposition at this rate would have input up to 0.7 kg N into an area 0 – 50 m downwind of the source of approximately 1 ha, or about 7 % of the annual critical load. Of course, this estimate of local deposition only applies for the

situation where a sensitive ecosystem is immediately downwind of the source and for the source geometry used in the field experiments.

A modelling exercise was undertaken using the KATCH model to predict the pattern of deposition downwind of a more realistically sized source. Assuming that slurry was produced from a dairy farm with 120 head of cattle, giving a net production of 1404 tonnes of slurry (Pain *et al.*, 1998), and that the farmer applies slurry on four occasions throughout the year at a rate of 39 t ha^{-1} then an area of 9 ha would be required for each application. Slurry was assumed to be applied to a square field, and the emission fluxes and meteorological data from Experiment 8 were used as input to the model. The surface resistances estimated during Runs 1 - 4 of Experiment 8 were used to characterise the deposition pattern. Deposition at this rate was also likely to be representative of deposition to moorlands (*e.g.* Fowler *et al.*, 1998c; Sutton *et al.*, 1992). The calculated deposition contour map is shown in Figure 5.23.

The highest deposition of N was modelled to occur immediately downwind of the source, as shown in Figure 5.23, with much lower deposition to the wider environment caused by the diluting effects of atmospheric dispersion. Deposition at the centreline of the plume reduced to 0.1 kg N ha^{-1} (1.0 % of the annual critical load) within 400 m of the source, with the majority of the downwind area receiving between 0.05 and 0.01 kg N ha^{-1}. This analysis demonstrates that the environmental impacts of deposition from an individual slurry source would be localised, with dispersion of material in the atmosphere resulting in negligible environmental burdens beyond about 600 m downwind. Of course, this analysis only considers a single slurry application. A far more difficult modelling exercise would be to try to determine the effects of multiple slurry applications on the environment. However, if the deposition plumes from multiple sources do not converge within 600 m of the source their influence on local critical loads should remain negligible. A far more significant contribution to critical load exceedances is therefore likely from the cumulative increase in background concentrations caused by NH₃-N emissions from slurry spreading.
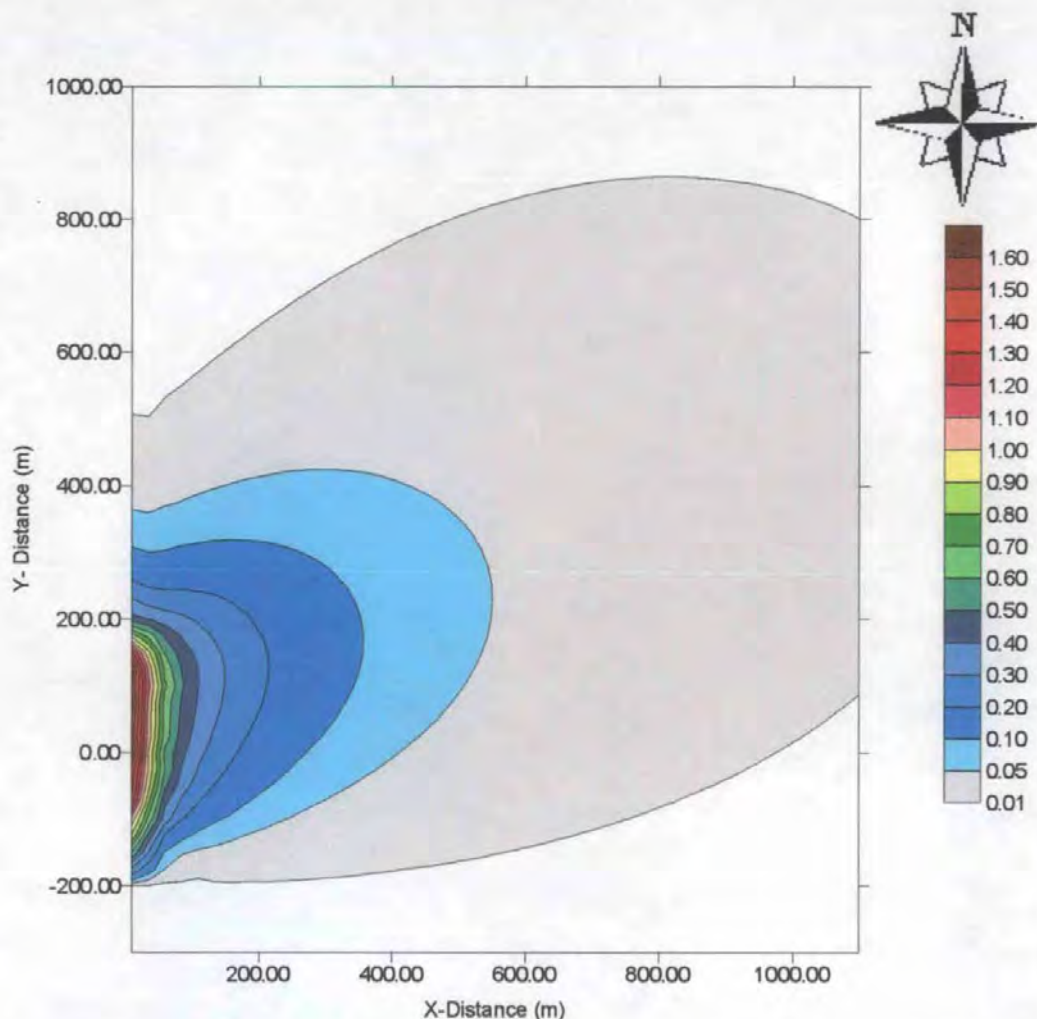
Figure 5.23: Spatial pattern of NH_3-N deposition (kg N ha^{-1}) downwind of a 300 m x 300 m field spread with slurry. The bottom right-hand corner of the source is positioned at (0, -150) on the graph. Emission data, meteorological data and surface resistances were taken from Experiment 8. Note: the last two isolines (0.05 kg ha^{-1} and 0.01 kg ha^{-1}) are not linearly related to the previous isolines.

6

EMISSION, DISPERSION AND LOCAL DEPOSITION OF AMMONIA VOLATILISED FROM FARM BUILDINGS: METHODS

6.1 INTRODUCTION

This chapter presents the methods and experimental designs used to determine the emission, dispersion and local deposition of NH_3 released from naturally ventilated farm buildings. Methods used by other researchers to determine emission and local deposition fluxes from naturally ventilated farm buildings were discussed in Chapter 2. The mass balance method, developed by Phillips *et al.* (1998), was identified for use in determining emission fluxes from the buildings whilst the N balance ("biomonitors") method, as used by Cowling and Lockyer (1981) and Sommer (1988), was identified for measuring local deposition fluxes.

Atmospheric dispersion models, suitable for determining the time-averaged dispersion of NH_3 from naturally ventilated buildings, were reviewed in Chapter 3. Dispersion downwind of a building is complicated by the enhanced turbulence generated by the building and by the complex re-circulating flows that occur around such structures. The consideration of these processes meant that the physically realistic atmospheric dispersion modelling approaches used in Chapters 4 and 5 could not be applied. Hence, the relatively detailed "building effects" module implemented within the UK-ADMS atmospheric dispersion model (Robins *et al.*, 1997) was used. The experiments described in this chapter were designed to evaluate both the applicability of the "building effects" module and to derive the appropriate emission and local deposition terms to enable the robust estimation of the spatial pattern of deposition around naturally ventilated buildings.

6.2 METHODS TO ESTIMATE NH₃ EMISSIONS FROM FARM BUILDINGS

Two methods were used to estimate the emissions of NH_3 from naturally ventilated farm buildings. The controlled release method was employed during the experiments at the Silsoe Research Institute (SRI) "Structures" building, as the building was used purely as a research tool and did not house livestock. While, emissions from a working dairy farm were estimated using the more labour intensive mass balance method developed by Phillips *et al.* (1998).

6.2.1 Controlled release

A controlled release of NH_3 from a cylinder of compressed liquefied gas was used to determine the NH_3 emission from the SRI Structures Building. Gaseous NH_3 was released within the building at a constant flow of 69 ml NH_3-N s^{-1}. Gas flow was regulated using a simple rotameter calibrated for NH_3 at atmospheric temperature and pressure (295 K, 1 ATM) (Flowbits, UK). A mass flux of 52 mg NH_3-N s^{-1} was calculated assuming ideal gas behaviour.

6.2.2 Estimation of NH₃ emissions from farm buildings using Ferm tubes

A simple mass balance method to estimate NH_3 emissions from naturally ventilated farm buildings was developed and validated by Phillips *et al.* (1998), as discussed in Chapter 2 Section 2.4.3. This method involves the direct measurement of the fluxes of NH_3 through the building ventilation components using passive flux samplers, "Ferm tubes", developed by Ferm (1986). These samplers measured the horizontal flux of NH_3 occurring across a single plane at a single point in space, and differ from the passive flux samplers used in Chapter 5 which rotated to measure the horizontal flux across a plane incident to the wind. The total flux from each ventilation aperture (in μg NH_3-N s^{-1}) was calculated from the Ferm tube flux measurements (in μg NH_3-N m^{-2} s^{-1}) and the open-face area of the ventilation aperture (in m^2). The total emission flux from the building was calculated as the algebraic sum of the fluxes from all the contributing ventilation apertures.

6.2.2.1 Theoretical basis of the Ferm tube method

The Ferm tube samplers comprised of three sections: two glass tubes (each 100 mm long with an inside diameter of 7 mm), and a third glass tube (30 mm long) with a stainless steel disc attached to one end. This disc had been laser drilled to create a precision 1.0 mm diameter orifice. The three sections were joined with greased silicone sleeves.
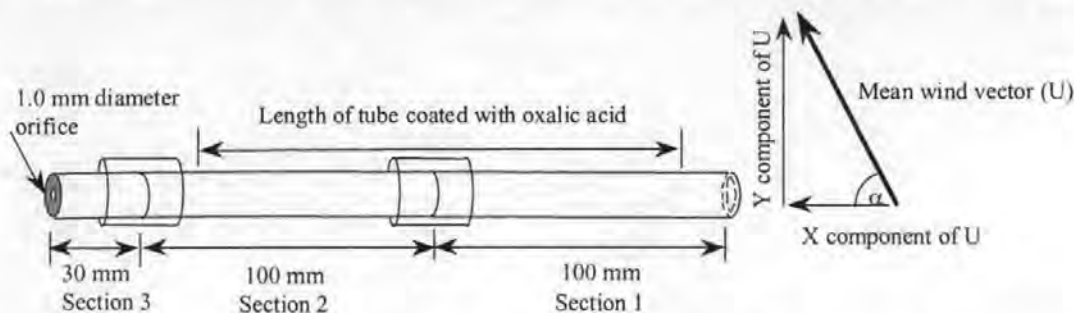
Figure 6.1:   Diagram of a Ferm tube flux sampler showing the three sub-sections and the outlet orifice. An example of the vector analysis of the wind flow through the sampler is also shown.

The "Ferm tube" samplers were similar to the "Shuttle" samplers, discussed in Chapter 4, in that air passively flowed through the sampler and NH_3 advected into the tube diffused to the sampler walls, coated with oxalic acid crystals. The orifice, attached to Section 3 of the Ferm tube, created laminar airflow through the sampler. This also ensured that the air was sufficiently retarded to enable all the NH_3 to react with the oxalic acid crystals, and that NH_4^+ particulate was not captured. As turbulent flow could occur at the inlets of the tube (Sections 1 and 3), these areas were not coated with oxalic acid and were not analysed. The sampler measured the flux of NH_3 in two directions. Gaseous NH_3 entering the sampler through Section 1 was trapped on the oxalic acid crystals in Section 1, whilst NH_3 entering the sampler through Section 3 was trapped on the oxalic acid coating of Section 2. Net fluxes were calculated as the difference between these two opposing fluxes.

Due to their fixed orientation, the Ferm tube samplers measured the vector component of the mean wind, as shown in Figure 6.1. Ferm (1986) showed that the samplers collect NH_3 at a rate decreasing more slowly than the cosine of the angle the wind makes with the inlet of the samplers for a wind incident with Section 1. Conversely, the samplers collect NH_3 at a rate decreasing more rapidly than the cosine of the angle the wind makes with Section 3 of the sampler. Because of this anomaly, the samplers were applied in oppositely facing pairs so that these artefacts approximately averaged out.

The net flux of NH_3 passing through the sampler was calculated using Equation 6.1, where M_{NH3-N} is the mass of NH_3-N, A is the cross sectional area of the sampler orifice, t is the time the sampler was exposed and R is an empirical factor to account for turbulence behind the orifice ($R= 0.7$).

$$F_{NH3} = \frac{M_{NH3-N}}{A\,R\,t}$$ Equation 6.1

6.2.2.2   Preparation of the Ferm tube samplers

Before preparation, the sections of the Ferm tubes were washed in a laboratory grade decontaminant (DECON 90). The glass sections of the samplers were oven dried at 100 °C, whilst the silicone sleeves and caps were dried in a fume cupboard on absorbent paper towels.

The interior walls of the two glass tubes (Sections 1 and 2) were coated with oxalic acid crystals by drawing a 30 g l^{-1} solution of oxalic acid dissolved in acetone into each tube using a syringe assembly. Acetone was used in preference to methanol due to the shorter drying times and as slightly elevated blank values would have a negligible effect on the determination of emission fluxes from a farm building using the Phillips *et al.* (1998) method. The tubes were only coated along the length of the interior surfaces where laminar air flow occurred, hence a 20 mm length of each glass tube was left un-coated. Glass tubes were coated in batches of five and were dried in a fume cupboard for approximately 300 s. Once assembled the Ferm tube samplers were fitted with polypropylene caps, to prevent contamination, and stored in sealed plastic bags at 5 °C.

6.2.2.3   Field application of the Ferm tube samplers

Pairs of Ferm tube samplers were mounted in the vents of the Yorkshire boarding, the ridge vent of the roof and across other large open areas of the Town Barton Farm building. The use of multiple sampling points was essential in order to account for the spatial variability in the emission of NH₃ from the building. A full description of the sites where Ferm tubes were applied is given in Section 6.5.2.2.

6.2.2.4   Extraction and analysis of the Ferm tube samplers

The Ferm tube samplers were removed from the farm building and capped at the end of each experimental run. The samplers were extracted by drawing a 10 ml aliquot of de-ionised water, measured using a calibrated automatic pipette, into each tube twice. To simplify the analysis, Section 1 of the inward facing tube was extracted into the same vial as Section 2 of the outward facing tube and *vice versa*, *i.e.* the total mass of NH₃ passing in each direction was calculated. The net flux through the sampler was calculated as the difference between the fluxes in either direction.

6.3 MEASUREMENT OF AIR CONCENTRATIONS OF NH₃ AROUND THE FARM BUILDINGS

Passive "Willems badge" samplers, developed by Willems (1990) were used to measure air concentrations around the SRI and Town Barton buildings. These samplers were chosen as triplicate sampling showed that standard deviations were typically less than +/- 10 % of the mean value and as they are well suited for application in large numbers due to their small physical size and light weight.

6.3.1 Theory

The Willems badge samplers, shown in Figure 6.2, measured ambient air concentrations of NH₃ according to Ficks first law which states that the diffusion of a gas is proportional to the concentration gradient, and the cross sectional area (A). The concentration gradient was linearized by treating $d\chi$ as the concentration difference between the air and the absorbent (χ_a-χ_o) and dl as a constant diffusion length (l). The diffusivity of gaseous NH₃ was included through the molecular diffusion co-efficient (D_{NH3}). The flux of NH₃ (F_{NH3}) in Equation 6.2 is the mass flux in $\mu g\ s^{-1}$.
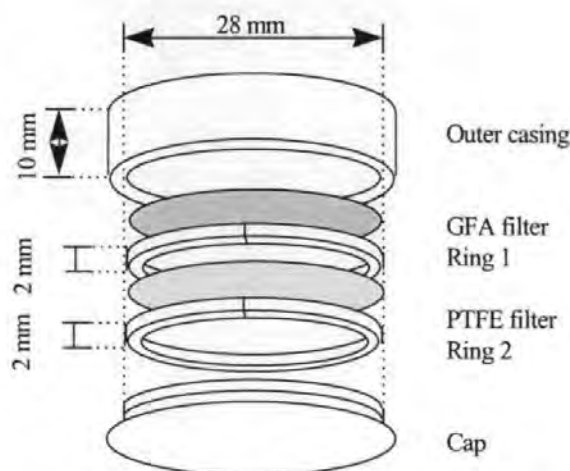
Figure 6.2:   Exploded diagram of a Willems badge showing the outer casing, the GFA absorption filter, the 2 mm spacers, the PTFE pre-filter and the cap.

$$F_{NH_3} = \frac{D_{NH3}\ A\ (\chi_a - \chi_o)}{l}$$

Equation 6.2

The concentration of NH₃ at the surface of the absorbent (χ_o) was assumed to be zero (*i.e.* the absorbent perfectly absorbs and binds NH₃), hence Equation 6.2 could be rearranged to calculate air concentrations, shown in Equation 6.3.

$$\chi_a = \frac{F_{NH_3}\ l}{D_{NH3}\ A}$$

Equation 6.3

The Willems badge samplers were designed to have a short diffusion length (l= 2 mm) and a relatively high cross sectional area (A= 615.7 mm^2) thereby increasing their sensitivity to NH$_3$ and reducing the limit of detection of the method. Samplers were found to reliably measure NH$_3$ concentrations below 1.0 µg m^{-3} over sampling durations of 24 hours. The short diffusion length was created by placing a PTFE pre-filter, with a 5.0 µm pore size, held on a rigid fibreglass frame (TE38, Schleicher and Shüll) close to the entrance of the sampler. The filter was held in place by a polystyrene clip and acted as a barrier to airflow into the sampler, creating an undisturbed air space behind itself. The 2.0 mm diffusion distance was created using a second polystyrene clip 2.0 mm in height. This clip separated the PTFE pre-filter from a glassfiber absorption filter (Whatman GFA), impregnated with tartaric acid. A polypropylene cap was used to seal the samplers once assembled.

The term l/D_{NH3} in Equation 6.3 represents the laminar boundary layer resistance (R_b) of the badge sampler to NH$_3$ diffusion. The PTFE filter also acted as a resistance to NH$_3$ diffusion R_f in series with R_b. Equation 6.3 was modified to include this additional resistance, the revised equation is shown as Equation 6.4. A further modification was included in Equation 6.4 as the mass flux (in µg s^{-1}) was split into the mass of NH$_3$ sampled (M_{NH3}) in µg and the sample duration (t) in seconds.

$$\chi_a = \frac{M_{NH_3}\,(R_b + R_f)}{A\,t} \qquad\qquad \text{Equation 6.4}$$

The value of R_f has been estimated by Willems (1990) to be 89 s m^{-1}, giving a combined resistance ($R_b + R_f$) of 180 s m^{-1} at 15 °C, based on the value of D_{NH3} discussed in Chapter 4, Section 4.2.5. Air concentrations were calculated following the determination of the mass of NH$_3$ collected on the GFA filter, using the total sampler resistance and the sample duration.

6.3.2 Laboratory preparation of the samplers

GFA filters were dipped in de-ionised water at approximately 90 °C to remove any excess fibres prior to being impregnated with tartaric acid. To speed up the drying process the wet filters were submerged in methanol before being placed on a drying rack in a glovebox supplied with NH$_3$ free air (created by passing air through a column containing dense glass wool impregnated with oxalic acid). Following approximately 30 minutes of drying, the filters were impregnated by submergence in a 24 g l^{-1} solution of tartaric acid in methanol and again dried in the glovebox. GFA filters were prepared in batches of 50 and stored in airtight polystyrene vials at 5 °C.

174

The PTFE filters also required preparation prior to field application to remove any NH_3 contamination that could volatilise and be transferred to the GFA filter. Due to the inert nature of the PTFE filters, the cleaning and drying of the filters was done in the open laboratory. The PTFE filters were dipped in a solution of 50 % methanol in deionised water to remove material from the hydrophobic surface of the filter. Following this, the filters were dipped sequentially in two beakers of pure methanol to remove excess water and to speed up the drying process. Once the PTFE filters were cleaned and dried they were stored flat in airtight sample vials.

The polystyrene clips and outer casings of the samplers were prepared by washing in deionised water and then drying on absorbent paper in the laboratory. Washed latex gloves were worn to prevent any contamination of the badges during construction. Separate washed forceps were used to handle the GFA and PTFE filters to prevent contamination of the PTFE filters with tartaric acid.

6.3.3 Field application of the Willems badges

The Willems badge samplers were mounted with the open end of the outer casing facing the ground. The samplers could be supported on simple masts made of garden cane due to their low weight. Each mast was made of three 2.4 m lengths of garden cane giving a total mast height of 4.5 m. The masts were secured, in the Town Barton Farm study, using six guy lines, as shown in Figure 6.3. Sample masts at the SRI Structures Building study were secured using metal base-plates. Despite the inherent flexibility of the garden cane masts, the use of three canes and the guying arrangement shown in Figure 6.3 enabled the masts to remain vertical in all wind conditions. The application of Willems badges in the sampling arrangement shown in Figure 6.3 enabled concentrations to be simultaneously measured at up to 32 sites, with a possible collection of 128 samples per run.

6.3.4 Analysis of the Willems badge samplers

At the end of each experimental run the Willems badge samplers were capped, labelled and returned to the laboratory. The samplers were immediately disassembled and the GFA filters were removed and stored at -15 °C in labelled sample vials. The GFA filters were later extracted in 5.0 ml of deionised water. The water was added slowly to each vial to preserve the structural integrity of the filter, as detached glass fibres could block the CFA system used to analyse the extractant for NH_4^+-N. Vials were left overnight to enable the

concentration of NH_4^+-N on the filter and in the water to reach an equilibrium[2]. A small quantity (approximately 0.5 ml) of the extractant was then removed from each vial using a washed dropping pipette for analysis on the CFA system described in Chapter 4.
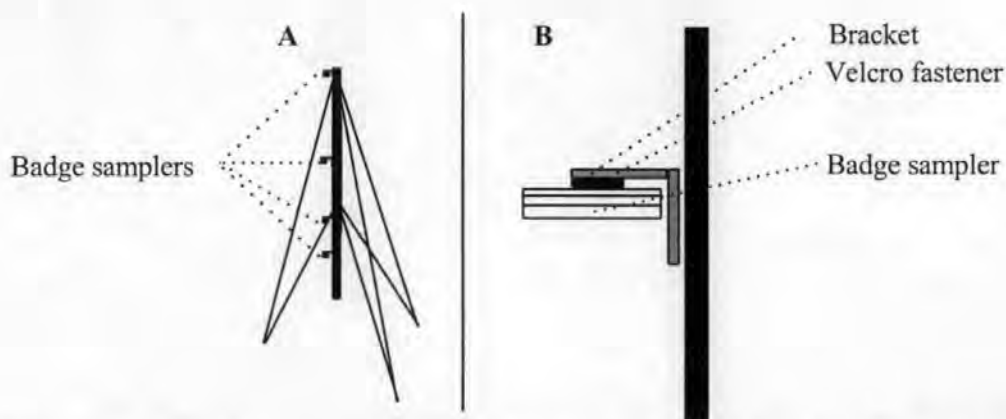
Figure 6.3:   **A**: Mast shown guyed for application in the field equipped with four Badge samplers. **B**: Badge sampler attached to mast.

6.4   ESTIMATION OF NH₃ DEPOSITION AROUND FARM BUILDINGS

Plant "biomonitors" were used to estimate NH_3 deposition fluxes around the farm buildings. These had the advantage of providing a time-average measurement of deposition fluxes that could be compared with the time-average air concentration measurements.

6.4.1   Theory

Deposition fluxes were calculated using a N balance technique, as discussed in Chapter 2, Section 2.3.4. The total N contents of potted hydrologically isolated perennial ryegrass plants (*Lolium perenne L.*) grown from seed in washed sand and precisely dosed with nutrient solution were determined from the N content of above and below ground plant parts, the N content of the sand, and the NH_4^+-N content of leaf washings. The net increase in plant N due to deposition of NH_3 emitted from the farm building was calculated by exposing plants upwind and downwind of the source and by harvesting a control group of unexposed plants.

---

[2] A test to compare concentrations of NH_4^+ in water extracted from the sample vials using the equilibrium method and the concentration of NH_4^+ in water extracted from pulverised filters confirmed that an equilibrium situation was reached within 24 hours.

6.4.2 Growth of plants

Several hundred *L. perenne* seeds were germinated on plastic gauze over a bath of deionised water. Germination of the seeds took approximately a week, with all the seedlings germinating at a similar time. Once the seedlings had grown to a uniform height, of about 50 mm, 20 seedlings were transplanted into each sealed plastic pot filled with washed horticultural grade sand. The seedlings were planted in an evenly spaced uniform pattern in the pots.

The plants were identically dosed with nutrient solution throughout the growth period using a calibrated dispenser (with a precision of +/- 0.1 %). The composition of the nutrient solution used is presented in Table 6.1. The nutrient solution was a modified version of "Arnon's solution" as described in Hatch and Murray (1994). The nutrient solution was modified to omit NH_4^+-N compounds, with the only source of nutrient N to the plant being KNO_3 (at a concentration of 200 mg N l^{-1}). This prevented inaccuracies in the dosage between plants due to NH_3 volatilisation and also ensured that any NH_3-N measured was present due to atmospheric deposition. Plants were initially dosed with nutrient solution diluted to a ratio of 1:5 nutrient solution to water to prevent "scorching" of the seedlings. After two weeks of further growth, the plants were supplied with undiluted nutrient solution.

Concentration (per litre)									
KNO_3	$MgSO_4$	$Ca(H_2PO_4)_2.$ H_2O	H_3BO_3	$MnCl_2.$ $4 H_2O$	$CuSO_4.$ $5 H_2O$	$ZnSO_4.$ $7 H_2O$	H_2MoO_4	$FeSO_4.$ $7 H_2O$	$8 M H_2SO_4$
1.44 g	0.49 g	0.13 g	2.86 mg	1.81 mg	0.08 mg	0.22 mg	0.09 mg	14.94 mg	0.50 µl

Table 6.1:   Composition of the nutrient solution used to dose the "biomonitors".

6.4.3 Field application of the biomonitors

A randomly selected control group of plants was harvested prior to the start of each biomonitor experiment. The control group enabled the determination of the N contents of plants before exposure to ambient atmospheric NH_3. The leaves of all the plants, including the control group, were washed in de-ionised water prior to the start of the experiments to remove any NH_3 on the leaf surfaces. Plants not in the control group were positioned around the buildings at specific sites, discussed in Section 6.5. Several plants were used at each site to provide a replicated sample and to enable the biological variability inherent in such a system to be addressed.

6.4.4   Analysis of the biomonitors

The N contents of all the sinks of the potted plants were determined in order to derive an accurate N budget. These sinks were: leaf surfaces, above ground plant tissues, below ground plant tissues and sand.

6.4.4.1   Analysis of the N content of biomonitor leaf washings

Above ground tissues were removed from the plants within two hours of the end of the experiment and washed in 40 ml of 0.05 M orthophosphoric acid. The NH_4^+-N concentration of the extractant from the washing process was determined on the CFA system described in Chapter 4.

6.4.4.2   Removal of below ground plant tissues

Due to the larger number of analyses from the Town Barton Farm experiment than from the SRI Structures Building study, below ground plant tissues were removed using slightly different methods. Following the SRI study, below ground tissues were extracted by adding 300 ml of deionised water to the roots and sand in each biomonitor pot, with the water serving to wet the roots sufficiently to allow them to be gently extracted. Following the Town Barton Farm study, roots and sand were removed from the pots and crudely separated. The crude root fraction was then freeze dried, following which the sand was dusted from the dried roots.

6.4.4.3   Determination of the N content of the sand.

The N present in the sand was determined, following the SRI study, by analysing a sample of the liquor from the washed roots for NO_3^--N and NH_4^+-N on the CFA system (Skalar, UK). The total water content of the sand was calculated by weighing then drying the samples. This enabled the water present in the pot, prior to the addition of that used to extract the samples, to be accounted for. The NO_3^--N and NH_4^+-N contents of the sand (in mg) were calculated from the aqueous concentrations (in mg N l^{-1}) and the volume of water used to extract the sample (in l).

Sand N contents were calculated, following the Town Barton Farm study, by extracting a weighed sample (approximately 200 g) of the sand in 100 ml of 1.0 M KCl and agitating for 30 minutes. A sample of the resulting liquor was analysed on the CFA system to determine the NO_3^--N and NH_4^+-N concentrations. The moisture content of a sub sample of the sand was determined by weighing then oven drying at 80 °C for 72 hours. This allowed a small correction to be made to the extractant volume to account for the water previously

present and to enable the NO_3^--N and NH_4^+-N concentrations to be expressed as mg per gram dry weight. The total dry mass of sand in the pots (in grams dry weight) was measured enabling the total NO_3^--N and NH_4^+-N contents to be calculated from their dry weight concentrations.

6.4.4.4   Determination of the N content of the plant tissues

Washed samples of above and below ground tissues were stored at -15 °C in sealed plastic bags. The frozen samples were freeze dried for 48 hours. A freeze drier was used in preference to a conventional oven to prevent the possible loss of volatile nitrogenous compounds. The dried samples were then weighed using a five figure digital balance before being milled to a fine powder using a ball mill. The N concentrations of the powdered samples were determined by gas chromatography (Carlo Erba). The total N content of each type of tissue (in mg) was calculated from the N concentration (in mg g^{-1}) and the dry mass of the above ground plant tissues (in g).

6.5   SITES

Two sites were used in these experiments: the experimental "Structures" building at Silsoe Research Institute (SRI), Bedfordshire, and a working dairy farm "Town Barton", at Sandford in Devon. The experimental building was used to investigate NH_3 emissions and dispersion in semi-controlled conditions, whilst the experiments at the working dairy farm were conducted to investigate emissions and dispersion of NH_3 in a realistic environment.

6.5.1   Structures Building

Experiments were conducted between 21 - 28 August 1996 at the SRI Structures Building, (national grid reference: TL 081826) shown in Figure 6.4. The Structures Building was an idealised model of a real farm building and not used to house livestock, thus NH_3 was emitted as a controlled release from the naturally ventilated mid section. The sections to either side of the mid-section were not ventilated and were used for the storage of the sampling and emission regulation equipment. These sections were hermetically sealed from the mid-section to prevent NH_3 leaks.

A map showing the SRI Structures Building and the land immediately surrounding the building is presented in Figure 6.5. The immediately local area was predominantly open grassland, with a sward height of 50 mm. A narrow road and a field of wheat stubble were to the south-east of the building whilst a young plantation was to the north of the building.
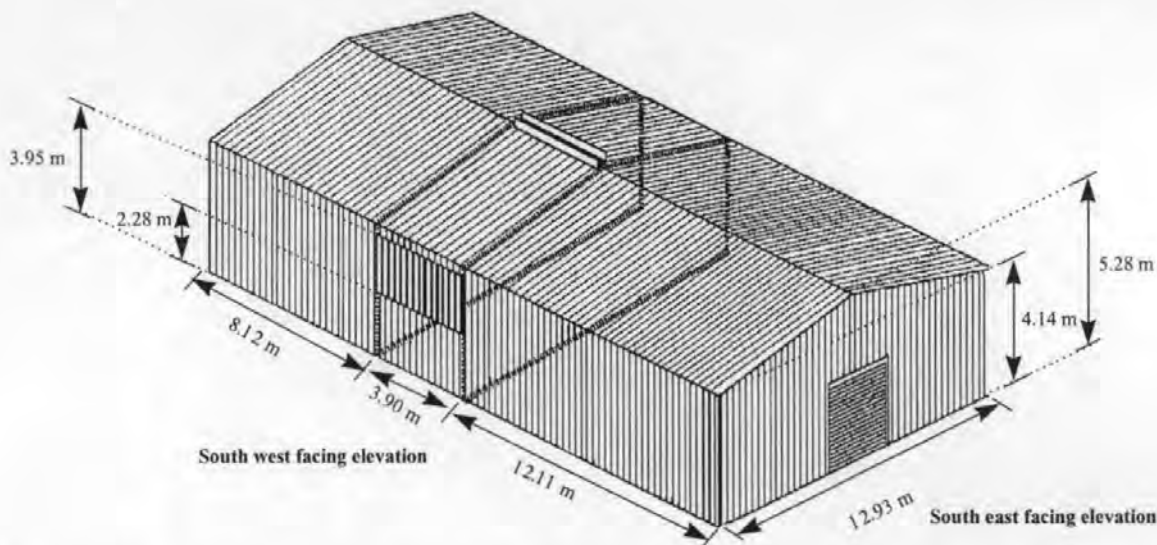
Figure 6.4:   Scale drawing of the SRI Structures Building showing the naturally ventilated mid section. Original drawing supplied by Silsoe Research Institute.
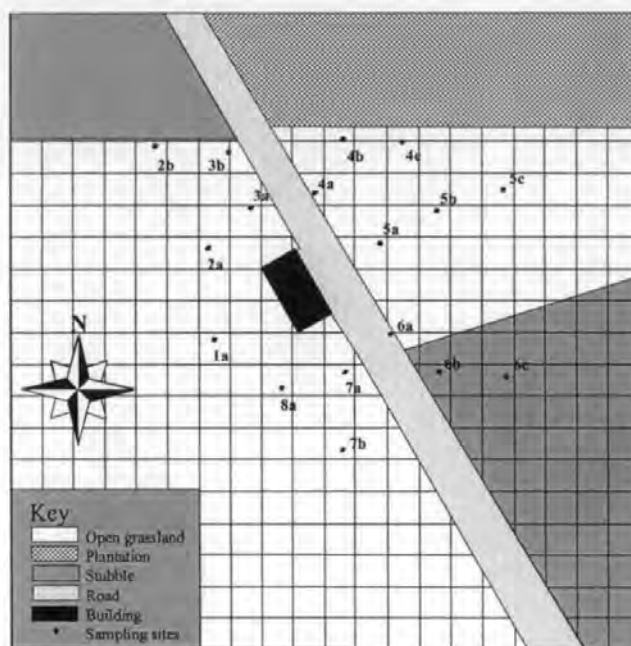
Figure 6.5:   Map showing the land use and location of sampling masts around the SRI Structures Building. Area is shown on a 10m x 10m grid. Plant biomonitors, used to estimate local deposition, were situated at Sites 5a, 6a, and 1a.

6.5.1.1   Arrangement of the sampling equipment

Masts, supporting vertical arrays of Willems badges, were positioned at several sites radiating around the Structures Building, as shown in Figure 6.5. This experimental design ensured that the dispersion of NH_3 could be measured for all wind directions. Though sampling masts were positioned at all the sites shown in Figure 6.5, Willems badges were mostly sited on the masts that were in a 180° sector downwind of the building.

Biomonitors were co-located with the passive diffusion samplers at three sites, one site upwind of the building (1a) and two sites downwind of the building (5a and 6a). The co-location of the biomonitors with the Willems badges throughout the duration of the experiment allowed the direct estimation of the time averaged deposition velocity using Equation 1.4. Details of the run times for the four experiments to measure the air concentration field around the SRI Structures Building and the single biomonitor experiment to determine the NH₃ deposition flux are shown in Table 6.2.

Experimental run	Start	End	Sites
Air concentration run 1	21/08/96 14:20	22/08/96 15:00	1a, 3a, 3b, 4a, 4b, 4c, 5b, 5c, 6a, 6b, 6c, 8a
Air concentration run 2	22/08/96 15:00	23/08/96 16:16	1a, 3a, 3b, 4a, 4b, 4c, 5a, 5b, 5c, 6a, 6b, 6c, 8a
Air concentration run 3	23/08/96 16:16	24/08/96 17:16	1a, 3a, 3b, 4a, 4b, 4c, 5a, 5b, 5c, 6a, 6b, 6c, 8a
Air concentration run 4	24/08/96 17:16	31/08/96 11:30	1a, 3a, 3b, 4a, 4b, 4c, 5a, 5b, 5c, 6a, 6b, 6c, 8a
Biomonitors	21/08/96 15:00	31/08/96 15:00	1a, 5a, 6a

Table 6.2:   Run times and sampling sites used during the SRI buildings study.

6.5.2   Town Barton Farm, Devon

A second series of experiments was conducted, between 18 March - 16 April 1997, at a working dairy farm "Town Barton" located in the south-west of England (national grid reference: SS 826024). This site was selected as the dairy and cowshed were present in the same building. Consequently, the source of NH₃ on the farm was well defined and the emission from the building could be adequately determined using the Ferm tube mass balance method (Phillips *et al.*, 1998).

6.5.2.1   Description of the site

A map of the Town Barton Farm and the immediate surrounding area is shown in Figure 6.6. The main Town Barton Farm dairy/cowshed building, designed to house 120 dairy cows, was much larger than the SRI Structures Building and occupied a ground area of 1875 m². Dairy cows are housed in open cubicles on matting. Slurry, deposited into the channels between the cubicles, was removed, approximately every 30 minutes, by a system of automatic scrapers. The slurry scrapers transferred the waste, through an underground channel, to an open slurry lagoon, 50 m long by 10 m wide, 25 m south of the building. The slurry lagoon was capped with a crust throughout the duration of the experiment.
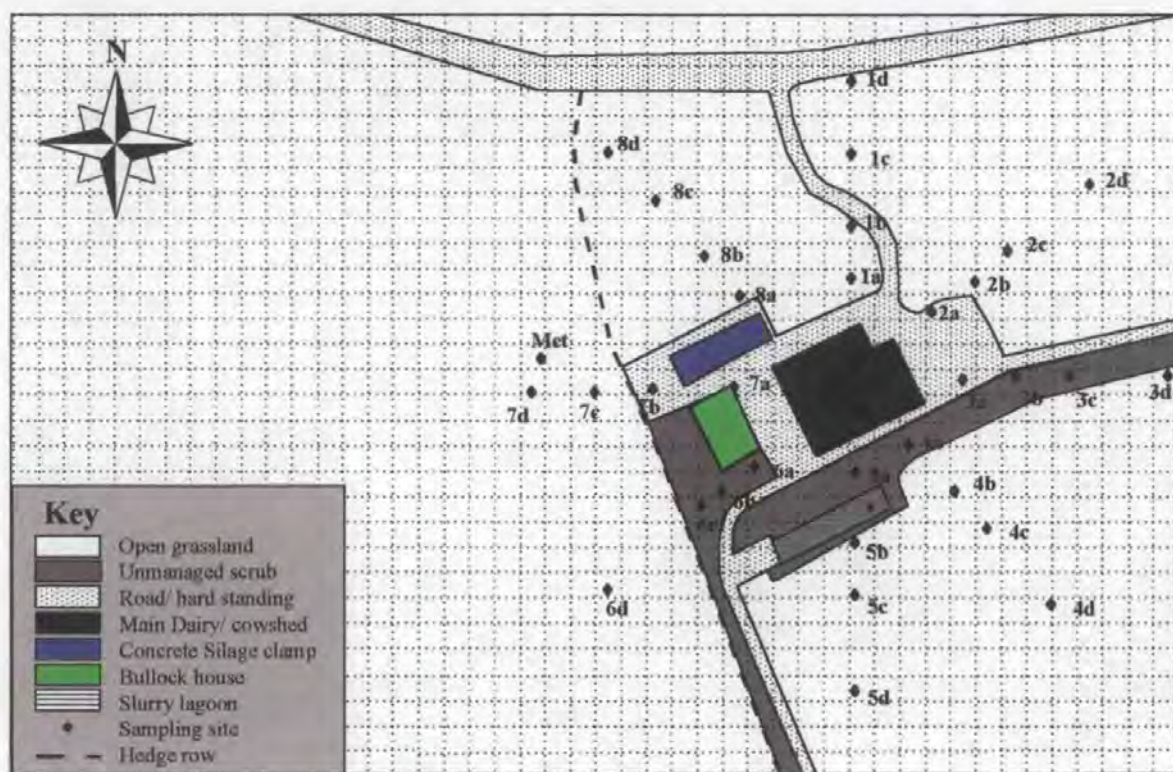
Figure 6.6:   Map of Town Barton Farm, Sandford, Devon showing the positions of the NH₃ sampling masts, and the layout of the buildings. The area is shown on a 10 m x 10 m grid.

During the housing period the dairy cows were fed on locally produced maize silage and received a concentrated feed supplement twice a day during milking, 06:00 and 16:00 (GMT). The milking parlour and collecting yard were adjacent to the cowshed. A second auxiliary cowshed, housing a small number of dairy cows in calf and their calves, was immediately to the west of the main dairy building. This building used a straw based waste management system and had a more open aspect than the main dairy building. The other main structure on the site was a large concrete silage clamp, 40 m long x 10 m wide x 2 m high.

The area around the farm was reasonably flat, with fields to the north and north-east of the building raised approximately 3m above the floor level of the building by an embankment. The fields to the south of the building were approximately 2 m lower than the floor level of the building.

6.5.2.2   Experimental design

Thirty two sampling masts (4.5 m in height) were positioned on a radial grid around the Town Barton Farm building. These masts were each equipped with four Willems badge

samplers (positioned at 0.5 m, 1.5 m, 2.5m, and 4.5 m), to measure vertical gradients in NH₃ concentration. A portable mast was also used to measure the vertical concentration gradient to 11.5 m using 13 Willems badge samplers. The positions of this mast are shown on a more detailed map, Figure 6.7.
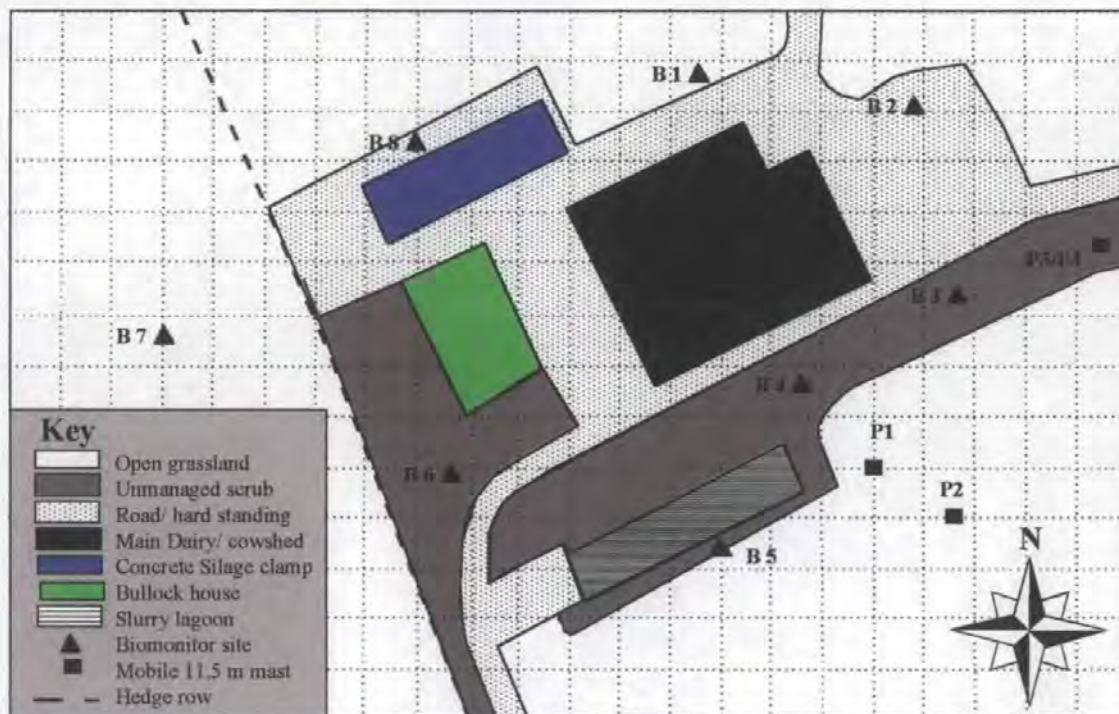
Figure 6.7:   Detailed map of Town Barton Farm showing the biomonitor sampling sites and the positions of the mobile 11.5 m mast. The area is shown on a 10 m x 10 m grid.

Enclosures containing 10 biomonitor plants were positioned at eight sites radiating around the farm, as shown in Figure 6.7. This sample arrangement ensured that measurements could be conducted in all wind directions. As the prevailing wind direction was from the west, the use of a radial sampling arrangement allowed NH₃ deposition measurements to be made across a concentration gradient formed by the non-uniform wind rose. An additional 10 biomonitor pots dosed with 20 mg N were placed at Sites B2, B3, and B4 to investigate whether modifying the N status of the plants affected the rate of uptake of atmospheric NH₃.

Emissions of NH₃ from the Town Barton Farm buildings were measured using Ferm tube flux samplers, as described in Section 6.2. The flux samplers were positioned at 94 sites on the farm building. Fifty nine pairs of Ferm tube samplers were positioned on the Yorkshire boarded walls and other openings of the main dairy/ cowshed, as shown in Figure 6.8.

Elevation facing to the south-west from the building

Elevation facing to the north-east from the building

Elevation facing to the north-west from the building

Elevation facing to the south-east from the building
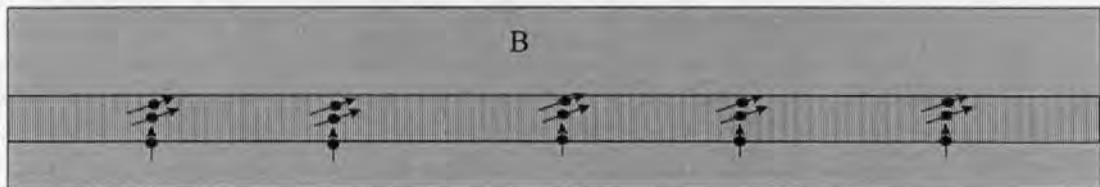
Scale   4 m   8 m

Figure 6.8:   Scale diagrams of the Town Barton Farm dairy/cowshed building showing the positions of the Ferm tube flux samplers used to measure NH_3 emissions from the walls of the building. Yorkshire boarding (vertical hatch) not shown to scale. A: dairy, **B**: cowshed, ✔: horizontally mounted pair of Ferm tube samplers, ✔: vertically mounted pair of Ferm tube samplers.

These sampling sites were chosen to provide a detailed dataset of the "point" fluxes from the building. The south-west and north-east facing sides of the building had large openings, allowing the building to be efficiently ventilated. Fluxes across these openings were measured by mounting a number of Ferm tubes on 5.0 m high vertical wooden posts. Where doors partially blocked the openings, Ferm tubes were mounted at two heights, whilst four heights were used where the openings were unblocked.

The north-west and south-east facing sections of the main dairy/cowshed were comprised of Yorkshire boarding (0.15 m planking with a 0.025 m spacing between planks). Emissions through the Yorkshire boarding were measured using horizontally mounted

184

Ferm tubes with the inlets, inside the building, positioned parallel to the Yorkshire boarding. A 0.5 m gap occurred between the lower solid section of the wall and the Yorkshire boarding. Fluxes of NH_3 through this gap were measured using pairs of vertically mounted Ferm tubes.

Emissions of NH_3 from the roof of the building were more difficult to measure, due to the technical difficulty of accessing the roof. Sampling sites were accessed using a platform mounted to the front forks of a "low loader". Flux measurements were made on the two distinct roofs on the main building, the cowshed roof and the dairy roof. The cowshed roof ventilated through a 0.2 m wide open ridge and through 45 0.025 m wide lateral vents. The dairy building ventilated through 20 covered, naturally ventilated, ducts orientated to ventilate to the north-west and south-east. The total open face area of these ducts was 0.081 m², equally split between the two directions. The positions of the sampling sites, used to measure emissions from the roof of the Town Barton Farm main building are shown in Figure 6.9.
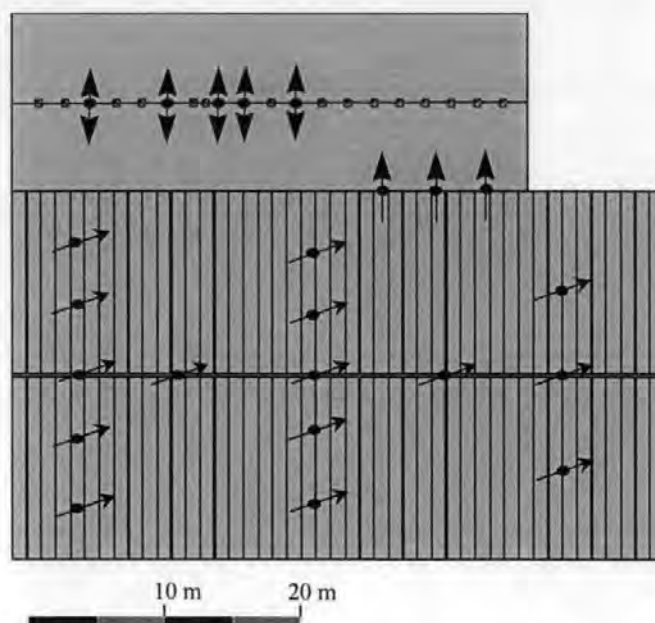
Figure 6.9:   Scale diagram of the plan view of the Town Barton Farm main building showing the positions of the Ferm tube flux samplers used to measure NH_3 emissions from the roof of the building. ●: horizontally mounted pair of Ferm tube samplers, ↑: vertically mounted pair of Ferm tube samplers.

A second building on Town Barton Farm, the auxiliary cowshed, is shown in Figure 6.10. Emissions from this building were measured at four positions using three pairs of Ferm tubes at each position. As the house was also used to store straw bales, which blocked ventilation on the south-east facing side, only emissions from the north-west, north-east

185

and south-west facing sides were measured. Ferm tubes were mounted on 5 m high wooden posts, which were positioned vertically on the sides of the building. Emissions from the roof of the auxiliary cowshed were not measured as the open area of the roof vents (0.18 m^2) was small in comparison to the largely open sides of the building and as there were practical difficulties in accessing the roof.

Elevation facing north-east from the building
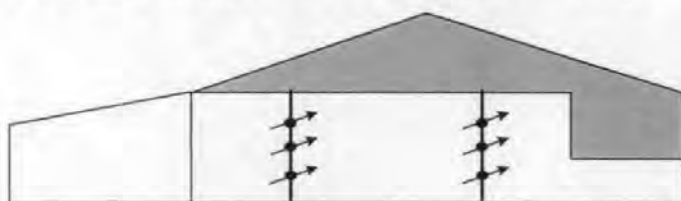
Elevation facing south-west from the building

Elevation facing north-west   **Elevation facing south-east**
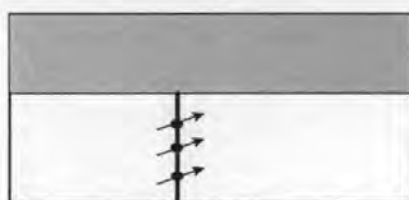
Scale   4 m   8 m

Figure 6.10:   Scale diagram of the second cowshed on Town Barton Farm showing the positions of Ferm tube samplers used to measure NH₃ emission fluxes. $\nearrow$: horizontally mounted pair of Ferm tube samplers, $\uparrow$: vertically mounted pair of Ferm tube samplers.

6.5.2.3   Timing of the experiments

The experiments to measure the emission, dispersion and local deposition around Town Barton Farm were conducted during March and April 1997. The times of the various experiments are given in Table 6.3. The 24 hour experiments were initially designed to measure NH₃ emissions and air concentrations simultaneously. However, due to problems that were encountered with the application of the Ferm tubes in wet conditions, reliable estimates of NH₃ emission were only obtained for the third and fourth experiments.

Experimental run	Start	End	Sites
Air concentration run 1	20/03/97 15:00	21/03/97 15:00	Arrays 3 to 7
Air concentration run 2	23/03/97 12:00	24/03/97 12:30	Arrays 1 to 5
Air concentration run 3	28/03/97 13:00	29/03/97 13:30	Arrays 2 to 6
Air concentration run 4	02/04/97 13:00	03/04/97 14:00	Arrays 1 to 5
Emission run 1	28/03/97 12:00	29/03/97 12:00	All
Emission run 2	02/04/97 12:00	03/04/97 12:00	All
Biomonitors	18/03/97 16:00	16/04/97 11:00	All

Table 6.3:   Experimental times for the experiments conducted at Town Barton Farm. Site positions are referenced to Figure 6.6 for air concentration measurements, Figure 6.7 for biomonitor measurement and Figures 6.8, 6.9 and 6.10 for emission measurements.

6.6   CONCLUSIONS

This chapter presented experimental methods for measuring the emission, dispersion and local deposition of NH_3 volatilised from two naturally ventilated farm buildings. These were the SRI Structures Building and a working dairy farm in the south-west of England, "Town Barton". The experimental designs and descriptions of the field sites were also presented. Results of the field experiments are presented in Chapter 7.

7

EMISSION, DISPERSION AND LOCAL DEPOSITION OF NH₃ VOLATILISED FROM FARM BUILDINGS: RESULTS

7.1 INTRODUCTION

This chapter presents the results of two series of experiments to measure the emission, dispersion and local deposition of NH_3 released from naturally ventilated farm buildings. The first series of experiments investigated dispersion and deposition of NH_3 released from an idealised building, the Silsoe Research Institute (SRI) Structures Building, whilst the second series of experiments investigated dispersion and local deposition of NH_3 released from a working farm, "Town Barton". The experimental methods and designs for these experiments can be found in Chapter 6.

7.2 SRI STRUCTURE BUILDING EXPERIMENT

The SRI Structures Building experiments were subdivided into four experimental runs. These runs were overlapping to provide continuous monitoring of the dispersion of NH_3 around the building. The initial three runs, to investigate the temporal variability of NH_3 dispersion, each had a duration of 24 hours, whilst the fourth run continued for 10 days to provide information on the longer time-average pattern of dispersion. The four runs also enabled the calculation of time-average ground level air concentrations that were used, in combination with deposition fluxes, estimated using biomonitors, to determine the time-averaged deposition velocity.

7.2.1 Meteorological conditions

Meteorological conditions were measured close to the experimental site, at the Silsoe Research Institute meteorological station. This station provided data on air temperature, wind speed, wind direction and rainfall every 10 minutes. A summary of the

meteorological conditions measured during each of the experimental runs is shown in Table 7.1.

Run	Temperature ($^\circ$C)			Relative humidity (%)			Wind speed {5 m} (m s^{-1})			Wind direction ($^\circ$)		Precipitation (mm)
	Mean	Max	Min	Mean	Max	Min	Mean	Max	Min	Mean	σ_θ	Total
1	17.6	24.2	9.3	70	100	42	2.4	5.3	0.1	232	22	0.0
2	17.0	21.7	14.6	84	100	47	2.9	5.5	0.4	178	32	18.5
3	16.8	20.7	13.7	78	93	56	4.2	6.9	1.9	214	13	0.2
4	14.2	20.1	7.8	87	100	55	3.3	9.6	0.1	275	61	24.6
ALL	15.1	24.2	7.8	84	100	42	3.3	9.6	0.1	254	62	43.3

Table 7.1:   Meteorological conditions measured during the experiments at the SRI Structures Building. Data were provided by Silsoe Research Institute.

In total 43.3 mm of rainfall were measured during the experiment. Rainfall did not occur continuously throughout the experiment, hence, a further analysis was conducted to investigate any wind direction dependence. The results of this analysis are presented in Table 7.2.

Run	Mid-point of 30° wind sector (degrees from north)											
	30	60	90	120	150	180	210	240	270	300	330	360
1	0.0	0.0	0.0	0.0	0.0	0.0	0.0	0.0	0.0	0.0	0.0	0.0
2	0.0	0.0	0.0	4.4	5.4	7.9	0.8	0.0	0.0	0.0	0.0	0.0
3	0.0	0.0	0.0	0.0	0.0	0.0	0.2	0.0	0.0	0.0	0.0	0.0
4	0.0	0.0	0.0	0.0	0.0	0.0	0.4	0.0	1.7	10.8	6.7	5.0
ALL	0.0	0.0	0.0	4.4	5.4	7.9	1.4	0.0	1.7	10.8	6.7	5.0

Table 7.2:   Sector distribution of total rainfall (in mm) measured during the SRI Structures Building experiment.

7.2.2   NH₃ dispersion

Ammonia concentrations around the SRI Structures Building were investigated using arrays of passive diffusion samplers (Willems badges), as discussed in Chapter 6, Section 6.3. These measurements were used to investigate the horizontal concentration distribution at 0.5 m above the surface, and the vertical concentration distribution to 4.5 m at the approximate centreline of the NH₃ plume

7.2.2.1 *Horizontal distributions of NH₃ concentrations*

Horizontal distributions of NH_3 concentrations around the SRI Structures Building were evaluated using measurements from the Willems badge samplers closest to ground level (0.5 m). Data from these samplers, and the Cartesian locations of the sampling site positions were imported into a contour mapping computer program (Surfer v 6.01, Golden software inc.). Concentration contour maps, shown in Figure 7.1, were calculated using the program's default "Kriging" methodology to interpolate between the data points. The Kriging interpolation method was chosen as it has been widely used in the literature for plotting trace atmospheric constituents (*e.g.* CLAG, 1994).

Run 1   Run 2

Run 3   Run 4
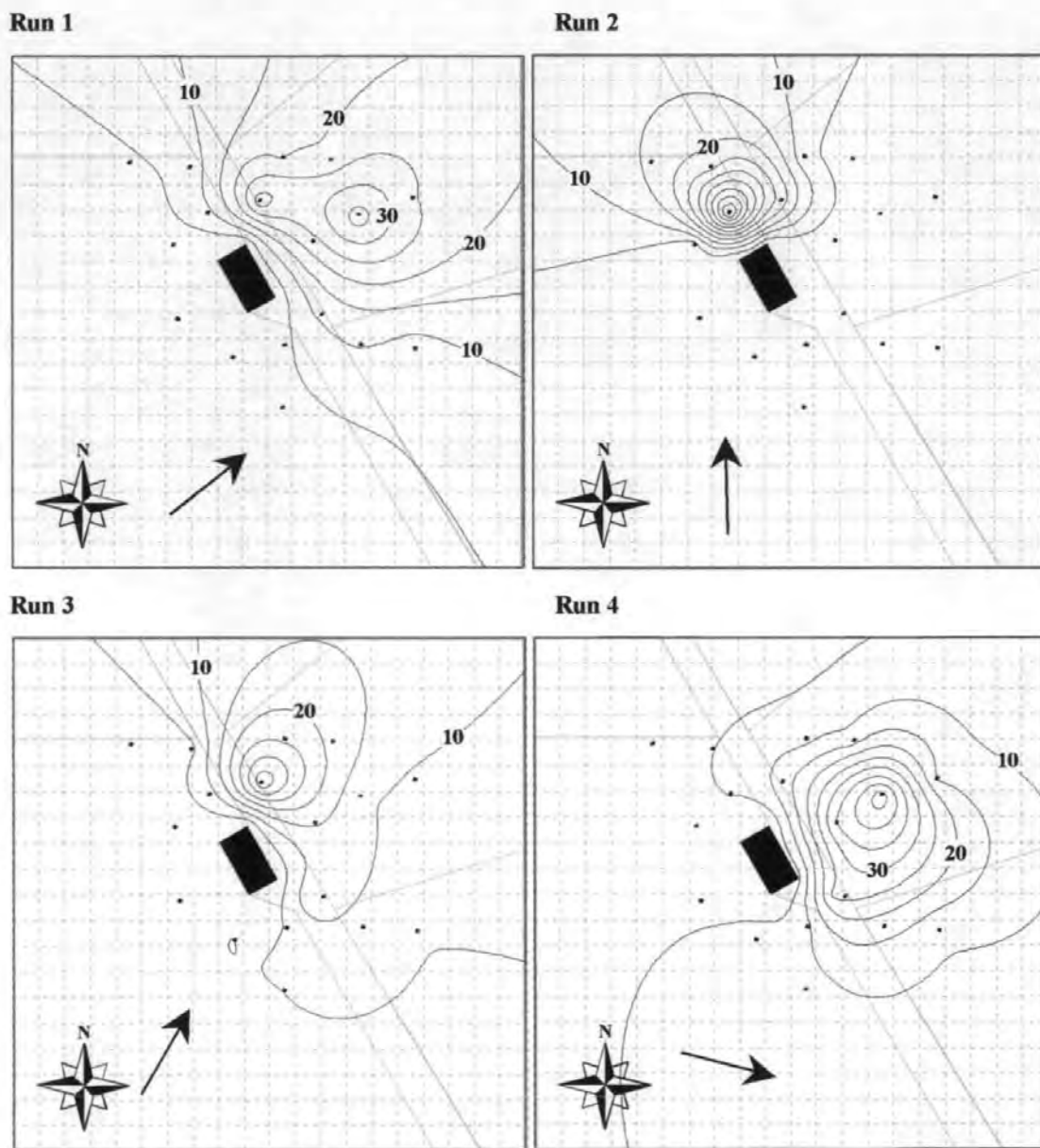
Figure 7.1: Contour plots of measured ground level air concentrations (in μg NH₃-N m⁻³) around the SRI Structures Building. Contours are shown with a resolution of 5.0 μg NH₃-N m⁻³. 1:2750 scale. Arrows show the median wind direction.

The concentration contour maps, shown in Figure 7.1, demonstrate that the trajectories of the NH_3 plumes released from the building correlated well with the median wind directions. Dispersion of NH_3 was measured over the fields to the north-east, north, north-north-east and north-east of the building for each of the four experimental runs.

Figure 7.1 shows that the initial dispersion of the plumes downwind of the building varied between the each run. Plumes, measured in Runs 1 and 4, were of a comparable width and were somewhat wider than those measured in Runs 2 and 3. The variability in the plume widths measured in Runs 3 and 4 could, in part, be explained by the variation in the standard deviation of the wind direction (σ_θ) between these runs, bearing in mind the relationship between σ_y and σ_θ discussed in Chapter 3, Section 3.2.1. However the differences in plume width between Runs 1 and 2 cannot be attributed to σ_θ and show good evidence that the orientation of the building caused a narrower cavity wake to form.

The spatial pattern of near-ground level NH_3 concentrations was also modelled using the UK-ADMS v2.2 atmospheric dispersion model. This model has a relatively detailed treatment of building influenced dispersion, as discussed in Chapter 3, Section 3.2.1.5. Contour plots of modelled ground level concentrations were calculated using the building dimensions and hourly averaged meteorological data. The source term for NH_3 was equally split between emissions from the roof and the Yorkshire boarding of the building. Modelled concentration contour maps for each run are shown in Figure 7.2.

A reasonable agreement was found between both the magnitude and spatial distribution of the modelled and measured concentrations for Run 1, however the other runs were in a much poorer agreement. Concentrations were overpredicted by the model to the north-east of the building for Runs 2 and 3 and to the south-east of the building for Run 4. Measured and modelled near-ground level concentrations within the NH_3 plume, defined as concentrations that were greater than the measured background level by a factor of 2.0, were also compared directly, results are shown in Figure 7.3.

Run 1

Run 2

Run 3

Run 4
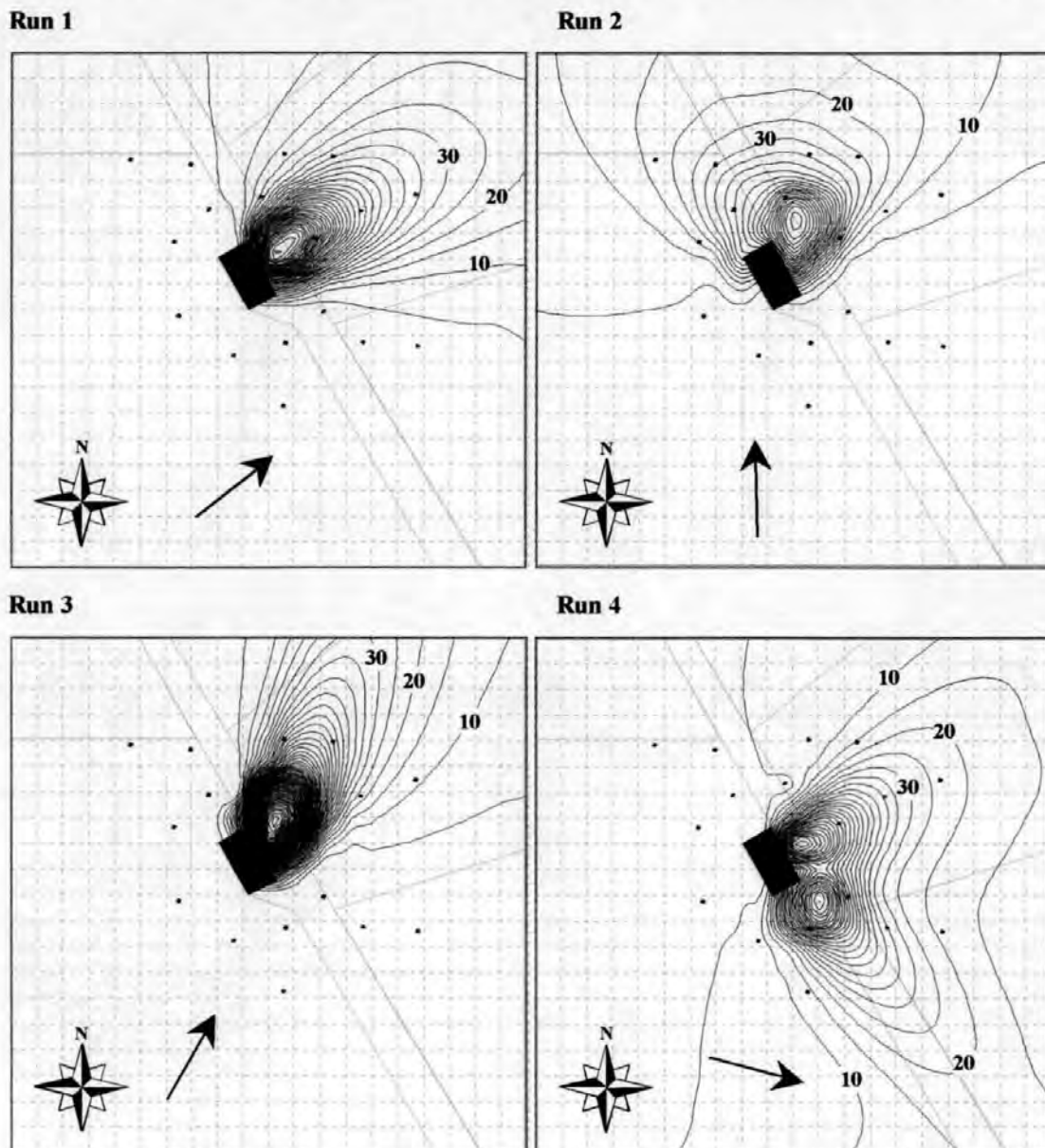
Figure 7.2:   Contour plots of ground level air concentrations (in μg NH$_3$-N m^{-3}) around the SRI Structures Building modelled using UK-ADMS 2.2. Contours are shown with a resolution of 5.0 μg NH$_3$-N m^{-3}. 1:2750 scale. Arrows show the median wind direction.

The direct comparison between the measured and modelled near-ground level concentrations, shown in Figure 7.3 demonstrated that the model described the dispersion of NH$_3$, within the measured plume, reasonably well. The gradient of the regression line was 1.19 and the y-intercept was 9.6 though the latter was not significantly different from zero. However, there was some scatter between the measurements and model predictions. The results showed that 62 % of the model predictions were within a factor of 2.0 of the measurements and the R^2 value of the relationship indicated that 32 % of the variation in the measurements was accounted for by the model.
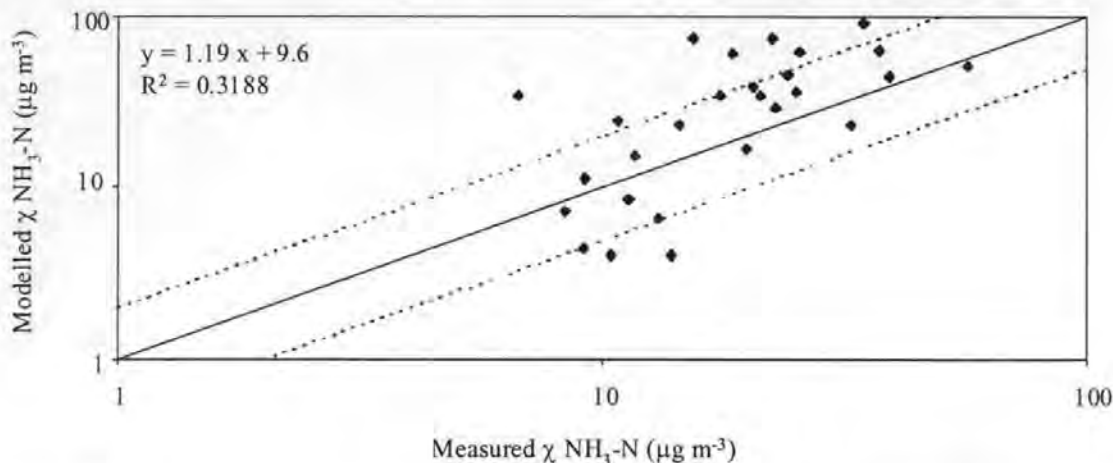
Figure 7.3: Comparison between measured ground level air concentrations and the predictions of the UK-ADMS model. Emissions sources were equally split between the roof and Yorkshire boarding of the building. Line fits are shown to indictate 1:1, 2:1 and 1:2 ratios of the data series.

The differences between the measured and modelled concentrations were hypothesised to be due to an oversimplification when modelling the source distribution of the building. The naturally ventilated mid-section of the building was likely to emit NH_3 through the Yorkshire boarding only when driven by a mass flux of air into the building. For conditions when there was little mass flux of air into the building (*i.e.* winds from the north-west and south-east) the mid section was hypothesised to ventilate principally through the roof, with NH_3 diffusing into the passing air stream. To test this hypothesis a second set of model runs were conducted. In these runs emissions were modelled from the roof and Yorkshire boarding of the building for winds between 225 and 255 degrees, whilst for other wind directions emissions were assumed to be from the roof only. The results of the second modelling study are presented in Figure 7.4.

A much improved agreement was found between the revised model predictions, shown in Figure 7.4, and the field measurements, shown in Figure 7.1. The horizontal distribution of NH_3 concentrations were found to be in close agreement for Runs 2 and 3, and the anomalous plume previously modelled to be travelling over the area to the south-east of the building during Run 4 was no longer apparent.

A statistical comparison of the revised model predictions and the field measurements is shown in Figure 7.5. The statistics of the regression analysis showed a higher proportion of the variability in the measurements was accounted for by the model when using the revised

source distribution ($R^2 = 0.37$). Furthermore, a higher proportion of the model predictions were within a factor of 2.0 of the measurements (69 %).

Run 1   **Run 2**

Run 3   **Run 4**
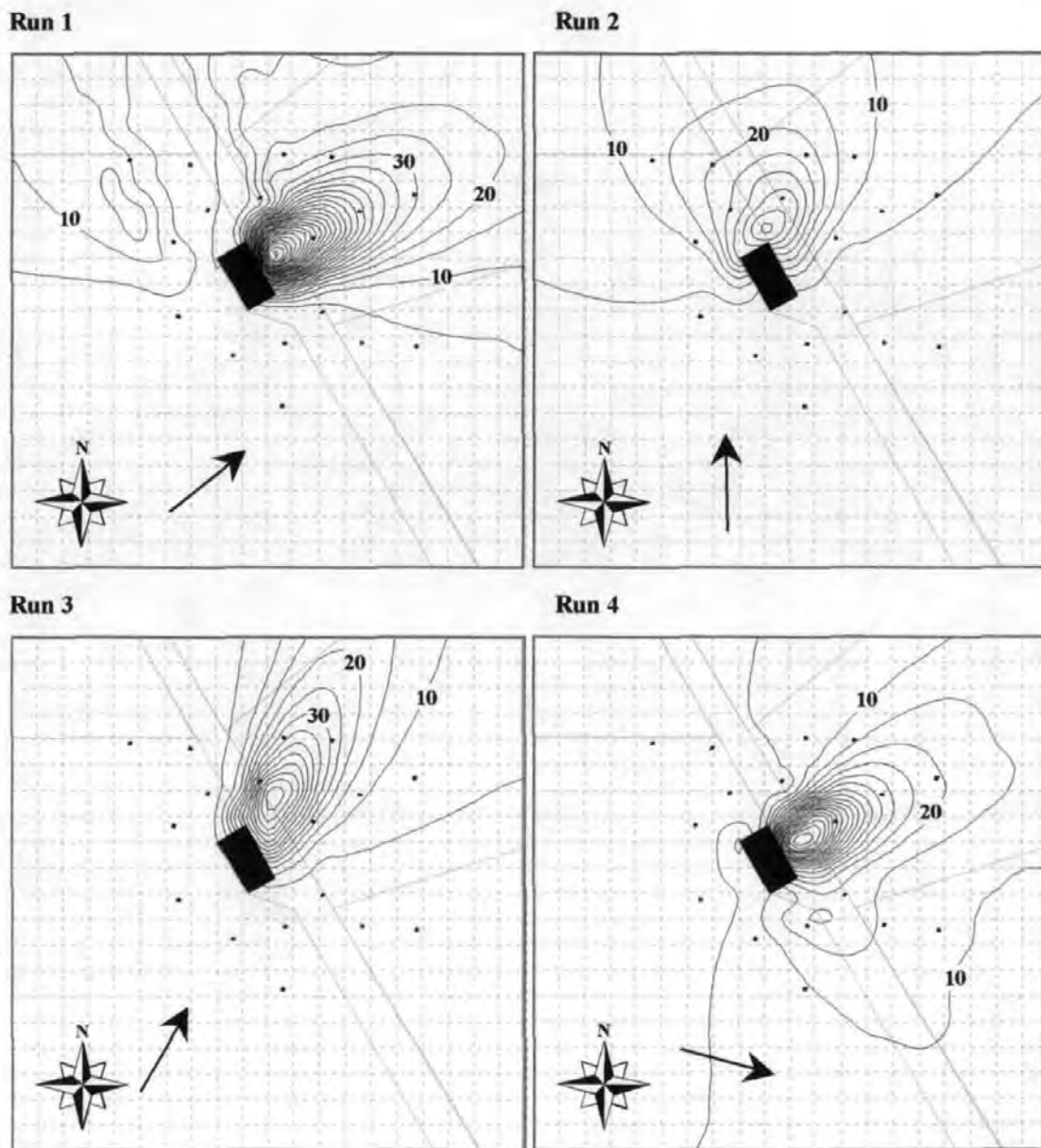
Figure 7.4:   Revised contour plots of ground level air concentrations (in μg NH_3-N m^{-3}) around the SRI Structures Building modelled using UK-ADMS 2.2. Emissions were modelled from the roof and walls for wind directions between 225 - 255°. For other wind directions emissions were modelled as a roof release. Contours are shown with a resolution of 5.0 μg NH_3-N m^{-3}. 1:2750 scale. Arrows show the median wind direction.

7.2.2.2   *Vertical distributions of NH₃ concentrations*

The vertical distribution of NH_3 concentrations was investigated using the field measurements made to 4.5 m at the centreline of the NH_3 plume. The measured concentration profiles and the predictions of the UK-ADMS atmospheric dispersion model

are shown in Figure 7.6. Emissions from the building were modelled using the revised source distribution as previously discussed.
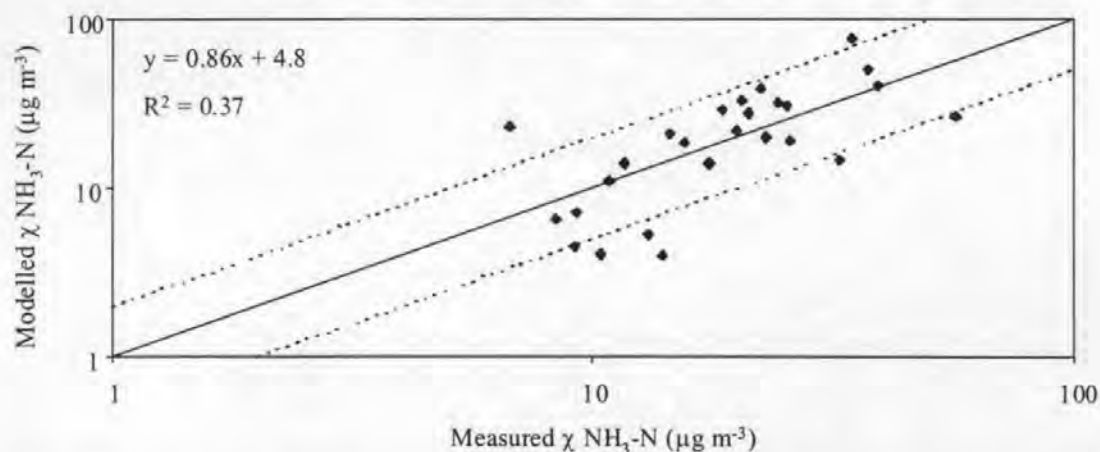
Figure 7.5:   Comparison between measured ground level air concentrations and the predictions of the UK-ADMS model. Emissions were modelled from the roof and walls for wind directions between 225 - 255°. For other wind directions emissions were modelled as a roof release. Line fits are shown to indictate 1:1, 2:1 and 1:2 ratios of the data series.

Figure 7.6 demonstrates that concentrations downwind of the building were uniformly distributed in the vertical. Measurements made during Runs 2 and 3 showed the most pronounced vertical concentration gradients, with concentrations increasing with height. Such a concentration distribution suggested that the roof of the building was the source of NH_3 for these runs. This provides further evidence to support the use of the previously discussed revised source distribution.

The predictions of the UK-ADMS model were in a reasonable agreement with the measurements of the magnitude and vertical distribution of air concentrations, with 87 % of the model predictions being within a factor of 2.0 of the measurements. The vertical concentration distributions modelled at sites close to the source for Runs 2 and 3 did not show the increase in concentration with height measured in the field. This was likely to be due to the approximate treatment of dispersion in the near-field wake implemented within UK-ADMS.
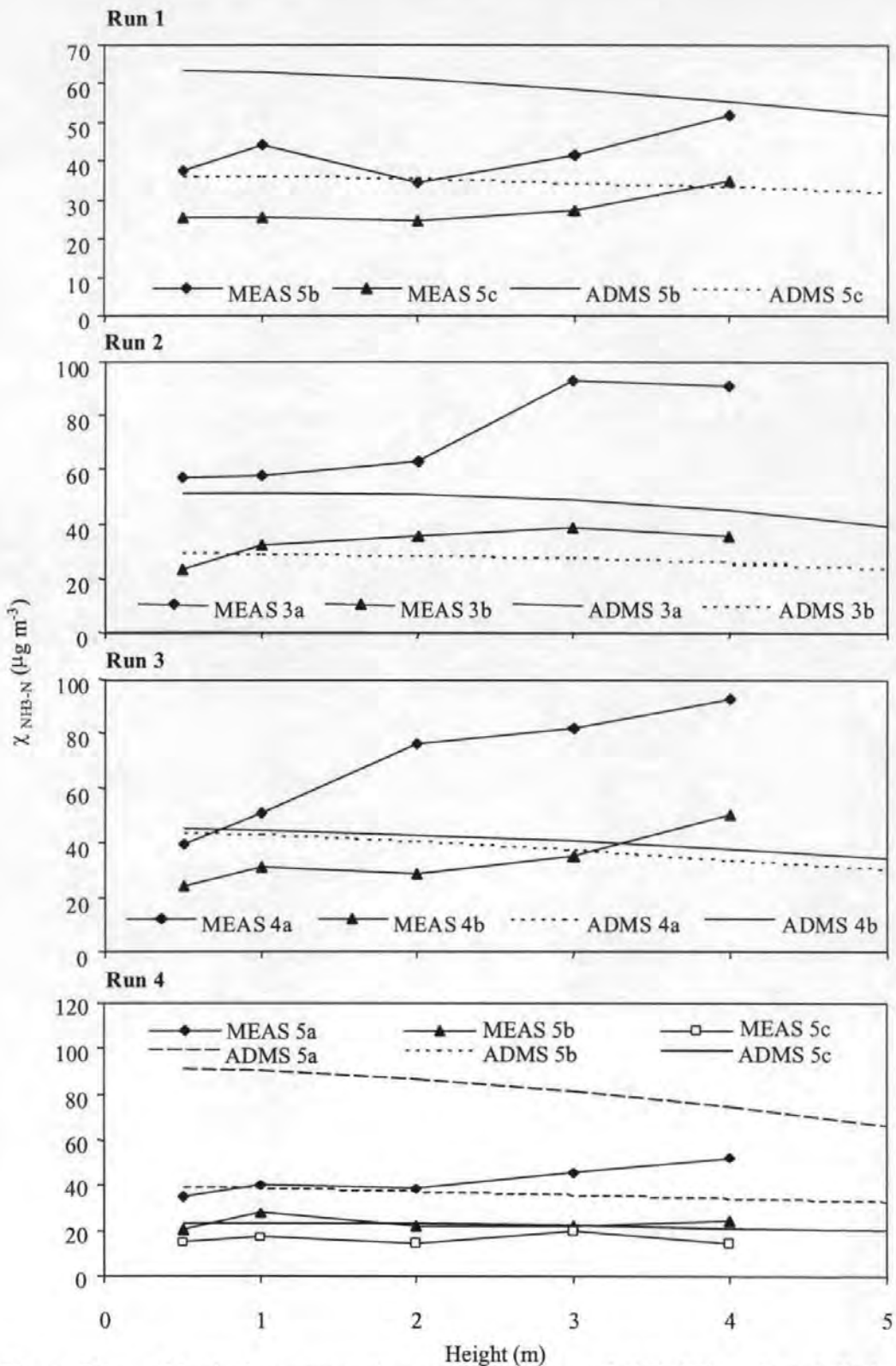
Figure 7.6:   Vertical concentration profiles measured (MEAS) and modelled using UK-ADMS 2.2 (ADMS) at the centreline of the NH₃ plume from the SRI Structures Building.

7.2.3   NH₃ deposition

Deposition of NH₃ was measured using biomonitors, as described in Chapter 6, Section 6.4. The partitioning of N in the biomonitors was investigated by determining the N contents of four fractions: above ground material (shoots and leaves), below ground

material (roots), sand, and surface N (as NH_x-N) bound to the leaves. The analysis was conducted tracing each fraction back to an individual biomonitors, rather than by simply calculating means from all the replicate biomonitors at a site. This enabled the subsequent analysis to account for any variability in the N partitioning between the biomonitors. Results, shown in Table 7.3, were statistically analysed using a one-way analysis of variance (ANOVA).

Site	Above ground material			Below ground material			Sand	Leaf	Total
	Mass (g)	N (%)	N (mg)	Mass (g)	N (%)	N (mg)	N (mg)	N (mg)	N (mg)
Pre	2.03_a	3.85_a	78.07_a	0.95_a	1.92_a	18.10_a	16.34_a	NM	112.51_a
1a	3.54_b	2.33_b	82.38_b	$2.54_{b,c}$	1.20_b	30.25_b	0.00_b	0.05_a	112.68_a
5a	$3.76_{b,c}$	2.36_b	88.54_c	2.68_b	1.13_b	$30.31_{b,c}$	0.00_b	0.09_b	118.94_b
6a	3.80_c	2.33_b	88.54_c	2.32_c	1.17_b	27.20_c	0.00_b	0.15_c	$115.89_{a,b}$

Table 7.3: Results of the biomonitor experiment at the Silsoe Structures Building to investigate NH_3 deposition. Results were statistically analysed using a one-way ANOVA to determine whether significant differences occurred between the sites. Numbers with the same subscripted letter are not significantly different at the $P<0.05$ level. NM: not measured. Thirteen replicate biomonitors were used at all sites with the exception of Site 6a where eight biomonitors were used.

7.2.3.1   Above ground dry mass

Biomonitors exposed in the field had significantly higher mean above ground dry mass than the pre-field control group. This increase in above ground mass indicated that significant metabolic activity had occurred during the exposure period. Biomonitors at both Sites 5a and 6a (downwind) also had significantly higher mean above ground dry mass, at the 90% confidence level, than those at Site 1a (upwind). However, only the biomonitors at Site 5a had significantly higher mean above ground dry mass than those at Site 1a at the 95% confidence limit. No significant difference was observed in above ground dry mass between biomonitors at Sites 5a and 6a.

7.2.3.2   Above ground percentage N

All biomonitors exposed in the field showed significant reductions in the % N levels in the above ground tissues when compared to the pre-field control group. No significant differences in the % N levels were found between biomonitor groups exposed in the field.

7.2.3.3   Above ground N contents

All the biomonitors exposed in the field had significantly higher above ground N contents than the pre-field control group. The biomonitors at Sites 5a and 6a also had significantly higher levels of above ground N than biomonitors at Site 1a. No significant differences were found between the biomonitors at the two downwind sites with the results, rather fortuitously, being identical to two decimal places. The significantly higher N contents of the biomonitors at the downwind sites provide good evidence that deposition of NH_3 occurred downwind of the building and that deposited NH_3 was assimilated in the above ground plant organs.

7.2.3.4   Below ground dry mass

The biomonitors exposed in the field had significantly higher below ground biomass than the pre-field control group. This demonstrated that, as found in the above ground plant material, a high rate of metabolic activity had occurred during exposure in the field. No significant differences in below ground biomass were found between the biomonitors at either of the downwind sites and those upwind of the building, showing that atmospheric NH_3 did not stimulate the production of below ground plant material. Significant differences in below ground dry mass were found between the biomonitors exposed at the two downwind sites, with significantly lower below ground dry mass being found at Site 6a. The reason for this last finding was not clear and could have resulted from experimental error in the extraction of root material.

7.2.3.5   Below ground percentage N

Lower percent N concentrations in root material were found in the biomonitor groups exposed in the field than the pre-field control group. No significant differences were observed in the below ground percent N concentration between biomonitors at the downwind sites and those at the upwind site.

7.2.3.6   Below ground N contents

The below ground N contents of the biomonitors exposed in the field were significantly higher than found in the pre-field control group. No significant differences in below ground N contents were found between the upwind and downwind sites. A significantly lower below ground N content was found at Site 6a than at Site 5a, due to the aforementioned differences in below ground dry mass.

7.2.3.7   Sand N contents

No measurable quantity of NH_4^+-N (<0.01 mg) or NO_3^--N (<0.1 mg) could be determined in the sand fraction of any of the biomonitors exposed in the field. This contrasted with the high levels of NO_3-N measured in the pre-field control group, showing that the N present in the sand prior to exposure in the field had been metabolised.

7.2.3.8   Leaf surface N contents

Leaf N (as NH_x-N) was not measured in the pre-field control group as leaf surfaces of all biomonitors were thoroughly washed prior to the distribution of plants between the various sites. Significant differences in leaf surface NH_x-N were measured between biomonitors groups exposed in the field. Biomonitors at Site 1a had the lowest surface N levels whilst the highest surface N levels were found on the biomonitors at Site 6a.

7.2.3.9   Total N contents

Biomonitors at Site 1a had similar (not statistically different) total N contents to the pre-field control group. This provided good evidence that the biomonitors were a closed system with the only unquantified pathway being surface-atmosphere exchange. The fate of the additional N supplied in the sand was investigated by comparing the N contents of the pre-field control group and the biomonitors at Site 1a. Approximately 75 % of the N, supplied in the sand was metabolised in the root organs, whilst 25 % was translocated to the stems and leaves.

No significant differences in total N contents were found between the pre-field control group and the biomonitors at Sites 1a and 6a. A significant increase in total N content was measured between the biomonitors exposed at Site 5a and both the pre-field control and the biomonitors at Site 1a. This demonstrated that NH_3 deposition had occurred at Site 5a. The N contents of biomonitors at both the downwind sites were not significantly different.

7.2.3.10   Estimation of a deposition velocity

Time averaged deposition fluxes were calculated for each of the biomonitor groups exposed in the field from the ground area of the pots, the experiment duration and the difference between the recovered N and the pre-field control. A time-averaged deposition velocity was calculated using Equation 1.4. However, as the deposition velocity relates to dry deposition, a correction was required to account for wet deposition to the biomonitors. Some uncertainly exists in the literature over the contribution of wet deposition to net local deposition fluxes, as discussed in Chapter 1, Section 1.4.3. Consequently, fluxes were

calculated both without wet deposition (following the recommendation in Jensen and Asman, 1995) and with wet deposition (using the experimental results of Couling, 1997).

Couling (1997) measured wet deposition around the SRI Structures Building for a similar emission rate of NH_3 to that used in this study. Rainwater concentrations of 3 µg NH_3-N ml^{-1} and 8 µg NH_3-N ml^{-1} were measured 15 m downwind at the plume centreline. The average of these two measurements (5.5 µg NH_3-N ml^{-1}) was used to estimate the rainwater concentration for comparison with these measurements. Wet deposition fluxes were calculated using the rainfall distribution shown in Table 7.2. Results, shown in Table 7.4, demonstrate that the best estimate of the deposition velocity for the SRI Structures Building study was 21 mm s^{-1}, based on the deposition flux calculated at Site 5a. Only a small contribution of wet deposition to the bulk deposition flux was estimated at this site.

Site	χ_{NH3-N} (µg m^{-3})	F_{NH3-N} (Bulk) (ng m^{-2} s^{-1})	F_{NH3-N} (Wet) (ng m^{-2} s^{-1})	F_{NH3-N} (Dry) (ng m^{-2} s^{-1})	V_d (Bulk) (mm s^{-1})	V_d (Dry) (mm s^{-1})
5a	29	610 (S)	10	600 (S)	21 (S)	21 (S)
6a	20	320 (NS)	70	250 (NS)	16 (NS)	13 (NS)

Table 7.4:   Air concentrations, deposition fluxes and deposition velocities calculated at sites downwind of the SRI Structures Building. Wet deposition fluxes were estimated from the data in Couling (1997). NS: Fluxes were not significantly different from zero, S: Fluxes were significantly different from zero ($P<0.05$).

7.2.4   Calculation of a local deposition budget for the SRI study

The deposition velocity, estimated above, was used as input to the UK-ADMS atmospheric dispersion model to determine the NH_3 deposition flux field around the building. Wet deposition was included in the model using the washout co-efficient method discussed in Chapter 3, Section 3.2.1.2 and the parameterisation of Jensen and Asman (1995) discussed in Chapter 1, Section 1.4.3. Results are presented in graphical form in Figure 7.7.

The mass budget for the building was also evaluated from the cumulative emission and the deposition around the site. Results, shown in Table 7.5, demonstrate that approximately 0.6 kg of NH_3-N was deposited over a 200 m x 200 m area around the SRI Structures Building. This represented a 2 % reduction in the quantity of NH_3 emitted from the site.

	Emitted	Wet deposition	Dry deposition	Bulk deposition	% Locally deposited
ng NH$_3$-N m^{-2} s^{-1}	-	0.7	97.6	98	-
g NH$_3$-N	30400	4.2	570	574	2

Table 7.5: NH$_3$-N budget for the SRI Structures Building calculated for emissions between 21 - 31 August 1996. Fluxes are shown as an average flux over a 200 m x 200 m grid around the building.

Wet deposition (ng NH$_3$-N m^{-2} s^{-1})   **Dry deposition (µg NH$_3$-N m^{-2} s^{-1})**

Bulk deposition (µg NH$_3$-N m^{-2} s^{-1})
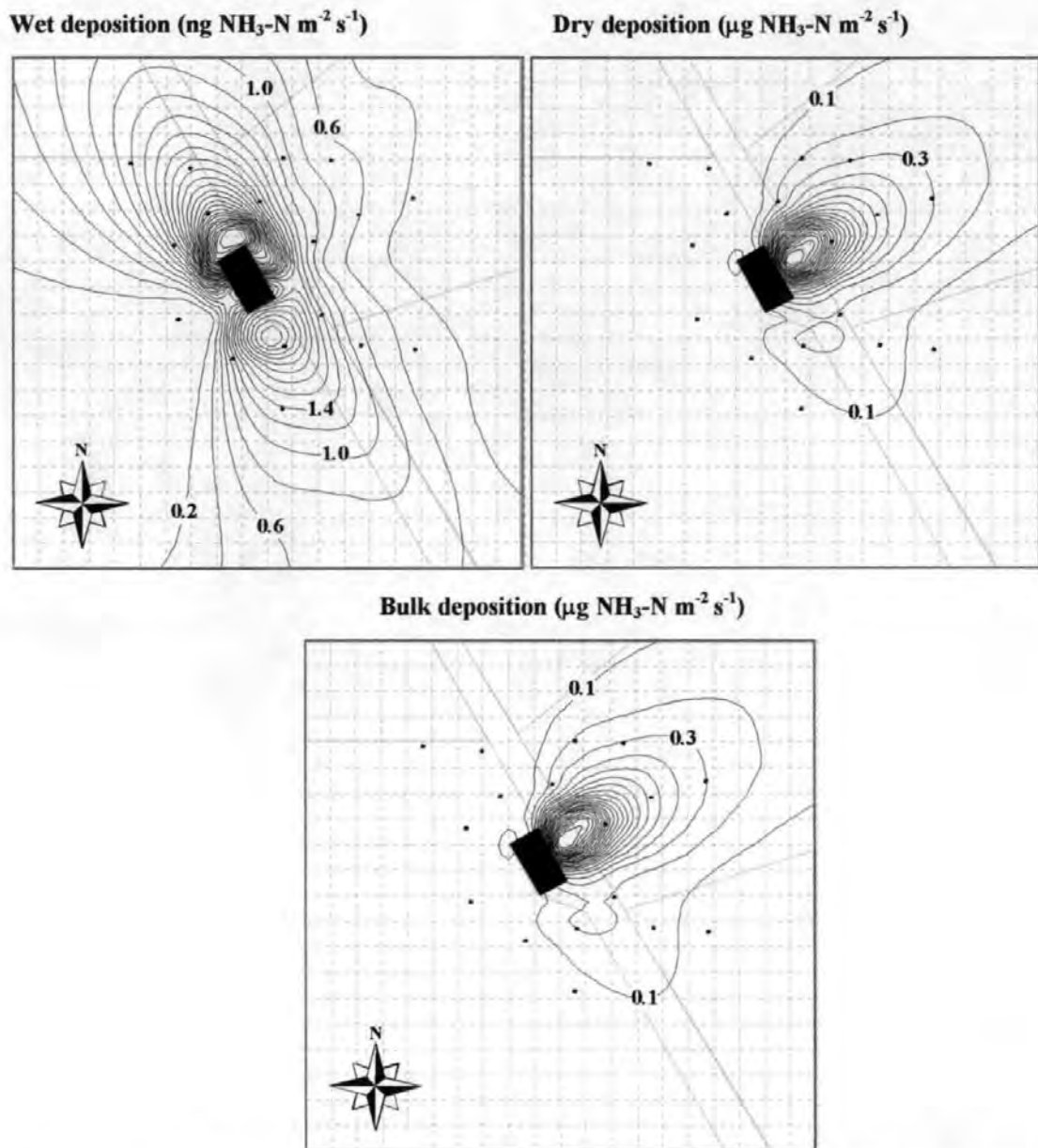
Figure 7.7: Contour plots of modelled wet, dry and bulk (wet + dry) deposition fluxes around the SRI Structures Building between 21 - 31 August 1996. Maps are shown to scale of 1:2750. 0.1 µg NH$_3$-N m^{-2} s^{-1} = 31.56 kg NH$_3$-N ha^{-1} a^{-1}.

7.3   TOWN BARTON FARM EXPERIMENT

Experiments were conducted at Town Barton Farm between 18 March - 16 April 1997. Full details of the experiments are given in Chapter 6. These experiments were designed to

replicate those conducted at the SRI Structured Building, providing data on the emission, dispersion and local deposition of NH₃ at an operational farm in contrast to the controlled research building previously used.

7.3.1   Meteorological conditions

Meteorological conditions measured during the Town Barton Farm experiment are shown in Table 7.6. The experimental period was mostly dry, with only 2.8 mm of rainfall, 50 % of which occurred during Run AC2. The wind direction was very variable during Runs AC1, AC2 and the long-term biomonitor experiment (BIOM). An analysis of the wind direction rose for each run is shown in Table 7.7. Winds were predominantly from the north-west for all the experimental runs, though a significant period of easterly winds occurred during Run AC2.

Run	Temperature (°C)			Relative humidity (%)			Wind speed {3 m} (m s⁻¹)			Wind direction (°)		Precipitation (mm)
	Mean	Max	Min	Mean	Max	Min	Mean	Max	Min	Mean	σ₀	Total
AC1	8.9	15.2	5.3	81	100	45	1.7	3.4	0.4	258	82	0.0
AC2	8.1	10.5	6.2	96	100	83	2.5	6.8	0.1	229	87	1.4
AC3	5.9	11.8	0.1	87	100	55	3.4	8.0	0.7	284	57	0.0
AC4	10.2	14.4	6.5	96	100	74	3.7	8.3	1.4	289	12	0.0
BIOM	8.4	20.1	-3.0	82	100	28	2.7	8.7	0.1	233	86	2.8

Table 7.6:   Meteorological conditions measured during the experiments at Town Barton Farm. AC air concentration measurements, BIOM: biomonitor flux measurements. NH₃ emissions from the building were measured during Runs AC3 and AC4.

Run	Mid-point of 30° wind sector (degrees from north)											
	30	60	90	120	150	180	210	240	270	300	330	360
AC1	0.0	0.0	0.0	16.7	8.3	0.0	0.0	4.2	8.3	37.5	20.8	4.2
AC2	0.0	3.9	19.2	0.0	3.9	0.0	7.7	3.8	11.5	50.0	0.0	0.0
AC3	0.0	0.0	0.0	3.9	0.0	3.9	3.9	15.4	3.9	30.8	38.5	0.0
AC4	0.0	0.0	0.0	0.0	0.0	0.0	0.0	0.0	44.4	51.9	3.7	0.0
BIOM	0.3	1.6	6.1	12.6	10.7	2.9	5.1	6.4	12.6	27.0	11.6	3.3

Table 7.7:   Percentage distribution of wind directions during the experiments at Town Barton Farm.

7.3.2   NH₃ emissions

Ferm tube passive flux samplers were used to measure the emission of NH₃ from the building during Runs AC3 and AC4. Fluxes of NH₃ were measured from each of the main

202

ventilation points of the building. The total emission was calculated from the algebraic sum of the emission from each of these points. The total emission from the building and the contribution of each of the ventilation points are shown in Table 7.8.

The overall emissions flux from the building was dominated by the contributions from the roof, the south-east facing wall and the north-east facing wall. Such a pattern of emission flux was likely to be due to the predominantly north westerly winds that occurred during the experiments. Ventilation points on the roof, particularly the lateral vents, were found to be a strong source of NH_3 emission, contributing to 42 % of the total flux measured during Runs AC3 and AC4.

		Run AC3		Run AC4	
		g NH_3-N day^{-1}	%	g NH_3-N day^{-1}	%
South-east facing wall	Yorkshire board	400	12	513	12
	Gap	443	13	598	14
North-west facing wall	Yorkshire board	33	1	115	3
	Gap	39	1	149	4
South-west facing wall	Door gaps	214	6	-11	0
North-east facing wall	Door gaps	856	25	1122	26
Dairy	Vents	38	1	26	1
Roof	Main axis	207	6	150	4
	Vents	1178	35	1588	37
Second building	Openings	0	0	0	0
	Total	3408	100	4250	100

Table 7.8: Emission of NH_3 from Town Barton Farm. The contribution of each of the ventilation points to the total emission flux is shown.

The total emission of NH_3 from the building was 25 % higher during Run AC4 than during Run AC3. This could have been due to the higher mean air temperature and wind speed which have been found to influence the volatilisation rate of NH_3, as discussed in Chapter 1, Sections 1.2.3.1 and 1.2.3.2. No detectable NH_3 emission was measured from the second farm building on the site used to house livestock bedded on straw.

In addition to the sources mentioned in Table 7.8, a further source of NH_3, present at Town Barton Farm, was the slurry lagoon. Emission fluxes from the slurry lagoon were estimated using a similar model back-calculation method to that discussed in McInnes *et al.* (1985). Fluxes were calculated, using Equation 3.15, from air concentration measurements at Site 5b and dispersion factors predicted with UK-ADMS. Data from Run AC3 were not

analysed as the wind direction distribution, shown in Table 7.7, suggested that the air concentration samples at Site 5b would have been significantly influenced by the dispersing plume of NH₃ from the building. Measured vertical NH₃ concentration profiles at Site 5b and the predicted dispersion factors are shown in Figure 7.8.
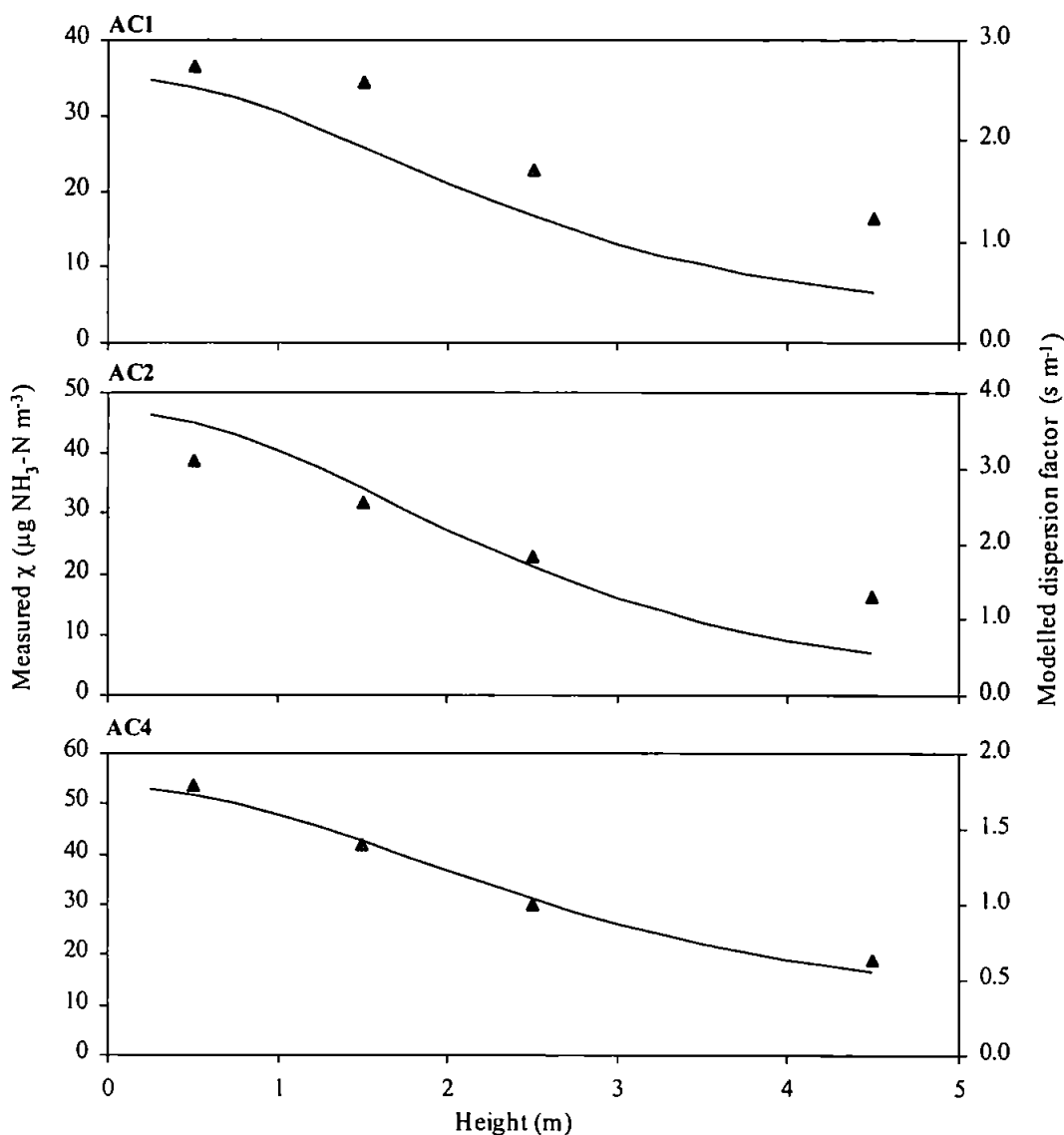
Figure 7.8:   Measured NH₃ concentrations (▲) and modelled (UK-ADMS) dispersion factors (—) at Site 5b for Runs AC1, AC2, and AC4.

The dispersion factor profile, predicted by UK-ADMS, agreed well with the shape of the measured NH₃ concentration profile, given the complexities of the terrain around the slurry lagoon. The emission fluxes for each run were calculated by dividing the measured air concentrations by the relevant dispersion factors, according to Equation 3.15. Mean fluxes and 95 % confidence limits were calculated assuming that each air concentration measurement and dispersion factor prediction produced an independent flux estimate. The

predicted NH$_3$ emission fluxes from the slurry lagoon were 16.8 +/- 2.3 µg m^{-2} s^{-1}, 12.0 +/- 1.6 µg m^{-2} s^{-1} and 29.9 +/- 1.2 µg m^{-2} s^{-1} for Runs AC1, AC2 and AC4.

7.3.3   NH$_3$ dispersion

A similar experimental design to that used at the SRI Structures Building was implemented at Town Barton Farm to measure the dispersion of NH$_3$ released to the atmosphere. The NH$_3$ concentration field around the building was measured, during Runs AC1 - AC4, using a radial arrangement of 4.5 m high sampling masts and a portable 11.5 m mast. These measurements were analysed to determine the vertical and horizontal NH$_3$ concentration distributions around the building. Again, the UK-ADMS atmospheric dispersion model predictions were compared with the field measurements.

7.3.3.1   Horizontal distribution of NH$_3$ concentrations

Concentration contour maps were calculated by interpolating measurements at 0.5 m using a similar method to that described in Section 7.2.2.1. The resulting concentration contour maps are shown in Figure 7.9. The measurements demonstrated that NH$_3$ plumes from the building and the slurry lagoon dispersed over the fields to the south-east of the farm, as would be expected from the predominant north westerly wind directions. Westerly winds were measured in Run AC4, and resulted in high concentrations to the east of the building. Maximum concentrations (up to 100 µg NH$_3$-N m^{-3}) were measured close to the building, decreasing to between 10 – 15 µg NH$_3$-N m^{-3} at 100 m from the building. Background concentrations were reasonably constant at around 4 µg NH$_3$-N m^{-3} for each run.

The UK-ADMS model was run using the buildings dimensions, meteorological data from the on site meteorological station and measured NH$_3$ emission data as described in Section 7.3.2. Emissions of NH$_3$ from the main building during Runs AC1 and AC2 were estimated from the average of the measurements during Runs AC3 and AC4. Likewise, the emission flux from the slurry lagoon during Run AC3 was estimated from the average of the fluxes measured during the other runs. Modelled ground level concentration contour maps are shown in Figure 7.10.

A reasonable agreement was found between the measured and modelled spatial concentration distributions, particularly for Runs AC1, AC3 and AC4. However, much higher concentrations were predicted to the north-east of the building during Run AC2 than were measured, though the predominant advection of the plume over the fields to the

south-east of the building was correctly predicted. The poorer agreement between the model and the measurements for Run AC2 was likely to be due to the substantial duration of calm conditions and very variable wind directions measured.
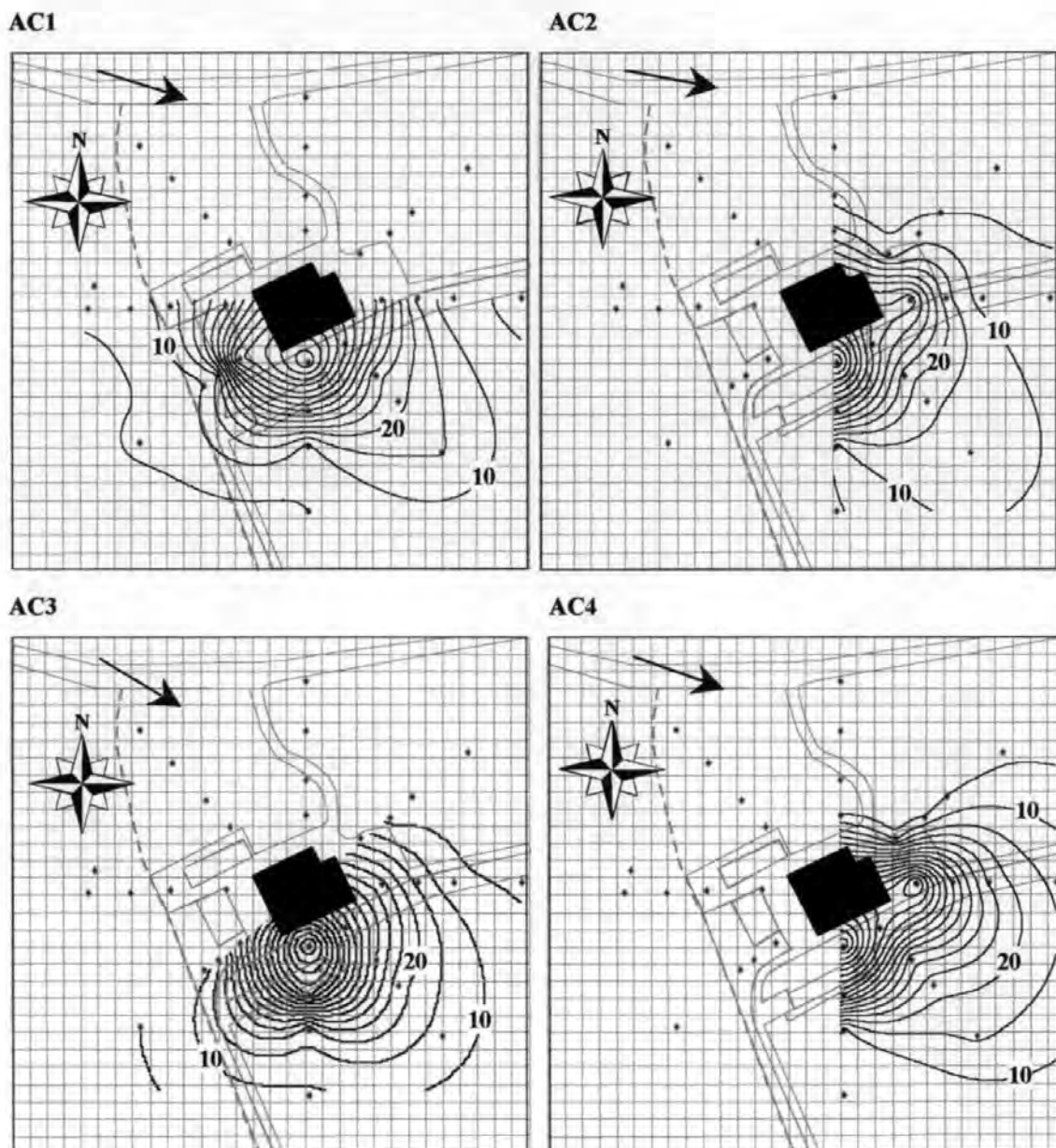
Figure 7.9:   Contour plots of measured ground level air concentrations (in µg NH₃-N m⁻³) around Town Barton Farm. Results are shown to scale of 1:4000. Arrows show the median wind direction.

A statistical comparison of the UK-ADMS models predictions of near-ground level air concentrations with the field measurements over the area influenced by the plume was also conducted. This comparison is shown in Figure 7.11. Overall, 85 % of the model predictions were found to be within a factor of 2.0 of the field measurements. A linear regression analysis was also conducted showing a significant gradient term (0.71 +/- 0.19)

and a significant y-intercept (7.92 +/- 7.10 µg NH_3-N m^{-3}). The R^2 value for the regression fit indicated that 55 % of the variation in the measurements was predicted by the model.

AC1   **AC2**

AC3   **AC4**
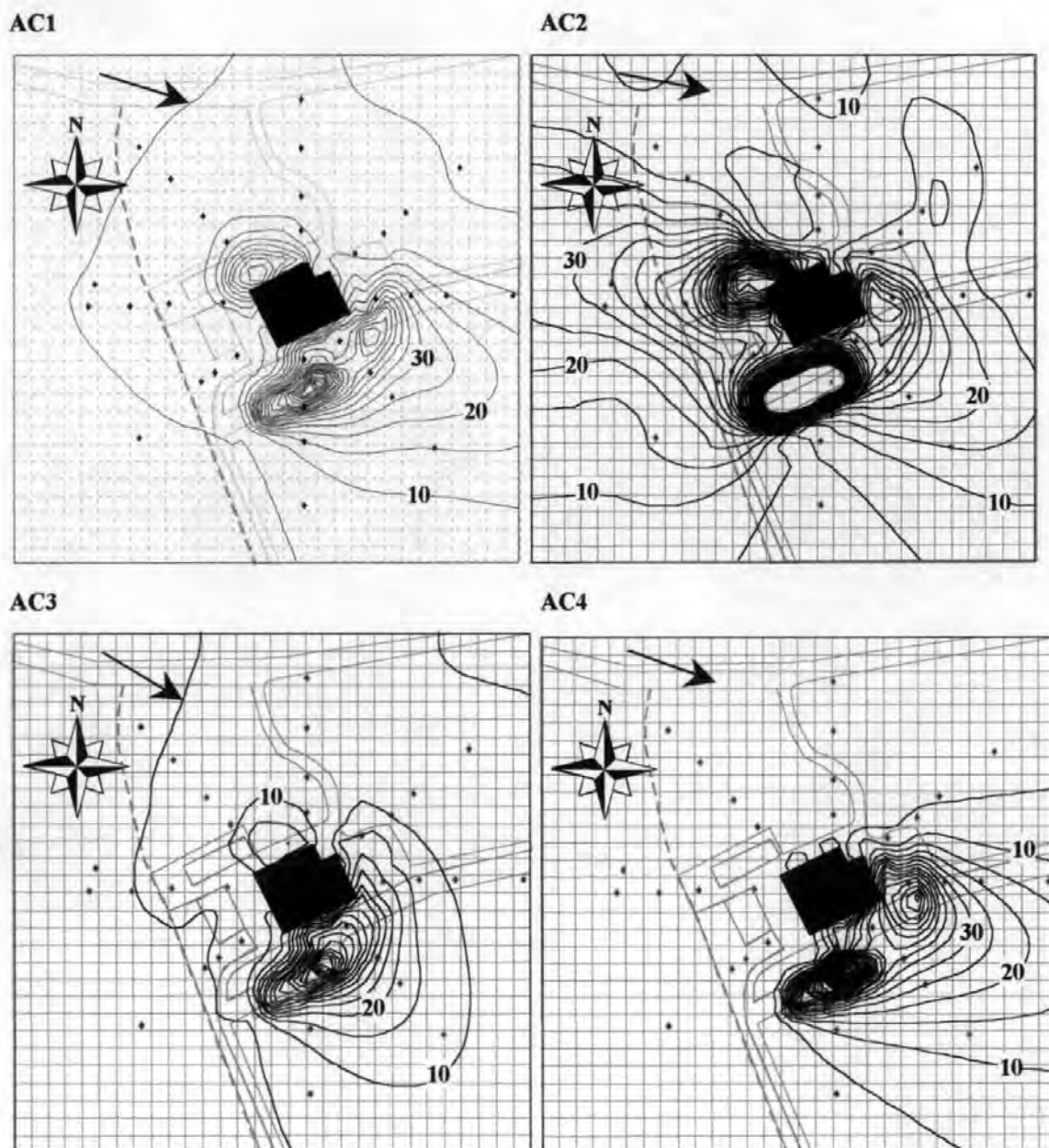
Figure 7.10:   Contour plots of ground level air concentrations (in µg NH_3-N m^{-3}) around Town Barton Farm modelled using UK-ADMS. Results are shown to scale of 1:4000. Arrows show the median wind direction.

7.3.3.2   Vertical distribution of NH₃ concentrations

The modelled and measured vertical distributions of NH_3 concentrations were compared at the centreline of the plume. The plume centreline was estimated to be to the south-east of the building for Runs AC1, AC2 and AC3 and to the east of the building for Run AC4. Results are presented in Figure 7.12.
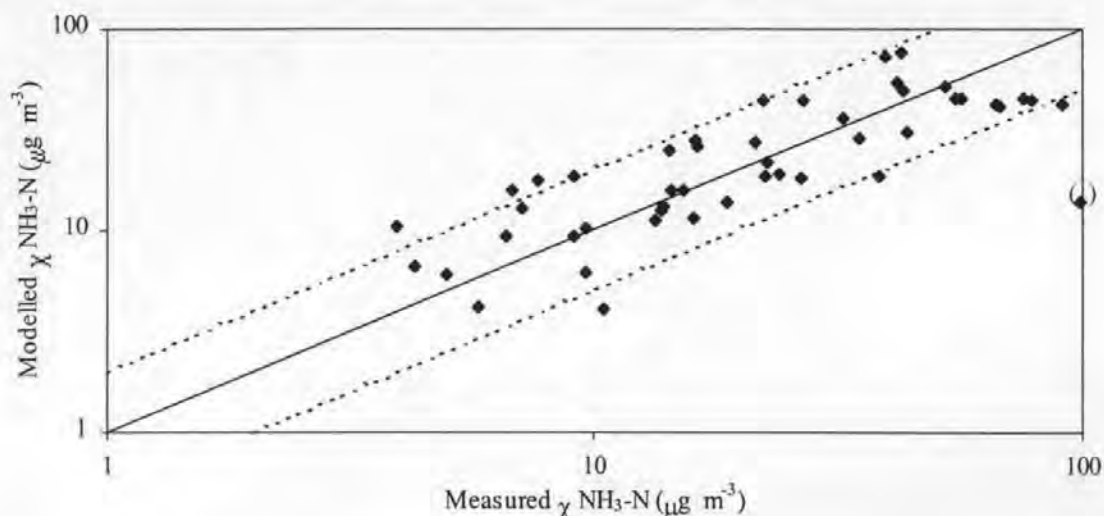
Figure 7.11: Comparison between measured and modelled ground level NH_3 concentrations around Town Barton Farm. Data point in parenthesis was excluded from the statistical analysis.

Both modelled and measured air concentrations showed a relatively uniform vertical distribution. This was likely to be due to the rapid mixing caused by turbulence generated by the building and due to the large number of emission points on the building. The uniform distribution of concentrations with height was well illustrated by the measurements and model predictions at the portable mast sites. Concentrations in excess of background levels by a factor of four were predicted at the highest sampling position (11.5 m) during Runs AC1 and AC2, whilst concentrations at 11.5 m were nearly an order of magnitude higher that background during Runs AC3 and AC4.

More pronounced vertical concentration distributions were measured close to the building, particularly during Runs AC3 and AC4, with maxima at the top and middle of the profiles respectively. The UK-ADMS model was unable to match the vertical concentration distributions at these points, though the magnitude of the predicted concentrations was reasonably close. In general, the UK-ADMS model predicted the magnitude of concentrations closely for Runs AC1 and AC2 and tended to underpredict concentrations, on the centreline of the plume, close to the building for Runs AC3 and AC4.
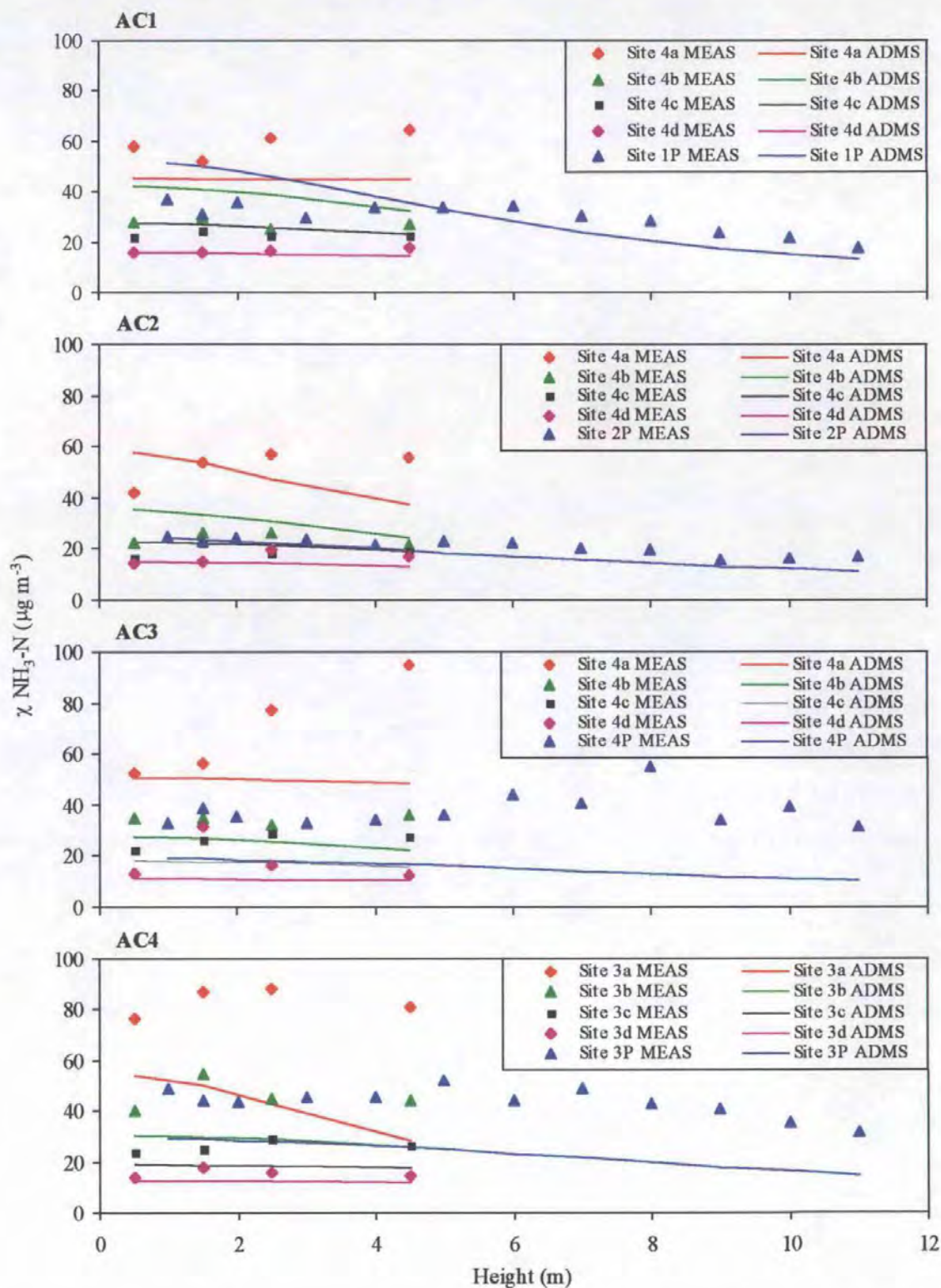
Figure 7.12: Vertical concentration profiles measured (MEAS) and modelled (ADMS) at the centreline of the NH₃ plume downwind of Town Barton Farm.

7.3.4 NH₃ deposition

The deposition of NH₃ around Town Barton Farm was estimated by exposing biomonitors at eight sites around the farm. Site locations are shown in Figure 6.7. Willems badge passive diffusion samplers were co-located with each of the biomonitor sampling sites,

enabling the calculation of time averaged deposition velocities. Ten biomonitors were exposed at each site. A further ten biomonitors, dosed with an additional 20 mg NO_3^--N were located at Sites B2, B3 and B4. A pre-field control group of 10 plants was analysed prior to the start of the experiment.

Plants were analysed, in a similar manner to that described in Section 7.2.3, to determine the N contents of four fractions: above ground biomass, below ground biomass, sand, and leaf surfaces. The results of the biomonitor analysis, and air concentration measurements are presented in Table 7.9. Results were statistically analysed using a one-way ANOVA.

Site	χ NH₃-N	Above ground material			Below ground material			Sand	Leaf	Total
	(μg m⁻³)	Mass	N	N	Mass	N	N	N	N	N
		(g)	(%)	(mg)	(g)	(%)	(mg)	(mg)	(mg)	(mg)
B1	4.07	$7.39_{a,b}$	$1.53_{a,c}$	$112.64_{a,c}$	$8.29_{a,b}$	$0.76_{a,b,e}$	$62.26_{a,b,c}$	$0.31_{a,f}$	$0.05_{a,e}$	$175.25_{a,c}$
B2	3.02	$6.92_{a,h}$	$1.60_{a,b,c,g}$	$109.99_{a,c}$	9.58_{a}	$0.74_{a,b,c}$	$68.46_{a,b}$	$0.19_{a,b,c,d,e,f}$	0.12_{b}	178.76_{a}
B2*	3.02	$7.81_{b,d}$	$1.66_{b,d,g}$	129.54_{b}	8.81_{a}	$0.82_{a,c,d}$	72.45_{a}	$0.27_{a,b,f}$	$0.06_{e,f,g}$	202.32_{b}
B3	24.38	7.17_{a}	$1.56_{c,e}$	$111.84_{a,c}$	$8.91_{a,b,c}$	$0.79_{a,b,c}$	$68.46_{a,b,d}$	$0.13_{b,c,g}$	0.11_{b}	180.55_{a}
B3*	24.38	$8.24_{c,e}$	$1.65_{b,g}$	$135.51_{b,d}$	$7.67_{a,b,c}$	$0.81_{a,b,c}$	$60.32_{b,c}$	$0.16_{a,b,c,d,g}$	0.13_{b}	196.11_{b}
B4	30.49	$7.57_{a,b,f}$	$1.58_{b,c}$	119.22_{c}	$8.53_{a,b}$	0.71_{b}	$60.01_{b,c}$	$0.08_{c,d,e}$	0.16_{d}	$179.48_{a,c}$
B4*	30.49	$8.21_{d,e,f}$	$1.74_{d,f}$	142.50_{d}	$7.80_{b,c}$	$0.74_{a,b}$	57.55_{c}	$0.12_{c,g}$	0.07_{c}	200.24_{b}
B5	40.00	$6.96_{a,h}$	$1.65_{b,e,f,h}$	$113.58_{a,c}$	$7.38_{b,c}$	$0.85_{c,d}$	$62.88_{a,b,c}$	$0.11_{c,d,e,g}$	$0.06_{c,g}$	$176.64_{a,c}$
B6	8.62	6.21_{g}	$1.69_{g,f}$	$104.58_{e,f}$	$6.77_{c,d}$	0.90_{d}	$61.52_{a,b,c}$	$0.06_{d,e}$	$0.05_{e,f,h}$	166.21_{c}
B7	3.06	$7.07_{a,h}$	1.54_{c}	$108.22_{a,c,f}$	$7.12_{b,c}$	$0.84_{c,d,e}$	$59.57_{c,d}$	0.05_{c}	0.12_{b}	167.97_{c}
B8	5.74	$6.57_{h,g}$	$1.56_{c,h}$	101.80_{f}	$8.30_{a,b,c}$	$0.87_{c,d}$	$70.00_{a,b,d}$	$0.21_{f,g}$	$0.06_{g,h}$	$172.07_{a,c}$
Pre	-	4.94_{i}	2.27_{i}	$111.37_{a,c,e}$	5.90_{d}	1.09_{f}	$61.85_{b,c}$	1.63_{h}	0.16_{d}	$175.01_{a,c}$

Table 7.9: Results of the biomonitor experiments to determine NH₃ deposition around Town Barton Farm. Results were statistically analysed using a one-way ANOVA to determine the effects of each treatment. Numbers with the same subscripted letter are not significantly different at the P<0.05 level. * Plants dosed with an additional 20 mg NO_3^--N.

7.3.4.1 Above ground dry mass

Biomonitors exposed in the field had statistically higher mean above ground dry mass than the pre-field control group. The sub-groups at Sites B2 and B3 which were dosed with an additional 20 mg NO_3^--N had significantly higher mean above ground dry mass than biomonitors at the same site that received the standard N dose. However, biomonitors at Site B4 that received the additional 20 mg N did not have significantly different above ground dry mass than the standard dosed biomonitors. The interpretation of the results for

the standard dosed plants exposed in the field was more uncertain, with significant differences between some individual groups but no clear explainable trends.

7.3.4.2 Above ground percentage N

The mean percentage N concentration in the above ground plant material of the pre-field control group was significantly higher than that measured in any of the biomonitor groups exposed in the field. No differences in percentage N levels were found between the standard dosed biomonitors and those at Site B2 that received the additional N dose, though significantly higher percentage N levels were measured in the biomonitors that received the additional N dose at sites B3 and B4. Site specific differences between the standard dosed biomonitors were difficult to interpret, with significant differences between some individual groups, though no clear trends.

7.3.4.3 Above ground N contents

Biomonitors receiving the additional 20 mg N dose had higher above ground N contents than either the pre-field control group or the biomonitors, at the same site, that received the standard dose. None of the standard dosed biomonitors had statistically higher (at the 95 % confidence limit) N contents than the biomonitors in the pre-field control group, though the increase in N measured at Site B4 was statistically significant at the 90 % confidence limit. Biomonitors at Site B8 had a significantly lower mean N content than the pre-field control group, indicating that either field losses occurred at this site or that N had been translocated from the above ground plant material.

7.3.4.4 Below ground dry mass

Below ground dry mass measured at all sites, except Site 6, was significantly higher than that measured in the pre-field control group, demonstrating that growth of the plant root organs had occurred during the experiment. No statistical differences in below ground dry mass were found between biomonitors dosed with additional N and the respective standard dosed biomonitors.

7.3.4.5 Below ground percentage N

Below ground percentage N levels were significantly higher in the pre-field control group than any of the biomonitor groups exposed in the field. No significant differences were found between biomonitors dosed with the additional N and the respective standard dosed biomonitors.

7.3.4.6   Below ground N contents

Only the biomonitors at Site B2 that received an additional N dose had a statistically different mean below ground N content than the pre-field control group. Below ground N contents were reasonably consistent between the biomonitors exposed in the field, with no detectable effects of the additional N dosage.

7.3.4.7   Sand N contents

All the groups of biomonitors exposed in the field had lower sand N contents than the pre-field control group. No differences in sand N contents were observed between the biomonitors which were dosed with the additional 20 mg N and the respective biomonitors which received the standard N dose. This indicated that the additional N dose had been metabolised. The highest sand N contents were found at Site B1 (0.31 mg) and the lowest sand N contents were found at Site B7 (0.05 mg).

7.3.4.8   Leaf surface N contents

High leaf surface N contents were measured on the pre-field control group despite the washing of the leaves several hours before the plants were harvested. All the biomonitors measured in the field, with the exception of those at Site B4 that received the standard N dose, had statistically lower surface N contents than the pre-field control group. Significantly lower surface N contents were measured in the biomonitors at Site B2 which were dosed with additional N than those receiving the standard dose. Whilst, no significant differences in surface N contents were found between biomonitors at Site B3 dosed with additional N and those receiving the standard dose. Surface N contents were significantly lower at Site B4 for the biomonitors receiving the additional N dose than those receiving the standard N dose.

7.3.4.9   Total N contents

Significant differences were found between all the biomonitors that received the additional N dose and the pre-field control group. This demonstrated that the analysis had correctly identified the "spiked" biomonitors. Biomonitors that received the additional N dose also had significantly higher mean total N contents than those that received the standard dose at the same site. The recapture of the N spike was calculated from the difference in total N between biomonitors that received the standard and additional N doses. Recaptures of 23.6 mg N, 15.6 mg N and 20.8 mg N were estimated from the analysis of biomonitors at Sites B2, B3 and B4 respectively.

The capture-recapture data was also used to investigate the partitioning of N in the biomonitors by comparing the N contents of the various plant fractions between the standard dosed biomonitors and those receiving the additional dose. Biomonitors at all the sites showed that the N applied to the roots as NO_3^--N was translocated to the above ground organs. Despite the generally high sensitivity of the biomonitor experiment, as demonstrated by the capture-recapture experiment, none of the standard dosed biomonitors exposed in the field had significantly different total N contents than the pre-field control group. This suggests that deposition of NH_3 to the biomonitors in the field occurred at a rate below the detection limit of the method (calculated as being approximately 10 mg N or 0.33 µg N m^{-2} s^{-1}).

7.3.4.10 Regression analyses

A series of regression analyses were performed in order to investigate the dependence of the various parameters measured in the biomonitor experiments (for the standard nutrient dosage) on the measured NH_3 air concentrations. Analyses of variance were performed to investigate whether the gradients of the regression lines were significantly different from zero and T-tests were performed to investigate whether the y-intercepts of the regression lines were significantly different from zero, results are shown in Table 7.10.

	Above Ground Material			Below Ground Material			Sand	Leaf	Total
	Mass (g)	N (%)	N (mg)	Mass (g)	N (%)	N (mg)	N(mg)	N(mg)	N (mg)
M	0.01	0.00	0.24	0.00	0.00	-0.05	>0.01	>0.01	0.19
C	6.84	1.57	106.68	8.16	0.81	64.85	0.18	0.08	171.79
R²	0.10	0.11	0.41	0.00	0.01	0.03	0.13	0.05	0.26
P {M}	0.44	0.42	0.09	0.90	0.81	0.70	0.38	0.59	0.19
P {C}	>0.01	>0.01	>0.01	>0.01	>0.01	>0.01	>0.01	>0.01	>0.01

Table 7.10: Regression analysis of the trends in the parameters measured in the biomonitor experiments with air concentration. *M*: gradient, *C*: y-Intercept, R^2: correlation statistic squared, *P*: probability.

The analyses in Table 7.10 show that none of the variables measured in the biomonitor experiments correlated with the NH_3 air concentrations at the 95 % confidence level. However the above ground N contents of the biomonitors did correlate with the measured NH_3 concentrations at the 90 % confidence level, and the total N correlated with the NH_3 concentrations at the 80 % confidence level.

7.3.4.11   Estimation of the short-range deposition velocity for Town Barton Farm

The above regression analysis shows that the below ground N contents were unaffected by atmospheric NH_3. Therefore, the below ground N contents could be removed from the analysis, so removing a substantial portion of the experimental uncertainty.

An estimation of the deposition velocity for the Town Barton Farm experiment was made from the rate of change of above ground N with air concentration. The numerator of the gradient was converted from an expression of mass (mg) to an expression of flux (μg m^{-2} s^{-1}) in order to calculate a deposition velocity in m s^{-1}. This calculation gave an estimate of the time averaged deposition velocity of 0.008 m s^{-1} which compares with an identical estimate of deposition velocity (rounded to three decimal places) determined from the increase in above ground N at Site B4.

7.3.5   Estimation of a local deposition budget for Town Barton Farm

The UK-ADMS model, parameterised with a dry deposition velocity of 0.008 m s^{-1}, was used to calculate the spatial pattern of NH_3 deposition around Town Barton Farm during the period 18 March to 16 April 1997. As only 2.8 mm of rainfall occurred during this period no account of wet deposition was made. A contour map showing the spatial pattern of deposition around Town Barton Farm is presented in Figure 7.13.

The deposition of NH_3, shown in Figure 7.13, occurred predominantly over the fields to the east and south-east of the building, as would be expected from the predominant north westerly winds. However, a peak in NH_3 deposition (0.4 μg NH_3-N m^{-2} s^{-1}) was found close to the north-west facing side of the building. This was likely to be due to the higher frequency of low wind speed conditions associated with winds from 105 - 165° than from 285 - 345°. Low wind speeds often result in reduced dispersion and would cause an increased proportion of the released material to be entrained in the cavity wake close to the building.

An NH_3 budget for Town Barton Farm was calculated from the measured emission estimate, presented in Section 7.3.2, and the deposition estimates discussed above. The results are presented in Table 7.11. The deposition budget shows that of the 132 kg NH_3-N released during the experiment, about 2 % was estimated to be locally deposited to a 300 m x 300 m grid around the farm.
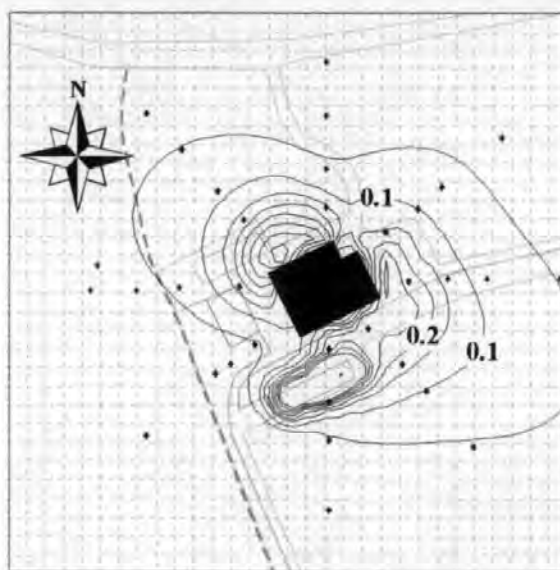
Figure 7.13: Contour map of deposition flux (μg NH$_3$-N m^{-2} s^{-1}) around Town Barton Farm. Contours are shown with a resolution of 0.05 μg NH$_3$-N m^{-2} s^{-1}. Map shown to a scale of 1:4000. 0.1 μg NH$_3$-N m^{-2} s^{-1} = 31.56 kg NH$_3$-N ha^{-1} a^{-1}.

	Emitted	Dry deposition	% Local deposited
ng NH$_3$-N m^{-2} s^{-1}	-	52	-
kg NH$_3$-N	132	2.9	2

Table 7.11: NH$_3$-N budget for Town Barton Farm calculated for emissions between 18 March and 16 April 1997. Fluxes were averaged over a 300 m x 300 m grid around the farm. Wet deposition was not considered in the calculations due to the low level of precipitation measured in the field.

7.4 SUMMARY AND DISCUSSION

7.4.1 NH$_3$ emissions

7.4.1.1 Estimated emission factors for the farm building and slurry lagoon

Mean emission factors of 340 μg NH$_3$-N s^{-1} (500 kg liveweight)$^{-1}$ and 74 μg NH$_3$-N s^{-1} (500 kg liveweight)$^{-1}$ were calculated for the naturally ventilated building and for the slurry lagoon at Town Barton Farm respectively. These emission factors were derived from the stocking rate at the farm (120 animals) and assuming each animal has a liveweight of 550 kg (Pain *et al.*, 1998).

The emission factors derived from the Town Barton Farm study were compared with data from the literature, as shown in Table 7.12. The emission factor for housing was somewhat higher than the literature values although, given the likely experimental uncertainty, was concluded to agree well with the emission factors determined by Demmers *et al.* (1998)

and Sutton *et al.* (1995). Of the emission factors presented in Table 7.11, the factor determined by Phillips *et al.* (1998) appears to be something of an outlier, being considerably lower than the other values. A reasonable comparison (within 35 %) was also found between the emission factor estimated in Chapter 1, Section 1.2.3.2, from research conducted by Swierstra *et al.* (1995), for total housing and storage losses and those reported in this work.

Source	Emission factor	Reference
Winter housing	340µg NH₃-N s⁻¹ (500 kg liveweight)⁻¹	This study
Winter housing	300 µg NH₃-N s⁻¹ (500 kg liveweight)⁻¹	Demmers *et al.* (1998)
Winter housing	57 µg NH₃-N s⁻¹ (500 kg liveweight)⁻¹	Phillips *et al.* (1998)
Housing (from loss rates)	279 µg NH₃-N s⁻¹ (500 kg liveweight)⁻¹	Sutton *et al.* (1995)
Housing + storage	624 µg NH₃-N s⁻¹ (500 kg liveweight)⁻¹	Swierstra *et al.* (1995)
Slurry lagoon	74 µg NH₃-N s⁻¹ (500 kg liveweight)⁻¹ or 20 µg NH₃-N m⁻² s⁻¹	This study
Collecting yard	87 µg NH₃-N s⁻¹ (500 kg liveweight)⁻¹	Misselbrook *et al.* (1998)
Slurry tank (stirred)	51 µg NH₃-N m⁻² s⁻¹	Pain *et al.* (1998)
Slurry lagoon	24 µg NH₃-N m⁻² s⁻¹	
Slurry store (stirred)	51 µg NH₃-N m⁻² s⁻¹	Sommer *et al.* (1993a)
Slurry store (crust)	10 µg NH₃-N m⁻² s⁻¹	
<u>Digested slurry:</u> Uncovered store	105 µg NH₃-N m⁻² s⁻¹	Sommer (1997)
Straw covered store	8.6 µg NH₃-N m⁻² s⁻¹	
Clay pebble covered store	3.2 µg NH₃-N m⁻² s⁻¹	
Slurry store	79 µg NH₃-N s⁻¹ (500 kg liveweight)⁻¹	Sutton *et al.* (1995)

Table 7.12: Comparison of the emission factors determined from the Town Barton Farm experiment with literature values.

The emission factor for the slurry lagoon was found to be comparable with those reported in the literature, despite the wide range of literature values. The emission factor estimated by Pain *et al.* (1998) was 20 % higher than the estimate reported herein and the emission measurements by Sommer *et al.* (1993a) were a factor of two lower. Perhaps rather fortuitously, the estimate of slurry store emissions by Sutton *et al.* (1995) was within 10 % of the emission factor estimate reported herein. The good agreement between the results of this study and the literature values provides some reassurance that the model back-calculation method was reasonably robust. This study presented the first application of such a method for determining emissions from stored slurry.

7.4.1.2   Estimation of the annual NH₃ emission budget for Town Barton Farm

The net annual emission from the dairy/cowshed building at Town Barton Farm was estimated to be 1.1 t NH_3-N a^{-1}. This was calculated assuming the housing period extending for 180 days and using the reduction in emissions between winter and summer discussed in Phillips *et al.* (1998). Annual emissions of 0.31 t NH_3-N a^{-1} from the slurry lagoon were calculated using the emission factor determined above and assuming that the lagoon emits NH_3 continuously throughout the year. Losses from grazing and slurry spreading at Town Barton Farm were not measured. However, emissions through these pathways were estimated from the emission factors discussed in Pain *et al.* (1998) of 6.0 g NH_3-N animal^{-1} day^{-1} for grazing animals and 8.4 kg NH_3-N animal^{-1} a^{-1} for slurry spreading emissions. The total NH_3 emission from the farm was estimated to be 2.5 t NH_3-N a^{-1}. The distribution of the total emission between the various pathways is shown in Figure 7.14.
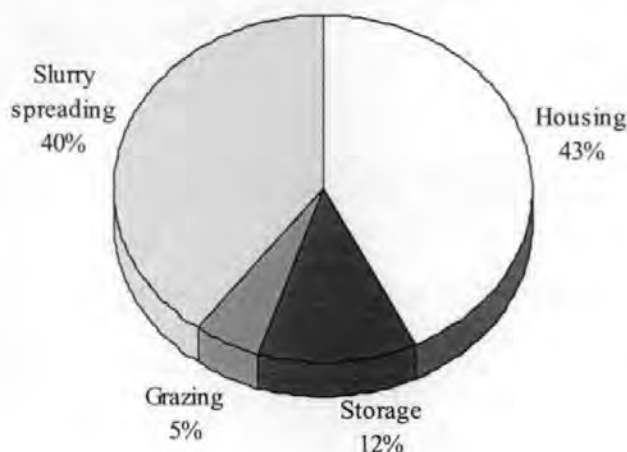
Figure 7.14:   Distribution of the net NH_3 emissions from Town Barton Farm between the four main loss pathways. Data on slurry spreading emissions and grazing emissions were estimated from data in Pain *et al.* (1998).

7.4.2   NH₃ dispersion

One of the main experimental aims was to determine the dispersion of NH_3 around a naturally ventilated farm building. The UK-ADMS model was used to predict the dispersion of NH_3 using the generalised building effects module to include the flow distortions, turbulence and wake effects generated by the building. The performance of the model was assessed using the measured air concentrations.

Results from both the Town Barton Farm study and the SRI Structures Building study showed that the UK-ADMS model predictions were typically within a factor of two of the

field measurements. The UK-ADMS predictions were slightly more precise for the Town Barton Farm study than for the SRI Structures Building study, which was likely to be due to the uncertainties in the distribution of emissions points in the SRI Structures Building study. The UK-ADMS model was generally in good agreement with the field measurements over the spatial and vertical distributions of NH_3 concentrations. Both studies showed that the comparison between the UK-ADMS model predictions and the measurements improved with distance from the source, and that the model tended to predict more uniform concentration profiles in the cavity wake than were measured.

Similar estimates of the uncertainty in the predictions of the UK-ADMS buildings effects module have been found by Robins *et al.* (1997). They evaluated the buildings effects module against wind tunnel data and field scale measurements, finding the agreement between the wind tunnel dataset and the model predictions was typically within a factor of two. A slightly poorer comparison was found between the model predictions and field measurement data.

Data presented in Hill (1997) on the comparison between CFD modelling and short term measurements of dispersion from a poultry farm also tended to show that model predictions were within a factor of two of the field measurements. Of course, such precise predictions of dispersion over short time scales would not be expected with the UK-ADMS model. However, the CFD techniques cannot be expected to yield better dispersion predictions over longer time scales as they require detailed input data (including emission data) and can be sensitive to the specification of the incoming wind field. Overall, the UK-ADMS model was concluded to provide robust estimates of dispersion downwind of both naturally ventilated farm buildings.

7.4.3 Local deposition of NH_3

7.4.3.1 Plant responses to atmospheric NH₃

The biomonitor experiments investigated the surface-atmosphere exchange of NH_3 at two contrasting periods in the growing cycle (late summer and spring). The physiological response of the plants to N addition through the soil was found to vary between the experiments. Nitrogen applied to the growth media was mostly metabolised in the root organs during the late summer, whilst N was translocated from the root organs to the leaves and stems during the spring experiments.

The observed seasonal variation in N allocation could be explained in terms of the seasonal balance of photosynthesis, producing carbohydrates and consuming energy, and respiration, which metabolises carbohydrates to produce energy (Fitter and Hay, 1987). During the late summer to early autumn, plants experience favourable conditions for both photosynthesis (light, water and temperature) and respiration (temperature), hence both processes are in a quasi-equilibrium state, with the excess energy produced being used for growth. As there are roughly equal pressures on plants to produce above ground material, which increases the rate of photosynthesis, and below ground material, which increases the rate of respiration, any excess N is likely to be metabolised close to the source of uptake. In spring, low temperatures suppress respiration whilst the increasing insolation enables a moderate rate of photosynthesis for a reduced energy cost. In such conditions it is well documented that plants take advantage of the favourable balance of respiration to photosynthesis by expanding their canopies, hence any additional N would be translocated to the above ground plant material.

The metabolism of N close to the site of uptake, found in the SRI buildings study, also enabled the site of metabolism of the deposited NH_3 to be investigated. As a statistically significant increase in N content (over the background biomonitors) was only found in the above ground N of downwind biomonitor it was likely that the site of deposition, and uptake into the plant was the above ground plant organs. This seemingly obvious conclusion poses some interesting further questions. The time averaged deposition velocity of 0.02 m s^{-1}, suggested that NH_3 deposition occurred at a rate in excess of stomatal resistance (Wesley, 1989). This would indicate that deposition to the leaf surface occurred, as found by Sutton *et al.* (1998a) and in Chapter 5 of this thesis. As the site of intake and metabolism of NH_3 was the above ground plant organs then rapid cuticular uptake must have occurred following leaf surface deposition.

The cuticular uptake of deposited NH_3 on the leaf surfaces may also explain the variability in leaf surface NH_x-N observed. Winds were mainly from the north during the last six hours of the SRI building study experiment, which could have caused the high surface NH_x-N concentrations observed at Site 6a, despite its lower time-averaged NH_3 air concentration and lower net deposition flux. Furthermore, modelled air concentrations over the last 12 hours of the Town Barton Farm experiment were mainly directed towards biomonitors at Sites B2, B3, B4, and B8. With the exception of biomonitors at Site B8, the sites modelled to receive a high air concentration over the last 12 hours of the experiments were found to have high levels of leaf surface NH_x-N.

The lower deposition of NH$_3$ to biomonitors measured at the Town Barton Farm study may also have been related to the metabolic processes that were occurring. Whilst N nutrition was mainly located at the site of uptake for biomonitors during the SRI building study, translocation and metabolism of NO$_3^-$ -N from the roots to the shoots was found in the Town Barton Farm study. This was likely to have occurred due to the N demand, for chlorophyll production, of the rapidly growing canopy. The metabolism of NO$_3^-$ -N in the shoots of plants releases hydroxyl ions (Pearson and Stewart, 1993) which may have resulted in the above ground plant organs becoming increasingly alkaline, hence reducing their affinity for atmospheric NH$_3$. The lower deposition velocity estimated during the Town Barton Farm study was also likely to be related to the lower temperatures measured in the field, as found in Chapter 5. Due to the temperature dependence of plant respiration a reduced assimilation of NH$_3$ would be expected at low temperatures. This would reduce the uptake of NH$_3$ from the leaf surface sinks, causing an increase in the leaf surface NH$_3$ concentration and an increase in the surface resistance to atmospheric deposition.

7.4.3.1   *Net deposition around naturally ventilated buildings*

Deposition to fields around the buildings, defined as a 200 m x 200 m grid in the SRI study and a 300 m x 300 m grid in the Town Barton Farm study was estimated to reduce the net emission of NH$_3$ by 2 %. These values are close to the estimated reduction in net emission of 3.2 % determined by Fowler *et al.* (1998b) to occur within 300 m of a poultry farm. The slightly lower percentage re-capture, when compared with the results of Fowler *et al.* (1998b), was likely to be due to the smaller area over which local deposition was calculated.

The percentage recapture estimated from the farm building study was compared with the recapture estimates from the slurry spreading experiments. For deposition velocities of 0.01 and 0.02 m s^{-1}, the recapture of NH$_3$ within 50 m of the source, measured during the slurry spreading experiments, was estimated to range from 2 - 15 % of the source term with a mean of 7 %. Clearly, the potential for local recapture (to grassland) of emissions around a farm building is much lower than downwind of a slurry application. This was due to the much higher and more dispersed plume of NH$_3$ that was released from the buildings, as can be seen by comparing Figures 7.6 and 7.12 with Figures 5.3 and 5.4. The well dispersed NH$_3$ plume from the building was generated by the enhanced turbulence created by the building as well as the elevated and well distributed release points on the building. Significant recapture of NH$_3$ from such a well dispersed plume would require the plume to

be intercepted by tall woodland close to the site. High levels of local deposition to woodland close to a poultry building have been predicted by Hill (1997).

The potential for local atmospheric pollution around a farm was evaluated by comparing the long-term averaged fluxes shown in Figure 7.13 with the critical loads for N discussed in Chapter 1, Section 1.7.1. Assuming that the receptor environment was a moorland, and that the time-average deposition velocity determined during the field experiments applied equally to both moorlands and grasslands, then local deposition within 100 m of the farm would exceed the critical load of 10 kg N ha^{-1}. Deposition to receptors further than 150 m from the source was not investigated this study. However, as the local dispersion and deposition estimates presented herein were similar to those presented in Fowler *et al.* (1998b), their conclusion that the environmental impacts of a single source would largely be confined to within 1 km seem realistic.

8

CONCLUSIONS

8.1   INTRODUCTION

The aim of this thesis, discussed in Chapter 1, was to estimate the emission, dispersion and local deposition of NH_3 volatilised from two sources: slurry spread onto grassland and naturally ventilated farm buildings. Models and methods were identified to address these aims in Chapters 2 and 3 and field experiments were designed in Chapters 4 and 6. The results of the field experiments were presented in Chapters 5 and 7.

This chapter presents a summary of the results of the field experiments. The implications of the findings presented herein on both the control of pollution and for the on-farm conservation of N are discussed later in the chapter. The chapter concludes with recommendations for further research to address issues raised by this project.

8.2   SUMMARY OF RESEARCH

The background of this project, discussed in Chapter 1, demonstrates an increasing interest amongst the scientific and political communities in the atmospheric behaviour of NH_3, a pollutant that is principally released to the atmosphere from agriculture. Legislation will regulate NH_3 emissions in the future in order to limit the transboundary transport of NH_x-N (the UN-ECE "multi-pollutant multi-effect" protocol) and to protect natural ecosystems close to sources of emission (the EC IPPC directive).

Atmospheric dispersion models have been developed, for example FRAME (Singles *et al.*, 1998) and HARM (Metcalfe *et al.*, 1998b) to predict the atmospheric transport of NH_3 and a large number of field studies have been conducted to measure deposition fluxes to natural and fertilised vegetation. However, little information was available on the atmospheric dispersion and local deposition of NH_3 close to the source of emission.

The ADEPT project, under which this study was conducted, aimed to address the issues of short-range transport and deposition of NH_3. The work conducted in this study investigated the atmospheric dispersion and deposition of NH_3 close to slurry spreading, within 50 m of the source, and investigated dispersion and deposition around naturally ventilated farm buildings.

8.2.1 NH₃ emissions

8.2.1.1   Emissions from slurry spreading

Eight field experiments were conducted to measure the emission of NH_3-N using the micrometeorological mass balance method discussed in Chapter 2. The experiments were timed to investigate the seasonal and diurnal controls over NH_3-N emissions.

♦ Patterns of NH_3-N emission were fairly consistent between experiments with 28 - 66 % of the total flux (measured over approximately 48 hours) occurring during the first 3 - 5 hours. This was followed by an exponential decline in emission rates during subsequent runs.

♦ NH_3-N emissions often showed a strong diurnal variability with emission maxima occurring during daytime and minima occurring overnight.

♦ The average NH_3-N emission, expressed as a percentage of TAN applied, was 18 %. This was in good agreement with the proportion of NH_3-N emission likely from dilute slurries as discussed in Pain *et al.* (1998).

♦ Emission fluxes measured during the first experimental run were strongly correlated with friction velocity (u_*). A multiple regression analysis was performed demonstrating that u_*, *RH*, and rainfall described 97 % of the variation in initial NH_3-N emissions.

8.2.1.2   Emissions from farm buildings and slurry lagoons

Emissions of NH_3-N were measured from the main dairy/cowshed building and the slurry lagoon at Town Barton Farm. Emission fluxes from the farm building were determined using passive flux samplers ("Ferm tubes"). Emissions from the slurry lagoon were determined using a back-calculation method, applying the dispersion predictions from the UK-ADMS atmospheric dispersion model. A summary of the findings of these experiments follows.

♦ The first use of a back-calculation method to determine NH_3-N emission from stored slurry was reported.

◆ Emission factors of 340 μg NH$_3$-N s^{-1} (500 kg liveweight)$^{-1}$ and 74 μg NH$_3$-N s^{-1} (500 kg liveweight)$^{-1}$ were derived for the farm building and slurry lagoon respectively. Comparable emission factors were found in the literature.

◆ The spatial distribution of NH$_3$-N emission points on a naturally ventilated farm building was investigated. Forty percent of the NH$_3$-N emitted from the building was released from the roof, with the remainder being released through the Yorkshire boarding and through other ventilation openings.

◆ The overall NH$_3$-N emission from Town Barton Farm was determined using the measured emission factors for housing and slurry storage and the emission factors from Pain *et al.* (1998) for grazing and slurry spreading. The calculations showed that 2.5 t NH$_3$-N a^{-1} were estimated to be emitted from the site. Forty three percent of the total emission estimate was derived from housing losses, 40 % from spreading losses, 12 % from storage losses and 5 % from grazing losses.

8.2.2   NH$_3$ dispersion in the atmosphere

8.2.2.1   Atmospheric dispersion from slurry spreading

A physically realistic model of dispersion in the constant flux layer of the atmosphere was developed in Chapter 3. This model was based on an exact analytical solution to the advection-diffusion equation, proposed by Huang (1979). The model used a power law parameterisation to include realistic profiles of wind speed and eddy diffusivity. The realism of these profiles was investigated and an optimal power law reference height was identified. Modifications were made to the model to include an exact surface depletion deposition scheme (Horst, 1977) and to allow the model to resolve line and area sources. A computational method was also developed to model the influence of wind angles oblique to the source. The model, termed the K-theory Atmospheric Transport and Exchange (KATCH) model, was shown to produce similar predictions of vertical dispersion to the more complex Lagrangian "Random Walk" model developed by Wilson *et al.* (1981a) and Wilson *et al.* (1981b).

The KATCH model predictions were compared, in Chapter 5, with non-dimensionalised field measurements of vertical dispersion at the immediately downwind site. Dispersion of NH$_3$ at this site could be assumed to be unaffected by dry deposition. The following conclusions were drawn from a comparison between the model predictions and the entire data set.

◆ The KATCH model was found to produce an unbiased estimate of vertical dispersion.

224

♦ The correlation between measured and modelled values demonstrated that 73 % of the variation in the measurements was described by the model.

♦ A high proportion (83 %) of the model predictions were within a factor of two of the field measurements and 38 % of the model predictions were within +/- 20 % of the field measurements.

The influence of the uncertainty in determining horizontal and vertical NH_3 fluxes on the above comparison was also investigated. Measurements of the vertical and horizontal fluxes of NH_3 during the first two runs of each experiment tended to be better quality (shown by well-defined logarithmic vertical profiles) due to the higher emission fluxes. Hence, a second comparison was made restricting the dataset to only consider measurements made in these runs.

♦ The correlation between the measurements and the model predictions increased, with 93 % of the variation in the measurements being accounted for by the model.

♦ The proportion of the model predictions that were within a factor of two of the field measurements increased to 92 %, with 56 % of the model predictions being within +/- 20 % of the field measurements.

The KATCH model was concluded to produce realistic dispersion estimates close to an area source. Measurement uncertainty was concluded to be the largest contributor to the differences between model predictions and field measurements.

8.2.2.2   *Atmospheric dispersion from a farm building*

Modelling the atmospheric dispersion of material released from a farm building was identified in Chapter 3 as being considerably more difficult than modelling dispersion from slurry spreading. This was due to the complex flows and turbulence associated with such structures. The UK-ADMS model, incorporating a reasonably detailed description of building influenced dispersion, was selected from the available modelling methods. The treatment of building effects within UK-ADMS, as described in Robins *et al.* (1997), was less detailed than the CFD approaches used by Hill (1997) to determine NH_3 dispersion from a poultry farm. However, when calculating time averaged air concentrations and deposition fluxes, particularly with emission data specified as 24 hour averages, the UK-ADMS approach was found to be adequate. The results of field experiments comparing the UK-ADMS model predictions with the measured air concentration field around Town

Barton Farm and the SRI Structures Building are listed below, full details of these experiments can be found in Chapter 7.

♦ UK-ADMS model predictions of the spatial pattern of ground level air concentrations were within a factor of two of field measurements for 65 % and 85 % of the comparisons at the Structures Building and Town Barton Farm studies respectively. The correlation statistic (R^2) showed that 37 % and 55 % of the variation in the measurements was accounted for by the model.

♦ Vertical concentration distributions were also compared at the approximate centreline of the NH_3 plume. Concentration profiles immediately downwind of the farm buildings were reasonably vertically homogeneous and much taller than those measured downwind of slurry spreading. This was likely to be due to the elevated height of the release and the increased turbulence, and associated vertical mixing, that would occur downwind of a building.

♦ The UK-ADMS model predictions were found to agree well with the field measurements on the vertical homogeneity of concentrations downwind of the source. This agreement was, again, typically within a factor of two, though the small-scale inhomogeneities measured close to the source could not be matched by the model.

8.2.3 Local deposition of NH_3

8.2.3.1 Estimation of mass budgets downwind of slurry spreading and farm buildings

Field scale estimates of the local deposition fluxes of NH_3 downwind of slurry spreading and farm buildings were determined using modified flux-gradient and N balance methods respectively. The modified flux-gradient method, developed in Chapter 4, was applied to account for the temporal variability of fluxes downwind of slurry spreading. The results from the slurry spreading experiments are detailed below.

♦ Eight field scale micrometeorological experiments, using a modified flux-gradient method, were conducted to estimate the deposition of NH_3 within 50 m of a surface level NH_3 source (slurry applied to grassland). The results reported herein are, to the author's knowledge, the first reported results of the application of such a micrometeorological technique in the immediate near-field of an emission source.

♦ Local dry deposition (within 50 m of a 30 m wide slurry source) at a rate limited by boundary later resistance was predicted, using the KATCH model, to result in a net reduction in the mass of NH_3 emitted from each experiment of between 21 – 25 %.

◆ Recapture of NH₃ during individual runs was not as consistent, with between 10 - 40 % of the emitted NH₃ depositing depending on the stability of the atmosphere. Highly stable atmospheric conditions, as often encountered during overnight periods, were found to entrain NH₃ close to the surface thus increasing the potential for local deposition. High rates of vertical dispersion during unstable periods, as often found during daytime periods with high insolation, reduced the surface level concentrations thus reducing the potential for local deposition.

◆ Field estimates of the local deposition of NH₃ demonstrated that high surface resistances often occurred downwind of the source. Forty six percent of the interpreted vertical profiles suggested that local deposition was not at a sufficiently high rate to affect the net emission from the site. The highest local deposition of NH₃ was measured during Experiment 8, where 18 % of the emitted NH₃ was estimated to deposit within 50 m of the source.

As micrometeorological methods were invalid in the complex flows around a building, an alternative method was required. The N balance method using "biomonitors", discussed in Chapter 6, was applied to determine the local deposition. This method produced long-term averaged estimates of fluxes, which are relevant downwind of a continuously emitting dairy farm. The experimental results are summarised as follows.

◆ Time averaged deposition velocities of 0.02 m s⁻¹ and 0.008 m s⁻¹ were estimated from air concentration measurements and fluxes, calculated using biomonitors, at the SRI Structures Building and Town Barton Farm respectively.

◆ Local deposition of NH₃ was estimated to result in a net recapture of 2 % of the NH₃ emitted from both the SRI Structures Building (within a 200 m x 200 m area) and Town Barton Farm (within a 300 m x 300 m area).

◆ For comparable deposition velocities, a lower percentage recapture was found around the farm buildings than was estimated in the slurry spreading experiments. This was identified to be due to the more dispersed NH₃ plume released from the buildings.

8.2.3.2   Mechanisms and controls over local deposition of NH₃

Flux estimates made with the modified flux-gradient and N-balance methods also provided useful information on the likely sites of deposition of NH₃ and the controls over the deposition process. The conclusions from the experimental results, presented in Chapters 5 and 7, are detailed overleaf.

♦ Both techniques demonstrated that estimated deposition velocities could be higher than would be expected from stomatal uptake alone, suggesting that deposition occurred to the leaf surfaces.

♦ Data from the "biomonitors" at both the SRI Structures Building and at Town Barton Farm demonstrated that deposited N was metabolised and incorporated into the structural N of the plants, providing strong evidence that uptake across the cuticle occurs. Both experiments also demonstrated that deposited N was metabolised close to the site of intake (*i.e.* in the leaves of the plants).

♦ Further evidence that deposition of NH_3 onto leaf surfaces occurred, followed by transfer of NH_x-N into the plant, was found from the higher NH_x-N concentrations measured on the surface of plants downwind of the source at the Structures Building study. In addition, both experiments found that surface NH_x-N concentrations were approximately related to the wind directions during the final hours of the experiment.

♦ Evidence that the leaf surface uptake mechanism could become saturated, following the application of fertilisers to grassland was found as no detectable deposition of NH_3 was measured from NH_3 plumes advected over fertilised grassland. The likely cause for the sink saturation was the expected strong and persistent emission of NH_3 from the stomata of the grass.

♦ Further evidence for the saturation of the leaf surface sink, measured during the slurry spreading experiments, was found from the increase in surface resistance measured over time. Such a saturation of the surface sinks for NH_3 was hypothesised to occur due to the accumulation of material on the surface though previous deposition to the plants. This provides additional evidence that the removal of material from the surfaces was not instantaneous.

♦ The saturation of surface sinks was found to occur faster during periods with a high variation in emission fluxes. This was hypothesised to be due to the dependence of deposition on the surface-atmosphere concentration gradient and the dependence of concentrations in the atmosphere on the emission flux from the slurry.

♦ Estimated deposition velocities were found to be strongly correlated with the ambient surface temperature, the latent heat flux and the roughness length. The first two of these terms were likely to influence deposition due to their influence on plant metabolism, and therefore the removal of material accumulated in the surface sink, whilst the last term affected deposition due to physical diffusion through the boundary layer. A multiple regression analysis showed that 57 % of the variation in deposition

velocities could be explained in terms of the aforementioned variables if runs where sinks saturation occurred were discounted.

8.3   IMPLICATIONS OF THE RESEARCH

The prevention of pollution and the conservation of resources can be seen as complimentary goals when regarding NH_3 emissions from agriculture. The emission of NH_3 has no benefit to the farmer and represents a significant loss of N from agricultural production systems. As this lost N is usually replaced with artificial fertilisers, the net cost to UK agriculture caused by NH_3-N emissions can be estimated to be in the order of £70 M per annum. This calculation is based on the cost of replacing the 200 kt NH_3-N that are estimated to be annually emitted from agriculture (Pain *et al.*, 1998) with ammonium nitrate fertilisers. The implications of the research reported in this thesis on both the prevention of pollution and the conservation of N are presented in this section.

8.3.1   Prevention of pollution

The research reported in this thesis has implications for the control of pollution at both a national and regional scale. The evaluation, at a national scale, of transboundary pollutants is largely the responsibility of the European Monitoring and Evaluation Project (EMEP). The atmospheric dispersion of pollutants emitted from each nation is currently determined using a *Lagrangian* atmospheric dispersion model, as discussed in EMEP (1996). The emission factors determined in this study were in good agreement with the emission factors presented in Pain *et al.* (1998) for emissions from the three main components of the UK NH_3 emission inventory: slurry spreading, housing, and loss from slurry stores. The current UK "official" emission estimates are not entirely consistent with those presented in Pain *et al.* (1998), however the results of this study provide additional evidence to support the emission factors used by Pain *et al.* (1998).

The assumption of instantaneous mixing in the EMEP atmospheric dispersion model, leads to the model significantly underpredicting the "sub-grid level" (or local) deposition (Krüger and Tuovinen, 1997). To account for this, sub-grid level factors are applied to incorporate local deposition. These result in 15 % of the net emission in each grid cell being locally recaptured (Krüger and Tuovinen, 1997). Such local deposition factors seem to be realistic, based on the measurements reported in this thesis. However, no firmer conclusion about the overall suitability of these factors could be reached. Deposition close to slurry spreading was found to be highly variable due to sink saturation and the influence of the plot dimensions. Whilst, the farm building experiments showed a relatively low

local recapture of emissions due to the increased vertical atmospheric dispersion. Lower local deposition factors are likely to be required to account for periods when local deposition is inefficient, such as over winter and immediately following the application of N fertiliser. Consequently, during such periods it is likely that the net export of NH_x from the UK will increase.

Particular attention should also be paid to the timing of emission events in atmospheric dispersion models, with most assuming that emissions are uniform throughout the year (*e.g.* EMEP, 1996; Singles *et al.*, 1998). This assumption is clearly an oversimplification when considering emissions from both farm buildings and slurry spreading. Emissions from the latter mainly occur during winter and therefore local deposition may be lower than the annual mean due to temperature effects, whilst the emissions from the former occur as a pulse, mostly within a few hours following application. As farmers are guided to spread slurry during periods with strong insolation and moderate winds (MAFF, 1998a) and often avoid spreading when rainfall is predicted, these effects should be included in the emission and local deposition modelling. Moreover, the timing of events in the agricultural calendar (*e.g.* silage cutting) mean that slurry spreading emissions have an increased probability of occurring during specific months of the year.

The local effects of a source were found to be strongly dependent on the distance between the source and the receptor. Of the two sources evaluated in this study, farm buildings had the largest potential for local pollution due to their fixed location, high emission rates and long emission duration. Indeed the critical load for moorlands was shown to be exceeded at distances greater than 100 m from the source. Atmospheric emissions from slurry spreading are less likely to cause local pollution as the source terms are more spatially dispersed and the emission duration is shorter. In general, a distance of 1.0 km between the source and receptor was likely to result in negligible local pollution from atmospheric emissions derived from either source.

8.3.2 Conservation of N on the farm

The conservation of N from farm wastes can be seen as being more efficient when emissions are reduced, or even prevented, at the source. Recapture of NH_3-N, once emitted into the atmosphere is a relatively inefficient process, with the highest recapture recorded in this study of about 20 % occurring downwind of surface applied slurry. Lower recaptures (<5 %) were estimated around farm buildings. Moreover, the local recapture was found to be dependent on the ambient temperature and on the management of the

230

downwind areas. A negligible local recapture was estimated over fertilised grassland. Further work on the conservation of NH_3-N, within the boundaries of individual farms, should concentrate on reducing emissions at the source. Although the influences of farm woodlands around a source need to be properly quantified before any clear conclusions can be reached over the potential for reducing net emissions from a site.

The influence of different meteorological conditions on NH_3 emission was investigated in Chapter 5. No clear meteorological controls over the net NH_3 emission fluxes were found. However, emissions during the initial run of each experiment were found to be strongly dependent on friction velocity, rainfall and relative humidity. The influence of friction velocity on net NH_3 emissions was likely to be buffered by the pulse of emission that often occurred when friction velocities increased.

The washing of NH_3 into soils during periods with rainfall and high humidities, as discussed in Menzi *et al.* (1998), Pain and Misselbrook (1997) and Sommer *et al.* (1991), would also be likely to reduce the net emission, though again no clear trends were observed in this study. However, it should be noted that the application of slurry during periods with high rainfall may result in the surface run-off of NH_x or the leaching of nitrates, formed from the microbial oxidation of NH_3.

Given the difficulties in managing NH_3 emissions through increased local deposition or through timing of slurry applications, successful reductions in NH_3 emissions from slurry require modified slurry application techniques. The use of more efficient methods, such as ploughing and injection can result in reductions in NH_3 emission of around 90 % (Pain *et al.*, 1991). Consequently, further research on the conservation of N should focus on these methods.

About 40 % of the net emission of NH_3-N from UK agriculture occurs from housed livestock (Pain *et al.*, 1998). The research reported in this thesis demonstrated that local recapture of emissions around a building is less efficient than recapture downwind of slurry spreading due to the enhanced dispersion caused by wake turbulence. Reducing emissions at the source is also difficult in naturally ventilated farm buildings due to the well distributed volatilisation and ventilation points. One possible way to reduce the net emission may be the recapture of N in farm woodlands near the site. Indeed, Sutton *et al.* (1997b) predicted high levels of local deposition to the edges of woodland. However, such woodlands would need to be immediately downwind of the farm and dense enough to

provide an efficient sink for NH_3. Deposition to woodlands some distance from a farm has been shown in Hill (1997) to be relatively low due to the increased dispersion caused by the higher roughness lengths of tall vegetation.

8.4   RECOMMENDATIONS FOR FURTHER RESEARCH

The research presented in this thesis has identified several topics that should be considered in order to develop and extend the conclusions reported.

♦ More research is required to investigate the physiology of the surface uptake mechanisms of plants. Clearly, the rate of uptake of deposited N from the surface is important in determining sink saturation and consequently can lead to time dependent deposition fluxes downwind of a source.

♦ Experiments are required to consider the importance of air concentration fluctuations on the exchange process and the adsorption-desorption that occurs on leaf surfaces.

♦ The local deposition of NH_3 over land use types other than agricultural grassland should also be considered. In particular, exchanges over tall vegetation, woodland and arable land immediately downwind of a source.

♦ More detailed descriptions of the temporal pattern of NH_3 emissions from farm buildings and slurry spreading should be determined for inclusion in long-range atmospheric dispersion models.

♦ Further research is required on the appropriate NH_3 emission factors for farm buildings. In particular, to investigate emissions from a range of different dairy buildings to enable the current variability in emission factors to be addressed.

REFERENCES

Allen A. G., Harrison R. M. and Wake M. T. (1988) A mesoscale study of the behaviour of atmospheric ammonia and ammonium. *Atmospheric Environment* **22**, 1347-1353.

Allen A. G., Harrison R. M. and Erisman J. (1989) Field measurements of the dissociation of ammonium nitrate and ammonium chloride aerosol. *Atmospheric Environment* **23**, 1591-1599.

Andersen H. V., Hovmand M. F., Hummelshoj P. and Jensen N. O. (1993) Measurements of ammonia flux to a spruce stand in Denmark. *Atmospheric Environment* **27**, 189-202.

Amon M., Dobeic M., Misselbrook T. H., Pain B. F., Phillips V. R. and Sneath R. W. (1995) A farm scale study on the use of de-odorase for reducing odour and ammonia emissions from intensive fattening piggeries. *Bioresource Technology* **51**, 163-169.

Aneja V. P., Rogers H. H. and Stahel E. P. (1986) Dry deposition of ammonia at environmental concentrations on selected plant species. *Journal of the Air Pollution Control Association* **36**, 1338-1341.

ApSimon H. M., Kruse M. and Bell J. N. B. (1987) Ammonia emissions and their role in acid deposition. *Atmospheric Environment* **21**, 1939- 1946.

ApSimon H. M., Barker B. M. and Kayin S. (1994) Modelling studies of the atmospheric release and transport of ammonia in anticyclonic episodes. *Atmospheric Environment* **28**, 665-678.

ApSimon H. M., Couling S., Cowell D. and Warren R. F. (1995) Reducing the contribution of ammonia to nitrogen deposition across Europe. *Water, Air and Soil Pollution* **85**, 1891-1896.

Artyomov V. M., Artyomov E. M. and Fridman S. H. D. (1994) Ammonia uptake by plants. *Environmental Monitoring and Assessment* **29**, 221-228.

Asman W. A. H. and Janssen A. J. (1987) A long range transport model for ammonia and ammonium for Europe. *Atmospheric Environment* **21**, 2099-2265.

233

Asman W. A. H., Pinksterboer E. F., Maas H. F. M., Erisman J. W., Waijers-Ypelaan A., Slanina J. and Horst T. W. (1989) Gradients of ammonia concentration in a nature reserve: model results and measurements. *Atmospheric Environment* **23**, 2259-2265.

Asman W. A. H. and Van Jaarsveld H. A. (1992) A variable resolution transport model applied for NH$_x$ in Europe. *Atmospheric Environment* **26**, 445-464.

Asman W. A. H. (1995) Parameterisation of the below cloud scavenging of highly soluble gases under convective conditions. *Atmospheric Environment* **29**, 1359-1368.

Asman W., Hertel O., Berkowicz R., Christensen J., Runge E., Sorensen L., Granby K., Nielsen H. and Jensen B. (1995) Atmospheric nitrogen input to the Kattegat. *OPHELIA* **42**, 5-28.

Asman W. A. H. (1998) Factors influencing local dry deposition of gases with special reference to ammonia. *Atmospheric Environment* **32**, 415-421.

Atkins D. H. F. and Lee D. S. (1993) Indoor concentrations of ammonia and the potential contribution of humans to atmospheric budgets. *Atmospheric Environment* **27**, 1-7.

Baldocchi D. D., Hicks B. B., and Meyers T. P. (1988) Measuring biosphere-atmosphere exchange of biologically related gases with micrometeorological methods. *Ecology* **69**, 1331-1340.

Baxter R., Emes M. J. and Lee J. A. (1992) Effects of an experimentally applied increase in ammonium on growth and amino acid metabolism of *Sphagnum cuspidatum* Ehrh. Ex. Hoffm. from differently polluted areas. *New Phytologist* **120**, 265-274.

Berkley D. D. (1988) Calculus: second edition. Saunders College Publishing.

Berthelot M. P. E. (1859) Violet d' aniline. *Rep. de Chim. Appl.* **1**, 284.

Bless H. G., Beinhauer R. and Sattelmacher B. (1991) Ammonia emission from slurry applied to wheat stubble and rape in North Germany. *Journal of Agricultural Science* **117**, 225-231.

Bobbink R. (1991) Effects of nutrient enrichment in Dutch chalk grassland. *Journal of Applied Ecology* **28**, 28-41.

Bobbink R., Gerrit W. H. and Raessen M. (1992) Atmospheric deposition and canopy exchange processes in heathland ecosystems. *Environmental Pollution* **75**, 29-37.

Bower K. N., Wells M., Choularton T. W. and Sutton M. A. (1995) A model of ammonia/ammonium conversion and deposition in a hill cap cloud. *Quarterly Journal of the Royal Meteorological Society* **121**, 569-591.

Briggs G.A. (1974) Diffusion estimation for small emissions in environmental research laboratories. Air resources atmospheric turbulence and diffusion laboratory 1973 annual report. USAEC Report ATDL-106, National Oceanic and Atmospheric Administration, December 1974.

Bristow A. W., Whitehead D. C. and Cockburn J. E. (1992) Nitrogenous constituents in the urine of cattle, sheep and goats. *Journal of the Science of Food and Agriculture* **59**, 387-394.

Brown M. J., Arya S. P. and Snyder W. H. (1997) Plume descriptors derived from a non-Gaussian concentration model. *Atmospheric Environment* **31**, 183-189.

Bruckner G., Gebauer G. and Schulze E. D. (1993) Uptake of $^{15}NH_3$ by *Picea abies* in closed chamber experiments. *Isotopes in Environmental and Health Studies* **29**, 71-76.

Buijsman E., Mass H. F. M. and Asman W. A. H. (1987) Anthropogenic ammonia emissions in Europe. *Atmospheric Environment* **21**, 1009-1022.

Bull K. R. and Sutton M. A. (1998) Critical loads and the relevance of ammonia to an effects based nitrogen protocol. *Atmospheric Environment* **32**, 565-572.

Burkhardt J. and Eiden R. (1994) Thin water films on coniferous needles. *Atmospheric Environment* **28**, 2001-2017.

Carruthers D. J. and Weng W. S. (1992) Boundary layer structure specification. CERC Technical Guide to UK-ADMS Version 1.0. CERC, Cambridge.

Carruthers D. J., Weng W. S., Hunt J. C. R., Holroyd R. J. and McHugh C. A. (1993) Plume/ puff spread and mean concentration module specifications. CERC Technical Guide to UK-ADMS Version 1.0. CERC, Cambridge.

Carruthers D. J., Holroyd R. J., Hunt J. C. R., Weng W. S., Robins A. G., Apsley D. D., Thomson D. J. and Smith F. B. (1994) UK-ADMS: A new approach to modelling dispersion in the Earth's atmospheric boundary layer. *Journal of Wind Engineering and Industrial Aerodynamics* **52**, 139-153.

Cass G. R., Gharib S., Peterson M. and Tilden J. W. (1982) The origin of ammonia in the atmosphere in an urban area. Open File Report 82-86 Environmental Quality Laboratory, California Institute of Technology, Pasadena.

Chambers B. J., Smith K. A. and Van der Weerden T. J. (1997) Ammonia emissions following the land spreading of solid manures. In: *Gaseous Nitrogen Emissions from Grasslands* (edited by Jarvis S. C. and Pain B. F), pp 275 – 280. CAB International.

CLAG (1994) Critical loads for acidity in the United Kingdom. Critical Loads Advisory Group Summary Report. Institute of Terrestrial Ecology, Edinburgh, UK.

CLAG (1997) Deposition fluxes of acidifying compounds in the UK. Critical Loads Advisory Group Sub-group Report on Deposition Fluxes. Institute of Terrestrial Ecology, Edinburgh, UK.

Clarke R. H. (1979) A model for short and medium range dispersion of radionuclides released to the atmosphere. National Radiological Protection Board – Harwell. NRPB-R91.

Corbett J. O. (1981) The validity of source depletion and alternative approximation methods for a Gaussian plume subject to dry deposition. *Atmospheric Environment* **15**, 1207-1213.

Couling S. (1997) Ammonia dispersion and deposition around livestock buildings In: *Gaseous Nitrogen Emissions from Grasslands* (edited by Jarvis S. C. and Pain B. F), pp.115-121. CAB International.

Cowan I. R., Castro I. P. and Robins A.G. (1997) Numerical considerations for simulations of flow and dispersion around buildings. *Journal of Wind Engineering and Industrial Aerodynamics* **67**, 535-545.

Cowling D. W. and Lockyer D. R. (1981) Increased growth of Ryegrass exposed to ammonia. *Nature* **292**, 337-338.

Dabney S. M. and Bouldin D. R. (1990) Apparent deposition velocity and compensation point of ammonia inferred from gradient measurements above and through Alfalfa. *Atmospheric Environment* **24**, 2655-2666.

Dawson P., Stock D. E. and Lamb B. (1991) The numerical simulation of airflow and dispersion in three dimensional atmospheric recirculating zones. *Journal of Applied Meteorology* **30**, 1005-1024.

Demmers T. G. M., Burgess L. R., Short J. L., Phillips V. R., Clark J. A. and Wathes C. M. (1998) First experiences with methods to measure ammonia emission from naturally ventilated cattle buildings in the UK. *Atmospheric Environment* **32**, 285-293.

Denmead O. T., Simpson J. R., and Freney J. R. (1974) Ammonia flux into the atmosphere from a grazed pasture. *Science* **185**, 609-610.

Denmead O. T., Freney J. R. and Simpson J. R. (1976) A closed ammonia cycle within a plant canopy. *Soil Biology and Biochemistry* **8**, 161-164.

Denmead O. T., Simpson J. R. and Feney J. R. (1977) A direct field measurement of ammonia emission after injection of anhydrous ammonia. *Soil Science Society of America Journal* **41**, 1001- 1004.

Denmead O. T., Nulsen R. and Thurtell G. W. (1978) Ammonia exchange over a corn crop. *Soil Science Society of America Journal* **42**, 840-842.

Denmead O. T. (1983) Micrometeorological methods for measuring gaseous losses of nitrogen in the field. In: *Gaseous Loss of Nitrogen from Plant Soil Systems* (edited by Freney J. R. and Simpson J. R.), pp. 133-157. Martinus Nijhoff/ Dr W. Junk publishers.

Denmead O. T. (1994) Measuring the fluxes of CH₄ and N₂O between agricultural systems and the atmosphere. In: *CH₄ and N₂O: Global Emissions and Control from Rice Fields and Other Agricultural and Industrial Sources* (edited by Minami K., Mosier A. and Sass R.), pp. 209-234. NIASES.

DoE (1995) Official UK emission figures agreed for submission by DoE and MAFF in 1995 between ADAS, Imperial College, IGER and ITE (based on 1993 census data). Air Quality Division, Department of the Environment, London.

Doran J. C. and Horst T. W. (1985) An evaluation of Gaussian plume-dispersion models with dual- tracer field measurements. *Atmospheric Environment* **19**, 939-951.

Draaijers G. P. J., Ivens W. P. M. F., Bos M. M. and Bleuten W. (1989) The contribution of ammonia emissions from agriculture to the deposition of acidifying and eutrophying compounds onto forests. *Environmental Pollution* **60**, 55-66.

Dragosits U., Sutton M. A. and Place C. J. (1996) The spatial distribution of ammonia emissions in Great Britain for 1969 and 1988 assessed using GIS techniques. In: *Atmospheric Ammonia: Emissions, Depositions and Environmental Impacts. Poster Proceedings* (edited by Sutton M. A., Lee D. S., Dollard G. J. and Fowler D.), pp 46-49. Institute of Terrestrial Ecology, Edinburgh.

Dragosits U., Sutton M. A., Place C. J. and Bayley A. A. (1998). Modelling the spatial distribution of agricultural ammonia emissions in the UK. *Environmental Pollution* **102**, 195- 203.

Duyzer J. (1994) Dry deposition of ammonia and ammonium aerosols over heathland. *Journal of Geophysical Research* **99**, 18757-18763.

Duyzer J. H., Verhagen H. L. M. and Westrate J. H. (1992) Measurement of the dry deposition flux of ammonia onto a coniferous forest. *Environmental Pollution* **75**, 3-13.

Duyzer J. H., Verhagen H. L. M., Weststrate J. H., Bosveld F. C. and Vermetten A. W. M. (1994) The dry deposition of ammonia onto a Douglas fir forest in the Netherlands. *Atmospheric Environment* **28**, 1241-1253.

Dyer A. J. and Hicks B. B. (1970) Flux-profile relationships in the constant flux layer. *Quarterly Journal of the Royal Meteorological Society* **96**, 715-721.

EMEP (1996) Transboundary air pollution in Europe MSC-W status report 1996 part 1: Estimating dispersion of acidifying agents and of near surface ozone. Norwegian Meteorological Institute.

EMEP (1997) Transboundary air pollution in Europe MSC-W status report 1997 part 1: Emissions, dispersion and trends in acidifying and eutrophying agents. Norwegian Meteorological Institute.

Erisman J., Vermetten A. and Asman W. (1988) Vertical distribution of gases and aerosols: The behaviour of ammonia and related components in the lower atmosphere. *Atmospheric Environment* **22**, 1153-1160.

Erisman J. and Wyers G. P. (1993) Continuous measurement of surface exchange of SO_2 and NH_3: Implications for their possible interaction in the deposition process. *Atmospheric Environment* **27**, 1937-1949.

Erisman J. W., Elzakker B. G., Mennen M. G., Hogenkamp J., Zwart E., Van der Beld L., Romer F. G., Bobbink R., Heil G., Raessen M., Duyzer J. H., Verhage H., Wyers G. P., Otjes R. P. and Mols J. J. (1994) The Espeetsche veld experiment on surface exchange of trace gases: Summary of results. *Atmospheric Environment* **28**, 487-496.

Fangmeier A., Hadwiger-Fangmeier A., Van der Eerden L. and Jager H. (1994). Effects of atmospheric ammonia on vegetation- a review. *Environmental Pollution* **86**, 43-82.

Farquhar G. D., Wetselaar R. and Firth P. M. (1979) Ammonia volatilisation from senescing leaves of maize. *Science* **278**, 1257-1258.

Farquhar G. D., Firth P. M., Wetselaar R. and Weir B. (1980) On the gaseous exchange of ammonia between leaves and the environment: Determination of the ammonia compensation point. *Plant Physiology* **66**, 710-714.

Ferm M. (1986) Concentration measurement and equilibrium studies of ammonium, nitrate and sulphur species in air and precipitation. PhD thesis. Chalmers Tekniska Högskola, Göteborg, Sweden.

Ferguson R. B., McInnes K. J., Kissel D. E. and Kanemasu E. T. (1988) A comparison of methods of estimating ammonia volatilisation in the field. *Fertiliser Research* **15**, 55- 69.

Findlay D. C., Colborne G. J. N., Cope D. W., Harrod T. R., Hogan D. V. and Staines S. J. (1984) Soils and their use in south west England. Lawes Agricultural Trust.

Fitter A. H. and Hay R. K. M. (1987) Environmental physiology of plants: Second edition. Academic Press, London.

Fowler D., Duyzer J. H. and Baldocchi D. D. (1991) Inputs of trace gases, particles and cloud droplets to terrestrial surfaces. *Proceedings of the Royal Society of Edinburgh* **97B**, 35-59.

Fowler D., Sutton M. A., Smith R. I., Pitcairn C. E. R., Coyle M., Campbell G. and Stedman J. (1998a) Regional mass budgets of oxidised and reduced nitrogen and their relative contribution to the nitrogen inputs of sensitive ecosystems. *Environmental Pollution* **102**, 337-342.

Fowler D., Pitcairn C. E. R., Sutton M. A., Flechard C., Loubet B., Coyle M. and Munro R. C. (1998b) The mass budget of atmospheric ammonia in woodland within 1 km of livestock buildings. *Environmental Pollution* **102**, 343-348.

Fowler D., Flechard C. R., Sutton M. A. and Storeton-West R. L. (1998c) Long term measurements of the land-atmosphere exchange of ammonia over moorland. *Atmospheric Environment* **32**, 453-459.

Galperin M.V. and Sofiev M. A. (1998) The long range transport of ammonia and ammonium in the northern hemisphere. *Atmospheric Environment* **23**, 372-380.

Garland J. A. (1977) The dry deposition of sulphur dioxide to land and water surfaces. *Proceedings of the Royal Society of London A* **354**, 245 – 268.

Genermont S., Cellier P., Flura D., Morvan T. and Laville P. (1998) Measuring fluxes after slurry spreading under actual field conditions. *Atmospheric Environment* **32**, 279-284.

Gifford F.A. (1976) Turbulent diffusion-typing schemes: A review. *Nuclear Safety* **17**, 68-86.

Golder D. (1972) Relations among stability parameters in the surface layer. *Boundary Layer Meteorology* **3**, 47-58.

Goulding K. W. T. (1990) Nitrogen deposition to land from the atmosphere. *Soil Use and Management* **6**, 61-63.

Grunhage L., Dammgen U., Haenel H. and Jager H. (1994) Responses of grassland ecosystems to air pollutants: III- The chemical climate: Vertical flux densities of gaseous species in the atmosphere near the ground. *Environmental Pollution* **85**, 42-49.

Hanna S. R., Briggs G. A. and Hosker R. P. (1982) Handbook on atmospheric diffusion (edited by Smith J. S.). Technical Information Centre U.S. Department of energy.

Hansen B., Nornberg P. and Rasmussen K. R. (1998) Atmospheric ammonia exchange on a heathland in Denmark. *Atmospheric Environment* **32**, 461-464.

Harkins J. H. and Nicksic S. W. (1967) Ammonia in auto exhaust. *Envionmental Scence and Technology* **1**, 751-752.

Harper L. A., Catchpoole V. R., Davis R. and Weir K. L. (1983) Ammonia volatilisation: Soil, plant, and microclimate effects on diurnal and seasonal fluctuations. *Agronomy Journal* **75**, 212-218.

Harper L. A., Sharpe R. R., Langdale G. W. and Giddens J. E. (1987) Nitrogen cycling in wheat: Soil, plant, and aerial nitrogen transport. *Agronomy Journal* **79**, 965-973.

239

Harper L. A. and Sharpe R. R. (1995) Nitrogen dynamics in irrigated corn: Soil-plant nitrogen and atmospheric ammonia transport. *Agronomy Journal* **87**, 669-675.

Harper L. A. and Sharpe R. R. (1998) Atmospheric ammonia: issues on transport and nitrogen isotope measurement. *Atmospheric Environment* **32**, 273-277.

Hartung J. and Phillips V. R. (1994) Control of gaseous emissions from livestock buildings and manure stores. *Journal of Agricultural Engineering Research* **57**, 173-189.

Hatch D. J. and Murray P. J. (1994) Transfer of nitrogen from damaged roots of white clover (*Trifolium repens* L.) to closely associated roots of intact perennial ryegrass (*Lolium perenne* L). *Plant and Soil* **166**, 181-185.

Healy T. V., McKay H. A. C., Pilbeam A. and Scargill D. (1970) Ammonia and ammonium sulphate in the troposphere over the United Kingdom. *Journal of Geophysical Research* **75**, 2317-2321.

Hesterberg R., Blatter A., Fahrni M., Rosset M., Neftel A., Eugster W. and Wanner H. (1996) Deposition of nitrogen containing compounds to an extensively managed grassland in central Switzerland. *Environmental Pollution* **91**, 21-34.

Hill J. (1997) Application of computational modelling to ammonia dispersion from agricultural sources. PhD thesis, Imperial College Centre for Environmental Technology, London.

Hornung M., Hall J. R., Gascoyne J., Ullyett J., Dyke H. and Sutton M. A. (1997) Predictions of effects of NH_x deposition on a national scale using critical load approaches. In: *Ammonia Distributions and Effects Project: Distributions, Deposition and Environmental Impacts of Ammonia Emitted by Agriculture. Volume 3: Annex to Final Report on WA0613 to MAFF*. Institute of Terrestrial Ecology, Edinburgh.

Horst T. W. (1977) A surface depletion model for deposition from a Gaussian plume. *Atmospheric Environment* **12**, 797-802.

Horst T. W. (1984) The modification of plume models to account for dry deposition. *Boundary Layer Meteorology* **30**, 413-430.

Horst T. W. and Weil J. C. (1994) How far is far enough? The fetch requirements for micrometeorological measurement of surface fluxes. *Journal of Atmospheric and Oceanic Technology* **11**, 1018-1025.

Hosker R. P. (1984) Flow and diffusion near obstacles. In: *Atmospheric Science and Power Production* (edited by Randerson D.), pp. 241-326. US Department of Energy Technical Information Centre.

Houdijk A. L. F. M. and Roelofs J. G. M. (1991) Deposition of acidifying and eutrophicating substances in Dutch forests. *Acta Botanica Neerlandica* **40**, 245-255.

Hov O. and Hjollo B. A. (1994) Transport distances of ammonia and ammonium in Europe 2: Its relation to emissions of SO₂ and NOₓ. *Journal of Geophysical Research* **99**, 18749-18755.

Huang C. H. (1979) A theory of dispersion in turbulent shear flow. *Atmospheric Environment* **13**, 453-463.

Huber A. H. (1989) The influence of building width and orientation on plume dispersion in the wake of a building. *Atmospheric Environment* **23**, 2109-2116.

Husted S. and Schjoerring J. K. (1995) A computer controlled system for studying ammonia exchange, photosynthesis and transpiration of plant canopies growing under controlled environmental conditions. *Plant, Cell and Environment* **18**, 1070-1077.

Hutchings N. J., Sommer S. G. and Jarvis S. C. (1996) A model for ammonia volatilisation from a grazing livestock farm. *Atmospheric Environment* **30**, 589-599.

Hutchinson G. L., Millington R. J. and Peters D. B. (1972) Atmospheric ammonia: Absorption by plant leaves. *Science* **175**, 771-772.

INDITE (1994) Impacts of nitrogen deposition in terrestrial ecosystems. Department of the Environment, London, UK.

Ineson P., Coward P. A., Benham D. G. and Robertson S. M. C. (1998) Coniferous forest as a secondary source of nitrous oxide. *Atmospheric Environment* **32**, 3321-3330.

IPCC (1992) Climate change, the IPCC scientific assessment (edited by Houghton J. T., Jenkins G. J. and Ephraums J. J). Cambridge University Press, UK.

Iribarne J. V. and Pyshnov J. (1990) The effect of freezing on the composition of supercooled droplets. Retention of HCl, HNO₃, NH₃ and H₂O₂. *Atmospheric Environment* **24**, 383-387.

Jackson D., Jones S. R., Fulker M. J., and Coverdale N. G. M. (1987) Environmental monitoring in the vicinity of Sellafield following the deposition of radioactivity from the Chernobyl accident. *Journal of the Society for Radiological Protection* **7**, 75-87.

Jarvis S. C., Hatch D. J. and Lockyer D. R. (1989) Ammonia fluxes from grazed grassland: Annual losses from cattle production systems and their relation to nitrogen inputs. *Journal of Agricultural Science, Cambridge* **113**, 99-108.

Jarvis S. C. and Pain B. F. (1990) Ammonia volatilisation from agricultural land. In: *Proceedings No. 298*. The Fertiliser Society, Peterborough, UK.

Jarvis S. C., Hatch D. J., Orr R. J. and Reynolds S. E. (1991) Micrometeorological studies of ammonia emission from sheep grazed swards. *Journal of Agricultural Science, Cambridge* **117**, 101-109.

241

Jensen P. K. and Asman W. A. H. (1995) General chemical reaction simulation applied to below-cloud scavenging. *Atmospheric Environment* **29**, 1619-1625.

Jones J. A. (1981) A procedure to include deposition in the model for short and medium range atmospheric dispersion of radionuclides. National Radiological Protection Board-Harwell. NRPB-R122.

Jones J. A. (1983) Models to allow for the effects of coastal sites, plume rise, and buildings on dispersion of radionuclides, and guidance on the value of deposition velocity and washout coefficients. National Radiological Protection Board-Harwell. NRPB-R157.

Kissel D. E., Brewer H. L. and Arkin G. F. (1977) Design and testing of a field sampler for ammonia volatilisation. *Soil Science Society of America Journal* **41**, 1133-1138.

Klarenbeek J. V., Pain B. F., Phillips V. R. and Lockyer D. R. (1993) A comparison of methods for use in the measurement of ammonia emissions following the application of livestock wastes to land. *International Journal of Environmental Analytical Chemistry* **53**, 205-218.

Krom M. D. (1980) Spectrophotometric determination of ammonia: A study on a modified Berthelot reaction using Salicylicate and Dichloroisocyanurate. *The Analyst* **105**, 305-316.

Krüger O. and Tuovinen J. P. (1997) The effects of variable sub-grid deposition factors on the results of the Lagrangian long range transport model of EMEP. *Atmospheric Environment* **31**, 4199-4209.

Kruse M., ApSimon H. M. and Bell J. N. B. (1989) Validity and uncertainty in the calculation of an emission inventory for ammonia arising from agriculture in Great Britain. *Environmental Pollution* **56**, 237-257.

Kuylenstierna J. C. I., Hicks W. K., Cinderby S. and Cambridge H. (1998) Critical loads for nitrogen deposition and their exceedance at European scale. *Environmental Pollution* **102**, 591-598.

Lee D. S. and Longhurst J. W. S. (1993) Estimates of emissions of SO_2, NO_x, HCl and NH_3 from a densely populated region of the UK. *Environmental Pollution* **79**, 37-44.

Lee D. S., Halliwell C., Garland J. A., Dollard G. J. and Kingdon R. D. (1998) Exchange of ammonia at the sea surface- a preliminary study. *Atmospheric Environment* **32**, 431-439.

Leuning R., Freney J. R., Denmead O. T. and Simpson J. R. (1985) A sampler for measuring atmospheric ammonia flux. *Atmospheric Environment* **19**, 1117-1124.

Lockyer D. R. (1984) A system for measurement in the field of losses of ammonia through volatilisation. *Journal of the Science of Food and Agriculture* **35**, 837-848.

Lockyer D. R. and Whitehead D. C. (1986) The uptake of gaseous ammonia by the leaves of Italian ryegrass. *Journal of Experimental Botany* **37**, 919-927.

MAFF (1998a) Code of good agricultural practice for the protection of air. Ministry of Agriculture Fisheries and Food, Welsh office.

MAFF (1998b) Code of good agricultural practice for the protection of water. Ministry of Agriculture Fisheries and Food, Welsh office.

Marshall V. G. and DeBell D. S. (1980) Comparison of four methods of measuring volatilisation losses of nitrogen following urea fertilisation of forest soils. *Canadian Journal of Soil Science* **60**, 549-563.

Massman M. J. (1998) A review of the molecular diffusivities of H_2O, CO_2, CH_4, CO, O_3, SO_2, NH_3, N_2O, NO and NO_2 in air O_2 and N_2 near STP. *Atmospheric Environment* **32**, 1111-1127.

McInnes K. J., Kissel D. E. and Kanemasu E. T. (1985) Estimating ammonia flux: A comparison between the integrated horizontal flux method and theoretical solutions of the diffusion profile. *Agronomy Journal* **77**, 884-889.

McLeod A. R., Holland M. R., Shaw P. J. A., Sutherland P. M., Darrall N. M. and Skeffington R. A. (1990) Enhancement of nitrogen deposition to forest trees exposed to SO_2. *Nature* **347**, 277 – 279.

Menzi H., Katz P. E., Fahrni M., Neftel A. and Frick R. (1998) A simple empirical model based on regression analysis to estimate ammonia emissions after manure application. *Atmospheric Environment* **32**, 301-307.

Metcalfe S. E., Derwent R. G., Whyatt J. D. and Dyke H. (1998a) Nitrogen deposition and strategies for the control of acidification and eutrophication across Great Britain. *Water Soil and Air Pollution* **107**, 121-145.

Metcalfe S. E., Whyatt J. D. and Derwent R. G. (1998b) Multi-pollutant modelling and the critical loads approach for nitrogen. *Atmospheric Environment* **32**, 401-408.

Misselbrook T. H., Pain B. F. and Headon D. M. (1998) Estimates of ammonia emissions from dairy cow collecting yards. *Journal of Agricultural Engineering Research* **71**, 127-135.

Moller D. and Schieferdecker H. (1985) A relationship between agricultural NH_3 emissions and the atmospheric SO_2 content over industrial areas. *Atmospheric Environment* **19**, 695-700.

Monteith J. L. and Unsworth M. H. (1990) Principles of Environmental Physics: Second Edition. Edward Arnold, London.

Nihlgard B. (1985) The ammonium hypothesis. An additional explanation to the forest dieback in Europe. *Ambio* **14**, 2-8.

Olesen J. E. and Sommer S. G. (1993) Modelling effects of wind speed and surface cover on ammonia volatilisation from stored pig slurry. *Atmospheric Environment* **27**, 2567-2574.

243

Owen P. R. and Thomson W. R. (1963) Heat transfer across rough surfaces. *Journal of Fluid Mechanics* **15**, 321 – 334.

Pain B. F., Phillips V. R., Clarkson C. R. and Klarenbeek J. V. (1989) Loss of nitrogen through ammonia volatilisation during and following the application of pig or cattle slurry to grassland. *Journal of the Science of Food and Agriculture* **47**, 1-12.

Pain B. F. and Thompson R. B. (1989) Ammonia volatilisation from livestock slurries applied to land. In: *Nitrogen in Organic Wastes Applied to Soils* (edited by Hausen J. A. and Henricksen K.), pp 202-211. Academic Press, London.

Pain B. F., Phillips V. R., Clarkson C. R., Misselbrook T. H., Rees Y. J. and Farrent J. W. (1990) Odour and ammonia emission following the spreading of aerobically treated pig slurry on grassland. *Biological Wastes* **34**, 149-160.

Pain B. F., Phillips V. R., Huijsmans J. F. M. and Klarenbeek J. V. (1991) Anglo-Dutch experiments on odour and ammonia emissions following the spreading of piggery wastes on arable land. IMAG- DLO, Wageningen, The Netherlands.

Pain B. F. and Misselbrook T. H. (1997) Sources of variation in ammonia emission factors for manure applications to grassland. In: *Gaseous Nitrogen Emissions from Grasslands* (edited by Jarvis S. C. and Pain B. F), pp. 293-301. CAB International.

Pain B. F., Van der Weerden T. J., Chambers B. J., Phillips V. R. and Jarvis S. C. (1998) A new inventory for ammonia emissions from U.K. agriculture. *Atmospheric Environment* **32**, 309-313.

Pasquill F. (1961) The estimation of the dispersion of windborne material. *Meteorological Magazine* **90**, 33-49.

Pasquill F. and Smith F. B. (1983) Atmospheric diffusion: Third edition. Ellis Horwood Ltd. England.

Paulson C. A. (1970) The mathematical representation of wind speed and temperature in the unstable atmospheric surface layer. *Journal of Applied Meteorology* **9**, 857-861.

Pearson J. and Stewart G. R. (1993) Tansley review no. 56: The deposition of atmospheric ammonia and its effects on plants. *New Phytologist* **125**, 283-305.

Pearson J. and Soares A. (1998) Physiological responses of plant leaves to atmospheric ammonia and ammonium. *Atmospheric Environment* **32**, 533-538.

Phillip J. R. (1997) Windward diffusion. *Journal of Applied Meteorology* **36**, 974-977.

Phillips V. R., Bishop S. J., Price J. S. and You S. (1998) Summer emissions of ammonia from a slurry based, UK, dairy house. *Bioscience Technology* 65, 213-219.

Pitcairn C. E. R., Leith I. D., Sheppard L. J., Sutton M. A., Fowler D., Munro R. C., Tang S. and Wilson D. (1998) The relationship between nitrogen deposition, species composition and foliar nitrogen concentrations in woodland flora in the vicinity of livestock farms. *Environmental Pollution* 102, 41-48.

Porter L. K., Viets F. G. jnr, and Hutchinson G. L. (1972) Air containing nitrogen-15 ammonia: Foliar absorption by corn seedlings. *Science* 175, 759-761.

Raupach M. R. and Legg B. J. (1984) The uses and limitations of flux-gradient relationships in micrometeorology. *Agricultural Water Management* 8, 119-131.

RGAR (1997) Acid deposition in the United Kingdom: Fourth report of the review group on acid rain. Department of the Environment, UK.

Robins A., Carruthers D. and McHugh C. (1997) The ADMS building effects module. *International Journal of Environment and Pollution* 8, 708-717.

Rodgers G. A. (1978) Dry deposition of atmospheric ammonia at Rothamsted in 1976 and 1977. *Journal of Agricultural Science, Cambridge* 90, 537-542.

Russell A. G., Winner D. A., Harley R. A., McCue K. F. and Cass G. R. (1993) Mathematical modelling and control of the dry deposition flux of nitrogen containing air pollutants. *Environmental Science and Technology* 27, 2772-2782.

Ryden J. C. and McNeill J. E. (1984) Application of the micrometeorological mass balance method to the determination of ammonia loss from a grazed sward. *Journal of the Science of Food and Agriculture* 35, 1297-1310.

Ryden J. C. and Lockyer D. R. (1985) Evaluation of a system of wind tunnels for field studies of ammonia loss from grassland through volatilisation. *Journal of the Science of Food and Agriculture* 36, 781-788.

Ryden J. C. (1986) Gaseous losses of nitrogen from grassland. In: *Nitrogen Fluxes in Intensive Grassland Systems* (edited by Van der Meer H. G., Ryden J. C. and Ennik G. C.), pp. 59-73. Martinus Nijhoff Publishers, Dordrecht.

Sapek A. (1997) Nitrogen balances in permanent grassland. In: *Gaseous Nitrogen Emissions from Grasslands* (edited by Jarvis S. C. and Pain B. F), pp. 391-395. CAB International.

Sargent G. P. (1980) Computation of vapour pressure, dew point, and relative humidity from dry and wet bulb temperatures. *Meteorological Magazine* 109, 238-246.

Schjoerring J. K., Kyllinsbaek A., Mortensen J. V. and Byskov-Nielsen S. (1993a) Field investigation of the exchange between barley plants and the atmosphere I: Concentration profiles and flux densities of ammonia. *Plant, Cell and Environment* **16**, 161-167.

Schjoerring J. K., Kyllinsbaek A., Mortensen J. V. and Byskov-Nielsen S. (1993b) Field investigation of the exchange between barley plants and the atmosphere. II. Nitrogen reallocation, free ammonium content and activities of ammonium-assimilating enzymes in different leaves. *Plant, Cell and Environment* **16**, 169-178.

Schneider T. and Heij B. J. (1990) Dutch priority program on acidification. Thematic report 200-07, RIVM Bilthoven, The Netherlands.

Searle P. L. (1984) The Berthelot or indophenol reaction and its uses in the analytical chemistry of nitrogen. *Analyst* **109**, 549-568.

Sievering H., Enders G., Kins L., Kramm G., Ruoss K., Roider G., Zelger M., Anderson L. and Dlugi R. (1994) Nitric acid, particulate nitrate and ammonium profiles at the Bayerischer wald: Evidence for large deposition rates of total nitrate. *Atmospheric Environment* **28**, 311-315.

Singles R., Sutton M. A. and Weston K. J. (1998) A multi-layer model to describe the atmospheric transport and deposition of ammonia in Great Britain. *Atmospheric Environment* **32**, 393-399.

Smith R. J. (1995) A Gaussian model for estimating odour emissions from area sources. *Mathematical Computer Modelling* **21**, 23-29.

Sommer S. G. (1988) A simple biomonitor for measuring ammonia deposition in rural areas. *Biology and Fertility of Soils* **6**, 61-64.

Sommer S. G. and Jensen E. S. (1991) Foliar absorption of atmospheric ammonia by ryegrass in the field. *Journal of Environmental Quality* **20**, 153-156.

Sommer S. G. and Olesen J. E. (1991) Effects of dry matter content and temperature on ammonia loss from surface applied cattle slurry. *Journal of Environmental Quality* **20**, 679-683.

Sommer S. G., Olesen J. E. and Christensen B. T. (1991) Effects of temperature, wind speed, and air humidity on ammonia volatilisation from surface applied cattle slurry. *Journal of Agricultural Science, Cambridge* **117**, 91-100.

Sommer S. G., Christensen B. T., Nielsen N. E. and Schjorring J. K. (1993a) Ammonia volatilisation during storage of cattle and pig slurry: Effects of surface cover. *Journal of Agricultural Science, Cambridge* **121**, 63-71.

246

Sommer S. G., Jensen E. S. and Schjorring J. K. (1993b) Leaf absorption of atmospheric ammonia emitted from pig slurry beneath the canopy of winter wheat. *Acta Agriculturæ Scandinavica Section B: Soil and Plant Science* 43, 21-24.

Sommer S. G., Mikkelsen H. and Mellqvist J. (1995) Evaluation of meteorological techniques for measurements of ammonia loss from pig slurry. *Agricultural and Forest Management* 74, 169-179.

Sommer S. G. (1997) Ammonia volatilisation from farm tanks containing anaerobically digested animal slurry. *Atmospheric Environment* 31, 863 – 868.

Sommer S. G., Friis E., Bach A. and Schorring J. K. (1997) Ammonia volatilisation from pig slurry applied with trail hoses or broadspread to winter wheat: Effects of crop developmental stage, microclimate and leaf ammonia absorption. *Journal of Environmental Quality* 26, 1153-1160.

Speirs R. B. and Frost C. A. (1987) The enhanced acidification of a field soil by very low concentrations of atmospheric ammonia. *Research and Development in Agriculture* 4, 83-86.

Sutton M. A. (1990) The surface atmosphere exchange of ammonia. PhD thesis, University of Edinburgh.

Sutton M. A., Dragosits U., Tang Y. and Fowler D. (2000) Ammonia emissions from non-agricultural sources in the UK. *Atmospheric Environment* 34, 855-869.

Sutton M. A., Monocrieff J. B. and Fowler D. (1992) Deposition of atmospheric ammonia on moorlands. *Environmental Pollution* 75, 15-24.

Sutton M. A., Fowler D., Hargreaves K. and Storeton-West R. L. (1993a) Interaction between NH$_3$ and SO$_2$ exchange inferred from simultaneous flux measurements over a wheat canopy. In: *General Assessment of Biogenic Emissions and Deposition of Nitrogen Compounds, Sulphur Compounds and Oxidants in Europe. Proceedings of the Joint CEC/ BIATEX Workshop.* Commission for European Communities, Brussels.

Sutton M. A., Fowler D. and Moncrieff J. B. (1993b) The exchange of atmospheric ammonia with vegetated surfaces. I: Unfertilised vegetation. *Quarterly Journal of the Royal Meteorological Society* 119, 1023-1045.

Sutton M. A., Fowler D., Storeton-West R. L. and Moncrieff J. B. (1993c) The exchange of atmospheric ammonia with vegetated surfaces II: Fertilised vegetation. *Quarterly Journal of the Royal Meteorological Society* 119, 1047-1070.

Sutton M. A., Pitcairn C. E. R. and Fowler D. (1993d) The exchange of ammonia between the atmosphere and plant communities. *Advances in Ecological Research* 24, 301-392.

Sutton M. A., Asman W. A. H. and Schjorring J. K. (1994) Dry deposition of reduced nitrogen. *Tellus* 46B, 255-273.

Sutton M. A., Place C. J., Eager M., Fowler D. and Smith R. I. (1995) Assessment of the magnitude of ammonia emissions in the United Kingdom. *Atmospheric Environment* **29**, 1393-1411.

Sutton M. A., Milford C., Dragosits U., Singles R., Fowler D., Ross C., Hill R., Jarvis S. C., Pain B. F., Harrison R., Moss D., Webb J., Espenhahn S., Halliwell C., Lee D. S., Wyres G. P., Hill J. and ApSimon H. M. (1997a) Gradients of atmospheric ammonia concentrations and deposition downwind of ammonia emissions: First results of the ADEPT Burrington Moor Experiment. In: *Gaseous Nitrogen Emissions from Grasslands* (edited by Jarvis S. C. and Pain B. F), pp. 131-139. CAB international.

Sutton M. A., Milford C., Dragosits U., Place C. J., Singles R. J., Smith R. I., Pitcairn C. E. R., Fowler D., Hill J., Wilson K., Brassington D., ApSimon H. M., Hill R., Ross C., Jarvis S. C., Pain B. F., Phillips V. R., Harrison R., Moss D., Clarke A., Webb J., Espenhahn S. E., Dore C., Lee D. S., Hornung M., Howard D. C., Hall J., Dyke H., Emmett B. A. and Lowe J. (1997b) In: *Ammonia Distributions and Effects Project: Distributions, Deposition and Environmental Impacts of Ammonia Emitted by Agriculture. Volume 2: Annex to Final Report on WA0613 to MAFF.* Institute of Terrestrial Ecology, Edinburgh.

Sutton M. A., Perhue E., Fowler D., Storeton-West R. L., Cape J. N., Arends B. G. and Mols J. J. (1997c) Vertical distribution and fluxes of ammonia at Great Dun Fell. *Atmospheric Environment* **31**, 2615-2624.

Sutton M. A., Burkhardt J. K., Guerin D., Nemitz E. and Fowler D. (1998a) Development of resistance models to describe measurements of bi-directional ammonia surface-atmosphere exchange. *Atmospheric Environment* **32**, 473-480.

Sutton M. A., Milford C., Dragosits U., Place C. J., Singles R. J., Smith R. I., Pitcairn C. E. R., Fowler D., Hill J., ApSimon H. M., Ross C., Hill R., Jarvis S. C., Pain B. F., Phillips V. R., Harrison R., Moss D., Webb J., Espenhahn S. E., Lee D. S., Hornung M., Ullyett J., Bull K. R., Emmett B. A., Lowe J. and Wyres G. P. (1998b) Dispersion, deposition and impacts of atmospheric ammonia: Quantifying local budgets and spatial variability. *Environmental Pollution* **102**, 349-361.

Svensson L. (1994) A new dynamic chamber technique for measuring ammonia emissions from land-spread manure and fertilisers. *Acta Agriculturæ Scandinavica, Section B, Soil and Plant Science* **44**, 35-46.

Swierstra D., Smits M.C.J. and Kroodsma W. (1995) Ammonia volatilisation from cubicle houses for cattle with slatted and solid floors. *Journal of Agricultural Engineering Research* **62**, 127-132.

Thom A. S. (1975) Momentum, mass, and heat exchange of plant communities. In: *Vegetation and the Atmosphere* (edited by Monteith J. L.), pp 57-109. Academic Press, London.

Thompson R. B., Pain B. F. and Lockyer D. R. (1990) Ammonia volatilisation from cattle slurry following surface application to grassland I: Influence of mechanical separation, changes in chemical composition during volatilisation and the presence of the grass sward. *Plant and Soil* **125**, 109-117.

Thompson R. B., Pain B. F. and Rees Y. J. (1990b) Ammonia volatilisation from cattle slurry following surface application to grassland II: Influence of application rate, wind speed and applying slurry in narrow bands. *Plant and Soil* **125**, 119-128.

Tirabassi T., Tagliazucca M. and Zannetti P. (1986) KAPPA-G, A non-Gaussian plume dispersion model: Description and evaluation against tracer measurements. *Journal of the Air Pollution Control Association* **36**, 592-596.

Van Breemen N., Burrough P. A., Velthorst E. J., Van Dobben H. F., De Wit T., Ridder T. B. and Reijnders H. F. R. (1982) Soil acidification from atmospheric ammonium sulphate in forest canopy throughfall. *Nature* **299**, 548-550.

Van der Eerden L. J., Dueck Th. A., Berdowski J. J. M., Greven H. and Van Dobben H. F. (1991) Influence of NH_3 and $(NH_4)_2SO_4$ on heathland vegetation. *Acta Botanica Neerlandica* **40**, 281-296.

Van der Eerden L., De Vries W. and Van Dobben H. F. (1998) Effects of ammonia deposition on forests in the Netherlands. *Atmospheric Environment* **32**, 525-532.

Van Hove L. W. A., Adema E. H., Vredenberg W. J. and Pieters G. A. (1989) A study of the adsorption of NH_3 and SO_2 on leaf surfaces. *Atmospheric Environment* **23**, 1479-1486.

Van Hove L. W. A., Bossen M. E., Mensink M. G. J. and Van Kooten O. (1992) Physiological effects of long term exposure to low concentrations of NH_3, NO_2 and SO_2 on Douglas fir, (*Pseudodotsuga menziesii*). *Physiologia Plantarum* **86**, 559-567.

Van der Molen J., Van Faassen H. G., Leclerc M. Y., Vriesema R. and Chardon W. J. (1990a) Ammonia volatilisation from arable land after application of cattle slurry. 1 Field estimates. *Netherlands Journal of Agricultural Science* **38**, 145-158.

Van der Molen J., Beljarrs A. C. M., Chardon W. J., Jury W. A. and Van Faassen H. G. (1990b) Ammonia volatilisation from arable land after application of cattle slurry. 2. Derivation of a transfer model. *Netherlands Journal of Agricultural Science* **38**, 239-254.

Voorburg J. H. and Kroodsma W. (1992) Volatile emissions of the housing systems for cattle. *Livestock Production Science* **31**, 57-70.

Webb E. K. (1970) Profile relationships: The log linear range and extension to strong stability. *Quarterly Journal of the Royal Meteorological Society* **96**, 67-90.

Wells M., Bower K. N., Choularton T. W., Cape J. N., Sutton M. A., Storeton-West R. L., Fowler D., Wiedensohler A., Hansson H. C., Svenningsson B., Swietlicki E., Wendisch M., Jones B., Dollard G., Acker K., Berner A., Krisz C., Laj P., Facchini M. C. and Fuzzi S. (1997) The reduced nitrogen budget of an orographic cloud. *Atmospheric Environment* **31**, 2599-2614.

Wesley M. L. (1989) Parameterisation of surface resistances to gaseous dry deposition in regional scale numerical models. *Atmospheric Environment* **23**, 1293-1304.

Whitehead D. C. (1970) The role of nitrogen in grassland productivity: A review of information. Commonwealth Agricultural Bureau. Farnham Royal, Buckinghamshire, UK.

Whitehead D. C. and Lockyer D. R. (1987) The influence of the concentration of gaseous ammonia on its uptake by the leaves of Italian Ryegrass with and without an adequate supply of nitrogen to the roots. *Journal of Experimental Botany* **38**, 818-827.

Whitehead D. C. and Lockyer D. R. (1989) Decomposing grass herbage as a source of ammonia in the atmosphere. *Atmospheric Environment* **23**, 1867-1869.

Wieprecht W. (1987) Zum Schwefel-und Sticksoffu in der Volkswirtschaft der DDR. Dissertation, Academy of Sciences, Berlin.

Willems J. J. H. (1990) A passive monitor for measuring ammonia. In: *Proceedings of a Field Intercomparison Exercise on Ammonia Measurement, Organised by CEE and the CNR-institute, Rome 1990.* CEE-Air Pollution Research Report 37.

Wilson J. D., Thurtell G. W. and Kidd G. E. (1981a) Numerical simulation of particle trajectories in inhomogeneous turbulence, i: Systems with constant turbulent velocity scale. *Boundary Layer Meteorology* **21**, 295-313.

Wilson J. D., Thurtell G. W. and Kidd G. E. (1981b) Numerical simulation of particle trajectories in inhomogeneous turbulence, ii: Systems with variable turbulent velocity scale. *Boundary Layer Meteorology* **21**, 423-441.

Wilson J. D., Thurtell G. W., Kidd G. E. and Beauchamp E. G. (1982) Estimation of the rate of gaseous mass transfer from a surface source plot to the atmosphere. *Atmospheric Environment* **16**, 1861-1867.

Wilson J. D., Catchpoole V. R., Denmead O. T. and Thurtell G. W. (1983) Verification of a simple micrometeorological method for estimating the rate of gaseous mass transfer from the ground to the atmosphere. *Agricultural Meteorology* **29**, 183-189.

Wilson J. D. and Shum W. K. N. (1992) A re-examination of the integrated horizontal flux method for estimating volatilisation from circular plots. *Agricultural and Forest Meteorology* **57**, 281-295.

Wyres G. P., Otjes R. P., Vermeulen A. T., De Wild P. J. and Slanina J. (1992a) Measurement of vertical concentration gradients of ammonia by continuous-flow denuders. In: *Air Pollution Report 39* (edited by Angeletti G., Beilke S. and Slanina J.). CEC, Brussels.

Wyers G. P., Vermeulen A. T. and Slanina J. (1992b) Measurement of dry deposition of ammonia on a forest. *Environmental Pollution* **75**, 25-28.

Wyers G. P. and Erisman J. W. (1998) Ammonia exchange over coniferous forest. *Atmospheric Environment* **32**, 441-451.

Yamulki S., Harrison R. M. and Goulding K. W. T. (1996) Ammonia surface-exchanges above an agricultural field in southeast England. *Atmospheric Environment* **30**, 109-118.

Yeh G. T. and Huang C. H. (1975) Three dimensional air pollution modelling in the lower atmosphere. *Boundary Layer Meteorology* **9**, 381-390.

Yin Z. H., Kaiser W., Herber U. and Raven J. A. (1998) Effects of gaseous ammonia on intracellular pH values in leaves of C3 and C4 plants. *Atmospheric Environment* **32**, 539-544.

APPENDIX 1: DEVELOPMENT OF THE KATCH MODEL

A1.1   INTRODUCTION

Computer models were developed in the Visual Basic Applications Edition (VBAE) programming language supplied with Microsoft Excel. The use of this language enabled the models to use the Excel "front end" and to transfer data seamlessly with the other spreadsheets used for data analysis. The main computer model developed was the K-theory Atmospheric Transport and exCHange model (KATCH), detailed in Chapter 4. A module was also developed to allow the calculation of the influence of non-orthogonal wind angles on the source, the SOURCEGEO module. The computer code of both these modules is described and presented in this appendix.

A1.2   THE KATCH MODEL

The KATCH model reads input data and writes output data to and from the underlying Excel spreadsheet. Columns A-M of the spreadsheet are used to store model input data, as shown in Figure A1.1. The model input data codes are shown in Table A1.1.

When the KATCH code is executed a "Dialog box" is presented to the user, as shown in Figure A1.1. This box allows the user to specify the integration intervals used by the model and to specify the output vertical concentration profiles. The model runs though each row of input data in turn, writing output concentrations in columns N onwards. Where positive values of deposition velocity are specified, the model also outputs the depleted concentrations at the roughness height for each deposition integration interval. Information on the progression of the model run, and on the run duration is shown in the Excel "status bar" at the bottom of the screen. The KATCH models architecture is shown in Figure

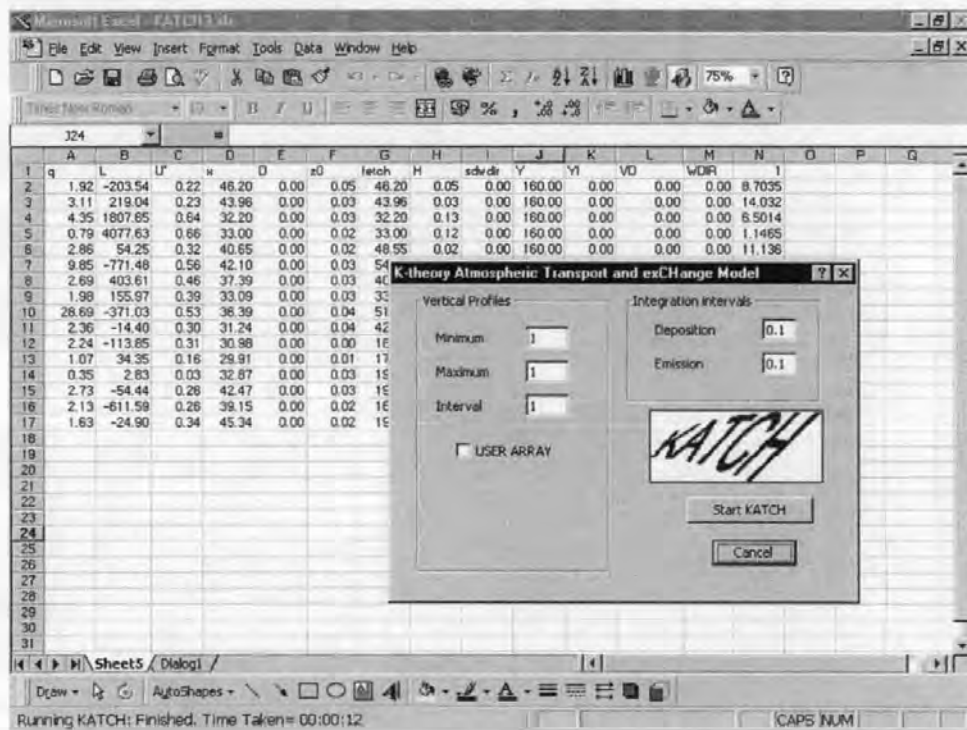A1.2. The model is compiled from 12 subroutines, three functions and two objects detailed in Table A1.2.

Figure A1.1: Screenshot showing the Microsoft Excel screen used by the KATCH model to read input data (colums A to M) and to write output data (column N onwards). The dialog box, used to define the vertical profiles and integration intervals, is also shown.

Model input	Data code	Units
Emission flux from source	Q	$\mu g\ m^{-2}\ s^{-1}$
Monin-Obukhov length	L	m
Friction velocity	U*	$m\ s^{-1}$
Downwind distance	x	m
Zero plane displacement height	D	m
Roughness length	z0	m
Source fetch	Fetch	m
Source height	H	m
Standard deviation of the wind direction	sdwdir	degrees
Source length	Y	m
Source centreline offset	Yi	m
Deposition velocity	Vd	$m\ s^{-1}$
Wind direction from centreline of source	WDIR	degrees

Table A1.1: Input data used by the KATCH model including the data code used to denote data within the model and the units of the data.
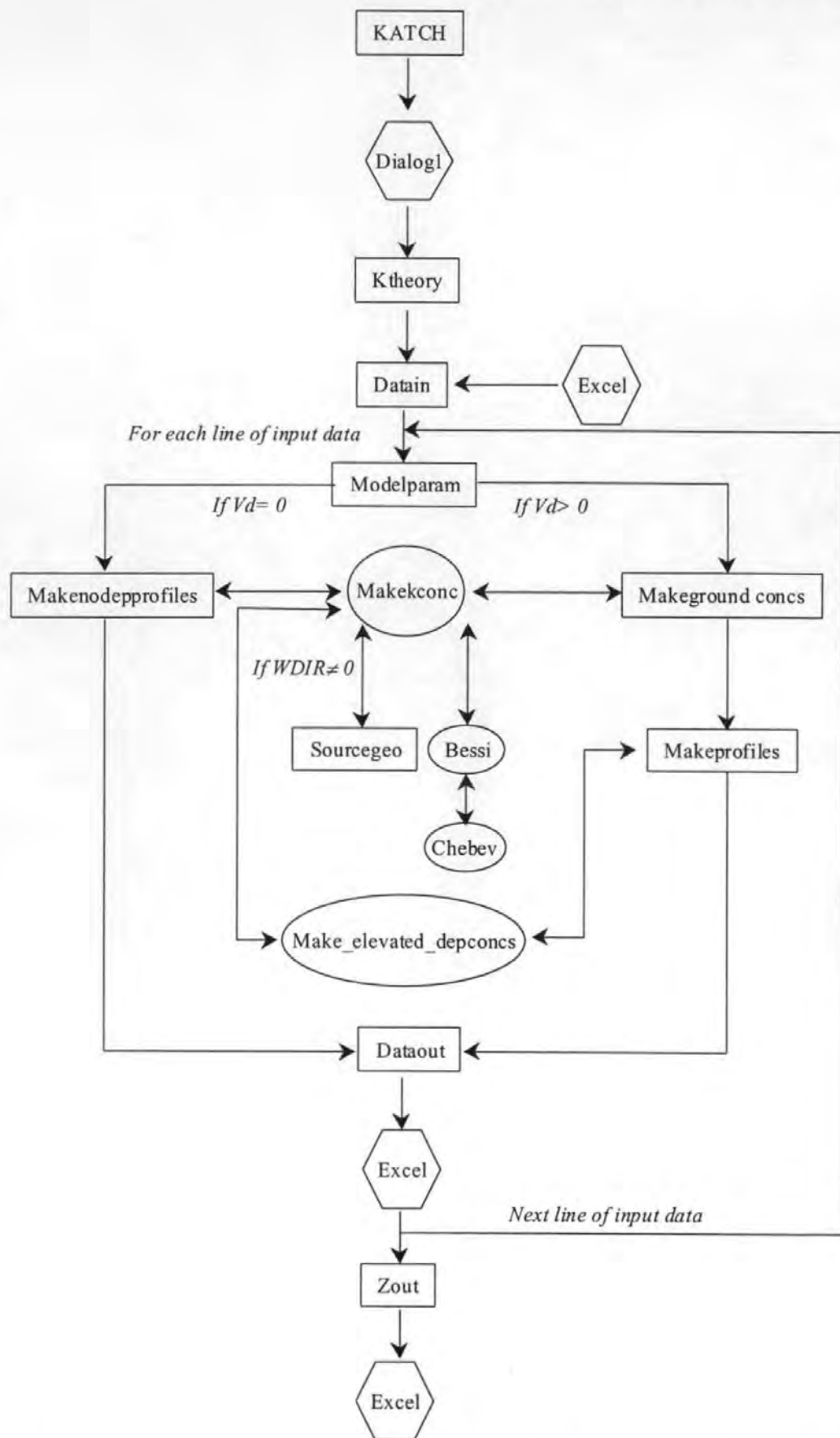
Figure A1.2: Architecture of the KATCH model. Subroutines shown as rectangles, functions shown as ovals and objects shown as hexagons.

Subroutine	Purpose
KATCH	Initial subroutine executed from Excel, shows the dialog box
Ktheory	Main program control subroutine executed from the dialog box, controls the calculation order and subroutine calls.
Datain	Determines the location and number of rows of input data, then reads input data into input arrays.
Modelparam	Calculates boundary layer parameters for use in the analytical K-theory function (Makekconc).
Makenodepprofiles	When the model is being run without deposition this subroutine is used to pass data to the Makekconc function and to collate the output air concentrations.
Makegroundconcs	When the model is being run with deposition, this module is used to determine the array of depleted ground level air concentrations.
Makeprofiles	When the model is being run with deposition, this module is used to determine the array of elevated depleted air concentrations.
Sourcegeo	If the wind direction from the centreline of the strip is greater than 0 then this module is used to determine the effect of wind direction changes on the downwind concentrations.
Dataout	Writes model results for each row of input data to the Excel spreadsheet.
Zout	When the model has processed all the input data this module writes the profile heights in row 1 of columns N onwards.
Function	
Makekconc	Calculates air concentrations according to the Huang (1979) analytical K-theory method.
Bessi	Modified Bessel function of the first kind and order -v (translated from FORTRAN to VBAE from Numerical recipes in Fortran: the art of scientific computing, 1992).
Chebev	Chebyshev evaluation of gamma functions used in Bessi (translated from FORTRAN to VBAE from Numerical recipes in Fortran: the art of scientific computing, 1992).
Make_elevated depconcs	Makes elevated depleted concentrations following the Horst (1977) surface depletion method.
Objects	
Dialog1	Dialog box used to define the vertical profiles and integration intervals used by the model.
Excel	Spreadsheet used to store input data and collate output data.

Table A1.2:   Subroutines, functions and objects used in the KATCH model.

A1.2   THE SOURCEGEO MODULE

The SOURCEGEO module was developed to simulate the edge effects caused by wind directions where the assumption that lateral dispersion was negligible could not be met. The conceptual method that SOURCEGEO was based on is described in Smith (1995) and discussed in Chapter 3, Section 3.2.1.1. The trigonometric expressions used in the KATCH

model were derived for this thesis as no suitable mathematical formulae were given by Smith (1995).

The SOURCEGEO solution was sub-divided into four separate calculations, as shown in Figure A1.3. Initially the wind aligned source width was calculated, shown as line *bd* in Section 1 of Figure A1.3. Line *bd* was calculated using Equation A1.1, with lines ac and *cd* being calculated from Equations A1.2 and A1.3 respectively, where Y is the strip length, X is the strip width and θ is the angle between the strip and the wind direction.
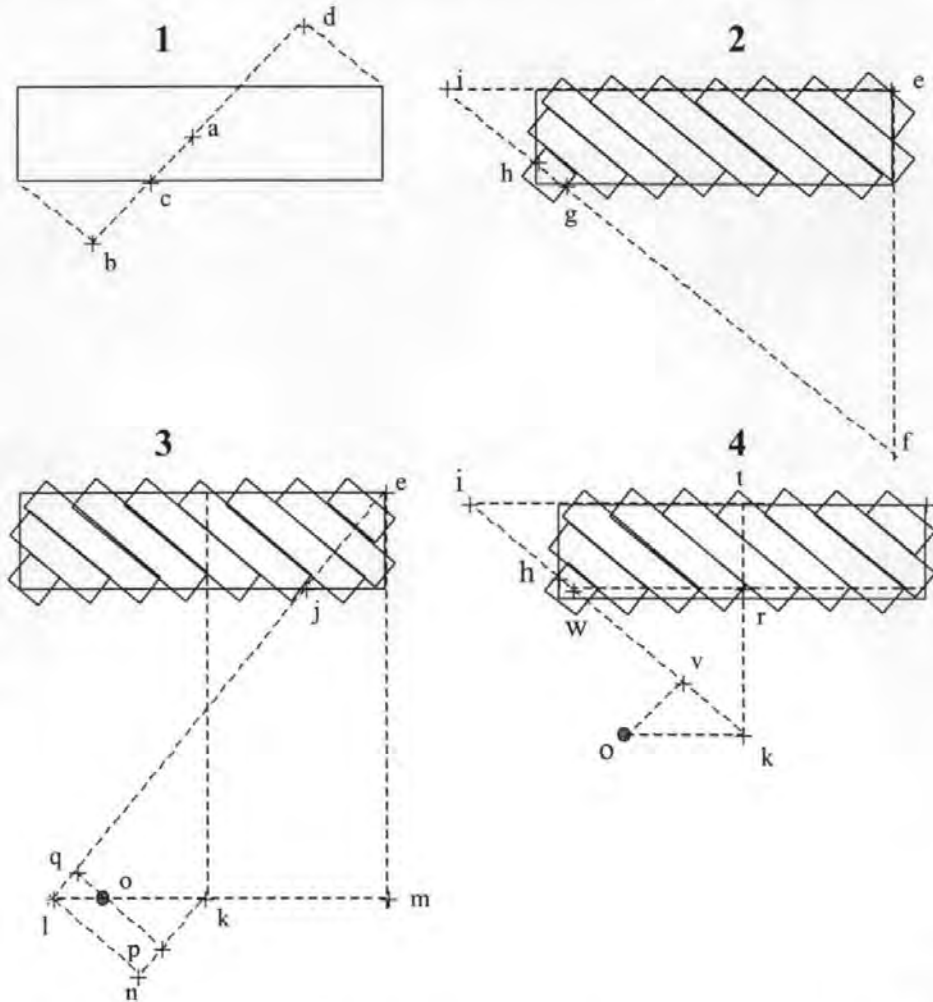

Figure A1.3: Diagram of the calculation sets used in the SOURCEGEO module. **1**: Determination of the wind aligned source width, **2**: Calculation of sub-strip widths (Y'), **3**: Calculation of maximum x' distance, **4**: Calculation of sub-strip lateral offsets (y').

$$bd = 2ac + 2cb \qquad\qquad \text{Equation A1.1}$$

$$ac = \frac{0.5Y}{\cos(\theta)} \qquad\qquad \text{Equation A1.2}$$

$$cb = [\sin(\theta)\, 0.5X] - [ac^2 - (0.5Y)^2]^{0.5} \qquad\qquad \text{Equation A1.3}$$

The number of sub-strips in the source (n) was calculated by subdividing the distance *bd* by the predefined width of the each sub-strip, termed x''. The length of each sub strip (Y', shown as line *gh* in Figure A1.3) was then determined, as shown in Figure A1.3, Section 2 where s is the sub-strip number, $s= 1$ being close to the upwind edge of the strip and $s= n$ being close to the downwind edge. Formulae to calculate Y' for each sub-strip are shown in Equations A1.4 to A1.8.

$$if \ s = 1, \ ef_s = \frac{s(0.5 \ x'')}{\cos(\theta)}, if \ s > 1 \ ef_s = \frac{(s + 0.5)(x'')}{\cos(\theta)}$$
Equation A1.4

$$fi_x = \frac{ef_s}{\sin(\theta)}$$
Equation A1.5

$$fg_s = \frac{ef_s - X}{\sin(\theta)}$$
Equation A1.6

$$hi_s = \frac{[fi_s \ \cos(\theta)] - Y}{\cos(\theta)}$$
Equation A1.7

$$Y'_s = gh_s = fi_s - fg_s - hi_s$$
Equation A1.8

Alongwind distances between each sub-strip and the receptor location (x') were determined following the determination of the wind aligned alongwind distance between the upwind corner of the strip (point *e*) and the receptor (line *el*). Line *el* was determined using Equations A1.9 to A1.15, where x is the physical distance between the downwind edge of the source and the receptor.

$$ej = \frac{X}{\cos(\theta)}$$
Equation A1.9

$$el = \frac{X + x}{\cos(\theta)}$$
Equation A1.10

$$ml = \sqrt{el^2 - (X + x)^2}$$
Equation A1.11

$$if \ ml < mk \ then \ kl = mk - ml, \ else \ kl = ml - mk$$
Equation A1.12

$$kn = kl \sin(\theta)$$
Equation A1.13

$$kp = ok \sin(\theta)$$
Equation A1.14

$$if \ ml < mk \ then \ eq = el + kn + kp, \ else \ eq = el - kn + kp$$
Equation A1.15

Alongwind distances from each sub-strip (x') were calculated using Equation A1.16.

$$if \ s = 1, \ x'_s = eq - (0.5x''), if \ s > 1 \ x'_s = eq - [(s + 0.5) x'']$$
Equation A1.16

The calculation of lateral offsets for each sub-strip (y') is illustrated in Figure A1.4, Section 4 by line *tk*. These positions are defined by Equations A1.17 to A1.21.

$$tr_s = (ih_s + 0.5hg_s)\sin(\theta)$$ Equation A1.17

$$rk_s = X - tr_s + x$$ Equation A1.18

$$wk_s = \frac{rk_s}{\sin(\theta)}$$ Equation A1.19

$$vk_s = \frac{x'_s}{\tan(\theta)}$$ Equation A1.20

$$y'_s = wv_s = wk_s - vk_s$$ Equation A1.21

A1.3   KATCH MODEL SOURCE CODE

```
Option Base 1

' *** Dimensionalise global (shared) variables ***
Dim ustar()
Dim d()
Dim z0()
Dim wdir()
Dim L()
Dim HE()
Dim emis()
Dim XMEAS()
Dim sdwdirMEAS()
Dim fetch()
Dim ypos()
Dim yi()
Dim VD()
Dim sdwdir()
Dim ZPRO
Dim KCONC()
Dim DEPCONCFROMSOURCE()
Dim KOUT()
Dim slcsg(), newxsg(), newysg(), nnnxsg, COUNTERSG As Double
Dim alpha, beta, lamda, v, Y, N, r, p, q, h0, U0, kz0, XINT, consa, consb, NZPRO, Time As Double
Dim rowcount, IT, nkout As Integer
Dim stepc, mult, stepdep, maxh, interval, startint As Single


'*** Main program control function ***
Sub KATCH ()
If DialogSheets(1).Show Then
ktheory
End If
End Sub


'*** Top level calculation subroutine for running the model ***
Private Sub ktheory()
stepc = CDbl(DialogSheets(1).EditBoxes(5).Text)
stepdep = CDbl(DialogSheets(1).EditBoxes(4).Text)

If DialogSheets(1).CheckBoxes(1).Value > 0 Then

'*** Code to allow the user to enter measurements heights ***
'*** NZPRO: number of heights ZPRO: Value of height ***
NZPRO = 8
ZPRO = Array(0.2, 0.45, 0.953, 1.93, 2.87, 3.89, 4.9, 5.9)
```

```
'*** Else calculate z heights ***
Else
maxh = CDbl(DialogSheets(1).EditBoxes(1).Text)
interval = CDbl(DialogSheets(1).EditBoxes(2).Text)
startint = CDbl(DialogSheets(1).EditBoxes(3).Text)
nkout = ((maxh + interval) - startint) / interval
End If

'*** Update status bar with message and note the start time of the calculations ***
gtime = Now
Application.DisplayStatusBar = True
Application.StatusBar = "Running KATCH: Reading Data"

'*** Run subroutine to read input data ***
datain

'*** Run each set of input data through the model and output results***
For IT = 1 To rowcount

'*** Array counter to update user on calculation progression ***
perleft = Int((IT - 1) / rowcount * 100)
Application.StatusBar = "Running KATCH: Processing data " + CStr(perleft) + "% Complete"

'*** Run subroutine to parameterise the boundary layer ***
modelparam

'*** Determine whether to include deposition and run relevant subroutines***
If VD(IT) > 0 Then
MAKEGROUNDCONCS
MAKEPROFILES
Else
makenodeprofiles
End If

'*** Output calculation results***
dataout

'***Calculate next set of data ***
Next IT

'*** Update the status bar with the duration of the run ***
Dim ntime As Double
ntime = Now
timetaken = (ntime - gtime)
Application.StatusBar = "Running KATCH: Finished. Time Taken= " + CStr(timetaken)

'*** Write the measurement heights to the spreadsheet ***
zout
End Sub

'***Subroutine handing input data ***
Private Sub datain()

Dim VBIG, irowcount, ITROW, USTARCOL, DCOL, LCOL, HECOL, EMISCOL As Integer
Dim XMEASCOL, sdwdirCOL, FETCHCOL, Z0COL, ycol, yicol As Integer

'*** constants ****
rowcount = 0
VBIG = 100000

'*** autodetection of columns ***
USTARCOL = Application.Match("U*", Range(Cells(1, 1), Cells(1, 20)), 0)
DCOL = Application.Match("d", Range(Cells(1, 1), Cells(1, 20)), 0)
```

```
LCOL = Application.Match("l", Range(Cells(1, 1), Cells(1, 20)), 0)
HECOL = Application.Match("h", Range(Cells(1, 1), Cells(1, 20)), 0)
EMISCOL = Application.Match("Q", Range(Cells(1, 1), Cells(1, 20)), 0)
XMEASCOL = Application.Match("x", Range(Cells(1, 1), Cells(1, 20)), 0)
sdwdirCOL = Application.Match("sdwdir", Range(Cells(1, 1), Cells(1, 20)), 0)
FETCHCOL = Application.Match("fetch", Range(Cells(1, 1), Cells(1, 20)), 0)
Z0COL = Application.Match("Z0", Range(Cells(1, 1), Cells(1, 20)), 0)
yposcol = Application.Match("y", Range(Cells(1, 1), Cells(1, 20)), 0)
yicol = Application.Match("yi", Range(Cells(1, 1), Cells(1, 20)), 0)
VDCOL = Application.Match("VD", Range(Cells(1, 1), Cells(1, 20)), 0)
wdircol = Application.Match("wdir", Range(Cells(1, 1), Cells(1, 20)), 0)

'*** Error handling ***
If Not IsNumeric(USTARCOL) Then
MsgBox ("U* not found")
GoTo 10
ElseIf Not IsNumeric(DCOL) Then
MsgBox ("d not found")
GoTo 10
ElseIf Not IsNumeric(LCOL) Then
MsgBox ("L not found")
GoTo 10
ElseIf Not IsNumeric(HECOL) Then
MsgBox ("H not found")
GoTo 10
ElseIf Not IsNumeric(EMISCOL) Then
MsgBox ("Q not found")
GoTo 10
ElseIf Not IsNumeric(XMEASCOL) Then
MsgBox ("x not found")
GoTo 10
ElseIf Not IsNumeric(sdwdirCOL) Then
MsgBox ("sdwdir not found")
GoTo 10
ElseIf Not IsNumeric(FETCHCOL) Then
MsgBox ("fetch not found")
GoTo 10
ElseIf Not IsNumeric(Z0COL) Then
MsgBox ("Z0 not found")
GoTo 10
ElseIf Not IsNumeric(yposcol) Then
MsgBox ("y not found")
ElseIf Not IsNumeric(yicol) Then
MsgBox ("yi not found")
GoTo 10
ElseIf Not IsNumeric(VDCOL) Then
MsgBox ("VD not found")
GoTo 10
ElseIf Not IsNumeric(wdircol) Then
MsgBox ("wdir not found")
GoTo 10
End If

'*** Counting number of rows ***
For ITROW = 2 To VBIG
If IsEmpty(Cells(ITROW, USTARCOL)) Then GoTo 1
rowcount = rowcount + 1
Next ITROW

'*** Create input arrays ***
1 ReDim ustar(rowcount)
ReDim d(rowcount)
ReDim z0(rowcount)
ReDim L(rowcount)
```

```
ReDim HE(rowcount)
ReDim emis(rowcount)
ReDim XMEAS(rowcount)
ReDim sdwdir(rowcount)
ReDim fetch(rowcount)
ReDim ypos(rowcount)
ReDim yi(rowcount)
ReDim KCONC(rowcount)
ReDim VD(rowcount)
ReDim wdir(rowcount)

'*** Fill input arrays ***
For irowcount = 1 To rowcount
ustar(irowcount) = Cells(irowcount + 1, USTARCOL)
d(irowcount) = Cells(irowcount + 1, DCOL)
z0(irowcount) = Cells(irowcount + 1, Z0COL)
L(irowcount) = Cells(irowcount + 1, LCOL)
HE(irowcount) = Cells(irowcount + 1, HECOL)
emis(irowcount) = Cells(irowcount + 1, EMISCOL)
XMEAS(irowcount) = Cells(irowcount + 1, XMEASCOL)
sdwdir(irowcount) = Cells(irowcount + 1, sdwdirCOL)
fetch(irowcount) = Cells(irowcount + 1, FETCHCOL)
ypos(irowcount) = Cells(irowcount + 1, yposcol)
yi(irowcount) = Cells(irowcount + 1, yicol)
VD(irowcount) = Cells(irowcount + 1, VDCOL)
wdir(irowcount) = Cells(irowcount + 1, wdircol)
Next irowcount

10 End Sub

'*** Subroutine to calculate boundary layer parameters ***
Private Sub modelparam()

'*** Reference height for u and Kz profiles (in cm) ***
proh = 100

'*** Dimensionalise variables ***
Dim kx()
ReDim kz(proh)
Dim u()
ReDim u(proh)
Dim z()
ReDim z(proh)
Dim vsmall, k, phih, phimx, phim, intwsp, tempintwsp As Double
Dim intbzp, tempintbzp, ubar, XINT As Double
Dim i2 As Integer

'*** Read Constants***
k = 0.41

'*** Create vertical height profile ***
Start = 0.01 + z0(IT) + d(IT)
z(1) = Start
For ZIPROFILE = 2 To proh
z(ZIPROFILE) = z(ZIPROFILE - 1) + 0.01
Next ZIPROFILE

'*** Generate wind speed and kz profiles ***
For i = 1 To proh Step 1

'*** Calculate stability correction factors***
If L(IT) < 0 Then
phih = (1 - (16 * ((z(i) - d(IT) / L(IT)))) ^ -0.5
phimx = (1 - (16 * ((z(i) - d(IT) / L(IT)))) ^ 0.25
```

```
phim = 2 * Log((1 + phimx) / 2) + Log((1 + phimx ^ 2) / 2) - 2 * Atn(phimx) + Application.Pi() / 2
ElseIf L(IT) > 0 Then
phih = 1 + (5.2 * ((z(i) - d(IT)) / L(IT)))
phim = -5.2 * ((z(i) - d(IT)) / L(IT))
End If

'*** Calculate wind speed ***
u(i) = (ustar(IT) / k) * (Log(z(i) - d(IT)) - phim) - ((ustar(IT) / k) * Log(z0(IT)))

'*** Calculate eddy diffusivity***
kz(i) = (k * ustar(IT) * (z(i) - d(IT))) / phih

Next i

'integrate wind speed  and Kz profiles
intwsp = 0
tempintwsp = 0
intKzp = 0
tempintKzp = 0

For i2 = 1 To proh
If i2 = 1 Then
   tempintwsp = z(i2) * u(i2) * 0.5
   tempintKzp = z(i2) * kz(i2) * 0.5
   GoTo 100
End If

   tempintwsp = (z(i2) - z(i2 - 1)) * ((u(i2) + u(i2 - 1)) / 2)
   tempintKzp = (z(i2) - z(i2 - 1)) * ((kz(i2) + kz(i2 - 1)) / 2)
100 intwsp = intwsp + tempintwsp
   intKzp = intKzp + tempintKzp
Next i2

'** Calculate model parameterisations of wsp and kzp
ubar = intwsp * (1 / z(proh))
KZBAR = intKzp * (1 / z(proh))
alpha = (u(proh) - ubar) / ubar
beta = (kz(proh) - KZBAR) / KZBAR
lamda = alpha - beta + 2
v = (1 - beta) / lamda
r = beta - alpha
p = (1 - beta) / 2
q = lamda / 2
h0 = (z(proh))
U0 = u(proh)
kz0 = kz(proh)

'*** Calculate Consa for sigma Y term ***
If L(IT) < 0 And -L(IT) <= 8 Then consa = 0.22
If L(IT) < 0 And (-L(IT) <= 16 And -L(IT) > 8) Then consa = 0.16
If L(IT) < 0 And (-L(IT) <= 66 And -L(IT) > 16) Then consa = 0.11
If L(IT) < 0 And -L(IT) > 66 Then consa = 0.08
If L(IT) >= 66 Then consa = 0.08
If L(IT) > 0 And (L(IT) <= 66 And L(IT) > 14) Then consa = 0.06
If L(IT) > 0 And L(IT) <= 14 Then consa = 0.04
End Sub

'*** Main dispersion calculation subroutine ***
Private Function makekconc(XCONC, ZCONC, HECONC, FETCHCONC, YICONC, YPOSCONC,
wdirconc, stepk)

'*** Error handler***
On Error GoTo 1011
```

```
'*** Dimensionalise variables ***
Dim mod1, mod2, mod2a, mod3, mod3a, KCONCTEMP, KCONCT2 As Double

'*** Determine whether to use sourcegeo subroutine***
If wdirconc <= 0 Then GoTo 3

'*** Run sourcegeo ***
sourcegeo YPOSCONC, FETCHCONC, XCONC, YICONC, wdirconc

'*** Set integration interval to 1
stepk = 1

'*** Integrate the dispersion calculations across the source width ***
For XINT = 1 To COUNTERSG

'*** Calculate sigma-Y
sigmay1 = consa * newxsg(XINT) * (1 + 0.0001 * newxsg(XINT)) ^ -0.5
syw = Application.Radians(sdwdir(IT)) * newxsg(XINT)
sigmay = Sqr(sigmay1 ^ 2 + syw ^ 2)

'*** Main dispersion code ***
mod1 = (emis(IT) * (ZCONC * HECONC) ^ p * h0 ^ beta) / (lamda * kz0 * (newxsg(XINT)))
mod2 = (U0 * h0 ^ r * (ZCONC ^ lamda + HECONC ^ lamda)) / (lamda ^ 2 * kz0 * (newxsg(XINT)))
mod2a = Exp(-mod2)
mod3 = (2 * U0 * h0 ^ r * (ZCONC * HECONC) ^ q) / (lamda ^ 2 * kz0 * (newxsg(XINT)))

'*** Call the Bessel function ***
mod3a = bessi(mod3, -v)

'*** Include lateral dispersion***
MOD4 = (newysg(XINT) + (slcsg(XINT) / 2)) / (Sqr(2) * (sigmay))
MOD5 = (newysg(XINT) - (slcsg(XINT) / 2)) / (Sqr(2) * (sigmay))

    If MOD4 < 0 And MOD4 > -5 Then mod6 = -erf(-MOD4)
    If MOD4 > 0 And MOD4 < 5 Then mod6 = erf(MOD4)
    If MOD4 > 5 Then mod6 = 1
    If MOD4 < -5 Then mod6 = -1
    If MOD5 < 0 And MOD5 > -5 Then mod7 = -erf(-MOD5)
    If MOD5 > 0 And MOD5 < 5 Then mod7 = erf(MOD5)
    If MOD5 > 5 Then mod7 = 1
    If MOD5 < -5 Then mod7 = -1

'*** Calculate concentrations***
KCONCTEMP = mod1 * mod2a * mod3a * ((mod6 - mod7) / 2)

'*** Integrate concentrations across source***
KCONCT2 = KCONCTEMP + KCONCT2
Next XINT

'*** If SOURCEGEO is not required run this calculation***
GoTo 4

3 For XINT = XCONC To XCONC + FETCHCONC Step stepk

sigmay1 = consa * XINT * (1 + 0.0001 * XINT) ^ -0.5
syw = Application.Radians(sdwdir(IT)) * XINT
sigmay = Sqr(sigmay1 ^ 2 + syw ^ 2)
mod1 = (emis(IT) * ((ZCONC * HECONC) ^ p) * (h0 ^ beta)) / (lamda * kz0 * XINT)
mod2 = (U0 * h0 ^ r * (ZCONC ^ lamda + HECONC ^ lamda)) / (lamda ^ 2 * kz0 * XINT)
mod2a = Exp(-mod2)
mod3 = (2 * U0 * h0 ^ r * (ZCONC * HECONC) ^ q) / (lamda ^ 2 * kz0 * XINT)
mod3a = bessi(mod3, -v)

If VD(IT) = 0 Then
```

263

```
MOD4 = (YICONC + (YPOSCONC / 2)) / (Sqr(2) * (sigmay))
MOD5 = (YICONC - (YPOSCONC / 2)) / (Sqr(2) * (sigmay))

    If MOD4 < 0 And MOD4 > -5 Then mod6 = -erf(-MOD4)
    If MOD4 > 0 And MOD4 < 5 Then mod6 = erf(MOD4)
    If MOD4 > 5 Then mod6 = 1
    If MOD4 < -5 Then mod6 = -1
    If MOD5 < 0 And MOD5 > -5 Then mod7 = -erf(-MOD5)
    If MOD5 > 0 And MOD5 < 5 Then mod7 = erf(MOD5)
    If MOD5 > 5 Then mod7 = 1
    If MOD5 < -5 Then mod7 = -1
Else
mod6 = 1
mod7 = -1
End If


KCONCTEMP = mod1 * mod2a * mod3a * ((mod6 - mod7) / 2)
KCONCT2 = KCONCTEMP + KCONCT2
Next XINT
GoTo 4


1011 KCONCT2 = 0

4 makekconc = KCONCT2 * stepk



End Function


'*** Calculate ground level depleted concentrations **
Private Sub MAKEGROUNDCONCS()

'***Create arrays for ground level functions ***
Dim CONCFROMSOURCE()
ReDim CONCFROMSOURCE((XMEAS(IT) / stepdep) + 1)
Dim CONCFROMSINK()
ReDim CONCFROMSINK((XMEAS(IT) / stepdep) + 1)
ReDim groundconc((XMEAS(IT) / stepdep) + 1)
ReDim DEPCONCFROMSOURCE((XMEAS(IT) / stepdep) + 1)

mult = stepdep

'*** Set inital value of downwind surface concentration from the slurry ***
CONCFROMSOURCE(1) = makekconc(0.075, z0(IT), HE(IT), fetch(IT), yi(IT) + yposoff, ypos(IT),
wdir(IT), stepc)


'*** Fill arrays with source and sink concentrations ***
For iin = 1 To (XMEAS(IT) / stepdep)
xposoff = (XMEAS(IT) - (iin * stepdep))
CONCFROMSOURCE(iin + 1) = makekconc(xposoff, z0(IT), HE(IT), fetch(IT), yi(IT) + yposoff, ypos(IT),
wdir(IT), stepc)
CONCFROMSINK(iin) = makekconc(xposoff, z0(IT), z0(IT), 0, yi(IT), ypos(IT), 0, 1) / emis(IT)
Next iin

'*** Calculate first integral from Horst (1977)***
For idep = 1 To (XMEAS(IT) / stepdep)
If idep = 1 Then
DEPCONCFROMSOURCE(1) = CONCFROMSOURCE(1)
GoTo 1
End If

    For depsumint = 1 To idep - 1
    depsumtemp = DEPCONCFROMSOURCE(depsumint) * CONCFROMSINK(idep - depsumint)
```

264

```
        depsum = depsum + depsumtemp
      Next depsumint


DEPCONCFROMSOURCE(idep) = CONCFROMSOURCE(idep) - (depsum * VD(IT) * mult)

depsum = 0
depsumtemp = 0

1 Next idep

End Sub

'*** Use ground level concentrations to calculate concs at z height ***
'*** NOTE: run as a function from within MAKEPROFILES subroutine ***
Private Function MAKE_ELEVATED_DEPCONCS(z)

Dim DFE()
ReDim DFE(XMEAS(IT) / stepdep)

'*** calculate non depleted concentration ***
ELEVATEDCONCFROMSOURCE = makekconc(XMEAS(IT), z, HE(IT), fetch(IT), yi(IT), ypos(IT),
wdir(IT), stepc)

'*** Perform second integration from Horst (1977) ***
totalxd = XMEAS(IT)
For dfeiN = 1 To (XMEAS(IT) / stepdep)
yposoffd = 0
XPOSOFFD = (dfeiN * stepdep)
DFE(dfeiN) = makekconc(XPOSOFFD, z, HE(IT), 0, yi(IT), ypos(IT), 0, 1) / emis(IT)
Next dfeiN

Sum = 0
SUMTEMP = 0

For iedep = 1 To (XMEAS(IT) / stepdep) - 1
SUMTEMP = DEPCONCFROMSOURCE(iedep) * DFE((XMEAS(IT) / stepdep) - iedep)
Sum = Sum + SUMTEMP
SUMTEMP = 0
Next iedep

MAKE_ELEVATED_DEPCONCS = ELEVATEDCONCFROMSOURCE - ((Sum) * VD(IT) * mult)

End Function


'*** Main subroutine for the calculation of vertical concentration profiles ***
Private Sub MAKEPROFILES()

'*** Determine whether to use input or calculated z heights ***
If DialogSheets(1).CheckBoxes(1).Value < 0 Then
ReDim KOUT(nkout)
i = 1
ZIN = startint

'*** Run the MAKE_ELEVATED_DEPCONCS subroutine with calculated z heights***
Do While Not ZIN > maxh
KOUT(i) = MAKE_ELEVATED_DEPCONCS(ZIN)
i = i + 1
ZIN = Application.Round(ZIN + interval, 5)
Loop

Else

'*** Run MAKE_ELEVATED_DEPCONCS function with inputted z heights***
```

```
nkout = NZPRO
ReDim KOUT(nkout)

  For i = 1 To nkout
  KOUT(i) = MAKE_ELEVATED_DEPCONCS(ZPRO(i))
  Next i

End If

End Sub

' *** Subroutine to calculate concentrations profiles without deposition ***
Private Sub makenodeprofiles()

'*** Determine whether program is being run with inputted or calculated z data ***
If DialogSheets(1).CheckBoxes(1).Value < 0 Then

'*** Running with calculated z data ***
ReDim KOUT(nkout)
i = 1
ZIN = startint
Do While Not ZIN > maxh
KOUT(i) = makekconc(XMEAS(IT), ZIN, HE(IT), fetch(IT), yi(IT), ypos(IT), wdir(IT), stepc)
i = i + 1
ZIN = Application.Round(ZIN + interval, 5)
Loop

Else

'*** Running with inputted z-data ***
nkout = NZPRO
ReDim KOUT(nkout)

For i = 1 To nkout
KOUT(i) = makekconc(XMEAS(IT), ZPRO(i), HE(IT), fetch(IT), yi(IT), ypos(IT), wdir(IT), stepc)
Next i

End If
End Sub

'*** Subroutine to write model output to the spreadsheet ***
Private Sub dataout()

'*** Write concentration profile ***
For i = 1 To nkout
Cells((IT + 1), 13 + i).Value = KOUT(i)
Next i

'*** Write surface concentrations ***
If VD(IT) > 0 Then
IIGROUND = 1
For iground = 1 To (XMEAS(IT) / stepdep) - 1
Cells(1 + IIGROUND, IT + 20 + nkout).Value = DEPCONCFROMSOURCE(iground)
IIGROUND = IIGROUND + 1
Next iground
Else
GoTo 1
End If

1 End Sub

'*** Write z heights to the spreadsheet ***
Private Sub zout()
```

```
'*** Zcell= number of columns into the spreadsheet to start output***
ZCELL = 14

'*** Write calculated z heights ***
If DialogSheets(1).CheckBoxes(1).Value < 0 Then
For ZZZ = startint To maxh Step interval
Cells(1, ZCELL).Value = ZZZ
ZCELL = ZCELL + 1
Next ZZZ

Else

'*** Write inputted z heights ***
For ZZZ = 1 To NZPRO
Cells(1, ZCELL).Value = ZPRO(ZZZ)
ZCELL = ZCELL + 1
Next ZZZ

End If
End Sub


'

'Sourcegeo
'

Sub sourcegeo(lsg, wsg, xsg, ysg, wdirsg)

If wdirsg < 0 Then
wdirsg = -wdirsg
ysg = -ysg
End If

Pi = Application.Pi()
COUNTERSG = 0
tanwd = Tan(wdirsg * Pi / 180)
sinwd = Sin(wdirsg * Pi / 180)
coswd = Cos(wdirsg * Pi / 180)

'number of strips to use

asg = wsg / 2
csg = asg / coswd
bsg = Sqr(csg ^ 2 - asg ^ 2)
dsg = (lsg / 2) - bsg
esg = sinwd * dsg
CROSS = 2 * csg + 2 * esg
linew = 1

NSG = Application.RoundUp((CROSS / linew), 0)

'CALCULATION OF STRIP LENGTHS
ReDim slcsg(NSG)
Dim corr2sg() As Double
ReDim corr2sg(NSG)

ndynsg = 1
For itsg = 1 To NSG Step 1
   hnsg = ((linew / 2) * ndynsg) / coswd
   slsg = hnsg / sinwd
   tlsgg = slsg * coswd
     If hnsg > wsg + 1 Then
     corr1sg = (hnsg - wsg) / sinwd
       Else
     corr1sg = 0
```

```
        End If
    If tlsgg > lsg Then
        corr2sg(itsg) = (tlsgg - lsg) / coswd
    Else
        corr2sg(itsg) = 0
    End If

If (slsg - corr1sg - corr2sg(itsg)) > 1 Then
slcsg(itsg) = slsg - corr1sg - corr2sg(itsg)
Else
slcsg(itsg) = 0.001
End If

ndynsg = ndynsg + 2

Next itsg

'Calculation of xsg max

a2sg = wsg / coswd
b2sg = Sqr(a2sg ^ 2 - wsg ^ 2)
c2sg = (xsg + wsg) / coswd
d2sg = c2sg - a2sg
e2sg = Sqr(c2sg ^ 2 - (wsg + xsg) ^ 2)

If e2sg < lsg / 2 Then
f2sg = (lsg / 2) - e2sg
Else
f2sg = e2sg - (lsg / 2)
End If

g2sg = f2sg * sinwd
i2sg = ysg * sinwd

If e2sg > lsg / 2 Then
maxxsg = a2sg + d2sg - g2sg + i2sg
Else
maxxsg = a2sg + d2sg + g2sg + i2sg
End If

maxxsg = Application.RoundUp(maxxsg, 1)
nnnxsg = CInt(maxxsg / linew)


'calculation of newxsg


ReDim newxsg(NSG + 1)
ixsg = 1
For inewxsg = 1 To NSG
    newxsg(inewxsg) = maxxsg - ((linew / 2) * ixsg)
    ixsg = ixsg + 2
If Not newxsg(inewxsg) <= 0 Then COUNTERSG = COUNTERSG + 1

Next inewxsg

'calculation of newysg

ReDim newysg(NSG)

For inewYsg = 1 To NSG
a3sg = ((slcsg(inewYsg) / 2) + corr2sg(inewYsg)) * sinwd
b3sg = wsg - a3sg
z3sg = b3sg + xsg
```

```
c3sg = z3sg / sinwd
d3sg = newxsg(inewYsg) / tanwd
newysg(inewYsg) = c3sg - d3sg
Next inewYsg

End Sub


'
'modified bessel function
'
Function bessi(x, XNU)

Dim MAXIT As Integer
Dim ri, rip, rk, rkp, xmin As Double
Dim eps, fpmin, Pi As Double
Dim i, L, nl As Integer
Dim a, a1, b, c, d, del, del1, delh, dels, e, f, Fact, fact2, ff, gam1, gam2, gammi, gamp1, h, p, pimu, q, q1, q2,
qnew, ril, ril1, rimu, RIPL, RIP1, ritemp, rk1, rkmu, rkmup, rktemp, s, Sum, sum1, x2, xi, xi2, xmu, xmu2 As
Double
Dim negorpos As Boolean

If XNU < 0 Then
XNU = -XNU
negorpos = True
Else
negorpos = False
End If

eps = 0.0000000001
fpmin = 1E-30
MAXIT = 10000
xmin = 2
Pi = Application.Pi()

If x <= 0 Or XNU < 0 Then MsgBox ("Bad Arguments in Bessi")

nl = Int(XNU + 0.5)
xmu = XNU - nl
xmu2 = xmu * xmu
xi = 1 / x
xi2 = 2 * xi
h = XNU * xi
If h < fpmin Then h = fpmin
b = xi2 * XNU
d = 0
c = h

For i = 1 To MAXIT
    b = b + xi2
    d = 1 / (b + d)
    c = b + 1 / c
    del = c * d
    h = del * h
    If (Abs(del - 1) < eps) Then GoTo 1
Next i
MsgBox ("Failed at first loop")

1 ril = fpmin
RIPL = h * ril
ril1 = ril
RIP1 = RIPL
Fact = XNU * xi
```

```
For L = nl To 1 Step -1
   ritemp = Fact * ril + RIPL
   Fact = Fact - xi
   RIPL = Fact * ritemp + ril
   ril = ritemp
Next L

f = RIPL / ril

If x < xmin Then
GoTo 20
Else
GoTo 30
End If

20 x2 = 0.5 * x
pimu = Pi * xmu

If Abs(pimu) < eps Then
Fact = 1
Else
Fact = pimu / Sin(pimu)
End If

d = -Log(x2)
e = xmu * d

If Abs(e) < eps Then
fact2 = 1
Else
fact2 = Application.Sinh(e) / e
End If

chex = (8 * xmu * xmu) - 1
gam1 = chebev(chex, 1)
gam2 = chebev(chex, 2)
gampl = gam2 - (xmu * gam1)
gammi = gam2 + (xmu * gam1)

ff = Fact * (gam1 * Application.Cosh(e) + gam2 * fact2 * d)
Sum = ff
e = Exp(e)
p = 0.5 * e / gampl
q = 0.5 / (e * gammi)
c = 1
d = x2 * x2
sum1 = p

For i = 1 To MAXIT
   ff = (i * ff + p + q) / (i * i - xmu2)
   c = c * d / i
   p = p / (i - xmu)
   q = q / (i + xmu)
   del = c * ff
   Sum = Sum + del
   del1 = c * (p - i * ff)
   sum1 = sum1 + del1
   If Abs(del) < (Abs(Sum) * eps) Then GoTo 2
Next i
MsgBox ("BESSI FAILED AT SECOND LOOP")

2 rkmu = Sum
rk1 = sum1 * xi2
GoTo 40
```

270

```
30 b = 2 * (1 + x)
d = 1 / b
delh = d
h = delh
q1 = 0
q2 = 1
a1 = 0.25 - xmu2
c = a1
q = c
a = -a1
s = 1 + q * delh

For i = 2 To MAXIT
    a = a - 2 * (i - 1)
    c = -a * c / i
    qnew = (q1 - b * q2) / a
    q1 = q2
    q2 = qnew
    q = q + c * qnew
    b = b + 2
    d = 1 / (b + a * d)
    delh = (b * d - 1) * delh
    h = h + delh
    dels = q * delh
    s = s + dels
    If Abs(dels / s) < eps Then GoTo 3
Next i
MsgBox ("BESSI failed at loop 3")

3 h = a1 * h
rkmu = Sqr(Pi / (2 * x)) * Exp(-x) / s
rk1 = rkmu * (xmu + x + 0.5 - h) * xi

40 rkmup = xmu * xi * rkmu - rk1
rimu = xi / (f * rkmu - rkmup)
ri = (rimu * ri11) / ril
rip = (rimu * RIP1) / ril

For i = 1 To nl
    rktemp = (xmu + i) * xi2 * rk1 + rkmu
    rkmu = rk1
    rk1 = rktemp
Next i

rk = rkmu
rkp = XNU * xi * rkmu - rk1


If negorpos = False Then
bessi = ri
Else
bessi = ri + ((2 / Pi) * Sin(XNU * Pi) * rk)
End If
End Function

'
'Chevbez function
'
Function chebev(CHEBx, arty)
Dim CHEBj, CHEBm As Integer

If arty = 1 Then
```

271

```
CHEBci = Array(-1.14202268037117, 6.5165112670737E-03, 3.087090173086E-04, -3.4706269649E-06,
6.9437664E-09, 3.67795E-11, -1.356E-13)
Else
CHEBci = Array(1.84374058730091, -7.68528408447867E-02, 1.2719271366546E-03, -4.9717367042E-06,
-3.31261198E-08, 2.423096E-10, -1.702E-13, -1.49E-15)
End If

CHEBa = -1
CHEBb = 1

     If ((CHEBx - CHEBa) * (CHEBx - CHEBb)) > 0 Then
     resp = MsgBox("X out of range for Chebev", vbExclamation, "Ooops")
     If resp = vbOK Then GoTo 100
     End If
CHEBd = 0
CHEBdd = 0
CHEBY = ((2 * CHEBx) - CHEBa - CHEBb) / (CHEBb - CHEBa)
CHEBy2 = 2 * CHEBY
CHEBm = 5

For CHEBj = CHEBm To 2 Step -1
CHEBsv = CHEBd
CHEBd = (CHEBy2 * CHEBd) - CHEBdd + CHEBci(CHEBj)
CHEBdd = CHEBsv
Next CHEBj

chebev = (CHEBY * CHEBd) - CHEBdd + (0.5 * CHEBci(1))
100 End Function
```

COPYRIGHT STATEMENT